Università degli Studi di Milano

Facoltà di Scienze Matematiche Fisiche e Naturali

Corso di Laurea Magistrale in Fisica

Black hole spin alignment in astrophysical environments

Relatore interno: **Prof. Giuseppe Lodato**
Relatore esterno: **Prof. Emanuele Berti**

Tesi di laurea di:
Davide Gerosa
Matr. 790648

Codice P.A.C.S.: 04.70.-s

Anno Accademico 2011-2012

Hey what else can we do now
Except roll down the window
And let the wind blow back your hair
Well the night's busting open
These two lanes will take us anywhere
We got one last chance to make it real
To trade in these wings on some wheels
Climb in back, heaven's waiting on down the tracks
Come take my hand
We're riding out tonight to case the promised land.

Bruce Springsteen

Abstract

According to the currently accepted paradigm, astrophysical black holes are described by the vacuum solutions of the Einstein equations of general relativity that were first obtained by Kerr (1963). Surprisingly, astrophysical black holes are very simple objects, characterized by only two parameters: their mass M and their angular momentum (or spin) χ. Observations suggest that black holes exist only in two well separated mass ranges: stellar-mass black holes with $M \sim 10 M_\odot$ and supermassive black holes with $M \sim 10^6 - 10^{10} M_\odot$. Stellar-mass black holes result from the gravitational collapse of the most massive stars: when nuclear reactions exhaust the available fuel, these stars explode as Supernovae, leaving black holes as remnants. On the other hand, supermassive black holes are hosted by galaxies in their central bulges: their origin is probably cosmological and their growth is due to accretion and repeated merging events. In both mass ranges, black holes can form binary systems. If the separation between the two black holes is small enough ($a \lesssim 0.001$ pc in the supermassive case and $a \lesssim 50 R_\odot$ for stellar-mass black holes, where a is the binary separation), the evolution of the binary is ruled by gravitational-wave emission, that carries energy away from the system leading to a merger. At wider separation the evolution is dominated by interactions with the astrophysical environment, which can alter the black-hole parameters: mass, spin magnitude and spin orientation. In this thesis we study the impact of the astrophysical environment on the orientation of spins in black-hole binaries, both in the stellar-mass and in the supermassive range. The physical interactions of the binary with its environment are very different in these two ranges. Stellar-mass black-hole binaries result from the evolution and explosion of stars in binary systems; supermassive black-hole binaries are the result of galaxy mergers, and in general they interact with huge amounts of gas in the form of accretion discs.

After a black-hole merger, the final black hole will have a recoil velocity (or *kick*) due to the non-isotropic emission of linear momentum during the inspiral and merger phase. Kicks can be as large as ~ 4000 km/s (González et al. 2007a; Campanelli et al. 2007a) if the black holes have nonzero spin. This could be particularly critical in the case of **supermassive black holes**: kicks of this magnitude can exceed the escape velocity of even the most massive galactic bulges (Merritt et al. 2004), opening the possibility that black holes could be expelled from their galaxies. The key element to determine the likelihood of *superkicks* is the alignment between the individual black-hole spins before merger and the orbital angular momentum of the binary, since the recoil velocity depends strongly on the spin orientation: in particular, superkicks will be less likely in the case of partial alignment. Black-hole mergers are expected to occur in gas-rich environments, where circumbinary discs play a key role in bringing the binary to separations close enough for gravitational-wave emission to drive the final coalescence. Accretion discs affect also the mutual orientation of each black-hole spin through Lense–Thirring precession and viscous torques (Bardeen and Petterson 1975; Rees 1978). If the spin is initially misaligned with the angular momentum of the disc, the inner disc is efficiently aligned by the presence of the black holes, while the outer disc retains its initial orientation: the disc is now warped (Pringle 1992), and the propagation of these warps can alter the orientation of the spin. If the alignment timescale is at least comparable with the merger timescale, the black holes retains a certain misalignment, which can produce large recoil velocities.

The alignment timescale was found by Natarajan and Pringle (1998) in the case of small-amplitude (linear) warps and used in detailed analyses by Perego et al. (2009) and Dotti et al. (2010). We generalize their results using the non-linear theory of warp propagation developed by Ogilvie (1999) and verified numerically by Lodato and Price (2010). Large initial misalignments in the Bardeen–Petterson geometry would inevitably produce discs with a sizable warp, for which the linear approximation is inappropriate. The non-linear theory predicts lower values for the warp-propagation coefficient α_2, and introduces a new key dependence on the initial misalignment. We perform Monte Carlo simulations of randomly distributed spin directions and accretion rates, varying the viscosity of the disc and the magnitude of the black-hole spin. We consider both co- and counter-aligned discs, by carefully modeling the accretion efficiency (Bardeen 1973; King et al. 2008). As the spin grows, the alignment timescale becomes comparable with typical merger timescales ($\sim 10^7$ yrs; Escala et al. 2005; Dotti et al. 2009b): highly spinning black holes are more likely to receive *superkicks* and to be expelled by galaxies. From this point of view, the current lack of observational recoiling candidates (Komossa 2012) could indicate that black-hole spin magnitudes are low, as suggested by the chaotic-accretion scenario (King and Pringle 2006) and by predictions based on the Soltan argument (Soltan 1982; Yu and Tremaine 2002). Our assumptions have been tested against the Scheuer and Feiler (1996) disc solution, which however relies on the assumptions that warps propagate linearly. Steady-state solutions which account for the non-linear theory in a self-consistent way are not available at the moment. We hope our work could stimulate further studies in this direction.

Our main motivation for studying spin alignment of **stellar-mass black-hole** binaries consists in the imminent birth of gravitational-wave astronomy. Ground-based gravitational-wave detectors such as Advanced LIGO and Virgo are expected to perform the first direct detection (of gravitational waves) in the next few years. Gravitational-wave signals need to be extracted from noisy data using matched filtering, which consists of computing the cross-correlation between the output coming from the detector and a predicted theoretical waveform, or template. Detection rates increase by a factor ~ 30 to ~ 100 if matched filtering is used, but a detailed knowledge of the incoming waveform is required (Sathyaprakash and Schutz 2009). A template bank for efficient gravitational-wave detection of a black-hole binary depends in general on 17 different parameters, 4 of which define the spin orientations. If the evolution of the binary can cluster the spin parameters in certain regions of the parameter space, gravitational-wave data analysts could place more templates in these regions, thus increasing the efficiency of possible detections. In the slow-motion/weak-field regime (i.e. from $a \simeq 1000GM/c^2$ to $a \simeq 10GM/c^2$, where M is the total mass of the binary), the evolution of the binary can be followed by solving the Einstein field equations using a series expansion in v/c (where v is the orbital velocity and c is the speed of light). This *post-Newtonian* approximation is currently used to build LIGO and Virgo templates (Buonanno et al. 2009). A leading effect in post-Newtonian evolution was discovered by Schnittman (2004) and developed by Kesden et al. (2010a,b) and Berti et al. (2012b). During the post-Newtonian inspiral, black-hole binaries can transition through coplanar equilibrium solutions of the post-Newtonian equations and remain locked in these resonant configurations. The presence of such *resonances* is a natural physical mechanism to cluster samples of binaries with well defined spin orientations: both the spins and the orbital angular momentum tend to lie in the same plane just before merger. The effect of resonances strongly depends on the initial conditions of the post-Newtonian inspiral, i.e. on the formation history of the binary. A unified treatment is therefore necessary.

Here we study the interplay between astrophysics (at large separations) and general relativity (at small separations) to determine the spin configurations when binaries become detectable. We develop a simple astrophysical model to investigate the influence of astrophysical formation scenarios on the precessional dynamics of spinning black-hole binaries, focusing on resonant effects. Stellar-mass black holes are formed from the core collapse of massive stars. Asymmetric supernova explosions in binaries tilt the orbital plane, therefore modifying the spin orientations (Kalogera 2000). Once spin-orbit misalignments are introduced, the direction of the spins is further modified by tidal interactions (Hurley et al. 2002;

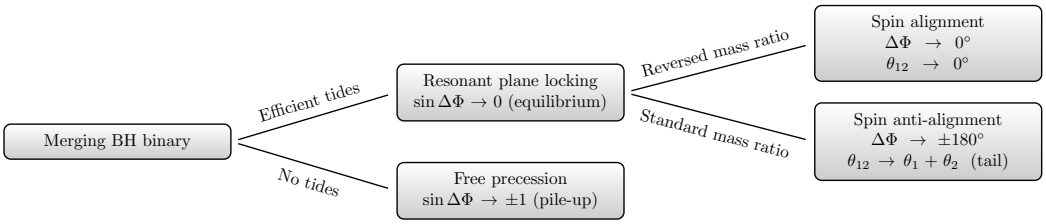

Figure 0.1: Schematic summary of our predictions for the spin orientation of stellar-mass black-hole binaries as they enter the Advanced LIGO/Virgo band.

Dominik et al. 2012). Tides are critical when the system is formed by a black hole and a stellar companion. Since the physical dimensions of the black hole are negligible, tides tend to align only the spin of the star, introducing a critical asymmetry between the two binary members. We generate samples of binaries using different formation scenarios, and we evolve them numerically by integrating the post-Newtonian equations of motion (Kidder 1995; Arun et al. 2009). Under the assumption that tidal interactions are efficient, we find that spin-orbit resonances should efficiently lock black-hole binaries in a "resonant plane" by the time they become detectable by gravitational-wave interferometers. This resonant plane is identified by the conditions $\Delta\Phi = 0^\circ$ or $\Delta\Phi = \pm 180^\circ$, where $\Delta\Phi$ is the angle between the components of the black-hole spins in the plane orthogonal to the orbital angular momentum. If tides are artificially removed from our simulations, binaries do not lock into resonant configurations, but rather their spins freely precess during the whole inspiral. Precessional motion slows down when $\Delta\Phi = \pm 90^\circ$, so binaries tend to pile up in these configurations. We also find that spin orientations encode information on mass-transfer events. If mass transfer between the binary members has been strong enough to produce mass-ratio reversal (so that the heavier black hole is produced by the initially lighter stellar progenitor), when black-hole binaries enter the sensitivity band of gravitational-wave detectors the two spins are aligned with each other, i.e. $\theta_{12} \sim 0^\circ$. On the other hand, if mass transfer is not efficient, binaries are expected to retain larger spin-spin misalignment angles even in the late inspiral. If the angles $\Delta\Phi$ and θ_{12} can be accurately measured for a large sample of gravitational-wave detections, their distribution will constrain models of compact-binary formation. In particular, it will tell us whether tidal interactions and mass transfer in massive binary stars are efficient (Fig. 0.1). Therefore our model offers a concrete observational link between gravitational-wave measurements and astrophysics. We also hope that it will stimulate further studies of precessional dynamics, gravitational-wave template placement and parameter estimation for binaries locked in the resonant plane.

This thesis has led to two scientific publications (Lodato and Gerosa 2013; Gerosa et al. 2013).

We organize our presentation as follows. Chapter 1 is dedicated to a review of the main properties of astrophysical black holes, focusing on spin effects. Supermassive black-hole mergers are introduced in Chapter 2, while in Chapter 3 we treat accretion discs around black holes and we discuss different warp-propagation theories. The alignment timescale between the spin of a supermassive black hole and its surrounding accretion disc is the main subject of Chapter 4, where we also present results from our Monte Carlo simulations. In Chapter 5 we show that a unified treatment is needed to model the evolution of the spins during the inspiral of stellar-mass black-hole binaries. We review the main properties of spin-orbit resonance in Chapter 6, where some test simulations are also presented. Finally, Chapter 7 discusses the predictions of our astrophysical model for the formation and evolution of stellar-mass black-hole binaries.

Contents

List of Figures

List of Tables

List of Acronyms

ΛCDM	Λ Cold Dark Matter
AGN	Active Galactic Nucleus
BH	Black Hole
CMB	Cosmic Microwave Background
GR	General Relativity
GW	Gravitational Wave
IMR	Inspiral Merger Ringdown
KAGRA	Kamioka Gravitational-Wave Detector
LAGEOS	Laser Geodynamics Satellites
LIGO	Laser Interferometer Gravitational-Wave Observatory
LISA	Laser Interferometer Space Antenna
NINJA	Numerical INJection Analysis
NS	Neutron Star
PN	Post-Newtonian
SMBH	Supermassive Black Hole
SN	Supernova
SNR	Signal-to-Noise Ratio
WMAP	Wilkinson Microwave Anisotropy Probe

Chapter 1

Spinning black holes

Initially introduced as pure mathematical solutions of the Einstein field equations, black holes (BHs) are observed in the Universe only in two well separated mass ranges[1]: stellar-mass BHs with $M \sim 1 - 100 M_\odot$ and supermassive black holes (SMBHs) with $\sim 10^6 - 10^{10} M_\odot$. Theoretical predictions do not restrict in any way BH masses to be in these two mass range: primordial BHs (Carr 2005) and intermediate-mass BHs (Miller and Colbert 2004) have also been predicted, but their existence is still a controversial topic. Even if their interactions with the astrophysical environment can be extremely complicated, astrophysical BHs are surprisingly simple objects defined by only two parameters: their mass and their angular momentum.

In this Chapter we introduce the main properties of astrophysical BHs, focusing on their spin effects. The Schwarzschild and the Kerr metrics are firstly introduced, together with the precessional motion of particles in their spacetimes. We then describe the experimental evidence for the existence of BHs in the Universe and the current measurements of their masses and spins. Gravitational-wave (GW) searches are introduced as promising channel to detect weak- and strong-field effects from compact objects (and BHs in particular). As relativists usually do, in this Chapter we will often use geometrical units $G = c = 1$. We will occasionally restore the fundamental constants to show some physical quantities.

1.1 Spin effects in black hole spacetimes

We introduce the Schwarzschild and the Kerr metrics to describe astrophysical BHs. Effects related to BH spin and/or the spin of a test particle orbiting around a BH are briefly described: these include the Penrose process, geodetic precession and Lense-Thirring precession.

1.1.1 Schwarzschild metric

Within Einstein's theory of general relativity (GR), the spacetime is assumed to be a 4-dimensional Lorentzian manifold. The spacetime outside a spherically symmetric body was first described by Schwarzschild (1916), only a few months after the publication of the Einstein field equations. In a suitable set of coordinates (t, r, θ, ϕ), the line element of the Schwarzschild geometry is (for a formal derivation, see e.g. Wald 1984)

$$ds^2_{\rm Sch} = -\left(1 - \frac{2M}{r}\right) dt^2 + \left(1 - \frac{2M}{r}\right)^{-1} dr^2 + r^2 (d\theta^2 + \sin^2 d\phi^2) \,. \tag{1.1}$$

It has the following important properties (e.g. Misner et al. 1973; Carroll 1997):

[1] $1 M_\odot \simeq 1.989 \times 10^{33}$ g and $1 R_\odot \simeq 6.955 \times 10^{10}$ cm are the mass and the radius of the Sun, respectively.

- *Asymptotically flat.* The Schwarzschild metric reduces to Minkowski's flat spacetime in the limit $r \to \infty$. The set of coordinates (t, r, θ, ϕ) has ben chosen precisely to stress this property: they reduce to the canonical polar coordinates centered on the object position.

- *Time-independent.* The metric is invariant under time translations.

- *Spherically symmetric.* the geometry of a two-dimensional surface of constant r and t in the 4-dimensional Schwarschild metric describes a sphere of radius r in a flat 3-dimensional spacetime.

- *Mass.* The only free parameter of the Schwarzschild metric M can be associated with the mass of the body considered. At large distances $r \to \infty$, the gravitational interaction described with (1.1) reduces to Newtonian gravity with a static potential

$$\phi = -\frac{M}{r}\,. \tag{1.2}$$

- *Schwarzschild radius.* The geometry presents an event horizon at $r = 2M$, which is called the *Schwarzschild radius*. It can be shown (Kruskal 1960) that the singularity of the metric (1.1) at

$$r = \frac{2GM}{c^2} \simeq 3\left(\frac{M}{M_\odot}\right)\mathrm{Km}\,, \tag{1.3}$$

  is only a coordinate singularity and it turns out to be an *event horizon*, i.e. the boundary of two detached spacetime regions (for a mathematical definition of event horizon, see Townsend 1997). A curvature singularity is present at $r = 0$, but it is screened by the event horizon and thus inaccessible from our Universe.

- *Uniqueness.* Any spherically symmetric solution of the Einstein vacuum field equations must be static and asymptotically flat (Birkhoff and Langer 1923), and it is necessarily equivalent to the Schwarzschild metric (Israel 1967). This result basically generalizes Gauss's theorem to GR; a complete proof is reported in Hawking and Ellis (1973).

1.1.2 Kerr metric

The assumption of spherical symmetry underlying the Schwarzschild geometry can be relaxed to axial symmetry, which is more appropriate for rotating objects. The related metric was first written down by Kerr (1963)

$$\begin{aligned} ds^2_{\mathrm{Kerr}} = &-\frac{r^2 - 2Mr + \chi^2M^2 - \chi^2M^2\sin^2\theta}{r^2 + \chi^2M^2\cos^2\theta}\,dt^2 + \frac{r^2 + \chi^2M^2\cos^2\theta}{r^2 - 2Mr + \chi^2M^2}\,dr^2 \\ &+ \frac{(r^2 + \chi^2M^2)^2 - (r^2 - 2Mr + \chi^2M^2)\chi^2M^2\sin^2\theta}{r^2 + \chi^2M^2\cos^2\theta}\sin^2\theta\,d\phi^2 \\ &+ (r^2 + \chi^2M^2\cos^2\theta)d\theta^2 - \frac{4\chi M^2 r\sin^2\theta}{r^2 + \chi^2M^2\cos^2\theta}\,dt d\phi\,, \end{aligned} \tag{1.4}$$

The Kerr metric has two free parameters, M and χ. We chose the set of coordinate proposed by Boyer and Lindquist (1967), for which it is straightforward to obtain the Schwarzschild metric in the limit $\chi = 0$, and the Minkowski spacetime if $r \to \infty$. As in the Schwarzschild case, M is the mass of the object, while χ is related to the total angular

momentum of the spacetime **J**

$$\mathbf{J} = \chi \frac{GM^2}{c} \hat{\mathbf{J}} \,, \tag{1.5}$$

where $\hat{\mathbf{J}}$ in a unit vector along the $\theta = 0$ direction. The Kerr solution thus describes the spacetime structure around a rotating BH: **J** is commonly called the "spin" of the BH and χ is the "dimensionless spin". The polar axis of the coordinates coincides with the rotation axis.

The solution(1.4) presents two horizons at

$$r_\pm = M \left(1 \pm \sqrt{1 - \chi^2} \right) , \tag{1.6}$$

while $r = 0$ is a curvature singularity. It is believed that every singularity in nature must be screened by an event horizon (*cosmic censorship conjecture*, Penrose 1969): this restricts the parameter χ to the range

$$0 \leq \chi \leq 1 \,, \tag{1.7}$$

in order to have at least one real solution of Eq. (1.6). Moreover, it can be shown that Kerr solutions with $\chi > 1$ are unstable (e.g. Pani et al. 2010). The condition $\chi \leq 1$ has also a heuristic explanation: equality corresponds to the maximum (Newtonian) angular frequency for a body of mass M, radius $R \sim GM/c^2$ and moment of inertia $\sim MR^2$. The solution with $\chi = 0$ corresponds to the non-rotating case, while the one with $\chi = 1$ is called "extreme Kerr BH".

The Kerr metric can be expanded as a Taylor series around $\chi = 0$ to describe slowly rotating bodies. To first order in χ we have

$$ds^2_{\rm Kerr} = ds^2_{\rm Sch} - \frac{4\chi M^2}{r} \sin\theta^2 d\phi dt + O(\chi^2) \,, \tag{1.8}$$

where $ds^2_{\rm Sch}$ is the non-rotating metric (1.1).

1.1.3 Penrose process

While a static observer can get arbitrarily close to a Schwarzschild BH, this is not possible for a Kerr BH. The effect is known as "frame dragging" (Thirring 1918; Lense and Thirring 1918; Thirring 1921). An observer located at separations $r < r_e$, where r_e is the *ergosphere boundary*

$$r_e = M \left(1 \pm \sqrt{1 - \chi^2 \cos^2\theta} \right) , \tag{1.9}$$

must move in the direction of the rotation of the BH. The spacetime is dragged by the BH rotation, along with all observers in it. Since $r_e > r_+$, the *ergosphere* is a region outside the event horizon, and thus accessible from our Universe. In other words, an observer should move faster than the speed of light to remain stationary with respect to another observer at $r = \infty$. It can be shown that test particles orbiting in this region must have negative energy and negative angular momentum.

Penrose (Penrose 1969; Penrose and Floyd 1971, see also Wagh and Dadhich 1989; Schutz 2009) pointed out how the existence of an ergosphere allows energy and angular momentum extraction from a spinning BH. Imagine dropping an unstable particle toward a Kerr BH, with zero orbital angular momentum. Inside the ergosphere it decays into two particles. One of the two particles falls into the BH, caring its negative angular momentum across the event horizon. If the other particle can escape from the ergosphere, it must then have positive angular momentum. Since the total angular momentum of the spacetime must be

conserved, the process necessarily involves a decrease in the BH spin.The same argument is valid for the energy of the particles, decreasing the BH mass. This conservation process can reduce the BH mass up to a final *irreducible mass* (Christodoulou 1970)

$$M_{\rm irr}^2 = \frac{1}{2}M^2\left(1+\sqrt{1-\chi^2}\right) \tag{1.10}$$

by the time all the angular momentum is extracted.

1.1.4 Geodetic precession

Besides gravitational attraction, BHs can act on their astrophysical environment by modifying the angular momentum of the surrounding particles. We review here two different effects, both of which cause a precessional motion of a test gyroscope in a BH spacetime. Derivations are carried out exactly only in simple cases, following Weinberg (1972) and Hartle (2003): we will refer to the complete results throughout this work when necessary.

Geodetic precession (de Sitter 1916b) is a consequence of the presence of a conserved space-like vector around a BH. Let us consider a test gyroscope or *test spin* in the Schwarzschild metric (1.1); a generalization to the Kerr metric can be found in Tsoubelis et al. (1986), Semerák (1999) and Kyrian and Semerák (2007).

In a frame where the test particle is at rest, the gyroscope spin is described by a space-like vector $s^\alpha = (0, \mathbf{s})$ moving in the background metric with a timelike 4-velocity $u^\alpha = (1, \mathbf{0})$. Thus the conditions $u^\alpha s_\alpha = 0$ holds, which must be true in any frame. We call S the magnitude of the $\mathbf{s}$ vector, $S \equiv \sqrt{s^\alpha s_\alpha}$.

In a coordinate basis where the metric is (1.1), the GR equations of motion for the test spin read

$$\frac{ds^\alpha}{d\tau} + \Gamma^\alpha_{\beta\gamma} s^\beta u^\gamma = 0\,, \tag{1.11}$$

where τ is the *proper time* (i.e. the time in the local inertial frame) and the Γs are the Christoffel symbols (cf. Eq. 1.31) of the Schwarzschild metric. For simplicity we restrict to the case where the test spin is moving on a circular orbit of radius R on the equatorial plane ($\theta = \pi/2$). The only non-vanishing spatial part of $u^\alpha = dx^\alpha/d\tau$ is in the ϕ-direction, $u^\phi = \Omega u^t$. The angular frequency Ω, formally defined as $\Omega \equiv d\phi/dt$, is related to the BH mass M and to the orbital radius R through Kepler's third law, which is still valid for circular orbits around a Schwarzschild BH (e.g. Hartle 2003): $\Omega^2 R^3 = M$.

We will solve now Eq. (1.11) for the four components of $\mathbf{s} = (s^t, s^r, s^\theta, s^\phi)$, taking as initial condition a test spin pointing in the r-direction. Initially $s^\theta = 0$, and s^θ must remain zero because the problem is symmetric with respect to the equatorial plane. The equation $u^\alpha s_\alpha = 0$ can be solved for s^t, yielding

$$s^t = R^2\Omega\left(1-\frac{2M}{R}\right)^{-1}\,. \tag{1.12}$$

The gyroscope equation (1.11) can then be expanded on the coordinate basis, and it results in two differential equations for s^r and s^ϕ:

$$\frac{ds^r}{dt} - (R-3M)\Omega s^\phi = 0\,, \tag{1.13}$$

$$\frac{ds^\phi}{dt} + \frac{\Omega}{R}s^r = 0\,, \tag{1.14}$$

where we used $dt = u^t d\tau$. The solution of the above equations with the initial condition

$s^\phi = 0$ is

$$s^r(t) = S\left(1 - \frac{2M}{R}\right)^{1/2} \cos(\Omega_{\rm GP}\, t)\,, \tag{1.15}$$

$$s^\phi(t) = -S\left(1 - \frac{2M}{R}\right)^{1/2} \left(\frac{\Omega}{\Omega' R}\right) \sin(\Omega_{\rm GP}\, t)\,, \tag{1.16}$$

where

$$\Omega_{\rm GP} = \left(1 - \frac{3M}{R}\right)^{1/2} \Omega \simeq \Omega - \frac{3}{2}\frac{M}{R}\Omega\,. \tag{1.17}$$

The first factor is the revolutionary motion around the BH mass M, the second terms is a new general relativistic effect: the spin components precess in the equatorial plane. After an orbital period $P = 2\pi/\Omega$, the test spin will return to the initial spatial position rotated by an angle

$$\Delta\Phi = 2\pi - P\Omega_{\rm GP} = 2\pi\left[1 - \left(1 - \frac{3M}{R}\right)^{1/2}\right]\,, \tag{1.18}$$

which reduces to $3\pi M/R$ in the weak-field limit ($M/R \ll 1$).

1.1.5 Lense-Thirring precession

Besides geodetic precession, a new effect arises if a test spin is orbiting around a Kerr BH. *Lense-Thirring* precession (Thirring 1918; Lense and Thirring 1918; Wilkins 1972) is produced by the coupling between the angular momentum of the particle and the BH spin. The following derivation is carried out in the slowly-rotating regime (Hartle 2003); the general case can be found e.g. in Merloni et al. (1999).

In the previous Section we studied geodetic precession by solving the geodetic equations (1.11) in the Schwarzschild metric, i.e. we considered the zeroth order in an expansion around $\chi = 0$ of the Kerr metric. Let us now consider now correction linear in χ. It is convenient to express the Kerr metric in the small-χ limit (1.8) using Cartesian coordinates (t, x, y, z), related to the previous ones (t, r, θ, ϕ) by the familiar relations

$$\begin{cases} x = r\sin\theta\cos\phi\,, \\ y = r\sin\theta\sin\phi\,, \\ z = r\cos\theta\,, \end{cases} \tag{1.19}$$

so that the rotation axis $\theta = 0$ corresponds to the z axis. The metric (1.8) becomes

$$ds^2_{\rm Kerr} = ds^2_{\rm Sch} - \frac{4\chi M^2}{r^2}\frac{x dy - y dx}{r} dt + O(\chi^2)\,. \tag{1.20}$$

We are interested in solving the gyroscope equation (1.11) only at the dominant post-Newtonian (PN) order. We postpone the treatment of the PN approximation to Sec. 6.1, because it will be one of the main topics of the second part of this work. Loosely speaking, physical quantities in GR can be expanded as a series in v/c (where v is the orbital angular velocity and c the speed of light), and only the leading-order terms are considered. Newtonian gravity is obtained to zeroth order in this expansion. In geometrical units, circular orbits $v^2/c^2 = M/r$. The spin χ appears in (1.20) multiplied by a factor M^2, thus the linear order in χ correspond to a PN order M^2/r^2. All the terms containing M/r in $ds^2_{\rm Sch}$ will be coupled to χ in terms like $\chi M^3/r^3$, which are not the dominant (first) PN order. As a

consequence, the calculation can be carried out setting $M = 0$ in $ds^2_{\rm Sch}$, i.e. using the flat metric in cartesian coordinates

$$ds^2_{\rm flat} = -dt^2 + dx^2 + dy^2 + dz^2 \,, \tag{1.21}$$

which simplifies the algebra.

We consider for simplicity a test particle freely falling along the z axis, with its spin lying the xy plane. The only non-vanishing components of u^α and s^α are respectively u^t, u^z, s^x and s^y. Eq. (1.11) restricted on the z axis leads to

$$\frac{ds^x}{dt} = -\frac{2\chi M^2}{z^3} s^y \,, \tag{1.22}$$

$$\frac{ds^y}{dt} = \frac{2\chi M^2}{z^3} s^x \,, \tag{1.23}$$

which is equivalent to a precession equation for the 3-dimensional vector $\mathbf{s}$

$$\frac{d\mathbf{s}}{dt} = \mathbf{\Omega}_{\rm LT} \times \mathbf{s} \,. \tag{1.24}$$

The frequency of the Lense-Thirring precession is therefore

$$\mathbf{\Omega}_{\rm LT} = \frac{2G^2\chi M^2}{c^3 z^3} \hat{\mathbf{J}} \,, \tag{1.25}$$

where z is the distance between the test spin and the mass M.

Geodetic precession (1.17) is an effect of order $R(\Omega_{\rm GP} - \Omega) \sim M/r$, while Lense-Thirring precession is a higher-order PN corrections $R\Omega_{\rm LT} \sim M^2/r^2$. We will find the same terms in the PN evolutionary equations treated in Sec. 6.2.

Both effects are present in general around a rotating body, and they combine in the total precession rate (Schiff 1960). Even if very small, both geodetic and Lense-Thirring precessional angles due to the Earth gravity have been measured. Measurements carried on with the LAGEOS (Laser Geodynamics Satellites) found precessional rates which agrees within 10% with the values predicted in GR (Ciufolini and Pavlis 2004). The Gravity Probe B

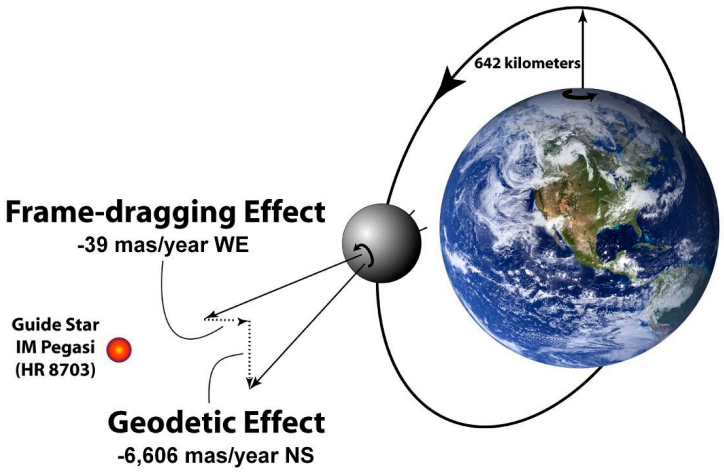

Figure 1.1: Gravity Probe B final results (Everitt et al. 2011). The Gravity Probe B experiment measured both geodetic precession and Lense-Thirring precession on four gyroscope around the Earth. Results are in spectacular agreement with the general relativistic predictions.

experiment (Everitt et al. 2011; Will 2011) carried four precision gyroscopes for 16 months on a polar orbit at 642 Km above the Earth surface (Fig. 1.1). Gravity Probe B results are a spectacular experimental confirmation of GR predictions in the weak-field limit. Analysis of the data gave a geodetic drift rate of 6601.8 ± 18.3 mas/yr and a frame-dragging drift rate of 37.2 ± 7.2 mas/yr, to be compared with the GR predictions of 6606.1 mas/yr and 39.2 mas/yr, respectively[2].

1.2 Black holes revealed

We briefly outline here the main astrophysical evidence for the existence of BHs. More details can be found in the review articles by Blandford (1987), Celotti et al. (1999), Narayan (2005), Berti et al. (2009) and references therein.

The main evidence that BHs are really present in our Universe comes from mass measurements, both for stellar-mass BHs (Sec. 1.2.1) and SMBHs (Sec. 1.2.2). Some spin estimates are also available today. However, the difficulty of such measurements and the strong dependence on the underlying astrophysical models make spin estimates still very controversial (Sec. 1.2.3).

1.2.1 Stellar-mass black holes in X-ray binaries

Stellar-mass BHs are extremely important in astronomy, because they are thought to the be one of the evolutionary endpoints for massive stars, and the collapse of their progenitor stars enriches the Universe with heavy elements (e.g. Woosley et al. 2002). Since neutron stars (NSs) cannot be more massive than about $3M_\odot$ (e.g. Rhoades and Ruffini 1974), mass measurements of compact objects above this limit are indirect observations of BHs. The first observation of a stellar-mass BH was announced in 1972 using X-ray and optical observations of the source Cygnus X–1 (Bolton 1972; Webster and Murdin 1972). Today ~ 50 systems are known to host a compact object too massive to be a neutron star (Özel et al. 2010). This is a small sample of a total number of $\sim 10^8$ to 10^9 stellar-mass BHs that are believed to exist in the Milky Way (Brown and Bethe 1994; Timmes et al. 1996). All those candidates have been identified in X-ray binaries, i.e. binary systems with an unusual strong X-ray emission. The X luminosity (often close to $L_{\rm edd} \sim 10^{38}$erg) and their short time variability ($\sim$ ms), support a model where X rays are supplied by accretion onto a compact object from a stellar companion. The key measurement to identify Cygnus X–1 and the other candidates as BHs was an estimate of its mass. Broad reviews on X-ray binaries can be found in Remillard and McClintock (2006) and Psaltis (2006).

The main observable used to measure the mass of X-ray sources is the radial velocity of the optical counterpart. Let us suppose we are observing a binary system made up by an X emitter (the BH) of mass $M_{\rm x}$ and an optical companion of mass M_c. When the optical companion is identified, e.g. the supergiant HD226868 associated with Cignus X-1, the radial velocity curve is obtained through Doppler measurements. The orbital period P and the radial velocity amplitude v_r of the optical companion combine in the *mass function* equation

$$f(M_{\rm x}) = \frac{P}{2\pi G} v_r = \frac{M_{\rm x}^3 \sin^3 i}{(M_c + M_{\rm x})^2} \,. \tag{1.26}$$

If an estimate of the companion star mass M_c is available, e.g. from stellar structure analysis, a lower limit on the mass of the X emitter $M_{\rm x}$ can be obtained. The main uncertainty here arises from the (usually unknown) inclination angle i.

We report in Fig. 1.2 experimental results for the stellar-mass BH population in the Milky Way. Many X-ray binaries present a compact object with a measured (or estimated) mass beyond $3M_\odot$, which is commonly interpreted as a stellar-mass BH.

[2] $1\,\text{mas} = 4.848 \times 10^{-9}\,\text{rad}$.

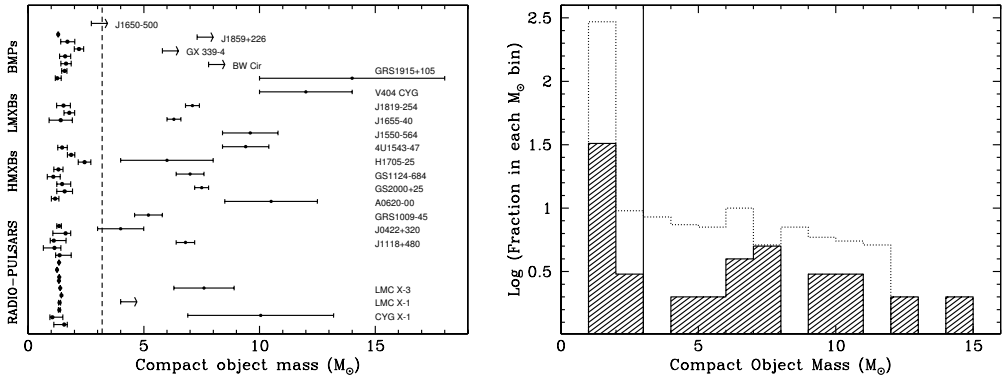

Figure 1.2: Observed stellar-mass BHs in the Milky Way (left panel, Casares 2007) and BH mass distribution compared with the core collapse model by Fryer and Kalogera (2001) (right panel, Casares 2007).

1.2.2 Supermassive black holes in AGNs and the case of SgrA*

Evidence of the existence of SMBHs comes from several energetic phenomena involving galactic cores, globally referred to as *active galactic nuclei* (AGNs) (for historical remarks on SMBH discoveries, see Melia 2003). In general, if the luminosity emitted by a source varies coherently on a given timescale timescale T, the different parts of the source must have had enough time to communicate with each other on that timescale. Causality implies that any signal within the source cannot propagate faster than the speed of light: this sets an upper limit on the physical dimensions of an astrophysical source of $L < Tc$. The main feature of the AGN phenomenon is the inferred compactness of the sources: luminosities of the order of $\sim 10^{48}$erg/s are emitted from regions smaller than a light-year ($\sim 10^{18}$cm). The tighter constraint is set by X-ray radiation variability, which in some cases can occur in less than one hour.

Two main facts suggest that AGNs could be powered by BHs (e.g. Begelman et al. 1984). First, efficient mass-to-light conversion is required to satisfy the observed luminosities: nuclear fusion has an efficiency of only 0.7%, while accretion onto BHs could reach even 40% (Sec. 3.2.1). Single super-massive objects with a mass in the range $\sim 10^6 - 10^{10} M_\odot$ can explain the observed luminosities easier than any other hypothesis, such as compact star clusters. Second, collimated structures (jets) are often associated with AGNs: the existence of jets requires the presence of a stable axis. Spinning BHs are therefore a promising hypothesis to explain these phenomena, with jet emission occurring along the spin axis.

Blandford and Znajek (1977) suggested that the Penrose process (Sec. 1.1.3) could be invoked to explain the presence of jets in AGNs. They consider a spinning BH surrounded by an accretion disc containing a magnetic field. The magnetic field facilitates the creation of positron/electron pairs inside the ergosphere, thus extracting energy from the BH by means of the Penrose process. A particle of each pair escapes, forming the energetic jets. In this way, AGN jets might be powered by energy extracted from the BH rotation (Rawlings and Saunders 1991; Nagar and Wilson 1999; Armitage and Natarajan 1999; Kinney et al. 2000; Tchekhovskoy et al. 2011). The issue is currently debated. Jet drivers might be the disc accretion energy rather than the BH spin (Blandford and Payne 1982; Livio et al. 1999; and Sec. 3.2.1). Jets are indeed observed in protostellar discs, where no BHs are present (Herbig-Haro objects, see Reipurth and Heathcote 1997 for a review).

SMBHs are today thought to be present at the center of most, if not all, galaxies (Kormendy and Richstone 1995; Magorrian et al. 1998; Ferrarese and Ford 2005) including our Milky Way. The most convincing proof of the existence of BHs comes precisely from the SMBH at the Galactic center, associated with the radio source Sgr A*. The Milky Way SMBH is an enormous source of discoveries and progress in astrophysics (e.g. Melia and

Falcke 2001; Genzel 2007; Reid 2009; Genzel et al. 2010). Since the distance to the Galactic Center is about 10^5 times closer than the nearest quasar, high-resolution observations of the Milky Way nucleus yield much more details and specific information than possible in any other galaxy nucleus. The central few parsecs of our Milky Way contain a dense and luminous star cluster, as well as several components of neutral, ionized gas. The discovery of the radio source SgrA* was made by Balick and Brown (1974) with the National Radio Astronomy Observatory and later confirmed using the Westerbork Radio Telescope (Ekers et al. 1975) and the Very Large Baseline Interferometry (VLBI; Lo et al. 1975). Three main line of evidence reinforce the case for the BH nature of SgrA*:

i) *Evidence from gas motion.* The first dynamical evidence for a central mass concentration emerged using the radial velocities of ionized gas (Wollman et al. 1977). Applying a virial analysis to these gas velocities, Lacy et al. (1980, 1982) suggested the presence of a central mass concentration of $2-4\times10^6 M_\odot$ in the central parsec: they concluded that this mass might be a massive BH, plausibly associated with the compact radio source Sgr A*.

ii) *Constraints from stellar orbits.* Besides stellar velocity dispersion measurements (Genzel et al. 1996; Haller et al. 1996a,b), the main evidence of the nature of SgrA* comes from observations of single star orbits, which are perfectly compatible with the motion induced by a Keplerian gravitational field from a point mass of $4.4\times10^6 M_\odot$ placed in SgrA* (Schödel et al. 2002, 2003; Ghez et al. 2003, 2005, 2008; Eisenhauer et al. 2005; Gillessen et al. 2009a,b). The stars closest to the Galactic center are called *S-stars*: nowadays 30 orbits have been well determined (Gillessen et al. 2009b), and for one of them (the star S2) a complete orbit is now available (Gillessen et al. 2009a). S2 is orbiting with a period of 15.8 years, on a highly eccentric orbit around SgrA* ($e = 0.88$). Its pericenter distance from Sgr A* is 17 light-hours, or 1400 Schwarzschild radii for a $4.4\times10^6 M_\odot$ BH.

iii) *VLBI observations.* VLBI performed the highest-resolution imaging and astrometry measurements of the Galactic center, which places strong additional constraints on the properties of Sgr A* (Bower et al. 2004, 2006; Shen et al. 2005; Doeleman et al. 2008). The currently best determinations of the intrinsic size of the radio source is 0.37mas, which corresponds to 3.7 Schwarzschild radii for a $4.4\times10^6 M_\odot$ BH at the Galactic center distance.

We strongly believe that BHs exists in nature because they are the only plausible way to explain these mass measurements. However, the first direct evidence for a BH event horizon is yet to come. An indirect argument has been proposed by Broderick and Narayan (2006) and Broderick et al. (2009), precisely in the case of SgrA*. Matter accreting onto a hypothetical hard surface lying outside the Schwarzschild radius, but within the upper limit of 3.7 Schwarzschild radii set by the VLBI images, will emit some of its gravitational energy as non-thermal radiation on the way. Once the matter hits the surface, it will shock, thermalize, and emit all its remaining energy as black-body radiation. Since this component is not observed, it sets an upper limit on the mass accretion rate. This limit is so low that the observed (non-thermal) emission from the infalling gas would require an accretion efficiency of nearly 100%. To avoid this unphysical conclusion, the central object cannot have a physical surface, but rather an event horizon.

1.2.3 Spin measurements

Precise measurements of BH spin magnitude are a major challenge for modern astrophysics. Four methods to measure BH spins have been proposed so far (Abramowicz and Fragile 2013):

i) fitting the continuum spectra of observed BH candidates using disc emission models (Davis et al. 2006; Middleton et al. 2006; Shafee et al. 2006; Remillard and McClintock 2006; McClintock et al. 2006, 2011);

ii) fitting the broadened iron line profiles with general relativistic predictions (Fabian et al. 1989, 2000; Karas et al. 2000; Wilms et al. 2001; Fabian 2002; Miller et al. 2002, 2004; Reynolds and Fabian 2008);

iii) in the case of quasi-periodic tobjects, matching the observed frequencies to those predicted by theoretical models (Cui et al. 1998; Abramowicz and Kluźniak 2001; Remillard et al. 2002; Török et al. 2005);

iv) analyzing the "shadow" cast by the BH on the surface of an accretion disc (Takahashi 2004a).

The continuum fitting and the iron line methods are perhaps the best developed to date. The former applies only to stellar-mass BH, while the latter con be applied to both classes.

In the continuum fitting method, one identifies the inner edge of the accretion disc with the radius of the innermost stable orbit $R_{\rm isco}$, which is estimated by fitting the X-ray continuum spectrum. Since $R_{\rm isco}$ is a function of the BH spin parameter χ (Eq. 3.27-3.29), knowing its value allows one to infer the value of χ. The following measurement however is model-dependent, since hypotheses on the disc structure (typically Shakura and Sunyaev 1973, or Novikov and Thorne 1973) are required to carry out this procedure. It is also essential to have accurate measurements of the distance to the source, the disc inclination, and the BH mass (Orosz et al. 2007, 2009, 2011; Cantrell et al. 2010). The main issue of the continuum fitting method is the uncertainty introduced by the inclination angle. The effect of the spin on the spectrum is indeed degenerate with the effect of the inclination angle (Li et al. 2009), that must therefore be measured independently (Steiner and McClintock 2012).

Accreting BHs present an iron line (Fe Kα) which is intrinsically narrow in frequency. The observed energy profile of the line is shaped by both special relativistic (i.e. light beaming and Doppler shifting) and general relativistic (i.e. gravitational redshifting) effects into a characteristic profile which can be used to infer the properties of the BHs. Fig. 1.3 shows these effects in a schematic way.

In a nonrelativistic disc, each radius of the disc produces a symmetric double-horned line profile. Emission comes from both approaching (blueshifted) and receding material (redshifted) (e.g. Marsh and Horne 1988). Relativistic effects arise near the BH, where the orbital velocities are higher. Special relativistic beaming enhances the emission of the incoming mass, i.e. the blue peak. Two effects then contribute to the redshifting of the line: transverse Doppler effect from the time dilation in special relativity, and gravitational redshift from the spacetime curvature around the BH. All these effects together cause an asymmetric broadened line profile. A sum over all the disc rings is required to obtain a final prediction to be compared with observations. This clearly requires to adopt a model of the disc structure upon which the Fe Kα results would depend. Predictions in the Schwarzschild case were first made by Fabian et al. (1989), while the Kerr case is reported in Laor (1991), Bromley et al. (1998) and Martocchia et al. (2000). The blue extent of the line is almost entirely a function of the inclination, thereby providing a way to measure the inclination of the disc. On the other hand, the redward width of the line is a sensitive function of the inner radius of the line-emitting annulus $R_{\rm isco}$, which encodes the information about the spin magnitude (Fanton et al. 1997; see also Eq. 3.27-3.29). The main issue is therefore to obtain a proper measurement of the red wing of the line. This wing extends to lower energies for a rapidly rotating BH because gas in this case can get closer to the event horizon, deep in the potential well of the BH. The Fe Kα method has also the virtue of being independent of the mass of the BH and the distance to the source.

This procedure was firstly applied by Tanaka et al. (1995) to the Seyfert Galaxy MCG-6-30-15. Broad emission lines are today the only viable tool to measuring SMBH spins. SMBH spin measurements seem to support a high-spin picture with $\chi \sim 0.6$ to $\chi > 0.98$. A summary of SMBH spin measurements published by January 2013 has been collected by Reynolds (2013), and it is reported in Table 1.1. However, it is critical to note that such observations regard only a handful of cases, and they are naturally biased in favor

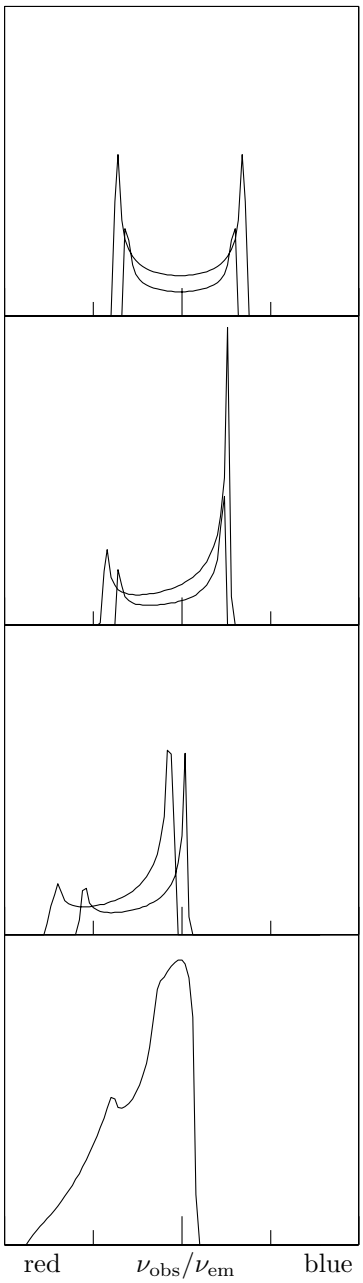

Newtonian: emission in a non-relativistic accretion discs comes from both approaching (blueshifted) and receding material (redshifted) in the same way, resulting in symmetric a double-horned profile.

Special relativity: special relativistic light beaming increases the number of photons coming from the approaching material (the blue wing) and transverse doppler shift causea a slight global redshift.

General relativity: gravitational redishift from particles close to the event horizon cause further frequency-dependent redshift. The red wing encodes information about $R_{\rm ISO}$ and thus about χ.

Line profile: contributions coming from all the disc annuli must be considered to predict the final line profile.

Figure 1.3: Broadening of the Fe Kα line profile (adapted by Fabian et al. 2000). Panels show the observed flux as a function of the ratio between the observed frequency $\nu_{\rm obs}$ and the emitted frequency $\nu_{\rm em}$. The first three panels shows the contributions produced by two disc rings in Newtonian gravity, considering only special relativity corrections and finally including the general relativistic gravitational redshift. The latest panel shows an hypothetical line profile obtained considering the emission coming from all the rings of the disc.

Object	$M/10^6 M_\odot$	χ	Mass Reference	Spin Reference
Mrk335	14.2 ± 3.7	$0.83^{+0.09}_{-0.13}$	Peterson et al. (2004)	Walton et al. (2013)
IRAS 00521–7054	—	> 0.84	—	Tan et al. (2012)
Tons180	~ 8.1	$0.92^{+0.03}_{-0.11}$	Zhou and Wang (2005)	Walton et al. (2013)
Fairall 9	255 ± 56	$0.52^{+0.19}_{-0.15}$	Peterson et al. (2004)	Lohfink et al. (2012)
Mrk359	~ 1.1	$0.66^{+0.30}_{-0.54}$	Zhou and Wang (2005)	Walton et al. (2013)
Mrk1018	~ 140	$0.58^{+0.36}_{-0.74}$	Bennert et al. (2011)	Walton et al. (2013)
1H0419-577	~ 340	> 0.89	Zhou and Wang (2005)	Walton et al. (2013)
Ark120	150 ± 19	$0.64^{+0.19}_{-0.11}$	Peterson et al. (2004)	Walton et al. (2013)
Swift J0501.9-3239	—	> 0.99	—	Walton et al. (2013)
1H0707-495	~ 2.3	> 0.97	Zhou and Wang (2005)	Zoghbi et al. (2010)
Mrk79	52.4 ± 14.4	0.7 ± 0.1	Peterson et al. (2004)	Gallo et al. (2011)
Mrk110	25.1 ± 6.1	> 0.89	Peterson et al. (2004)	Walton et al. (2013)
NGC3783	29.8 ± 5.4	> 0.88	Peterson et al. (2004)	Brenneman et al. (2011)
NGC4051	1.91 ± 0.78	> 0.99	Peterson et al. (2004)	Patrick et al. (2012)
RBS1124	—	> 0.97	—	Walton et al. (2013)
RAS13224–3809	~ 6.3	> 0.987	González-Martín and Vaughan (2012)	Fabian et al. (2013)
MCG–6-30-15	$2.9^{+1.8}_{-1.6}$	> 0.98	McHardy et al. (2005)	Brenneman and Reynolds (2006)
Mrk841	~ 79	> 0.52	Zhou and Wang (2005)	Walton et al. (2013)
Swift J2127.4+5654	~ 1.5	0.6 ± 0.2	Malizia et al. (2008)	Miniutti et al. (2009)
Ark564	~ 1.1	$0.96^{+0.01}_{-0.11}$	Zhou and Wang (2005)	Walton et al. (2013)

Table 1.1: Summary of published AGN/SMBH spin measurements that pass the quality-criteria described in Reynolds (2013). Masses are quoted with 1σ error bars whereas spins are quoted with 90% error ranges. Many of these measurements are still debated: for instance, the SMBH in NGC3783 has been found to have a prograde spin of $\chi > 0.88$ by Brenneman et al. (2011), while the analysis of Patrick et al. (2012) gives a retrograde spin of $\chi > 0.35$.

of large values of χ. This is because astronomers can distinguish only lines with significant broadening.

Alternative models for the production of broad Fe Kα lines were considered by Fabian et al. (1995), including lines from mildly relativistic outflows, the effect of absorption edges on the observed spectrum, and broadening of the line via Compton scattering. The idea of producing a broad line via Comptonization (Misra and Sutaria 1999) relies on the possibility that the spectrum initially consists of a narrow iron line superposed on a power-law continuum. Comptonization in a surrounding cloud with optical depth $\tau \sim 4$ can produce the broad line. The cloud must be both cold ($kT < 0.5$ keV in order to predominatly downscatter rather than upscatter the incoming photons) and fully ionized. The cloud is kept fully ionized and yet cool by postulating that the continuum source has a very luminous optical/UV component. In another alternative model, Skibo (1997) has proposed that energetic protons transform iron in the surface of the disc into chromium and lower-Z metals, which then enhances their fluorescent emission. With limited spectral resolution, such a line blend might appear as a broad skewed iron line. These alternative models have been ruled out very recently at least for the case of NGC 1365 (Risaliti et al. 2013), which is found to host a spinning BH with $\chi = 0.97^{+0.01}_{-0.04}$.

To summarize, BH spin measurements are currently an open and very controversial topic in modern astrophysics in both the stellar-mass and the SMBH case. A case in point is Cyg X-1, which was initially estimated to be non-rotating ($\chi = 0.05 \pm 0.01$; Miller et al. 2009) and later to be almost maximally spinning in a follow-up analysis performed by the same group ($\chi > 0.95$; Fabian et al. 2012); as well as the SMBH in NGC3783, where even the direction is unclear: Brenneman et al. (2011) claim prograde accretion from a spinning BH with $\chi > 0.88$, and Patrick et al. (2012) found a $\chi > 0.35$ BH counter-aligned with the accretion material.

1.3 Gravitational waves

Observational evidence for spinning BHs should come soon not only from the indirect detection of light emitted via interactions with their astrophysical environment, but also from GWs. GWs will provide a new window to Universe, that is intrinsically different from the electromagnetic one. The Big Bang, supernova (SN) explosions, perturbed BHs and compact binaries are all GW sources: the Universe is expected to be full of gravitational signals that have not been detected yet. GW observations are very important to characterize the spin properties of astrophysical BHs. The SMBH spin distribution could be measured very accurately with future space-based interferometers (see e.g. Lang and Hughes 2006, 2008), and provide precious information on how SMBHs are formed and evolve (see Hughes and Blandford 2003, Berti and Volonteri 2008 and our discussion in Sec. 2.1.1).

We firs introduce the key ideas of GW emission, and in particular the famous quadrupole formula first derived by Einstein himself. Then we briefly describe the Hulse-Taylor binary pulsar as the first indirect proof of the existence of GWs. Finally we give a brief overview of the main efforts towards direct detections.

1.3.1 Linearized gravity

GWs are ripples of curvature in the spacetime produced by the motion of massive bodies. The existence of wavelike solutions of the GR equations was soon realized by Einstein himself (Einstein 1916). Here and below, we use a metric signature $(-,+,+,+)$; greek indeces vary over the four spacetime dimensions ($\mu = 0, 1, 2, 3$), while latin indeces vary over only the three space dimensions ($i = 1, 2, 3$).

Propagation effects in the gravitational equations can be studied in the weak-field limit. Given a metric tensor $g_{\mu\nu}$ and the stress-energy tensor $T_{\mu\nu}$, gravity is described by the

Einstein field equations (in geometrical units $G = c = 1$)

$$R_{\mu\nu} - \frac{1}{2g_{\mu\nu}R} = 8\pi T_{\mu\nu}\,. \tag{1.27}$$

The Ricci tensor $R_{\mu\nu}$ and the scalar curvature R are defined as contractions of the Riemann tensor $R^{\nu}_{\mu\rho\sigma}$ as follows:

$$R^{\nu}_{\mu\rho\sigma} = \frac{\partial\Gamma^{\nu}_{\mu\sigma}}{\partial x^{\rho}} - \frac{\partial\Gamma^{\nu}_{\mu\rho}}{\partial x^{\sigma}} + \Gamma^{\nu}_{\lambda\rho}\Gamma^{\lambda}\mu\sigma - \Gamma^{\nu}_{\lambda\sigma}\Gamma^{\lambda}\mu\rho\,, \tag{1.28}$$

$$R_{\mu\nu} = g^{\rho\sigma}R_{\rho\mu\sigma\nu}\,, \tag{1.29}$$

$$R = g^{\mu\nu}R_{\mu\nu}\,, \tag{1.30}$$

where $\Gamma^{\mu}_{\nu\rho}$ are the affine connections

$$\Gamma^{\mu}_{\nu\rho} = \frac{1}{2}g^{\mu\lambda}\left(\frac{\partial g_{\lambda\nu}}{\partial x^{\rho}} + \frac{\partial g_{\lambda\rho}}{\partial x^{\nu}} - \frac{\partial g_{\nu\rho}}{\partial x^{\lambda}}\right)\,. \tag{1.31}$$

We assume that far from the source, gravitational effects are small, so we can write

$$g_{\mu\nu} = \eta_{\mu\nu} + h_{\mu\nu}\,, \tag{1.32}$$

with $\eta_{\mu\nu} = \mathrm{diag}(-1, +1, +1)$ and $|h_{\mu\nu}| \ll 1$. At linear order in $h^{\mu\nu}$, the affine connections and the Riemann tensor read

$$\Gamma^{\mu}_{\nu\rho} = \frac{1}{2}\eta^{\mu\lambda}\left(\frac{\partial h_{\lambda\nu}}{\partial x^{\rho}} + \frac{\partial h_{\lambda\rho}}{\partial x^{\nu}} - \frac{\partial h_{\nu\rho}}{\partial x^{\lambda}}\right)\,, \tag{1.33}$$

$$R_{\mu\nu\rho\sigma} = \frac{1}{2}\left(\frac{\partial^2 h_{\mu\sigma}}{\partial x^{\rho}\partial x^{\nu}} + \frac{\partial^2 h_{\nu\rho}}{\partial x^{\sigma}\partial x^{\mu}} - \frac{\partial^2 h_{\nu\sigma}}{\partial x^{\rho}\partial x^{\mu}} - \frac{\partial^2 h_{\mu\rho}}{\partial x^{\sigma}\partial x^{\nu}}\right)\,. \tag{1.34}$$

Let us now define the *trace-reverse* tensor

$$\bar{h}_{\mu\nu} = h_{\mu\nu} - \frac{1}{2}\eta_{\mu\nu}\left(\eta_{\alpha\beta}h^{\alpha\beta}\right) \tag{1.35}$$

and impose the Lorenz gauge

$$\frac{\partial\bar{h}^{\mu\nu}}{\partial x^{\nu}} = 0\,. \tag{1.36}$$

Using (1.33) and (1.34), the Einstein field equations (1.27) can be written as

$$\left(\eta^{\rho\sigma}\frac{\partial}{\partial x^{\rho}}\frac{\partial}{\partial x^{\sigma}}\right)\bar{h}^{\mu\nu} = -16\pi T^{\mu\nu}\,, \tag{1.37}$$

which is a wavelike equations with signals propagating at the speed of light. The general solution can be built up by adding waves from δ-function sources with the standard Green-functions method (e.g. Hartle 2003):

$$\bar{h}^{\mu\nu} = 4\int d^3x' \left.\frac{T^{\mu\nu}(t', \mathbf{x}')}{|\mathbf{x} - \mathbf{x}'|}\right|_{t'=t-|\mathbf{x}-\mathbf{x}'|}\,. \tag{1.38}$$

Let us now study the propagation of GWs in vacuum ($T^{\mu\nu} = 0$), for which (1.37) admits

plane-wave solutions: $\bar{h}^{\mu\nu} \propto \cos[\omega(t-z)]$ for a wave propagating along the z-axis. Being a symmetric four-dimensional tensor, $h^{\mu\nu}$ has ten independent components. Four of these are fixed by imposing the Lorenz gauge (1.36), leaving six independent components. Within the Lorentz gauge, we can always consider a coordinate transformation $x^\mu \to x^\mu + \xi^\mu$ such that the four ξ^μ solve the wave equation without sources. There are therefore four more conditions we can impose to simplify the metric perturbation $\bar{h}^{\mu\nu}$. More specifically, we impose $\eta_{\alpha\beta}h^{\alpha\beta} = 0$ (and thus $\bar{h}^{\mu\nu} = h^{\mu\nu}$) and $h^{i0} = 0$, working in the so-called *transverse-traceless* gauge. The only two remaining independent components h_+ and $h_\times$ refer to the two GW polarizations. Without loss of generality, we can consider a plane wave propagating along the z-axis with frequency ω; then

$$h_{\mu\nu} = \bar{h}_{\mu\nu} = \begin{pmatrix} 0 & 0 & 0 & 0 \\ 0 & h_+ & h_\times & 0 \\ 0 & h_\times & -h_+ & 0 \\ 0 & 0 & 0 & 0 \end{pmatrix} \cos[\omega(t-z)] \,, \tag{1.39}$$

which can be used to construct the general solution of the linearized Einstein equations in vacuum via a Fourier sum.

1.3.2 The quadrupole formula

We first introduce the momenta of the mass density T^{00}:

$$M = \int d^3x T^{00}(t, \mathbf{x}) \,, \tag{1.40}$$

$$M^i = \int d^3x T^{00}(t, \mathbf{x}) x^i \,, \tag{1.41}$$

$$M^{ij} = \int d^3x T^{00}(t, \mathbf{x}) x^i x^j \,. \tag{1.42}$$

From the energy-momentum conservation $\partial T^{\mu\nu}/\partial x^\mu = 0$, valid in linearized gravity, we have that the mass M and the linear momentum $\partial M^i/\partial t$ are conserved, i.e.

$$\frac{\partial M}{\partial t} = 0 \,, \tag{1.43}$$

$$\frac{\partial^2 M^i}{\partial t^2} = 0 \,. \tag{1.44}$$

Moreover we have (Buonanno 2007; Maggiore 2007)

$$\frac{\partial^2}{\partial t^2} M^{ij} = 2 \int d^3x T^{ij} \,. \tag{1.45}$$

Eq. (1.38) is the general solution of linearized gravity assuming outgoing waves. We consider here the propagation of GWs at a space point far from a weak, slowly-moving source. If R is the characteristic size of the source, we assume that the distance from the source to the detector $r \gg R$ and also that $\lambda \gg R$, where λ is the wavelength associated with the characteristic frequency of variation of the source. In this limit, Eq. (1.38) reduces to

$$\bar{h}^{\mu\nu} \to \frac{4}{r} \int d^3x' T^{\mu\nu}(t - r, \mathbf{x}') \,. \tag{1.46}$$

Over a limited range of angles about any direction, the wave described by equating (1.46)

is approximately a plane wave at large r. In this limit we can apply the analysis performed above for plane waves, where only the spatial part of $\bar{h}^{\mu\nu}$ is important (cf. Eq. 1.39). From (1.45) we have

$$\bar{h}^{ij} \to \frac{2}{r}\frac{\partial^2}{\partial t^2} M^{ij}(t-r)\,. \tag{1.47}$$

Eq. (1.43) shows that, as in the case of electromagnetic waves, where charge is conserved, there are no monopole contributions to the radiation field. In other words, there are no spherically symmetric waves in either electromagnetism or in gravity. However, while the leading term in electromagnetism is electric dipole radiation, this also vanishes for gravity, because linear momentum is conserved (cf. Eq. 1.44). The gravitational counterpart of the magnetic moment is the angular momentum (an integral of one power of x^i times the mass/charge-current), which is also conserved. The leading multipolar order for gravitational radiation is therefore the quadrupole term M^{ij}, as illustrated by Eq. (1.47).

To lowest order, the form of the total power radiated in GWs can be guessed from simple considerations (Hartle 2003). Being a wave propagation phenomenon, we expect the energy flux (energy per unit time and unit surface) to be quadratic in the wave amplitude (1.47). The power emitted (energy per unit time), must be quadratic in M^{ij} and its derivatives. The number of derivatives needed can be determined by dimensional analysis. Since in geometrical units the emitted power is dimensionless, it can contain only *third* time derivatives of M^{ij} (which are also dimensionless). The only two possible quadratic terms are

$$\left(\frac{\partial^3}{\partial t^3} M_{ij}\right)\left(\frac{\partial^3}{\partial t^3} M^{ij}\right) \qquad \text{and} \qquad \left(\frac{\partial^3}{\partial t^3} M^k_k\right)^2 . \tag{1.48}$$

The right combinations can be guessed by the fact that energy cannot be radiated from a spherically symmetric system, because this would violate mass conservation. For a spherically symmetric system the three axes x, y and z are all equivalent, thus

$$M^{ij}_{(\mathrm{sph})} = \frac{1}{3} M^k_k \delta^{ij}\,. \tag{1.49}$$

The combination of the two terms M_{ij} and M^k_k that vanishes for a spherically symmetric system is therefore

$$Q^{ij} = M^{ij} - \frac{1}{3} M^k_k \delta^{ij}\,. \tag{1.50}$$

In conclusion, the total power radiated P must be proportional to the quadratic contraction of the third-time derivatives of Q^{ij}. A more careful analysis (e.g. Misner et al. 1973; Buonanno 2007; Maggiore 2007) shows that the numerical factor is 1/5, i.e.

$$P = \frac{G}{5c^5}\left\langle \frac{d^3 Q_{ij}}{dt^3}\frac{d^3 Q_{ij}}{dt^3}\right\rangle , \tag{1.51}$$

where we restored the physical units and $\langle\cdot\rangle$ denotes the average over a period. This results is called the "quadrupole formula".

1.3.3 The Hulse-Taylor binary pulsar

The binary pulsar B1913+16 was the first binary pulsar to be observed (Hulse and Taylor 1975). Hulse and Taylor won the 1993 Nobel prize "*for the discovery of a new type of pulsar, a discovery that has opened up new possibilities for the study of gravitation*"[3]. The

[3] `www.nobelprize.org/nobel_prizes/physics/laureates/1993`

system is composed of two NSs, one of which is a pulsar with a flux density of about $10^{-26}\,\mathrm{erg\,s^{-1}cm^{-2}Hz^{-1}}$ at 1400 Hz. PSR B1913+16 is the first (indirectly) measured source of GWs; data from this source have now been available over a 35-year time span and they are in perfect agreement with GR predictions in the weak-field limit (Weisberg and Taylor 2003, 2005).

The main observable of PSR B1913+16 are the arrival times of the pulses. Non-relativistic analysis of arrival time data from this system yields five orbital parameters: (i) the projected semimajor axis of the pulsar orbit $a\sin i$, describing the dimension of the orbit; (ii) the orbital eccentricity e, describing the shape of the orbit; (iii) the epoch of periastron T_0, describing the bodies position on the orbit; (iv) the orbital period P; and (v) the argument of periastron ω_0, describing the orientation of the ellipse on the orbital plane. Relativistic effects can give us three additional quantities: (vi) the mean rate of advance of periastron $\langle\dot{\omega}\rangle$; (vii) a parameter linked to the GR time-dilation γ; and (viii) the orbital period derivative $\dot{P}$. The pulsar orbit is fully specified by only seven parameters, i.e six Keplerian elements plus the total mass of the system. Taylor and Weisberg (1982, 1989) provide the relevant formulae to compute all the orbital elements from the first seven observables just mentioned. For instance, the masses of the pulsar and companion are found to be $M_\mathrm{p} = 1.4414 \pm 0.0002 M_\odot$ and $M_c = 1.3867 \pm 0.0002 M_\odot$. Note that a value for G is needed in this evaluation, and its uncertainties are now comparable to the quoted uncertainties in M_p and M_c (Weisberg and Taylor 2005).

The eighth measured orbital parameter $\dot{P}$ overdetermines the system dynamically, and thus provides a test of the gravitation theory used to interpret the data. Using the quadrupole formula (1.51), Peters and Mathews (1963) showed that at the lowest order in GR the rate of period decrease is given by (see Sec. 5.2.1, and in particular Eq. 5.5)

$$\dot{P} = \frac{dP}{dt} = -\frac{194\pi}{5}\frac{G^{5/3}}{c^5}\left(\frac{P}{2\pi}\right)^{-5/3} M_p M_c (M_p + M_c)^{-1/3}(1-e^2)^{-7/2}\left(1 + \frac{73}{24}e^2 + \frac{37}{96}e^4\right). \tag{1.52}$$

Besides the fundamental constants G and c, all quantities in (1.52) can be either measured or derived from the observations. The variation of the orbital period causes a secular shift of the time at which the system is at periastron. The cumulative shift of the periastron time is shown in Fig. 1.4, together with the theoretical predictions from Eq. (1.52). Similar studies have also been performed other double NS systems (Lorimer 2008).

A small correction is needed to compare the measured value of $\dot{P}$ with the theoretical value predicted in the weak-field limit of GR. This is due to the relative acceleration between the Solar System and binary pulsar system projected onto the line of sight (Damour and Taylor 1991), and it depends on several poorly known quantities, such as the distance and proper motion of the pulsar and the radius of the Sun's galactic orbit. The accuracy of the test for gravitational radiation damping is now dominated by this correction term.

While we wait for spin effects to be detected in stellar-mass BH binaries (Sec. 5.1), the Hulse-Taylor binary pulsar provides an indirect proof of the relativistic spin-orbit couplings. Detailed predictions for PSR B1913+16 have been computed soon after its discovery by Barker and O'Connell (1975b) and Esposito and Harrison (1975). As shown in Sec. 1.1, the leading spin effect is geodetic precession, which for PSR B1913+16 has a period of $\sim 300\,\mathrm{yr}$. Assuming that the direction of the radio beam tracks the spin direction, geodetic precession should cause a secular change in the pulse shape, as observed from Earth. Variations of the pulse shape were reported by Weisberg et al. (1989) and these data were fitted by the models developed by Kramer (1998) and Weisberg and Taylor (2002). Measurements are compatible with geodetic precession as predicted in GR, with a misalignment between the pulsar spin and the orbital angular momentum of $\sim 20^\circ$. The theoretical calculations also predicts that the pulsar beam will no longer intersect our line of sight by 2025.

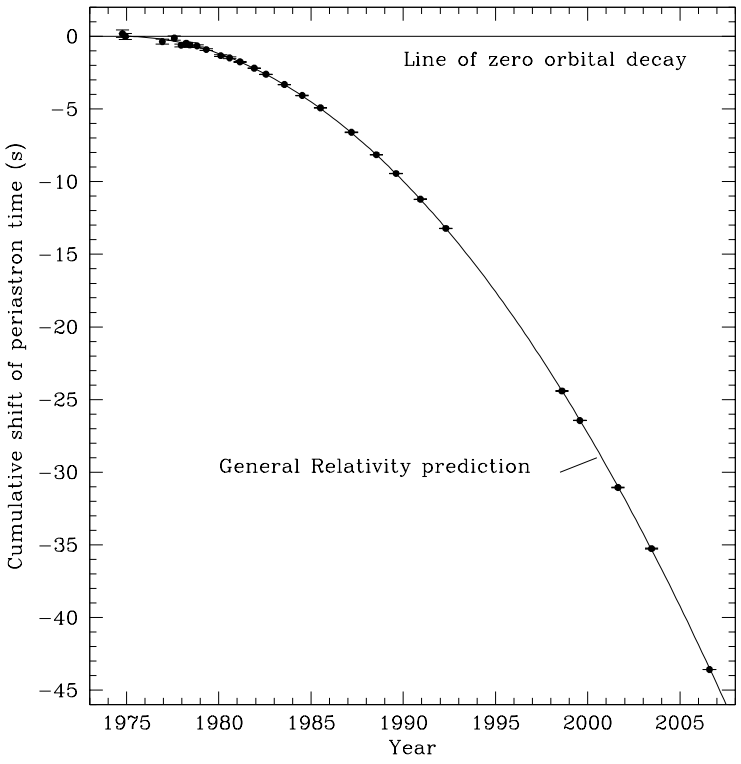

Figure 1.4: Orbital decay caused by GWs in the binary pulsar B1913+16 (Weisberg et al. 2010). The solid lines shows the expected shift of periastron time relative to an unchanging orbit, according to GR at the lowest PN order. Data points represent radio measurements, with error bars mostly too small to see.

1.3.4 Direct detections: methods and facilities

The direct detection of GWs is experimentally challenging. For example (Saulson 1994), a pair of $1.4M_\odot$ NSs near the center of the Virgo galactic cluster (15 Mpc away) in a circular orbit of 20-km radius (i.e. with imminent coalescence) which have an orbital frequency of 400 Hz will emit gravitational waves at ~ 800 Hz with an amplitude of the order

$$h \sim 10^{-21} \left(\frac{r}{15\,\mathrm{Mpc}} \right)^{-1} . \tag{1.53}$$

Therefore, GW detectors with characteristic length scales $L \sim 1$ km (4 km for LIGO, 3 km for Virgo) must perform length measurements with a precision $\Delta L = hL \sim 10^{-18}$m in order to detect GWs. This is an exceptional experimental challenge, but with the ongoing installation and commissioning of the Advanced LIGO and Advanced Virgo detectors, direct discovery of GWs may happen soon. Five approaches can be pursued to detect GWs in different part of the GW spectrum (for recent reviews, see (Sathyaprakash and Schutz 2009) and Riles 2013):

i) *Resonant bars.* Joseph Weber (1961) pioneered design and implementation of GW detectors, building the first resonant bar (Fig. 1.5). If two masses on a spring are momentarily stretched apart and then compressed by a GW, potential energy is imparted to the spring. If the characteristic frequency of the wave is near the resonance fre-

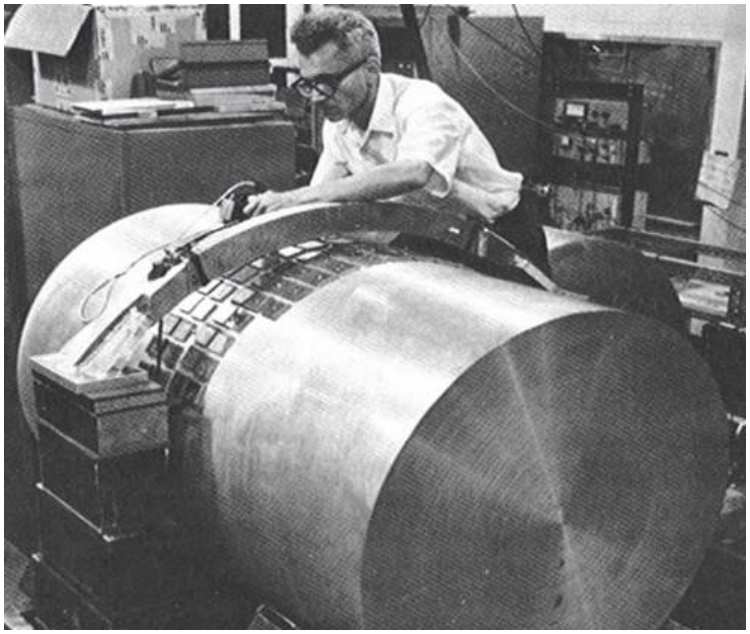

Figure 1.5: Joseph Weber working on an the very first GW detector, circa 1965 (Credit: University of Maryland). When a GW passes through the bar, it changes the distance between the two ends of the bar. The bar then absorbs energy from the wave, and this makes it vibrate. Sensors around the bar detect the vibrations and turn them into electrical signals that can be analyzed.

quency of the mechanical system, the response to the wave is magnified, and may thus be detected. Since it is only the elastic energy that matters, the first GW detectors were simple metal cylinders, where the energy converted to longitudinal oscillations of the bar was measured via piezoelectric materials near the surface of the bar. The severe technical challenges of bar detectors come fundamentally from their small size: any detector based on the resonances of a metal object cannot be larger than a few meters in size, and that seriously limits the size of the tidal stretching induced by a GW. Laser interferometric detectors can instead be built on km-scales (or million km-scale if in space). Moreover, bar detectors are sensitive only to GWs with frequencies close to the fundamental frequency of the cylinder, while GW interferometers can detect signals on a broader range of wavelengths.

Five major (cryogenic) bar detectors were operating in the late 1990s before GWs interferometers came online (Astone et al. 2007, 2010), and only two of them are still collecting data in 2013, since the interferometric detectors LIGO and Virgo reached better sensitivities on a broader band.

ii) *Interferometers.* A simple right-angle Michelson laser interferometer is a natural GW detector: a linearly polarized wave impinging normally to the interferometer with its polarization axis aligned with the arms will alternately stretch one arm while contracting the other. Interference patterns can then be analyzed and the properties of the stretching GW reconstructed. The optical structure of modern interferometers includes Fabry–Perot cavities for the interferometer arms to increase the time of exposure of the laser light to GWs, introduction of a *recycling* mirror between the laser and beam-splitter to increase effective laser power, and introduction of another mirror between the beam splitter and photodetector to allow tuning of the interferometer's frequency response (Freise and Strain 2010; Pitkin et al. 2011). The great advantage of GW interferometers is that a broader sensitivity band can be achieved, and thus more

GW sources are potentially detectable. At low frequencies ($\lesssim 45\,\mathrm{Hz}$ for the LIGO detectors) the noise is dominated by seismic ground motion, despite the strong isolation provided by the multiple stages of passive oscillators. At high frequencies ($\gtrsim 100\,\mathrm{Hz}$), quantum *shot* noise dominates, as determined by the Poisson statistics of photon detection (Riles 2013). At intermediate frequencies important known contributions come from the positions of the beam splitter and recycling mirrors, from thermal noise in the suspension wires and from various sources of noise in the auxiliary electronics (Abbott et al. 2009).

Besides the initial prototype interferometers used to demonstrate new technology developments (Saulson 1994), there are currently six major GW interferometer facilities around the world: LIGO (Laser Interferometer Gravitational Wave Observatory), which consists of two 4000-m arms interferometers and a third one with 2000-m arms, located in the Washington and Louisiana states (Fig. 1.6; Abramovici et al. 1992; Barish and Weiss 1999; Abbott et al. 2009; Smith 2009); Virgo a single 3000-m arms interferometer near Pisa (Acernese et al. 2005); GEO-600 near Hannover (Willke et al. 2002) and TAMA near Tokyo (Takahashi 2004b), with arms of 600 m and 300 m respectively. LIGO and Virgo scientists are currently working together on a joint collaboration (Abadie et al. 2012b,c; Aasi et al. 2013). The LIGO and Virgo detectors are now undergoing major upgrades to become Advanced LIGO (Harry 2010) and Advanced Virgo. These upgrades are expected to improve the broadband sensitivity by about an order of magnitude, which would increase the accessible volume of the Universe (and therefore the expected detection rate) by a factor 1000. One of the three LIGO detectors should soon be moved to India, to improve the network baseline. An underground 3-km interferometer (KAGRA; Somiya 2012) is under construction, and a 10-km cryogenic underground trio of triangular interferometers (Einstein Telescope; Sathyaprakash et al. 2012) is currently being planned.

Due to the frequency range involved, only stellar-mass BH binaries will be detected by ground-based GW interferometers (cf. Eq. 5.10). Astrophysically interesting sensitivities to detect SMBH inspirals at lower frequencies ($\sim 10^{-2}\,\mathrm{Hz}$) are unachievable on

Figure 1.6: Aerial view of the LIGO observatory in Livingston, Louisiana (USA). The large corner building hosts the laser generator and one of the main mirror of each arm. The beam pipes extend for 4 km in each direction covered by the arched, concrete enclosures seen in this picture (Credit: LIGO Laboratory).

Earth due to seismic noise. This will likely require placing interferometers in space. The proposed LISA (Laser Interferometer Space Antenna) project foresees a triangular configuration (roughly equilateral with sides of 5×10^6 km) of three satellites. Timing of lasers to and from each satellite would yield two linearly independent Michelson interferometers.

iii) *Pulsar timing arrays.* Galactic millisecond pulsars are extremely regular clocks when correcting for tiny, measurable spindows. Being a perturbation in the spacetime, if GWs are present between the emitting pulsar and the observer, they will perturb the regular structure of the pulse times. The basic concept is to treat the Earth and a distant pulsar as opposite ends of an imaginary interferometer arm in space. The pulsar acts as the reference clock at one end of the arm, sending out regular signals which are monitored by an observer on the Earth over some time-scale T. The method is thus sensitive to frequencies as low as $1/T$. If more pulsars are considered, GW signals can be separated from the timing noise of each pulsar, because the signal would be common to all pulsars in the array. A very low-frequency ($\sim$ several nHz) stochastic background of GWs can therefore be detected by comparing the arrival times of many pulsars (Lorimer 2008).

Efforts in the pulsar timing technique are currently pursued by several groups (Manchester 2008; Janssen et al. 2008; Jenet et al. 2009) which are now collaborating on a joint analysis to improve sensitivity, forming the *International Pulsar Timing Array* (Hobbs et al. 2010). Recent stochastic background searches using the pulsar timing array are reported by van Haasteren et al. (2011, 2012) and Demorest et al. (2013): they achieve limits on a stochastic background GW amplitude h in the several-nHz band of the order of 10^{-15}. The important aspect is to identify systematic uncertainties, some of which are instrumental (e.g., radio observatory clock synchronization) while some are terrestrial (e.g., ionosphere effects) and some are astrophysical (e.g., plasma fluctuations in the intervening interstellar medium, variable pulsar torque, and magnetospheric motions of emission regions).

iv) *Spacecraft tracking.* The idea is to look for anomalies in the communication data between Earth and interplanetary spacecraft. These anomalies can be due to interactions with a GW between emission and reception of the radio signal. The sensitivity of these searches is quite low because of atomic clock stability issue and delay caused by plasma in the solar wind. Unlike searches performed with resonant bars and ground-based interferometers, the spacecraft-tracking method applies to lower frequencies ($\sim$ mHz) (Armstrong 2006).

v) *CMB.* Signatures of gravitational waves from the Big Bang may be found in the cosmic microwave background (CMB) temperature and polarization distributions. Detection of these signatures is one of the main goals of the Planck mission. Since the CMB was affected by GWs when the Universe was only a few hundred thousand years old, the frequencies of those waves today are of order 10^{-16} Hz.

1.3.5 Matched filtering

Matched filtering is considered to be the optimal processing technique to detect GW signals. We describe here the main ideas of this technique following Thorne (1987) and Owen and Sathyaprakash (1999). In the frequency domain, a matched filter is a best-guess predicted waveform (or template) of the expected signal divided by the interferometer's spectral noise density in order to emphasize those frequencies to which the interferometer is most sensitive. The interferometer output is cross-correlated with the matched filter, and a signal-to-noise ratio (SNR) is computed. The SNR is compared to a predetermined threshold to decide if a signal is present in the noise. If the signal from which the matched filter was constructed is present, then it will contribute coherently to the cross-correlation, while if only noise is present the response is reduced.

The task is therefore to find the way to maximize the SNR. Let us consider a GW detector characterized by its noise spectral density $S_h(f)$ (with dimension Hz^{-1}), which describes the sensitivity of the detector at a given GW frequency f. We assumed the detector output to be $x(t) = h(t) + n(t)$, so that a *known* waveform $h(t)$ (with arrival time t_0) is buried in the instrumental noise $n(t)$. The best possible SNR is computed in three steps:

i) One constructs the *Wiener filter* $K(t)$, i.e. that function of time whose Fourier transform[4] is the same as the Fourier transform of the signal weighted by the noise density of the detector, so that noisy frequencies are suppressed:

$$\tilde{K}(f) = \frac{\tilde{h}(f)}{S_h(f)}\,. \tag{1.54}$$

ii) One computes the cross correlation between the output of the detector, which includes noise and possibly a signal, and the filter:

$$W = \int_{-\infty}^{+\infty} K(t - t_0)x(t)dt\,. \tag{1.55}$$

iii) The previous integral can be worked out to separate into a contribution which depends only on the noise N, and a remaining part S encoding the information from the signal (i.e. $W = N + S$). The signal to noise ratio is defined as S/N, and turns out to be (Thorne 1987)

$$\left(\frac{S}{N}\right)^2 = \int_0^{+\infty} \frac{2|\tilde{h}(f)|^2}{S_h(f)}\,. \tag{1.56}$$

The *Wiener filter* $K(t)$ it that filter with the property to give the highest possible SNR (Michelson and Taber 1984; Sathyaprakash and Schutz 2009).

This method of finding the highest SNR can be used only if the waveform $h(t)$ is known, i.e. if some previous knowledge of the GW signal is inserted in the search algorithm. Searches are more efficient if the parameters of a filter and its shape are precisely matched with that of a signal, as opposed to the case when no knowledge of the signal is available. If the signal shape is completely unknown we can only Fourier transform the detector output and compare it in a frequency bin to noise in that bin. For quasiperiodic signal (i.e. those coming from compact binary inspirals), matched filtering can increase the SNR in proportion to the square root of the number of signal cycles in the detector band. In typical interferometers, matched filtering increases the detection rates by a factor $30 - 100$ for compact binary inspiral signals. A quick look at the expected rates in Table 5.2 (where the use of matched filtering is considered) shows that the matched filtering technique is required to perform efficient GW searches.

Detailed predictions of the incoming waveforms are needed to use the matched filtering technique. It is therefore extremely important to model astrophysical GW sources and predict their configurations by the time they enter the sensitivity band of the detectors (Sec. 5.1.2).

[4]We define the Fourier transform of a quantity $g(t)$ to be

$$\tilde{g}(f) = \int_{-\infty}^{+\infty} g(t)e^{i2\pi tf}\,.$$

Part I

Spin-disc alignment in supermassive black-hole binaries

In my entire scientific life, extending over forty-five years, the most shattering experience has been the realization that an exact solution of Einstein's equations of general relativity, discovered by the New Zealand mathematician, Roy Kerr, provides the absolutely exact representation of untold numbers of massive black holes that populate the universe. This shuddering before the beautiful, this incredible fact that a discovery motivated by a search after the beautiful in mathematics should find its exact replica in Nature, persuades me to say that beauty is that to which the human mind responds at its deepest and most profound.

S. Chandrasekhar, Truth and Beauty:
Aesthetics and Motivations in Science (1987)

Chapter 2

Recoiling black holes

Numerical simulations in GR have found that spinning SMBHs could be ejected from their host galaxies as a consequence of a merger. We firstly describe the different stages of BH mergers and we later detail the *superkick* fitting formula to understand which BH spin configurations are required to avoid BH ejections.

2.1 From galaxy to black-hole merger

The existence of scale laws suggests that a galaxy and the SMBH at its center should share a common evolution. SMBH mergers are introduced and described as a direct consequence of larger-scale galactic mergers.

2.1.1 Supermassive black-hole formation and scale laws

Observations show that most galaxies with bulges, if not all of them, host a central SMBH (Kormendy and Richstone 1995; Magorrian et al. 1998; Ferrarese and Ford 2005). This observational discovery prompts questions about the formation processes of such massive objects in the Universe. Current modeling involves the growth of large-scale structures from cosmological primordial perturbations. Simulations have been carried out using Press-Schechter theory (Press and Schechter 1974; Lacey and Cole 1993), Monte-Carlo realizations of merger trees (Kauffmann and Haehnelt 2000; Volonteri et al. 2003; Bromley et al. 2004) and cosmological N-body simulations (Di Matteo et al. 2003, 2005).

SMBH seeds are often assumed to be remnants of the first stars formed in the Universe at redshift $z \sim 20$ (Haiman and Loeb 1998; Wyithe and Loeb 2005). Numerical simulations suggests that stars at very early times are expected to be relatively massive, and thus produce BH seeds with a mass of $\sim 100 M_{\odot}$ (Abel et al. 2000; Bromm et al. 2002). Optically bright quasars have been detected up to $z \sim 6$ (Fan et al. 2001, 2003, 2004, 2006) or even $z \sim 7$ (Mortlock et al. 2011) in the Sloan Digital Sky Survey. As we will see in Sec. 3.2.3, spinning BH requires far more than 1 Gyr to reach typical SMBH masses ($\sim 10^8 M_{\odot}$) from stellar-mass BH seed ($\sim 100 M_{\odot}$). These observations have prompted work on alternate channels to explain SMBH mass build-up. Observations can be matched only if SMBHs from stellar-mass seeds undergo brief but extremely strong growth episodes during which the accretion rate onto them is well in excess of the Eddington rate (Sec. 3.2.2) (Volonteri et al. 2003; Volonteri and Rees 2005; Begelman et al. 2006).

There are two possible ways to circumvent this issue: SMBH seeds are far more massive than $100 M_{\odot}$ or in some way SMBHs grow quicker. The first possibility has been addressed by Lodato and Natarajan (2006, 2007); Volonteri et al. (2008) and more recently by Johnson et al. (2012). They propose a model in which SMBH seeds result from the central mass concentrated via disc accretion in collapsed haloes at extremely high redshift ($z \sim 10 - 15$).

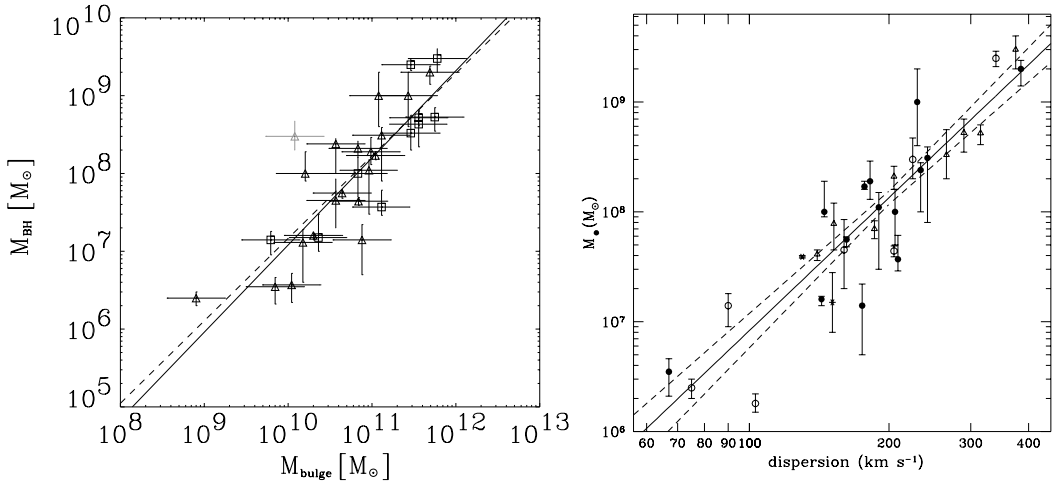

Figure 2.1: SMBH masses are correlated with the properties of their galactic bulge. Heavier BHs tend to be hosted by more massive galactic bulges (left panel, Häring and Rix 2004) with larger dispersion velocity (right panel, Tremaine et al. 2002).

They found that the evolution of these discs is driven by angular momentum redistribution induced by the development of gravitational instabilities. They predict $\sim 10^5 M_\odot$ initial seeds, from which SMBHs with masses $\sim 10^9 M_\odot$ can be easily built up by $z = 6$ to power the bright quasars observed. Alternatively, the only way to easily obtain fast-growing BHs is to provide a mechanism according to which they can maintain low spins (see further discussion in Sec. 3.2.3). Volonteri et al. (2005) found that SMBH mass growth is mainly due to gas accretion rather than mergers (see below), and BH spin-up is a natural consequence of prolonged accretion from gas-disc structures (Bardeen 1970; Thorne 1974). King and Pringle (2006, 2007) argued that SMBHs could accrete through a sequence of randomly oriented accretion events, rather than from a single prograde disc. If the angular momentum of the accretion disc is misaligned with respect to the direction of the BH spin, accretion of counter-rotating material can cause a spin-down of the hole and consequently a faster growth.

Moreover, SMBHs and their host galaxies evolve together. Coupled evolution is suggested by the presence of scale laws: the properties of SMBHs in galactic bulges are correlated with the properties of the central region of their galaxies (Fig. 2.1). The mass of the BH $M_{\rm BH}$ is correlated both with the stellar dispersion velocity σ_* within the galactic bulge (Ferrarese and Merritt 2000; Gebhardt et al. 2000; Ferrarese et al. 2001; Tremaine et al. 2002; Gültekin et al. 2009)

$$\log\left(\frac{M_{\rm BH}}{M_\odot}\right) = (8.13 \pm 0.06) + (4.02 \pm 0.32)\log\left(\frac{\sigma_*}{200{\rm km/s}}\right) ; \tag{2.1}$$

and with the mass of the bulge itself (Magorrian et al. 1998; Marconi and Hunt 2003; Häring and Rix 2004)

$$\log\left(\frac{M_{\rm BH}}{M_\odot}\right) = (8.20 \pm 0.10) + (1.12 \pm 0.06)\log\left(\frac{M_{\rm bulge}}{10^{11} M_\odot}\right) . \tag{2.2}$$

Whether they really form from stellar-mass seed or through a different mechanism, SMBHs are hosted into galactic bulges out to large redshifts, at least $z \sim 6$. In the early Universe, galaxies have been observed to merge with each other (e.g. Barnes and Hernquist 1992; Kennicutt et al. 1996; Conselice 2007). Moreover, galaxy mergers are predicted to be

frequent in the present models of large-scale structure formation. In the current ΛCDM cosmological scenario, the Universe evolution is described by the Einstein field equations with a non-vanishing cosmological constant Λ and a matter content mostly under the form of cold dark matter (CDM). The Nine-Year Wilkinson Microwave Anisotropy Probe (WMAP) observations (Bennett et al. 2012; Hinshaw et al. 2012) indicated that 71.4% of the energy-matter content of the Universe is contained the cosmological constant term, while 24% is under the form of cold (i.e. moving at non-relativistic speed) dark matter and only 4.6% is made of visible (baryonic) matter. Structures in the ΛCDM cosmological model form hierarchically: starting from primordial fluctuations, our Universe initially developed small structures that later combined with each other growing in mass and size. Visible mass follows the potential wells created by the evolving dark matter distribution. Only low-mass dark matter halos are present at early times, while higher mass dark matter structure are formed by repeated merger of the smaller ones. Galaxies associated with these merging structures should therefore merge too. Galaxies that we see today are the final outcome of this hierarchical growth.

After a galaxy merger, one would expect a single larger galaxy hosting two SMBHs, coming from the two progenitor spheroids. Observations are in clear contradiction with this picture: only ~ 20 SMBH binary candidates have been identified (Merritt and Milosavljević 2005; Colpi and Dotti 2009; Dotti et al. 2012). Objects have been discovered because of the presence of two resolved X- ray sources wandering in the merged galaxy (Komossa et al. 2003; Hudson et al. 2006; Barth et al. 2008; Bianchi et al. 2008; Comerford et al. 2009; Green et al. 2010a,b), or using radio interferometry measurements (Rodriguez et al. 2009; Maness et al. 2004). Current lack of dual-AGN observations (Van Wassenhove et al. 2012) suggests the SMBH may form from the merger of the lighter BHs in the progenitor galaxies. SMBH mergers could be a direct consequence of larger scale galactic mergers. We mention however, that sub-parsec binaries are not excluded by the present observations: if SMBH binaries stall at very low separations, they would be detected as a single AGN (Volonteri et al. 2009; Montuori et al. 2011, 2012).

2.1.2 Dynamical, gas-dominated and gravitational-wave inspiral

The merger of two SMBHs happens in three subsequent phases (Begelman et al. 1980; Yu 2002), as summarized in Fig. 2.2. After a galaxy merger, each BH sinks towards the center of the newly formed galaxy through interactions with the stellar environment. If a black hole of mass $M_{\rm BH}$ moves in a stellar environment where the average stellar mass is m_* and the velocity dispersion is σ_*, it will lose energy and sink towards the center on the dynamical friction timescale (Chandrasekhar 1943)

$$t_{\rm df} = \frac{\sigma_*^3}{8\pi n G^2 M_{\rm BH} m_* \log\Lambda}\,, \tag{2.3}$$

where n is the number of star per unit volume and $\log\Lambda$ is the Coulomb logarithm, which encodes all the uncertainties about the impact parameter (for derivation and discussion, see Bertin 2000).

The binary becomes "hard" when its binding energy is comparable with the kinetic energy of the surrounding stars. This typically happens at separations close to

$$a_H = \frac{GM}{\sigma_*^2} \simeq 10.8 \left(\frac{M}{10^8 M_\odot}\right)\left(\frac{\sigma_*}{200{\rm Km/s}}\right)^{-2} {\rm pc}\,. \tag{2.4}$$

where M is the total mass of the binary. Dynamical interactions between the stars and a single BH are negligible in this stage, but the binary can still get rid of energy and angular momentum through three-body interactions (Frank and Rees 1976). A single stars approaching the binaries is ejected with velocities comparable with the binary orbital speed $v \sim \sqrt{GM/a}$. Since for a hard binary the orbital velocity is larger than the average veloc-

ity of the surrounding stars, after the encounter the binary loses potential energy and the separation decreases. However, as stars are ejected the available region of the phase space (*loss-cone*) could be quickly depleted and the process may stall at separations close to 1 pc (Milosavljević and Merritt 2001, 2003). SMBHs will actually merge only if some astrophysical mechanism can further shrink the binary orbit. Interactions with a gaseous environment such as an accretions disc could in principle provide the necessary mechanism (Armitage and Natarajan 2002; Cuadra et al. 2009). However, under more reasonable assumption, Lodato et al. (2009) find that if the disc is massive enough to contribute to the inspiral, it will also fragment, thus preventing further accretion. The issue is still open, and it is now known as *the final parsec problem*.

The chaotic accretion picture proposed by King and Pringle (2006, 2007) could provide a possible solution. Nixon et al. (2011a,b, 2012a,b) have shown that a sequence of accretion episodes where the disc can be either co- or counteraligned with the binary could be much more effective than a single disc to shrink the binary separation.

At smaller separations, GW emission becomes an efficient way to emit energy and angular momentum. The inspiral timescale in this regime is given by (Peters and Mathews 1963; Peters 1964; see Junker and Schaefer 1992 for higher order corrections)

$$t_{\rm GW} = 8.1 \times 10^{12} \left(\frac{M}{10^8 M_\odot}\right)^{-3} \left(\frac{a}{\rm pc}\right)^4 \frac{(1+q)^2}{q} f^{-1}(e)\,{\rm yr}\,, \tag{2.5}$$

where q is the binary mass ratio and $f(e)$ is a function of the eccentricity e which is equal to 1 for circular orbits (see Eqs. 5.8). The critical separation a_{GW} that binaries have to reach to coalescence in a Hubble time is given by

$$a_{GW} = 6.3 \times 10^{-2} \left(\frac{M}{10^8 M_\odot}\right)^{3/4} \frac{q^{1/4}}{(1+q)^{1/2}} f^{1/4}(e)\,{\rm pc}\,. \tag{2.6}$$

This estimate is obtained in the weak field limit and correctly gives the timescale of the process. The detailed evolution when the binary approach the merger must be followed using the full non-linear theory of GR.

2.2 Black hole recoils

The final stage of BH mergers involve highly curved, dynamical spacetime that can only be simulated with fully numerical relativity. Simulating a curved spacetime is extremely difficult and became possible only recently (Pretorius 2005; Baker et al. 2005; Campanelli et al. 2006). Numerical relativists can now accurately determine the evolution of the spacetime, and the consequent emission of GWs, during the last orbits of black hole mergers. Whenever the binary is asymmetric for some reason (different masses, or spin vectors), GWs are preferentially emitted in one direction during a merger. Conservation of linear momentum requires that the final black hole produced in that merger recoils in the opposite direction. Recoil velocities, or *kicks*, were initially found to be of several hundreds of km/s using various approaches (Fitchett 1983; Favata et al. 2004). More accurate simulations of extremely asymmetric configurations recently found that the magnitude of the recoil velocity is critically different if spinning BHs are considered. While simulations of non-spinning BHs can only produce kicks of $\simeq 200$ km/s (González et al. 2007b), the merger of two maximally spinning BHs can result in recoil velocities as large as 4000 km/s, that have been called *superkicks* (González et al. 2007a; Campanelli et al. 2007a; Schnittman and Buonanno 2007; Herrmann et al. 2007). Kicks this large exceed the escape velocities of even the most massive galaxies (Fig. 2.3, Merritt et al. 2004), and would thus eject SMBHs from their hosts. SMBH ejections would have both cosmological and astrophysical consequences. Many galaxies could find themselves to be lacking a central SMBH, which is not considered likely by current observational evidences (see Sec.1.2.2). Predictions of BH merger rates will

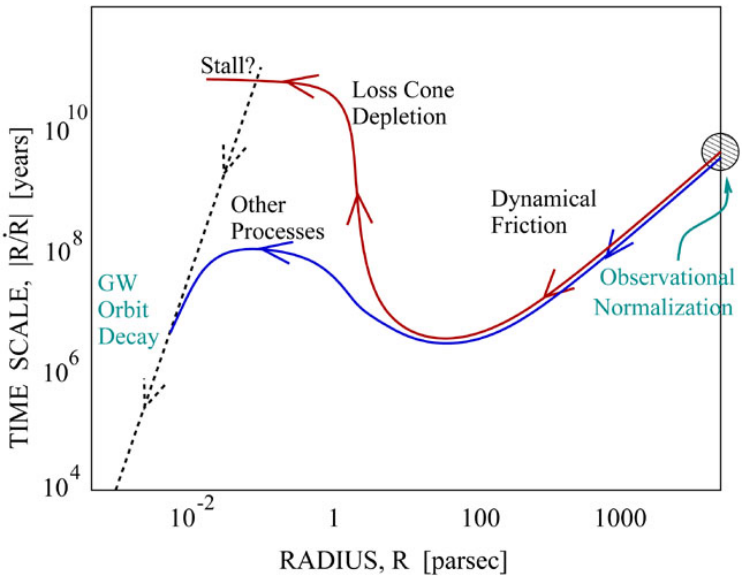

Figure 2.2: SMBH binary shrinking history (Backer et al. 2004). At large separation the two BHs sink toward the center of the merging galaxy via dynamical friction. As the binary become "hard", the process becomes inefficient (increasing timescale). If only star-binary collision are considered (red line), the process stalls at separation close to 1 pc. Other processes are needed (blue line) to solve the *final parsec problem* and bring the binary to separation where GW can finally drive the inspiral towards the merger.

also be affected (Madau and Quataert 2004; Volonteri 2007), with strong consequences on both future GW and electromagnetic observations (Schnittman 2011). If the final SMBH is not ejected, the recoil causes it to wander through the galaxy and the dark matter halo for $\sim 10^6 - 10^9$yr, before settling back to the galactic centre (Blecha and Loeb 2008; Gualandris and Merritt 2008; Guedes et al. 2011; Sijacki et al. 2011).

Strongly recoiling BHs present electromagnetic signatures, such as (i) broad emission-line shifts, (ii) flaring accretion discs and (iii) hypercompact stellar systems (for a review see Komossa 2012).

i) After the kick, the accretion disc and the surrounding matter typically remain bound to the SMBH while the bulk of the host galaxy remains behind. The accreting recoiling SMBH will therefore appear as an off-nuclear quasar as long as its accretion supply lasts. Precise observational signatures include the presence of blue-shifted broad lines over a set of narrow lines from the galaxy (Bonning et al. 2007). The source J092712.65+294344.0 has been discovered with this method within the Sloan Digital Sky Survey data by Komossa et al. (2008), and it is probably the best recoiling SMBH observational candidate known at time of writing. The case is still debated: the same data have been interpreted as a superposition of two AGNs in the same galaxy cluster (Heckman et al. 2009; Shields et al. 2009a) or as a close pre-merger SMBH binary (Bogdanović et al. 2009; Dotti et al. 2009a). Less clean candidates have been reported also by Shields et al. (2009b) and Robinson et al. (2010)

ii) In gas-rich mergers, an accretion disc is likely present. A prompt afterglow should come from shocks induced in the circumbinary disc by the recoil, just after the merger (Milosavljević and Phinney 2005). Lippai et al. (2008) developed a simple model by simply adding a recoil velocity to the newly formed SMBH at the center of the disc and found that the orbits of the fluid elements of the disc are thus perturbed and they intersect with each other. The intersection of supersonic orbits induces shocks in the disc that causes luminous flares. Further studies along this line have been performed

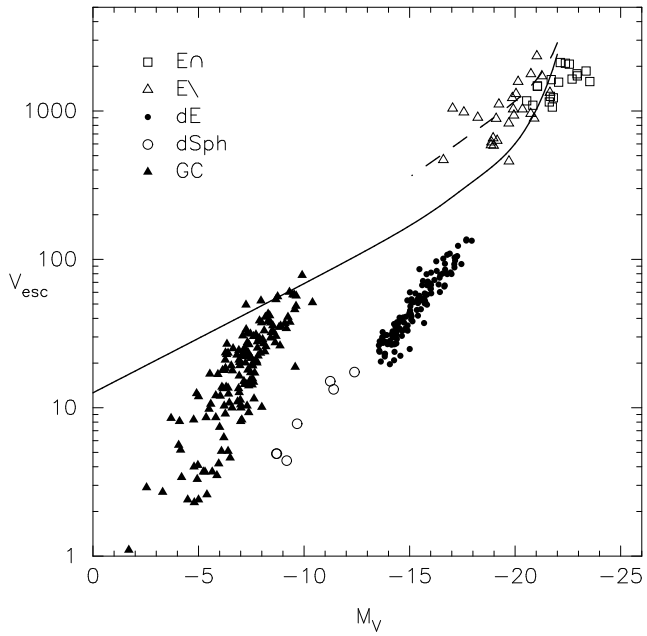

Figure 2.3: Escape velocity (in unit of km/s) from stellar systems that could host BH mergers as function of their absolute magnitude (Merritt et al. 2004). Escape velocities $v_{\rm esc} = (2\phi_0)^{1/2}$ are derived from estimation of the central gravitational potential of the system ϕ_0 estimated using stellar dynamics measurements. Observational data are taken from: Faber et al. (1997) [E], Binggeli and Jerjen (1998) and Mateo (1998) [dE], Webbink (1996) [GC,dSph]. The solid line show the prediction computed by Merritt et al. (2004) modeling dark matter halos associated with the luminous stellar systems with the typical profile predicted by Navarro et al. (1996).

by Shields and Bonning (2008); Schnittman and Krolik (2008); Rossi et al. (2010) and Corrales et al. (2010). A late afterglow instead may result from the viscous refilling of the inner disc (Loeb 2007). The role of the angle between the kick direction and to the orbital angular momentum vector of the pre-kicked disc has been specifically addressed by Ponce et al. (2012). Other signatures could be due to the reaction of the disc to the mass reduction of the holes, because the merged BH will generally be lighter than the total mass of the binary before the merger (Megevand et al. 2009; Rosotti et al. 2012).

iii) Even in the absence of an accretion disc, ejected SMBHs will always carry out bound stars. Merritt et al. (2009) related the properties of these *hyper-compact stellar systems* to the structure of their host galaxies and to the amplitude of the kick. At least in principle, future detections of these clusters could allow us to determine empirically the kick velocity distribution. Moreover, luminous events may come from tidal disruptions under recoil conditions (Komossa and Merritt 2008).

Particularly interesting is the recent case of the galaxy CID-42, which present an unusual morphology with two apparent optical nuclei (Comerford et al. 2009). Civano et al. (2010, 2012) interpreted the source as a recoiling SMBH, or alternatively, an SMBH ejection following 3-body interaction in a triple SMBH system. However, the hypothesis that the system could be a binary BH cannot be ruled out with the present data (Blecha et al. 2013).

SMBH ejections are in clear contradiction with observations that all galaxies with bulges appear to host a central SMBH (Ferrarese and Ford 2005), but whether strong BH recoils really happen in our Universe is currently an open issue both theoretically and observationally.

2.3 Superkick configurations

The goal of the first part of the present work is precisely to investigate theoretically the likelihood of large SMBH recoils. To this purpose, it can be useful to adopt the opposite point of view: how can SMBH ejection be avoided?

As discussed above, BH recoils have been predicted using fully non-linear numerical relativity. Numerical simulations in GR are computationally very expensive, making it impossible to explore the whole parameter space (Blanchet 2002; Buonanno et al. 2009). Semi-analytic approaches have been developed to reproduce the numerical results using fitting formulae (see Rezzolla 2009 for more details). To understand how galaxies can retain their BHs, we present a closer look to the *superkick* fitting formula. We indicate with $\parallel$ and $\perp$ the vector components parallel and perpendicular to the orbital angular momentum of the binary just before the merger. Given an orthonomal basis $(\mathbf{e}_{\perp 1}, \mathbf{e}_{\perp 2}, \mathbf{e}_{\parallel})$ the kick velocity $\mathbf{v}$ is typically fitted with (Lousto et al. 2010a)

$$\mathbf{v} = v_m \mathbf{e}_{\perp 1} + v_\perp (\cos\xi\, \mathbf{e}_{\perp 1} + \sin\xi\, \mathbf{e}_{\perp 2}) + v_\parallel \mathbf{e}_\parallel \,, \tag{2.7}$$

$$v_m = A\eta^2 \frac{1-q}{1+q}(1 + B\eta) \,, \tag{2.8}$$

$$v_\perp = H\eta^2 \frac{q}{1+q} (\boldsymbol{\chi_2} - \boldsymbol{\chi_1}) \cdot \mathbf{e}_\parallel \,, \tag{2.9}$$

$$v_\parallel = K\eta^2 \frac{q}{1+q} \cos(\Theta - \Theta_0) \, |\boldsymbol{\chi_2} - \boldsymbol{\chi_1}|_\perp \;; \tag{2.10}$$

where $\eta = q/(1+q)^2$ is the symmetric mass ratio; the vector $\boldsymbol{\chi_i}$ $(i = 1, 2)$ are defined having magnitude χ_i and the same direction of the BH spins; and Θ is the angle between the vector $|\boldsymbol{\chi_2} - \boldsymbol{\chi_1}|_\perp$ and the vector joining the two BHs. The remaining parameters are estimated using best-fitted values from numerical simulations, in particular

- $A = 1.2 \times 10^4$ km/s (González et al. 2007b);
- $B = -0.93$ km/s (González et al. 2007b);
- $H = (6.9 \pm 0.5) \times 10^3$ km/s (Lousto and Zlochower 2008);
- $K = (6.0 \pm 0.1) \times 10^4$ km/s (Campanelli et al. 2007b);
- $\xi = 135°$ (Lousto and Zlochower 2008);
- Θ_0 depends only on the mass ratio q (Lousto and Zlochower 2009).

A slightly different parametrization has been adopted by Baker et al. (2008) and van Meter et al. (2010). These studies have been addressed to bound encounters, likely to occur in astrophysical environments. In unbound BH collisions, the kick velocity can exceed 15000 km/s (Sperhake et al. 2008b, 2011b, 2012; Healy et al. 2009).

The maximum kick velocity is obtained when $|\boldsymbol{\chi_2} - \boldsymbol{\chi_1}|_\perp$ is maximum, i.e. when maximally spinning BHs approach the merger with both the spins lying in the orbital plane and counter-aligned with each other. From the fitting formula above, only two conditions can be found to avoid kick velocity larger than ~ 3000 km/s:

- BH are slowly spinning (both $v_\parallel$ and $v_\perp$ vanish if $\chi_1 = \chi_2 = 0$);
- both spins are aligned with the orbital angular momentum of the binary (only $v_\perp$ vanishes if $|\chi_1|_\perp = |\chi_2|_\perp = 0$, but note that the coefficient H is almost an order of magnitude smaller than K).

BH ejections have not to be considered likely if astrophysical SMBHs are found in one of these two categories.

Recent numerical simulations reported in Lousto and Zlochower (2011, 2012) and Lousto et al. (2012) claimed that slightly different configurations could produce kicks as large as 5000 km/s (*hang-up kicks*). These recent findings do not change the main conclusions of this Chapter: numerical relativity indicates that galaxies can retain their SMBHs either if they are slowly spinning or if they are aligned with the orbital angular momentum of the binary. In this work we investigate the likelihood for SMBH of being aligned with the the orbital angular momentum of the binary, as a consequence of the interaction with the surrounding accretion discs.

Chapter 3

Dynamics of accretion discs

In this Chapter we introduce accretion discs as a typical astrophysical environment for SMBH interactions. We firstly introduce the dynamics of Keplerian flat accretion discs following Pringle (1981) and Frank et al. (2002), as reported by Lodato (2008). We introduce two generalizations to describe discs around binary systems and in warped configuration. Detailed expressions to compute the accretion efficiency around a Kerr BH are also derived.

3.1 Keplerian disc physics

Accretion discs are the astrophysical mechanism for interstellar medium to accrete onto a central object, in our case a SMBH. We consider in this Section only Keplerian accretion discs, i.e. discs in which the gravitational field felt by each particle is due only to the central object gravity, neglecting the disc self-gravity, i.e. mutual gravitational interactions between different gas particles.

If a central object of mass M is surrounded by a gaseous cloud with a net orbital angular momentum, gas particles tend to reach equilibrium orbits on a plane perpendicular to the angular momentum itself, where they are kept in balance by the centrifugal force. On this plane, that would be the plane of the disc, particles are in general on elliptical Keplerian orbits. Each particle has specific energy and angular momentum given by

$$E = -\frac{GM}{2a}\,, \qquad \mathbf{L}^2 = GMa(1-e^2)\,, \tag{3.1}$$

where a and e are respectively the semimajor axis and the orbital eccentricity. If the gaseous medium is dissipative, particles can lose energy but angular momentum is conserved in the absence of tangential forces. Particles settle down in the minimum energy orbits for a given specific angular momentum $\mathbf{L}$, i.e. circular orbits ($e = 0$).

After the formation of a disc structure, accretion onto the central object is possible only if angular momentum can be removed. Angular momentum removal can be provided by fluid viscosity within the interstellar medium. The laws to describe the evolution of an accretion disc follow from the classical fluid equation of motion, when applied to the disc geometry. We use cylindrical coordinated with the z axis oriented along the orbital angular momentum of the disc, while R and ϕ vary on the disc plane. We call r the spherical radius, centered on the central object. The medium is described by fluid elements with velocity $\mathbf{v} = (v_R, v_\phi, v_z)$ and mass density ρ; its the evolution obeys to mass (continuity equation) and angular momentum (Navier-Stokes equations) conservation. The following derivation is carried out assuming that the timescale over which particles change their radial position (which correspond to the viscous timescale, see below), is much longer than every other timescale involved: both the sound propagation timescale and the orbital timescale. This

corresponds to the following ordering of the velocities

$$v_R \ll c_s \ll v_\phi \,, \tag{3.2}$$

where we indicated the sound speed with c_s: the first inequality states the approximation just mentioned and the second one will be demonstrated below.

The thin-disc approximation. Accretion discs are typically assumed to be thin. We introduce the aspect ratio of the disc H/R, where H the height of the disc. The thin-disc approximation consists into assuming that $H/R \ll 1$ along the whole disc profile. This condition is verified in astrophysical systems, from protostellar disc ($H/R \sim 0.1$) to SMBH accretion discs ($H/R \simeq 10^{-2}$). Since the disc is assumed to be thin in the z directions, it is more reasonable to use surface quantities. Given the volume mass density ρ, the surface density is defined integrating along the z axis

$$\Sigma = \int_{-\infty}^{+\infty} \rho \, dz \,. \tag{3.3}$$

The continuity equation integrated in the z direction reads

$$\frac{\partial \Sigma}{\partial t} + \frac{1}{R}\frac{\partial}{\partial R}(R\Sigma v_R) = 0 \,. \tag{3.4}$$

Newton's second law corresponds to the Navier-Stokes equations (still using volume quantities)

$$\frac{\partial \mathbf{v}}{\partial t} + (\mathbf{v}\cdot\boldsymbol{\nabla})\mathbf{v} = -\frac{1}{\rho}(\boldsymbol{\nabla} P - \boldsymbol{\nabla}\sigma) - \boldsymbol{\nabla}\phi \,. \tag{3.5}$$

The first term at the right-hand side encodes pressure forces. The second term contains the stress tensor σ and describes the effect of viscous forces. The stress tensor σ in cartesian coordinates is given by

$$\sigma_{ij} = \nu\rho\left[\frac{\partial v_i}{\partial x_j} + \frac{\partial v_i}{\partial x_j} - \frac{2}{3}(\boldsymbol{\nabla}\mathbf{v})\delta_{ij}\right] \,, \tag{3.6}$$

where ν is called *kinematic viscosity coefficient*. Viscous forces act only in the tangential direction in bulk viscosity is neglected and axisymmetry is imposed. The only non-vanishing components of the stress tensor σ is

$$\sigma_{R\phi} = \rho\nu R\frac{\partial \Omega}{\partial R} \,, \tag{3.7}$$

where $\Omega = v_\phi/R$ is the angular velocity. Viscous interactions are due to the differential rotation that causes different annuli to shear with each other. In particular it vanishes for a rigidly rotation flow ($\partial\Omega/\partial R = 0$). Finally, the third term in the right-hand side of (3.5) describes the gravitational interaction. Since we are neglecting the disc self-gravity, the gravitational potential ϕ is only given by the central object. Considering only gas particles sufficiently far from the object where GR effect can be neglected, we have

$$\phi = -\frac{GM}{r} \,. \tag{3.8}$$

Disc structure and dynamics are obtained by projecting the Navier-Stokes equations (3.5) on the three different directions of the cylindrical reference frame.

Vertical structure. The projection of Navier-Stokes equations (3.5) on the z axis is a restatement of the hydrostatic equilibrium, because the left-hand side can be neglected within the thin-disc approximation. This can be easily solved under the assumption that the gas is barotropic and that the sound speed does not depend on z. The vertical density results

$$\rho(z) = \rho_0 \exp\left(-\frac{z^2}{2H^2}\right), \tag{3.9}$$

where ρ_0 is the midplane mass density. The parameter H is the typical vertical size of the disc, and it is defined as

$$H = R\frac{c_s}{v_k}, \tag{3.10}$$

using the sound speed

$$c_s^2 = \frac{\partial P}{\partial \rho}, \tag{3.11}$$

and the Keplerian velocity

$$v_k^2 = \frac{GM}{R}. \tag{3.12}$$

The thin-disc approximation $H/R \ll 1$ consists in requiring $c_s \ll v_k$. This is clearly a condition on the temperature of the disc annuli. Due to thermal motion, the disc would expand in the vertical direction counteracting the gravitational force.

Radial equilibrium. Let us now project the Navier-Stokes equations on the R direction. The time variation of the radial velocity can be neglected, because of the ordering (3.2). The radial component of (3.5) gives rise to a condition on the tangential fluid velocity

$$v_\phi = v_k\sqrt{1 + \left(\frac{c_s}{v_k}\right)^2 \frac{d\log\rho}{d\log R}}. \tag{3.13}$$

Since ρ is typically a decreasing function of R, the tangential velocity v_ϕ is smaller than the Keplerian velocity v_k: gravitational energy is converted both into orbital motion and into thermal motion of the gas particles. Thermal contributions are neglegted in the thin-disc approximation, which leads to (cf. Eq. 3.2)

$$c_s \ll v_k \simeq v_\phi. \tag{3.14}$$

Angular momentum conservation. The ϕ component of (3.5), together with the continuity equation (3.4), states the angular momentum conservation though the disc

$$\frac{\partial}{\partial t}\left(\Sigma R v_\phi\right) + \frac{1}{R}\frac{\partial}{\partial R}\left(R^2 v_R \Sigma v_\phi\right) = \frac{1}{R}\frac{\partial}{\partial R}\left(\nu\Sigma R^3\frac{\partial\Omega}{\partial R}\right). \tag{3.15}$$

The above expression has the typical structure of a continuity equation: the left-hand side is the Lagrangian derivative of the angular momentum per unit mass $\Sigma R v_\phi$, while the source term at the right-hand side is the torque exerted by viscous forces.

The evolutionary law for the surface density is obtained combining angular momentum conservation (3.15) and continuity equation (3.4). The following expression is obtained

assuming Keplerian rotation (Eqs. 3.12 and 3.14)

$$\frac{\partial \Sigma}{\partial t} = \frac{3}{R}\frac{\partial}{\partial R}\left[R^{1/2}\frac{\partial}{\partial R}(\nu \Sigma R^{1/2})\right] . \tag{3.16}$$

It is a diffusion equation, where the diffusion coefficient is the kinematic viscosity ν.

Viscous timescale. The typical timescale over which the disc changes its properties can be inferred from the diffusion equation (3.16)

$$t_\nu \sim \frac{R^2}{\nu} , \tag{3.17}$$

and it is called *viscous timescale*. Being the timescale over which mass flows in the radial direction ($v_R \simeq R/t_\nu$), t_ν is also called *accretion timescale*. At the beginning of the Chapter, we assumed that the accretion timescale is much larger than the dynamical timescale ($t_{\rm dyn} = \Omega^{-1} = R/v_\phi$), which is equivalent to require $v_R \ll v_\phi$ as stated in (3.2).

Accretion rate. The mass that flows through a ring at a distance R from the central object is given by

$$\dot{M}(t, R) = -2\pi R v_R \Sigma , \tag{3.18}$$

which is called *accretion rate*. Given the viscosity coefficient ν, the diffusion equation (3.16) and the angular momentum conservation equation (3.15) can in principle be solved to find Σ and v_R, thus determining the accretion rate $\dot{M}$. In a stationary state, i.e. when the left-hand term of (3.15) can be neglected, the accretion rate is constant and it is given by (for Keplerian discs)

$$\dot{M} = 3\pi \nu \Sigma . \tag{3.19}$$

The above expression is strictly valid only in the outer disc, i.e. far from the central object.

The α prescription. The disc dynamics is ultimately ruled by the viscosity coefficient ν. The microscopic viscosity due to molecular collision is not sufficient to transport angular momentum on the observed timescales: accretion disc viscosity is thought to be due to turbulent motions triggered by magneto-rotational instabilities (Balbus and Hawley 1991) or gravitational instabilities (Lodato and Rice 2004; Lodato 2007). A critical discussion about various viscosity sources can be found in Lodato 2008. Our ignorance on the physical nature of disc viscosity is usually bypassed introduced the dimensionless parameter α (Shakura and Sunyaev 1973)

$$\nu = \alpha c_s H . \tag{3.20}$$

A precise measurement of α is the most important observational challenge in disc physics. The best constraint are obtained from observations of dwarf novae outbursts (Lasota 2001; Kotko and Lasota 2012) which seem to indicate a value $\alpha \simeq 0.1$. Oservational and computational attempts in determining the actual viscosity have been reviewed by King et al. (2007), who present a typical range $0.1 \lesssim \alpha \lesssim 0.4$ according to the best observational evidences.

3.2 Accretion onto spinning black holes

We present formulae to compute the radius of the last stable orbit and the accretion efficiency of a Kerr BH. The accretion efficiency enters in the definition of the Eddington accretion rate and sets the e-folding time at which spinning BHs grow. Since the accretion efficiency depends only on the spin magnitude χ, observations of the total luminosity emitted by accreting SMBH in AGNs can give constraints on the average SMBH spin magnitude.

3.2.1 Accretion efficiency

Accretion is a powerful source of energy. When a particle falls into a BH, all the available gravitational potential energy can be released outside. Consider a test particle of mass m falling into a Kerr BH of mass M and dimensionless spin χ. We restrict our studies to circular orbit on the equatorial plane, i.e. the plane orthogonal to the spin direction. This is not a critical assumption: particles accreting from an accretion disc are typically on circular orbits (Sec. 3.1) and the inner disc plane is orthogonal to the spin vector (Sec. 4.1).

Given a set of coordinates x^α ($\alpha = 1, 2, 3, 4$) and an affine parameter τ, we define the four-momentum of the test particle $p^\alpha = m dx^\alpha/d\tau$. The geodetic motion (i.e. when no other forces but gravity are present) of a test particle in GR follows from the conservation of p^α

$$g^{\mu\nu} p_\mu p_\nu = -m^2 \,. \tag{3.21}$$

In this case $\mu, \nu = t, r, \theta, \phi$ and $g^{\mu\nu}$ are the elements of the Kerr metric (1.4). The symmetries of the Kerr metric give immediately two constant of motion: the energy and the angular momentum

$$E = -p_t \,, \tag{3.22}$$

$$L = p_\phi \,. \tag{3.23}$$

The explicit form of (3.21) for the Kerr metric, when restricted to the equatorial plane ($\theta = \pi/2$), is

$$\begin{aligned} \frac{E^2 - m^2}{2m} = \frac{1}{2} m \left(\frac{dr}{d\tau}\right)^2 - \frac{Mm}{r} + \frac{L^2}{2mr^2} - \frac{ML^2}{mr^3} \\ + \chi \left(\frac{m^2 - E^2}{2m}\right) \frac{M^2}{r^2} + \chi \left(\frac{2EL - E^2}{m}\right) \frac{M^3}{r^3} \,. \end{aligned} \tag{3.24}$$

This correspond to the motion of a classic particle of constant total energy $(E^2 - m^2)/2m$ moving on the radial direction with kinetic energy $m\,(dr/d\tau)^2/2$. The effective potential is given by the classical Newtonian attraction Mm/r, the centrifugal term $L^2/2mr^2$, the GR correction in spherical symmetry ML^2/mr^3 (which is one PN order higher than the centrifugal potential), and two terms due to the spacetime rotation (at the M^2/r^2 and the M^3/r^3 PN level respectively). Circular orbit are obtained by (3.24) by solving

$$\left(\frac{dr}{d\tau}\right) = 0 \qquad \text{and} \qquad \frac{d}{dr}\left(\frac{dr}{d\tau}\right) = 0 \,, \tag{3.25}$$

for E and L as function of r. Considerable algebraic manipulation leads to the following

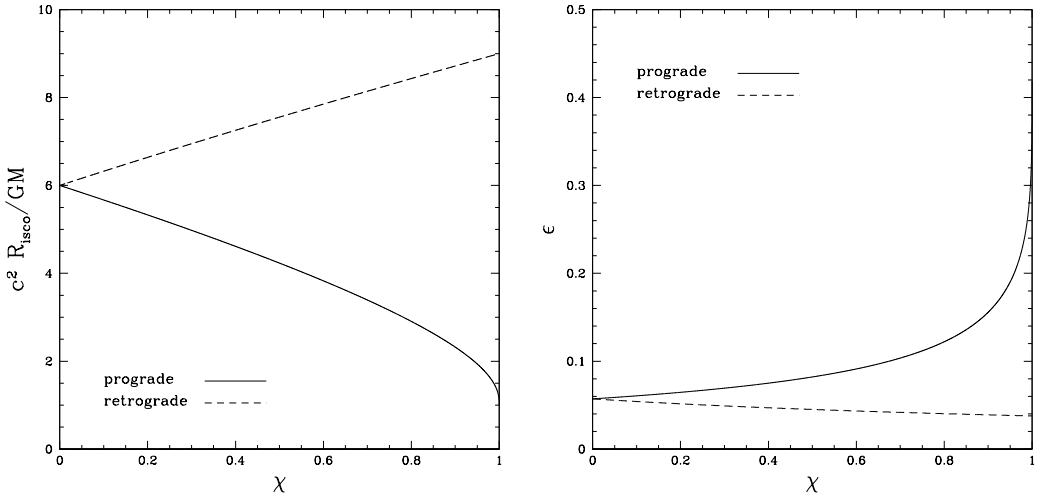

Figure 3.1: Accretion onto a spinning BH: radius of the innermost stable orbit (left panel) and accretion efficiency (right panel) as a function of the dimensionless spin χ. Particles can get much closer to the BH and extract more energy through accretion if their orbital angular momentum is directed along the spin axis (solid line, prograde), than in the counteraligned case (dashed line, retrograde).

expression for the particle energy (Bardeen 1970, 1973; Bardeen et al. 1972)

$$E(R) = mc^2 \frac{r_g^{3/2} - 2r_g^{1/2} \pm \chi}{r_g^{3/4}\left(r_g^{3/2} - 3r_g^{1/2} \pm 2\chi\right)^{1/2}}\,, \tag{3.26}$$

where we restored the fundamental constants and we defined $r_g = Rc^2/GM$ as the radial coordinate in unit of the gravitational radius. The two signs refer to infalling particles with angular momentum either aligned or counteraligned with the spin direction. An analogous expression can be obtained for L.

The effective potential in (3.24) presents a maximum, which corresponds to the radius of the innermost stable circular orbit

$$R_{\rm isco} = \frac{GM}{c^2}\left[3 + Z_2 \mp (3 - Z_1)^{1/2}(3 + Z_1 + 2Z_2)^{1/2}\right]\,, \tag{3.27}$$

$$Z_1 = 1 + (1-\chi^2)^{1/3}\left[(1+\chi)^{1/3} + (1-\chi)^{1/3}\right]\,, \tag{3.28}$$

$$Z_2 = (3\chi^2 + Z_1^2)^{1/2}\,. \tag{3.29}$$

The innermost stable orbit for a Schwarzshild BH ($\chi = 0$) is at $R_{\rm isco} = 6GM/c^2$ while for an extreme Kerr BH ($\chi = 1$) it is located at $R_{\rm isco} = GM/c^2$ for direct orbits and at $R_{\rm isco} = 9GM/c^2$ for retrograde orbits (see Fig. 3.1, left panel).

The maximum efficiency of energy extraction is defined as the fraction of the available energy at the last stable orbit and the rest mass energy of the infalling particle

$$\epsilon = 1 - \frac{E(R_{\rm isco})}{mc^2}\,, \tag{3.30}$$

and it depends only on the spin magnitude: $\epsilon = \epsilon(\chi)$. Accretion processes onto a BH can convert mass into energy with an efficiency in the range $5\% \lesssim \epsilon \lesssim 40\%$ (Fig. 3.1, right

panel). This makes accreting BHs among the most efficient energy sources in the Universe. For a comparison, the hydrogen burning reaction that powers main sequence stars has an efficiency of just 0.7%.

The difference between prograde and retrograde orbits becomes critical in the random accretion picture of King and Pringle (2006, 2007). In this scenario, prograde and retrograde accretion episodes are assumed to be equally probable: the effective efficiency can been computed using (King et al. 2008, see their Fig.5)

$$\epsilon_{\rm CA} = \frac{1}{2}\left(\epsilon_+ + \epsilon_-\right) , \tag{3.31}$$

where ϵ_+ and ϵ_- refer to the two sings in (3.26-3.29).

3.2.2 The Eddington limit

A spinning BH accreting with a rate $\dot{M}$ could be as luminous as

$$L = \epsilon(\chi)\,\dot{M}c^2 . \tag{3.32}$$

However, there is a theoretical limit on the total luminosity that can be reached by accretion (Eddington 1926). After an accretion event, the emitted radiation will act through radiation pressure on the infalling material counteracting gravity. If the luminosity increases, radiation pressure can overwhelm the gravitational force, preventing further accretion and consequently further radiation emission.

Let us consider a fluid element of a neural plasma placed at a distance R from a central object of mass M. Assuming that charges in the plasma cannot be separated, we can write the total force acting on an electron-proton couple. The gravitational force acting on it is only due to the proton mass m_p, because the electron mass is negligible. The main interaction between the outcoming radiation and the plasma is given by Thompson scattering with the electrons. To allow accretion, the gravitational force must be grater than the radiation pressure times the Thompson cross-section σ_T

$$\frac{GMm_p}{R^2} \geq \sigma_T \frac{L}{4\pi c R^2} , \tag{3.33}$$

which leads to

$$L \leq L_{\rm Edd} = \frac{4\pi c G m_p}{\sigma_T} M \simeq 1.3\times 10^{38}\left(\frac{M}{M_\odot}\right)\mathrm{erg} . \tag{3.34}$$

We call *Eddington limit* the situation in which gravity and radiation pressure are exactly balanced, i.e. when the equality in the above equation holds. Eq. (3.34) defines the maximum luminosity that can be reached accreting material onto a central object. In this derivation we neglected thermal pressure effects, which further decrease the maximum luminosity. The *Eddington luminosity* $L_{\rm Edd}$ is a very useful concept to compute the order of magnitude of typical accretion rates using only fundamental constants.

Three other related quantities can be defined. The *Eddington time* (or *Salpeter time*, see Sec. 3.2.3) is defined as the timescale over which the mass of the central object changes if it accretes continuosly at the Eddington limit

$$t_{\rm Edd} = \frac{Mc^2}{L_{\rm Edd}} = \frac{\sigma_T c}{4\pi G m_p} \simeq 4.5\times 10^8 \mathrm{yr} . \tag{3.35}$$

The *Eddington accretion rate* is the accretion rate of a BH of spin χ which is emitting at

the Eddington limit

$$\dot{M}_{\rm Edd} = \frac{L_{\rm Edd}}{\epsilon\, c^2}\,. \tag{3.36}$$

Finally, accretion rates are often expressed using the *Eddington fraction*

$$f_{\rm Edd} = \frac{\dot{M}}{\dot{M}_{\rm Edd}} = \frac{\dot{M}}{M}\,\epsilon\, t_{\rm Edd}\,, \tag{3.37}$$

with $0 \leq f_{\rm Edd} \leq 1$.

3.2.3 Black-hole mass growth

When particles accrete, the central object will consequently grow in mass. BH accretion is regulated by the efficiency ϵ which depends on the spin χ. We show here how the spin magnitude affects BH mass growth as firstly proposed by Salpeter (1964) and reported in King and Pringle (2006) and Volonteri et al. (2012).

If $\dot{M}$ is the actual accretion rate, only a fraction $\epsilon\dot{M}$ will be converted in emitted energy while a fraction $(1-\epsilon)\dot{M}$ will increase the BH mass. The variation rate of the BH mass is

$$\frac{dM}{dt} = (1-\epsilon)\dot{M} = \frac{1-\epsilon}{\epsilon}\frac{M f_{\rm Edd}}{t_{\rm Edd}}\,, \tag{3.38}$$

where Eqs. (3.35-3.37) have been used. If the BH spin χ and the Eddington fraction $f_{\rm Edd}$ can be assumed to be constant during the integration time, Eq. (3.38) easily leads to

$$M(t) = M_0 \exp\left(\frac{1-\epsilon}{\epsilon} f_{\rm Edd} \frac{t}{t_{\rm Edd}}\right)\,, \tag{3.39}$$

where M_0 is an integration constant. The Eddington timescale (3.35) is thus roughly the e-folding time of the BH mass growth. It is interesting to note its dependance on the BH spin χ, which enters in (3.39) through the accretion efficiency ϵ. Spinning BHs grow in mass faster than Schwarzshild BHs only if the angular momentum accreted is counteraligned with the BH spin, while for prograde orbits the growth is slower because mass is converted in outcoming radiation more efficiently. Some examples are shown in Fig. 3.2, where we chose values that belong to the same range of spin magnitude and accretion rates explored in the Monte Carlo simulations presented in this work (Sec. 4.4). Since the Salpeter timescale is a sizable fraction of the Hubble time, BH mass growth is a slow process: SMBH masses ($\sim 10^6 M_\odot$) can be reached within a few Gyrs only from massive seeds ($\sim 10^5 M_\odot$) or from stellar mass seed ($\sim 10^2 M_\odot$) if SMBHs are slowly spinning (see our discussion in Sec. 2.1.1).

If χ and $f_{\rm Edd}$ are not constant, Eq. (3.38) must be integrated in a self-consistent way with the evolutionary equations for $\epsilon(t)$ and $f_{\rm Edd}(t)$

$$\int_{M_0}^{M} \frac{dM}{M} = \int_0^t \frac{1-\epsilon(t')}{\epsilon(t')} f_{\rm Edd}(t') \frac{dt'}{t_{\rm Edd}}\,. \tag{3.40}$$

3.2.4 The Soltan argument

Accretion efficiency plays a key role in estimating the likelihood of SMBH in galaxies and their average spin magnitude. We present here the argument firstly suggested by Soltan (1982) as it is presented in the textbooks by Longair (2008, 2011).

Since accretion luminosity is linked to the properties of the accreting source ϵ and $\dot{M}$, the total luminosity emitted by all quasars in the Universe provides an estimate of the amount of mass which must have collapsed to form SMBH over the cosmic time. Let us suppose for

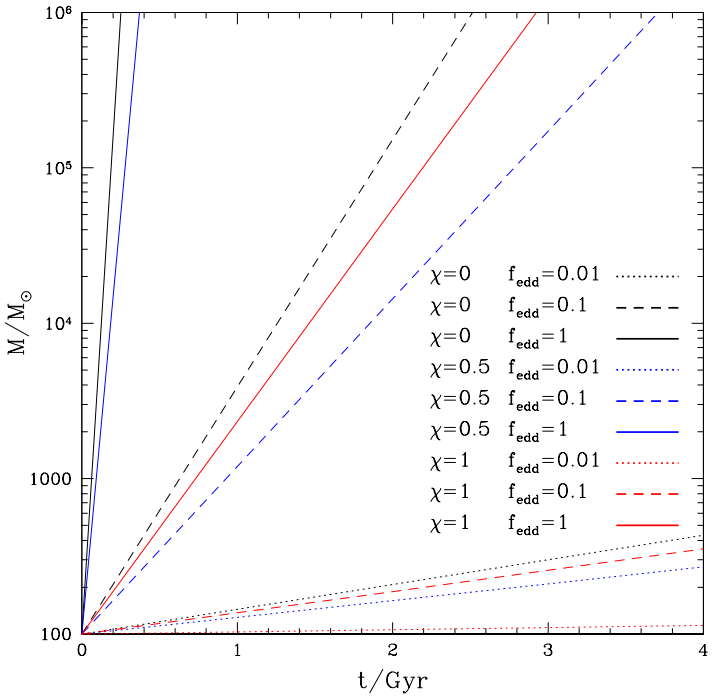

Figure 3.2: SMBH mass as function of time, varying over different spin magnitudes χ and Eddington fraction $f_{\rm Edd}$. The e-folding time is proportional to the Salpeter time $t_{\rm Edd}$ but it is regulated by the accretion rate and the accretion efficiency, see Eq (3.39). The initial mass M_0 has been set equal to $10^2 M_\odot$ and only prograde orbits have been considered.

simplicity that the (bolometric) luminosity L of quasars is only due to accretion of matter onto BHs. The mass of a single source can be estimated integrating the luminosity $L(t)$ over the quasar lifetime

$$M_{\rm BH} = \frac{1}{c^2} \int \frac{1-\epsilon}{\epsilon} L dt \,. \tag{3.41}$$

From this expression, the luminosity can now be integrated to consider all quasars at all epochs. The luminosity function can be expressed as $n(L,z)dL$, i.e. the number density of sources at a given redshift z. The total mass of SMBH per unit volume in quasars is thus expected to be (cf. Shen 2013)

$$\rho_{\rm BH} = \frac{1}{c^2} \int \int \frac{1-\epsilon}{\epsilon} \, L \, n(L, z(t)) \, dL \, dt \,, \tag{3.42}$$

where the relationship between t and z depends on the cosmological model. The number density $n(L,z)$ can now be related to the number counts of quasars. The number of quasars N, at a redshift z with a bolometric flux F is defined by

$$N(F,z) \, dF \, dz = n(L,z) \, dL \, D^2 \, dr \,, \tag{3.43}$$

where D is the distance to the sources and r is the comoving radius, i.e. a radial coordinate which follows the Hubble expansion: $dr = c\,(1+z)dt$. On cosmological scales, flux and

distance are related to the luminosity by

$$L = 4\pi D^2 (1+z)^2 F \,. \tag{3.44}$$

The mass density (3.42) thus results (Soltan 1982)

$$\rho_{\rm BH} = \frac{4\pi}{c^3} \int\int \frac{1-\epsilon}{\epsilon} (1+z)\, F\, N(F,z)\, dF\, dz \,. \tag{3.45}$$

The average density of mass in the Universe in the form of SMBHs is determined by integrals over the observed number–flux density relation for quasars and the observed redshift distribution in each flux density interval.

The latest expression must be related to observable quantities, such as the flux in a given waveband. Krolik (1999) provides a convenient relation which can be derived from Soltan's analysis. He normalised the mass density in black holes to the number density of galaxies $n_{\rm gal}$, thus obtaining an estimate of the typical BH mass in a galaxy

$$\langle M_{\rm BH} \rangle = 1.6 \times 10^7 \left(\frac{F}{10 F_B} \right) \left(\frac{\langle 1+z \rangle}{3} \right) \left(\frac{h}{0.75} \right)^{-3} \left(\frac{\epsilon}{0.1} \right)^{-1} M_\odot \ \text{ per galaxy}, \tag{3.46}$$

where brackets indicates averaged values over the counted sources, F_B is the flux in the B waveband and h is the Hubble parameter[1]. This analysis suggests that the typical galaxy should possess a BH remnant of mass about $10^7 M_\odot$, which is consistent with the observations.

Conversely, Yu and Tremaine (2002) developed the same argument using the observed BH mass distribution as input (see also Marconi et al. 2004; Shankar et al. 2004, 2013; Treister and Urry 2006; Wang et al. 2006b; Hopkins et al. 2007). They showed that the local BH mass density is consistent with the density accreted by quasars only if they have a mass-to-energy conversion efficiency $\epsilon \simeq 0.1$. Since the accretion efficiency is a function of the BH spin, this is also an argument on the average spin magnitude on SMBH in the Universe (see Sec. 4.6).

3.3 Warp propagation

Here we briefly introduce the physics of non-planar, or *warped*, accretion discs: such configurations are typically formed around spinning BHs through the Bardeen-Petterson effect (Sec. 4.1). This Section is largely based on Ogilvie (1999).

Let us consider a warped disc as composed of rings, each of them arbitrarily oriented in space at a distance R from the central object; in this context R should be interpreted as a spherical coordinate, rather than the cylindrical radius. We call β the tilt angle between the z axis and the plane of the each rings. In a warped disc, β can be an evolving function of the separation: $\beta = \beta(t, R)$; while the flat case is relized if β is constant. The orientation of the tilt on the xy plane is described by an azimuthal angle γ. The direction of the angular momentum of the ring is defined by a unit vector $\mathbf{l}(R,t)$, which is related to the angles β and γ by

$$\mathbf{l} = (\cos\gamma \sin\beta \,,\, \sin\gamma \sin\beta \,,\, \cos\beta) \ , \tag{3.47}$$

when projected onto an orthonormal basis. A useful dimensionless parameter to characterized the warp amplitude is

$$\psi = R \frac{\partial \beta}{\partial R} \,. \tag{3.48}$$

[1] The parameter h is related to the Hubble constant by $H_0 = 100\, h\, {\rm km\, s^{-1}\, Mpc^{-1}}$.

If the disc is warped, vertical shearing appears as a new angular momentum dissipation effect. Mathematically it corresponds to a non-vanishing Rz component in the stress tensor, besides the one reported in Eq. (3.7) (Papaloizou and Pringle 1983). This term causes warps to diffuse with a diffusive coefficient ν_2, that in general is different from the shearing viscosity ν. As in the α-prescription (3.20), it is useful to introduce a new dimensionless parameter α_2 defined by

$$\nu_2 = \alpha_2 c_s H \,. \tag{3.49}$$

Warp propagation theories have been carried out both in the small-amplitude ($\psi \ll H/R$) regime and in the general case. Attempts to built a complete theory were firstly carried on by Petterson (1977a,b, 1978), but their equations turned out to be wrong and they were corrected by Papaloizou and Pringle (1983). Their result basically generalizes what presented here in Sec. 3.1 and it is valid in the case of thin viscous discs: $H/R < \alpha$. Papaloizou and Pringle (1983) found that warps propagate trough the disc following a complex diffusion equation (see their Eq. 5.1). Their theory has been generalized to thick and inviscid discs by Papaloizou and Lin (1995), which discovered a new regime in which warps propagate via bending waves.

Pringle (1992) developed the first generalization to study also the large-amplitude regime. The equation derived for the angular momentum conservation in a disc with isotropic viscosity ν is

$$\frac{\partial}{\partial t}\left(\Sigma R^2 \Omega \mathbf{l}\right) + \frac{1}{R}\frac{\partial}{\partial R}\left(R^2 v_R \Sigma v_\phi \mathbf{l}\right) = \frac{1}{R}\frac{\partial}{\partial R}\left(\nu_1 \Sigma R^3 \frac{\partial \Omega}{\partial R}\mathbf{l}\right) + \frac{1}{R}\frac{\partial}{\partial R}\left(\frac{1}{2}\nu_2 \Sigma R^3 \Omega \frac{\partial \mathbf{l}}{\partial R}\right) . \tag{3.50}$$

If $\mathbf{l}$ is constant, then $\nu_1 \to \nu$ and $\nu_2 \to 0$ and this equation reduces to (3.15) which correspond to a planar configuration. A new term containing ν_2 appears at the right-had side, beside the usual term depending by ν_1. It corresponds to angular momentum which can propagate through the warps. This approach has been confirmed and extended by Ogilvie (1999) which developed a complete non-linear theory of warp propagation valid in the large-amplitude warp regime as well as in the small-amplitude one (see also Ogilvie 2000; Ogilvie and Dubus 2001; Ogilvie and Latter 2013a,b).

As the shear viscosity α controls the accretion onto the central object, the vertical viscosity α_2 controls the propagation of the warp through the disc. Different parts of the disc can communicate with each other through vertical shears on a timescale

$$t_{\nu 2} \sim \frac{R^2}{\nu_2} \,, \tag{3.51}$$

which is the analogous of the accretion timescale (3.17). The problem of the warp propagation could in general be very complicated, because the vertical viscosity depends not only on the α parameter, but also on the warp amplitude

$$\alpha_2 = \alpha_2 \left(\alpha, \psi\right) . \tag{3.52}$$

Even if α can be considered constant, $\psi = \psi(t, R)$ introduces new non-linear effects in the angular momentum conservation equation. This dependance disappears in the small-amplitude regime and the vertical viscosity is (Ogilvie 1999)

$$\alpha_2 = \frac{1}{2\alpha}\frac{4(1+7\alpha^2)}{4+\alpha^2} \qquad (\text{if } \psi \ll 1), \tag{3.53}$$

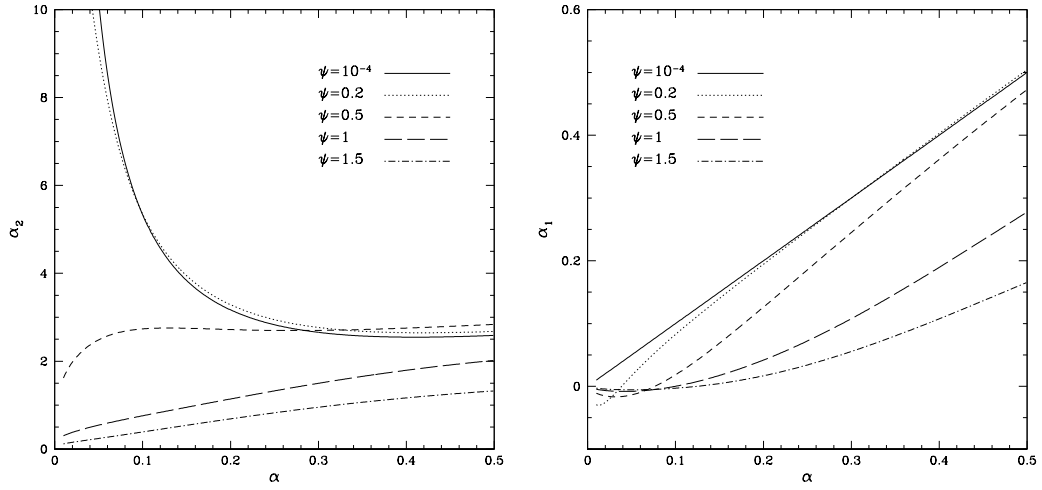

Figure 3.3: Vertical viscosity α_2 (left panel) and azimuthal viscosity α_1 (right panel) in the non-linear theory of warp propagation by Ogilvie (1999). As the warp amplitude ψ increases, the value of α_2 is completely determined by non-linear corrections, while α_1 shows larger deviations from α and could even formally be negative.

which can be approximated to

$$\alpha_2 = \frac{1}{2\alpha} \qquad (\text{if } \psi \ll 1 \text{ and } \alpha \ll 1), \tag{3.54}$$

when restricted to small value of α (Papaloizou and Pringle 1983). Bulk viscosity can in principle introduce further complications, but we assume its effect can always be neglected. Ogilvie (1999) evaluates the viscosity α_2 in the large-amplitude regime $\psi \sim 1$ by providing a slowly converging Taylor series to compute additional corrections[2]. However, the full non-linear result must be computed numerically. In the present work we compute the coefficient α_2 using a Fortran code kindly provided by G. Ogilvie. We show in Fig. 3.3 (left panel) the behavior of α_2 as a function of α varying over different warp amplitudes ψ.

For large ψ and small α, the theory of Ogilvie (1999) predicts that the azimuthal viscosity coefficient α_1 is different from α and in particular becomes negative (Fig. 3.3, right panel). The break point formally happens when

$$\alpha_1 = \alpha - \frac{1}{24}\frac{\psi}{\alpha} + O(\psi^4) < 0\,. \tag{3.55}$$

The behavior of the disc in such cases is unclear, and it could break up in two distinct planes at the radius where ψ becomes too large (Nixon and King 2012; Lodato and Price 2010). We address this issue in Sec. 4.3.3.

Warp propagation theories have been largely verified numerically. The bending waves regime has been tested by Nelson and Papaloizou (1999, 2000), while the thin-disc diffusive regime has been largely addressed by Lodato and Pringle (2006, 2007) and Lodato and Price (2010). While Lodato and Pringle (2007) find a disagreement comparing their simulations with the linear theory of Eq. (3.54), the new smoothed-particle hydrodynamics simulations reported in Lodato and Price (2010) are in spectacular agreement with the whole non-linear theory by Ogilvie (1999). We report their main result in Fig. 3.4.

[2]Note that Ogilvie (1999) defines the viscous coefficient using a different notation: $Q_1 = -3\alpha_1/2$ and $Q_2 = \alpha_2/2$.

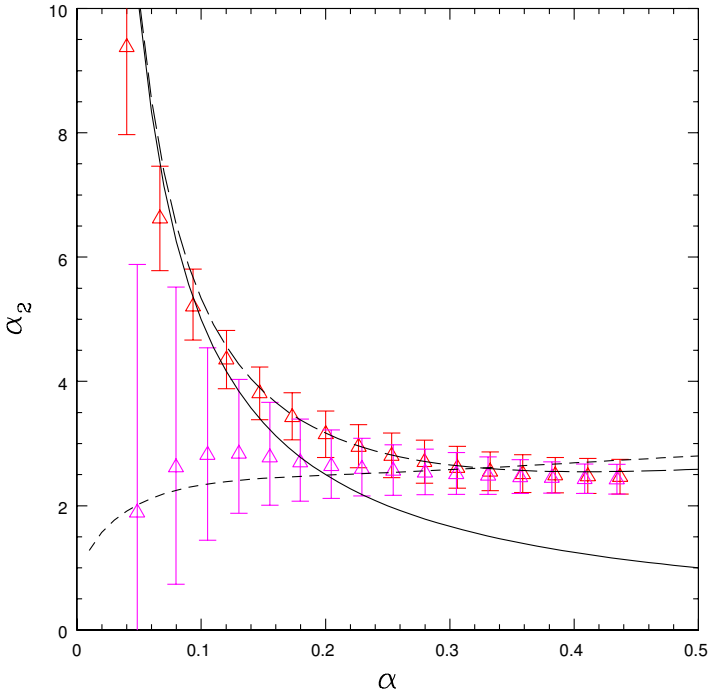

Figure 3.4: Warp diffusion coefficient as a function of the disc parameter α (Lodato and Price 2010). Solid line shows the analytical prediction (3.54), long-dashed line includes the correction (3.53) for large value of α, while short-dashed line is computed using the complete non-linear theory by Ogilvie (1999) with a fixed $\psi = 0.55$. Triangles show numerical results obtained by Lodato and Price (2010) in both the small-amplitude (red) and the large-amplitude (magenta) regime, which accurately confirm the non-linear theory.

3.4 Discs around binary systems

We describe here the main results on the dynamics of accretion discs around binary system and their effects on the binary evolution. Calculations and discussions about the inspiral timescale in different mass ratio regimes are postponed to Sec. 4.5.

Even if the disc and the binary orbit define in general two different planes, the analysis could be restricted to coplanar systems. Inclined discs around binaries have been studied numerically by Larwood and Papaloizou (1997) and a complete analytical theory has been developed by Ivanov et al. (1999). Orbits within the gravitational potential generated by a binary system would not in general be closed, because the binary potential cannot be treated as Keplerian. The first non-Keplerian term in a multipolar expansion of the gravitational potential is the quadrupole component, which causes a precession of the major axis of elliptical orbits. The same phenomenon happens on the solar system where the oblateness of the sun introduce a quadrupolar correction to its mostly Keplerian potential. If an inclined disc is considered, particles in different positions with respect to the binary major axis will precess with different frequencies. The system, now in a twisted configuration, dissipates viscously and evolves toward a coplanar configuration. The problem is analogous to the one studied in details in the next Chapter: in the spin-alignment process, the external torques is due to Lense-Thirring precession; while here is due to the binary potential. In the small-warp approximation, the alignment timescale of the process is (Ivanov et al. 1999, see also

King et al. 2013)

$$t_{\rm plane} = \begin{cases} (H/R)^{-1}\, t_{\rm dyn} & \text{if} \quad \alpha < H/R\,, \\ \alpha\,(H/R)^{-2}\, t_{\rm dyn} & \text{if} \quad \alpha > H/R\,, \end{cases} \tag{3.56}$$

which could be only one or two orders of magnitude bigger that the orbital period. It means that after just 10-100 particle orbits the disc and the binary can be considered on the same plane. To the best of our knowledge, a generalization of the above result considering large-amplitude warps is still missing.

A binary in a gaseous environment may have in general three different discs: two individual discs around each object (which we will call *circumprimary* or *circumsecondary* disc) as well as a *circumbinary* disc around the binary orbit. The binary evolution depends on the mutual relationship between the mass of the disc and the masses of the two BHs. If one of the two BHs is much lighter than the other (extreme mass ratio inspiral), then the secondary is able to migrate towards the primary exchanging angular momentum with the disc. If the secondary is massive enough, it can open a gap in the disc, around its orbit (Lin and Papaloizou 1979; Artymowicz and Lubow 1994; Armitage 2010). In this regime, both the secondary BH and the disc particles can be considered as orbiting around the primary BH. The secondary BH will generally collide with gas particles orbiting with a radius R close to the binary separation a. Particles just outside the binary orbit ($R > a$) move slower than the secondary BH. The BH speed is reduced by these collisions, which act exactly as in the dynamical friction scenario where a gives object interact with a collection of smaller point (see Sec.2.1 and Bertin 2000). Angular momentum is transferred from the secondary to the disc, increasing the orbital radius of the involved gas particles and decreasing the binary separation. The situation is reversed for particles colliding with $R < a$. The direction of the secondary migration depends on which of these two effects dominate. Integrating over every possible collision, it can be shown that the for typical disc structure, the disc gains angular momentum interacting with the secondary BH that consequently moves inwards (e.g. Armitage 2010).

The problem becomes more complicated whenever the BH mass ratio gets close to unity, because gas particles cannot be considered as orbiting around the primary. The problem has been studied using both grid-based (Günther and Kley 2002; MacFadyen and Milosavljević 2008) and smoothed-particle hydrodynamics simulations (Artymowicz and Lubow 1994; Escala et al. 2005). The binary produces a cavity in the disc that could be as big as $1.5a - 2a$ in which the two BHs orbit. Accretion within the cavity is not completely prevented and can still cause the binary shrink (Artymowicz and Lubow 1996). The effect of eccentric orbits in this regime could also be interesting for future GW observations (Armitage and Natarajan 2005).

When GW emission becomes an efficient source of angular momentum dissipation (see our discussions in Secs. 2.1 and 4.5), the disc and the binary decouple from each other (Armitage and Natarajan 2002). The two BHs quickly inspiral (the explicit calculation is reported in Sec. 5.2.1), while the disc cannot react on the same timescale. The behavior of the disc during the GW-driven evolution is still unclear and can lead to different predictions (Lodato et al. 2009; Chang et al. 2010; Baruteau et al. 2012; Noble et al. 2012; Bode et al. 2012).

Chapter 4

Black-hole spin alignment

In this Chapter we address the problem of the alignment between the spin of a Kerr BH and its surrounding accretion disc (Bardeen-Petterson effect). For the complete theory of accretions discs around Kerr BHs we refer to the recent review by Abramowicz and Fragile (2013). When spinning BHs form a binary system, we estimate if the BHs can reach an aligned configuration by comparing the BH-disc alignment timescale and the merger timescale. Interesting conclusions can be obtained regarding the likelihood of large BH recoil and about astrophysical BH properties.

4.1 The Bardeen-Petterson effect

The dynamics of accretion discs around a spinning BHs has been firstly studied by Bardeen and Petterson (1975) and it is now known as the *Bardeen-Petterson effect*. They showed that a viscous disc initially misaligned with the equatorial plane of the Kerr BH, would be expected to quickly reach an alignment configuration only in the inner regions. Out to a certain transition radius the outer disc retains its initial misalignment. Rees (1978) pointed out that because of Newton's third law, the disc may also cause the alignment the hole. The outer disc can pull the BH spin to a compete aligned configuration on a longer timescale. The detailed calculation of this BH-disc alignment timescale is one of the main purposes of this project.

Since a warp propagation theory was not available at the time, Bardeen and Petterson (1975) computed the disc structure assuming that the warps propagate through the disc with the same viscosity coefficient that produces the mass inflow (in our notation: $\alpha_2 = \alpha$). Their studied were improved later by Kumar and Pringle (1985) and Scheuer and Feiler (1996) considering the linear, small-α warp theory. Ivanov and Illarionov (1997) include also some PN corrections. Hydrodynamical simulations of the Bardeen-Petterson effect have been performed by Nelson and Papaloizou (2000), Fragile and Anninos (2005) and Fragile et al. (2007), while the inner disc behavior has been studied analytically by Lubow et al. (2002). A slightly different approach has been used by Martin et al. (2007) and Chen et al. (2009), where they derived stationary solutions of the disc structure assuming both viscosities ν and ν_2 to have power-law form. The numerical solution by Martin et al. (2009) consider the disc structure under the Bardeen-Petterson effect with a stellar companion embedded in the disc.

On the observational side, the Bardeen-Petterson effect has been invoked to explain peculiar observations, such as misaligned jets in AGNs (Kondratko et al. 2005; Caproni et al. 2006a,b, 2007; Martin 2008; Martin et al. 2008; Falceta-Gonçalves et al. 2010), oscillations in X-ray binaries (Fragile et al. 2001; Maccarone 2002) and X-ray transient sources due to tidal disruption events (Lei et al. 2013). We mention in particular the analysis performed by Caproni et al. (2006a) to the Seyfert Galaxy NGC 1068. If the occurrence of a misalignment

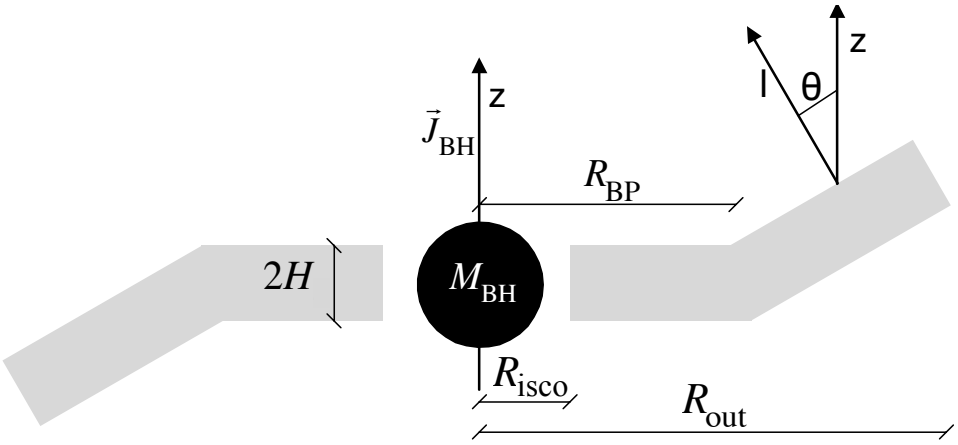

Figure 4.1: Bardeen-Petterson effect: schematic behavior of an accretion disc around a spinning BH (adapted by Caproni et al. 2006a). The inner disc is aligned with the BH equatorial plane, while at separation larger than the Bardeen-Petterson radius $R_{\rm BP}$ the outer disc orbital angular momentum l is generally misaligned by angle θ with the BH spin axis z.

between the inner disc (orthogonal to the galaxy's radio jets) and outer parts of the disc (identified by H_2O maser emission lines) is interpreted as due to the Bardeen-Petterson effect, the estimated timescale is well compatible with the expected AGN lifetime. A fundamental ingredient of their conclusion is the non-trivial relationship between α and α_2 of Eq. (3.53) previously neglected: however, the full-non linear expression has not been considered.

4.1.1 Warp radius

The geometry of the system is summarized in Fig. 4.1. The Bardeen-Petterson effect is due to the combination of the general relativistic Lense-Thirring precession and the viscous dissipation of the disc. Let us consider gas particles with $R \gg R_{\rm isco}$ where we can use the first-PN order approximation derived in Sec.1.1.5. We obtained that the orbital angular momentum of a particle around a BH precesses with a frequency given by (e.g. Wilkins 1972)

$$\Omega_{\rm LT} = \frac{2G^2M^2}{c^3R^3}\chi\,. \tag{4.1}$$

Each ring that forms the accretion disc will precess with a different frequency because $\Omega_{\rm LT}$ depends on the separation R. The disc does not precess as a whole, but it gets warped and twisted. Warps introduce a new substantial way to transfer angular momentum. If the timescale over which warps can propagate is shorter than the precessional timescale, the disc can quickly react to the twisting induced by the Lense-Thirring precession and reach an aligned configuration to avoid further dissipation. However, if the disc cannot react quickly, the misaligned configuration is maintained. The *Bardeen-Petterson radius* or *warp radius* $R_{\rm BP}$ is defined as the boundary radius between these two behaviors[1]. It can be found

[1]Slightly different definitions are present in the literature. For instance, Perego et al. (2009) define both a warp radius, which correspond to our $R_{\rm BP}$, and a Bardeen-Petterson radius, which is defined as the point where the warp amplitude ψ is maximum. These values can in general be different by a factor of order unity (see e.g. Fig. 4.3), depending on the disc structure.

equating the Lense-Thirring timescale $\Omega_{\rm LT}^{-1}$ and the warp propagation timescale $t_{\nu 2}$

$$R_{\rm BP} = \frac{2G^2M^2\chi}{c^3\nu_2}\,. \tag{4.2}$$

Using the α-prescription (3.49) and the thin-disc approximation (3.10), the viscosity coefficient ν_2 can be written as

$$\nu_2 = \alpha_2 H^2 \Omega_{\rm BP}\,, \tag{4.3}$$

where $\Omega_{\rm BP} = (GMR_{\rm BP}^{-3})^{1/2}$ is the Keplerian angular frequency evaluated at the warp radius. The Bardeen-Petterson radius is thus given by

$$\begin{aligned} R_{\rm BP} &= 2^{-1/3}\left(\frac{\chi}{\alpha_2}\right)^{2/3}\left(\frac{H}{R}\right)^{-4/3}\left(\frac{2GM}{c^2}\right) \\ &\simeq 1.58\times10^5\left(\frac{\chi}{\alpha_2}\right)^{2/3}\left(\frac{H/R}{0.01}\right)^{-4/3}\left(\frac{M}{10^8M_\odot}\right)R_\odot\,. \end{aligned} \tag{4.4}$$

The location of the warp radius depends on the BH properties M and χ, the aspect ratio of the disc H/R and the warp diffusion coefficient α_2. This expression is somewhat new (Lodato and Gerosa 2013), because the coefficient α_2 has not been substituted with any approximate expression. In the small-ψ, small-α regime (i.e. $\alpha_2 = 1/2\alpha$) it reduces to

$$R_{\rm BP} = 2^{1/3}\left(\frac{2GM}{c^2}\right)(\chi\alpha)^{2/3}\left(\frac{H}{R}\right)^{-4/3}\ {\rm yr}\,, \tag{4.5}$$

as reported by Natarajan and Pringle (1998). Note that H/R might be in general a function of R; however the dependance introduced by this factor is rather low (cf. Sec. 4.2).

4.1.2 Alignment timescale

The inner disc $R < R_{\rm BP}$ becomes aligned with the BH orbital plane on the viscous timescale $t_{\nu 2}$, as quickly as the disc is able to dissipate the differential precession induced by the Lense-Thirring term. On this timescale, the outer disc $R > R_{\rm BP}$ remains misaligned because the disc cannot dissipate the tilts. On a longer timescale, the outer disc exert a torque on the BH spin causing it to precess and finally to align with the outer disc angular momentum. We will refer to the timescale of this process as "BH-disc alignment timescale" or just "alignment timescale". In the following derivation we assume that the alignment timescale is greater than t_{ν_2}. We are implicitly assuming that the alignment is a quasi-equilibrium process and a stationary configuration is reached by the disc at every time step. This assumption is worth of further investigations (see Sec. 4.4.4).

The BH spin $J_{\rm BH}$ is pulled on the alignment timescale $t_{\rm align}$ as a reaction to the Lense-Thirring precession. The torques acts on the angular momentum of the disc rings close to the warp radius $L_d(R_{\rm BP})$ on a timescale $\Omega_{\rm LT}^{-1}(R_{\rm BP})$: $t_{\rm align}$ can be found equating the angular momentum per unit time which is exchanged between the disc and the hole (Scheuer and Feiler 1996; Natarajan and Pringle 1998; Lodato and Pringle 2006)

$$\frac{J_{\rm BH}}{t_{\rm align}} = L_d(R_{\rm BP})\,\Omega_{\rm LT}(R_{\rm BP})\,. \tag{4.6}$$

Sice the warp radius $R_{\rm BP}$ is by definition the distance at which $\Omega_{\rm LT}^{-1} = t_{\nu 2}$, the alignment

timescale can be written as

$$t_{\rm align} = \frac{\chi G M^2}{c\, L_d(R_{\rm BP})} \frac{R_{\rm BP}^2}{\nu_2}\,, \tag{4.7}$$

where the BH spin $J_{\rm BH}$ has been expressed using (1.5). The angular momentum $L_d(R_{\rm BP})$ can be estimated by considering the mass $\Sigma\pi R_{\rm BP}^2$ moving at a radius $R_{\rm BP}$ with a velocity $\Omega_{\rm BP} R_{\rm BP}$

$$L_d(R_{\rm BP}) = \pi \Sigma R_{\rm BP}^{5/2} (GM)^{1/2}\,, \tag{4.8}$$

where here Σ is the surface mass density at the warp radius. Since we are assuming that the process happens in a quasi-equilibrium configuration, the stationary expression (3.19) can be used. This leads to

$$t_{\rm align} = 3\chi \frac{\alpha}{\alpha_2} \frac{M}{\dot M} \left(\frac{R_{\rm BP}}{GM/c^2} \right)^{-1/2}\,, \tag{4.9}$$

where we used $\nu/\nu_2 = \alpha/\alpha_2$. This heuristic estimate can be confirmed using the disc structure computed by Scheuer and Feiler (1996), up to a factor $\sqrt{2}$

$$t_{\rm align} = 3\chi \frac{\alpha}{\alpha_2} \frac{M}{\dot M} \left(\frac{R_{\rm BP}}{2GM/c^2} \right)^{-1/2}\,. \tag{4.10}$$

We decide to adopt the latest expression to allow more immediate comparisons with the previous results in the literature, such as Natarajan and Pringle (1998) and Lodato and Pringle (2006). We stress however, that a factor $\sqrt{2}$ do not affect our main results. Like ours, also the Scheuer and Feiler (1996) derivation relies on the assumption that a steady state configuration is quickly reached by the disc while the mutual direction of the BH spin and the outer disc can be considered constant. Plugging (4.4) and (3.37) into (4.9), we obtain (Lodato and Gerosa 2013)

$$\begin{aligned} t_{\rm align} &= 3 \times 2^{1/6} \alpha \left(\frac{\chi}{\alpha_2} \right)^{2/3} \left(\frac{H}{R} \right)^{2/3} \frac{\epsilon\, t_{\rm edd}}{f_{\rm edd}} \\ &\simeq 7 \times 10^6 \left(\frac{\chi}{\alpha_2} \right)^{2/3} \left(\frac{\alpha}{0.1} \right) \left(\frac{H/R}{0.01} \right)^{2/3} \left(\frac{f_{\rm edd}}{0.1} \right)^{-1} \left(\frac{\epsilon}{0.1} \right) {\rm yr}\,. \end{aligned} \tag{4.11}$$

Note that the warp propagation coefficient α_2 has been kept explicitly indicated, without using any small-amplitude approximation. The alignment timescale vanishes for a Schwarzschild BH ($\chi = 0$) simply because there is no spin direction to be aligned with. The dependance of the alignment timescale on the BH spin χ is not trivial, because of the accretion efficiency $\epsilon = \epsilon(\chi)$: in particular it depends on the prograde/retrograde direction of the accreted particles (Sec. 4.3.2). Our expression is apparently independent on the BH mass, but the mass of the central object would generally affect the shape of the disc, that enters in $t_{\rm align}$ through H/R.

4.2 Alignment and merger

The key argument to predict if large SMBH recoils happen in astrophysics or not, is the expected misalignment between the binary orbital angular momentum and the spins just before the merger (Sec. 2.3). It is considered likely that the SMBH mergers typically happen in a gas-rich environment (Escala et al. 2004, 2005; Dotti et al. 2009b) where an accretion disc can drive the inspiral. Even warps are treated in the low-amplitude regime, the binary

orbit and the cimcumbinary disc are expected to reach a coplanar configuration quickly (see Sec. 3.4 and Ivanov et al. 1999), thus SMBH ejection likelihood can be estimated by comparing the direction of the spins with the orbital angular momentum of the disc. To predict recoil velocities, we should know the residual misalignment after the alignment process due to the Bardeen-Petterson effect. It is very difficult to approach the complete problem because the whole binary history is involved and the structure of the disc needs to be modeled in detail; moreover, additional general relativistic effects can further modify the misalignment angles in the GW-driven inspiral just before the merger (Sec. 4.6).

Critical conclusions can be obtained using just a timescale argument, which is the main analysis presented in this work. We compare the alignment timescale with the merger timescale $t_{\rm m} \simeq 10^7$ yr, i.e. the timescale over which the binary separation decreases. If $t_{\rm align} < t_{\rm m}$, then each BH has enough time to be aligned by with its own accretion discs, otherwise a residual misalignment is maintained. If this misalignment is not small and it is not greatly modified in the GW-driven inspiral, the BHs approach the merger in a configuration that can likely produce a superkick. Our procedure is implemented through Monte Carlo simulations as presented in Sec. 4.3 and 4.4. Before describing our results, we review previous attempts by Bogdanović et al. (2007), Perego et al. (2009) and Dotti et al. (2010).

- Bogdanović et al. (2007) present order-of-magnitude estimates of the Bardeen-Petterson effect. They consider the alignment timescale for a single BH and its accretion disc. They find that it is always shorter than the merger timescale, and conclude that each black hole is effectively aligned with its disc preventing any strong recoil. They evaluate the accretion time-scale by considering the flow properties at the Bondi radius (Bondi 1952), estimated to be at 40pc from the hole

$$R_{\rm Bondi} = \frac{GM}{v_{gas}^2} \simeq 40 \left(\frac{M}{10^8 M_\odot}\right) \left(\frac{v_{gas}}{100{\rm km/s}}\right)^{-2} {\rm pc}\,, \tag{4.12}$$

  where v_{gas} is an estimate of the gas speed. The accretion at $R_{\rm Bondi}$ is then computed using the Bondi-Hoyle accretion rate (Hoyle and Lyttleton 1941; Bondi and Hoyle 1944) as $\dot{M}_{\rm Bondi} \simeq 1 M_\odot/{\rm yr}$. Their conclusion is that the mass accreted in $t_{\rm m} \simeq 10^7$yrs at this rate is at least $1\% - 10\%$ of the BH mass. Since the alignment timescale is only $\sim 1\%$ of the accretion timescale, the inspiral lasts 1 to 10 alignment timescales and thus complete alignment is reached.
  We point out that such estimates at $R_{\rm Bondi} \simeq 40$pc cannot accurately describe the accretion properties at the warp radius $R_{\rm BP} \simeq 10^5 R_\odot \simeq 10^{-3}$pc, which is the location where most of the warp dissipation occur. Moreover, the viscous time at these distances from the hole is even larger than the Hubble time.

- Perego et al. (2009) improve their study finding slightly longer timescale. They consider the joint evolution of the mass and the spin vector of the BH under the Bardeen-Petterson effect caused by a misaligned accretion disc with a formal infinite radius. This means in practice that the outer disc angular momentum direction is considered fixed, while only the BH properties are evolved. Three disc configurations are considered, with initial misalignment angles $\theta_0 = \pi/3, \pi/6, \pi/30$; the BH mass and the Eddington fraction are taken within $10^5 M_\odot < M < 10^7 M_\odot$ and $10^{-4} < f_{\rm edd} < 1$ respectively; and each run is performed adopting two different prescriptions to model the viscosity profile.
  They assume that the rapid time evolution of the warped disc and the BH alignment can be decoupled (adiabatic approximation): after a timestep δt the disc quickly reaches the quasi-steady-state computed by Martin et al. (2007), while the BH properties are updated because some material has been accreted at the innermost stable orbit. They treat the warp propagation using $\alpha_2 = f_2/2\alpha_1$ where the values of f_2 are taken from the numerical simulations reported by Lodato and Pringle (2007). The

alignment timescale obtained with this procedure is (see Eq. 43 in Perego et al. 2009)

$$t_{\rm align}^{\rm P09} = 1.13\times10^5\left(\frac{\alpha}{0.1}\right)^{58/35}\left(\frac{\chi}{f_2}\right)^{5/7} f_{\rm edd}^{-32/35}\left(\frac{\epsilon}{0.1}\right)^{-32/35}\left(\frac{M}{10^6 M_\odot}\right)^{-2/35}{\rm yr}$$
$$\simeq 1.13\times10^5\left(\frac{\alpha}{0.1}\right)^{1.66}\left(\frac{\chi}{f_2}\right)^{0.71} f_{\rm edd}^{-0.91}\left(\frac{\epsilon}{0.1}\right)^{0.91}\left(\frac{M}{10^6 M_\odot}\right)^{-0.06}{\rm yr}\,. \tag{4.13}$$

Their result is compatible within a factor 2 with our expression (4.11), which can be restricted to $\alpha_2 = f_2/2\alpha_1$ and rescaled to give

$$t_{\rm align} \simeq 2.3\times10^5\left(\frac{\alpha}{0.1}\right)^{1.67}\left(\frac{\chi}{f_2}\right)^{0.67} f_{\rm edd}^{-1}\left(\frac{\epsilon}{0.1}\right)\left(\frac{H/R}{0.01}\right)^{1.33}{\rm yr}\,. \tag{4.14}$$

The only apparent difference is the factor containing the BH mass M, which comes from the disc structure considered in their derivation. Our expression instead keeps the shape of the disc H/R explicitly indicated (see also the equivalent in Natarajan and Pringle 1998). However, this M-dependace is very small suggesting that it is not a key factor.

Using the quasi-equilibrium procedure just described, Perego et al. (2009) found that the residual misalignment angle distribution is independent on the initial tilt angle θ_0. This conclusion relies on the alignment timescale expression (4.13) which does not contain the misalignment θ neither explicitly nor implicitly. Different initial misalignment will modify the warped disc structure and consequently the warp propagation that cause the Bardeen-Petterson alignment. The source of this missing dependance on θ is ultimately the linear warp-propagation theory considered (Sec. 4.4.2). One of the goal of the present work is to include non-linear effects as predicted by Ogilvie (1999). For future comparisons, we report in Fig. 4.2 the main result by Perego et al. (2009).

- Dotti et al. (2010) test this suggestions by performing a series of smoothed particle hydrodynamics simulations of two $4\times10^6 M_\odot$ SMBHs inspiraling within a $10^8 M_\odot$ circumbinary disc in their orbital plane. One of the SMBHs is initially at the center of the disc, while the second SMBH spirals inwards on an eccentric orbit ($e = 0.7$) from an initial separation of 50pc to a final separation of 10pc. Gas particles within the Bondi radii around the SMBH are accreted, and the BH properties are updated using the same algorithm presented in Perego et al. (2009). Gas is evolved assuming a polytropic equation of state with index $\gamma = 5/3$ (*hot* case) or $\gamma = 7/5$ (*cold* case). The hot medium is an adiabatic monoatomic gas and is meant to simulate an extreme case in which radiative cooling has been completely suppressed during the merger (Mayer et al. 2007b), while the *cold* gas is taken to approximate a solar metallicity medium heated by a starburst (Spaans and Silk 2000; Klessen et al. 2007). They found that the BH spins approach the merger aligned to within 10° (30°) with the orbital angular momentum of the cold (hot) disc. The difference between cold and hot gas can be understood from the alignment timescale (4.11) derived above. The cold disc will form a thinnest disc, thus H/R will be smaller than in the hot case. Since $t_{\rm align}$ is a monotonically increasing function of H/R, a cold disc will take less time to be aligned and it will also likely keep a smaller misalignment. However, we stress that the timescale expression could not determine in any way the residual misalignment distribution, for which galactic-scale simulations like the ones performed in Dotti et al. (2010) are needed (Sec. 4.6).

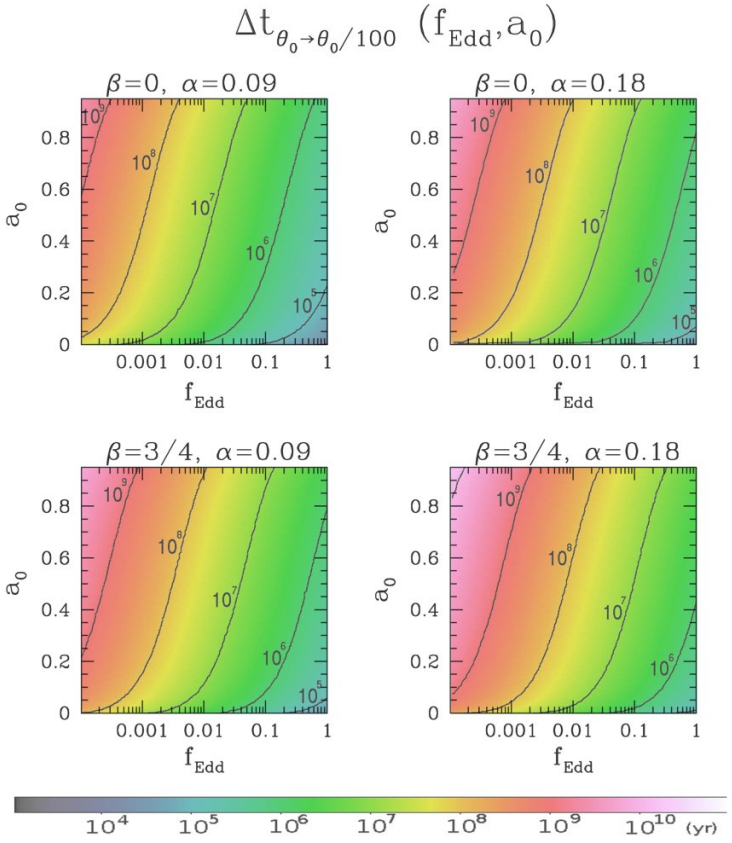

Figure 4.2: Alignment timescale by Perego et al. (2009), as a function of the Eddington factor $f_{\rm edd}$ and of the initial BH spin parameter a_0 (in our notation, χ). The colour scale represents $t_{\rm align}^{\rm P09}$ in years, for two value of $\alpha = 0.09, 0.18$ and two viscosity profiles $\nu_1, \nu_2 \propto R^\beta$. Distributions do not depend on the initial misalignment θ_0.

4.3 Modeling spin alignment

We compute for the first time the alignment timescale considering the full non-linear theory of warp propagation. We consider a system composed by a single BH and a single accretion disc, which is pulling the BH spin as predicted by the Bardeen-Petterson effect. We define $\theta = \beta(R_{\rm out})$ to be the angle between the orbital angular momentum of the outer disc and the spin of the BH (see Fig. 4.1), so that $0 < \theta < 2\pi$ with $\theta = 0, 2\pi$ corresponding to full alignment and $\theta = \pm\pi$ corresponding to full counteralignment. The alignment timescale that has been analytically derived in (4.11) should be evaluated considering the proper warp propagation coefficient $\alpha_2 = (\alpha, \psi)$. Before showing our results, three technical aspects must be discussed in more detail.

4.3.1 Warp amplitude ψ

To compute the warp evolution accurately, an estimate of $\psi = \partial\beta/\partial \ln R$ is needed. One would need to know not only the misalignment between the outer disc axis and the BH spin θ, but also how steep its gradient is. This requires a detailed calculation of the shape of the disc. Unfortunately, studies of disc structure around spinning BHs are available only in the small-amplitude regime (Scheuer and Feiler 1996; Natarajan and Armitage 1999; Martin et al. 2007). In our preliminary attempt to test the effect of the non-linear warp propagation, we decided to adopt a much simpler prescription: $\psi \simeq \theta$. We test this approximation against

the stationary solution computed by Scheuer and Feiler (1996). If $\beta \ll 1$, the components of $\mathbf{l}$ (3.47) orthogonal to the spin direction reduce to $\beta \sin\gamma$ and $\beta\cos\gamma$. They can be written using a single complex variable (Pringle 1996)

$$W(R) = \beta(R) e^{i\gamma(R)} . \tag{4.15}$$

The Scheuer-Feiler solution reads[2]

$$W^{\rm SF}(R) = \theta \exp\left[2(\pm i - 1)\left(\frac{R_{\rm BP}}{R}\right)^{1/2}\right] , \tag{4.16}$$

where the sings refer to BH co- or counter-alignment respectively. The tilt angle β results

$$\beta^{\rm SF}(R) = \theta \exp\left[-2\left(\frac{R_{\rm BP}}{R}\right)^{1/2}\right] , \tag{4.17}$$

which correctly returns $\beta = \theta$ if $R \to \infty$ and $\beta = 0$ if $R \to 0$. They predict a warp amplitude

$$\psi^{\rm SF}(R) = \theta \left(\frac{R_{\rm BP}}{R}\right)^{1/2} \exp\left[-2\left(\frac{R_{\rm BP}}{R}\right)^{1/2}\right] . \tag{4.18}$$

The function $\psi^{\rm SF}$ has is maximum in $R = 4R_{\rm BP}$ where its value is $0.18 \times \theta$ (Fig.4.3): the error computed by assuming $\psi^{\rm SF} = \theta$ is always less than a factor $1/0.18 = 5.56$. The Scheuer-Feiler solution can in principle be used only where the outer disc misalignment is small $\theta \ll 1$ and consequently the warp propagation can be treated linearly ($\psi \ll 1$). In this case the viscosity α_2 and the alignment timescale $t_{\rm align}$ do not depend on ψ (see Eq. 3.53): the small-θ regime where our approximation is affected by the larger error (up to a factor ~ 6), corresponds to the case where the net effect of ψ is negligible. If $\theta \sim 1$ we are fully in the non-linear regime: the vertical viscosity coefficient α_2 is smaller than in the linear approximation (see Fig. 3.3) and consequently the warp radius $R_{\rm BP}$ in (4.4) moves outwards. The location where the BH and the disc can exchange angular momentum through warps gets closer to the outer disc, where the local misalignment is θ.

A model of the disc shape would be needed to describe in detail the angular momentum exchanged between the disc and the BH and thus predict the final configuration.We decided to approach the problem within the approximation $\psi = \theta$ using a timescale argument. We hope our study will stimulate further works toward a complete modeling of the disc dynamical structure in the case of large misalignment angles.

4.3.2 Co- and counter-alignment

Up to now we loosely used the term *alignment* to indicate a configuration where the disc plane is orthogonal to the spin direction. The disc angular momentum can be either co- or counter-aligned with the BH spin.

The symmetry of the problem around the z axis is contained in the Kerr metric (1.4): the alignment process from a disc misaligned by θ or $-\theta$ is completely equivalent. For the same reason, the problem also presents a symmetry around $\theta = \pm\pi/2$. This means that if $|\theta| < \pi/2$, the system would go naturally towards a co-aligned configuration ($\theta \to 0$), while if $|\theta| > \pi/2$ it would tend to counter-alignment ($\theta \to \pm\pi$). Both these symmetries must be considered: the warp induced in the disc has the same amplitude in both co- and counter-aligned cases, only the BH spin verse changes. In other words, the warp propagation is independent on the sing of the Lense-Thirring differential precession (4.1). As a matter of fact, we never considered the sign of $\Omega_{\rm LT}$ in the above derivation.

[2]In the notation used by Scheuer and Feiler (1996) (see their Eqs. 8 and 16): $\theta = K$ and $R_{\rm BP} = \omega_p/\nu_2$.

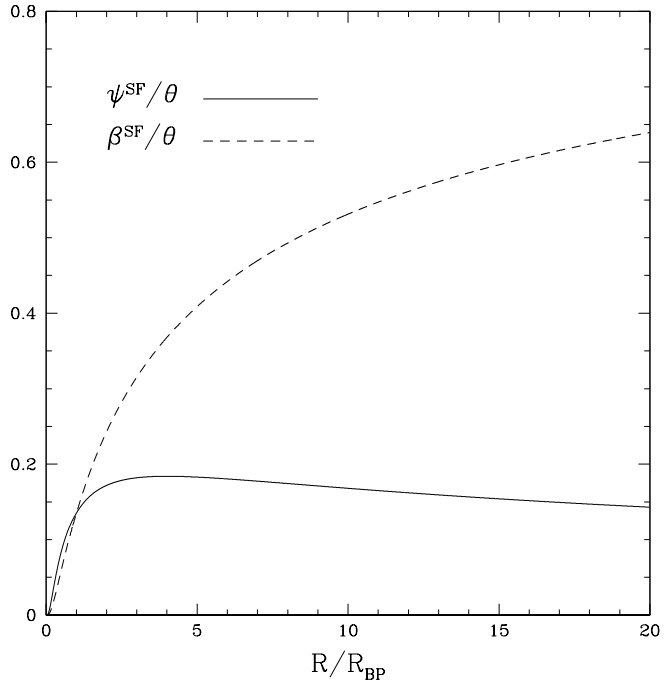

Figure 4.3: Tilt angle $\beta^{\rm SF}$ and warp amplitude $\psi^{\rm SF}$ as predicted with the Scheuer-Feiler analytical solution (Scheuer and Feiler 1996). Even in the small amplitude regime, the error computed by assuming $\psi = \theta$ is less than a factor 6 at the maximum warp location $R = 4R_{\rm BP}$.

The actual warp propagation coefficient α_2 is computed within the approximation $\theta = \psi$ after being symmetrized around $\theta = 0$ and $\theta = \pm\pi/2$, as shown in Fig. 4.4. This figure contains the new critical dependence on the misalignment angle that will enter in the computation of $t_{\rm align}$. The symmetry between co- and counter-alignment timescale is broken by the accretion efficiency ϵ because both the location and the potential energy of the innermost stable orbit change with the direction of the BH spin (Sec. 3.2.1). Accretion from aligned disc will occur on prograde orbits, while retrograde orbits are expected in a counter-aligned configuration. The difference between these two cases becomes critical for rapidly spinning BHs where the values of ϵ can be different up to a factor ~ 8 (Fig. 3.1).

King et al. (2005) show how the condition $|\theta > \pi/2|$ is not sufficient to predict counter-alignment. With a simple geometric argument, they show that counter-alignment is reached for a gas ring at a radius R only if

$$|\theta| > \pi/2 \qquad \text{and} \qquad L_d(R) < 2J_{\rm BH}\,, \tag{4.19}$$

where $L_d(R)$ is the angular momentum of the gas particles inside R. This is essentially a condition on the surface density Σ. The above condition is clearly verified for small R, where the evolution is dominated only by the presence of the BH and the influence of the outer disc is negligible. If $|\theta| > \pi/2$ the inner disc always counter-aligns with the BH spin, which consequently accrete from retrograde orbits. However, there could be some radius $R_{\rm counter}$ where the condition above becomes false: the outer disc forces the BH to an aligned configuration. A sharp transition occur at $R_{\rm counter}$ between the counter-aligned inner disc and the co-aligned outer disc. This case has been studied analytically by King et al. (2005) using the AGN disc model given by Collin-Souffrin and Dumont (1990) and numerically by Lodato and Pringle (2006).

In this work we simply assume that this transition never occurs, i.e. $R_{\rm counter} > R_{\rm out}$. A

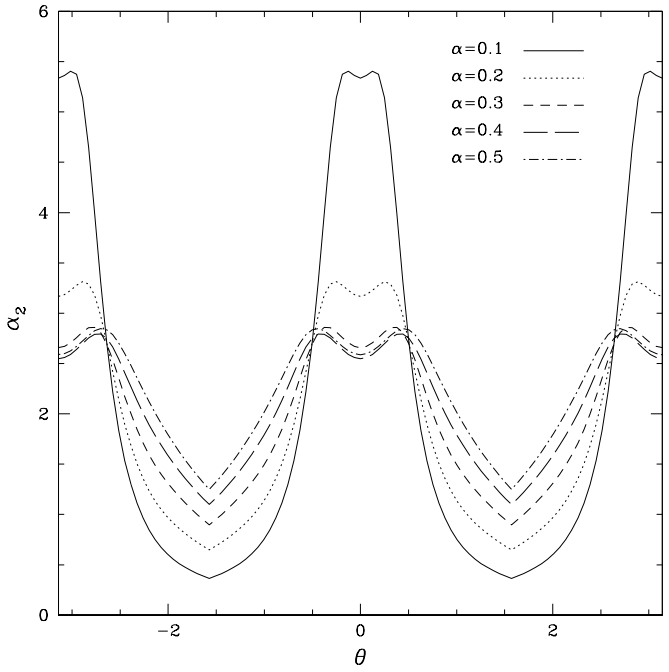

Figure 4.4: Warp propagation coefficient α_2 as function of the misalignment angle θ (Lodato and Gerosa 2013). We used the full non-linear theory of warp propagation within the approximation $\theta = \psi$, and implementing both the axial symmetry and the co-/counter-alignment symmetry.

more precise treatment cannot be adopted within our timescale argument, because a model for the disc structure is needed to predict $L_d(R)$. Our assumption is formally true only in the case where the mass of the disc is low enough. As we noted above, this assumption does not affect our treatment of the accretion efficiency, since the inner disc is counter-aligned even in these peculiar configurations. Unfortunately it does affect the viscosity coefficient α_2: the symmetrization point between co- and counter-alignment discussed above does not generally happen at $\theta = \pm\pi/2$, but it should contain both the conditions reported in (4.19).

4.3.3 Negative viscosity

We already mentioned as the non-linear theory of Ogilvie (1999) predicts a negative azimuthal viscosity for low values of α and large values of ϕ (see Eq. 3.55 and Fig. 3.3). The disc could break up in two distinct planes and maybe settle down in a stable counter-aligned configuration (Nixon 2012). In such cases, Nixon and King (2012) find that the disc splits into a co-aligned or counter-aligned inner disc while the outer disc remains misaligned. This configuration is very different from Fig. 4.1: it does not present a warp radius, but rather a sharp transition between aligned and counter aligned gas rings. The present derivation cannot be valid in this regime. However, since the alignment process in only based on Newton's third law, even those discs which present a sharp transition will be aligned. The alignment timescale will presumably be longer in this case because warp propagation through the transition is expected to be less effective. In practice, we assume that whenever $\alpha_1 < 1$, the alignment timescale $t_{\rm align}$ is grater than any other timescale involved in the process and in particular greater than the merger timescale $t_{\rm m}$. Broken discs affect our result only for $\alpha = 0.1$ and $\theta \sim \pm\pi/2$, where our procedure can lead to unphysical situations (see e.g. the $\chi \to 0$ limit in Fig. 4.7 and related discussion).

4.4 Monte Carlo simulations

We finally present the main results of our timescale argument. We use Monte Carlo simulations to compute alignment timescale distributions, fully considering the non-linear theory of warp propagation. The values of the alignment timescale obtained are then compared with estimates of the merger timescale, to predict likelihood of large recoil after SMBH merger events. We draw conclusions on the average spin properties of SMBH in the Universe.

4.4.1 Numerical setup

We compute the alignment probability through Monte Carlo realizations of $N = 10^4$ events. The alignment timescale (4.11) depends on five different parameter: θ, α, χ, H/R and $f_{\rm edd}$. The warp coefficient α_2 is uniquely determined by α and $\theta = \psi$ (Fig. 4.4), while the efficiency ϵ is determined by χ (Fig. 3.1).

We decide to keep the aspect ratio fixed to $H/R = 0.01$ because this factor is expected to produce a very weak dependance on the BH mass (see Eq. 4.13). The initial angles θ are randomly distributed between $-\pi$ and π, thus including also cases where the disc and the BH end up in a counter-aligned configuration. Being θ a polar angle, we take a uniform distribution in $\cos\theta$ to have an isotropic distribution in three dimensions. As for the Eddington fractions $f_{\rm edd}$, we carry out runs using a fixed value $f_{\rm edd} = 0.1$ and others where they are randomly generated between 10^{-4} and 1 with uniform logarithmic distribution. The alignment timescale can finally be computed for each choice of the remaining two free parameters α and χ. We vary χ between 0 and 1, and α between 0.1 and 0.5.

4.4.2 Alignment timescale distributions

Figs. 4.5 and 4.6 show histograms with some of our Monte Carlo realizations. Each panel contains probability distributions for a given spin parameter χ and three different values of α, with two different prescriptions for $f_{\rm edd}$.

The distributions collected in Fig. 4.5 are computed with a fixed valued $f_{\rm edd} = 0.1$. Let us stress the fact that even in this case we need Monte Carlo simulations, because we have to sample over the initial misalignment. Unlike Perego et al. (2009), who found that the alignment timescale is independent on the initial misalignment, we find that θ is a key parameter because it determines the warp propagation coefficient and consequently the warp radius location.

An interesting feature arises for rapidly rotating BHs, for which the alignment timescale distribution assumes a bimodal shape. The efficiency ϵ strongly divides the events with $|\theta| < \pi/2$ from those with $|\theta| > \pi/2$. For high spins, the efficiency of accretion $\epsilon(\chi)$ differs significantly between the co- and the counter-aligned cases (Fig. 3.1), so that for half of the events we have rapid (counter-)alignment, while for the remaining half we have relatively slower (co-)alignment. For extreme Kerr BHs ($\chi = 1$) the peak containing the co-aligned cases can occour at timescale as large as $\sim 50\,$Myr.

Fig. 4.5 shows probabilities where the Eddington fraction $f_{\rm edd}$ is drawn from a uniform logarithmic distribution between 10^{-4} and 1. This is the same range already explored by Perego et al. (2009). These distribution are the generalization to non-linear warps of their previous result reported in Fig. 4.2. Since we are sampling uniformly in $\log f_{\rm edd}$ like in the scale of their plots, our distributions are equivalent to lines at constant χ in their color-coded map. A crucial difference is that we cannot avoid using Monte Carlo simulations, because of the new dependence on θ. It can be seen that our timescale values are sensibly larger than their previous result, especially for high spins. Warp non-linearities become critical for large value of χ, where the distributions significantly move towards longer alignment timescale. *Rapidly spinning BHs need much more time to be aligned with the disc: this picture emerges only when non-linear warp propagation is considered.*

We report in Table 4.1 the average values of the alignment timescale computed in 50 different Monte Carlo runs, using both the linear and the non-linear warp propagation

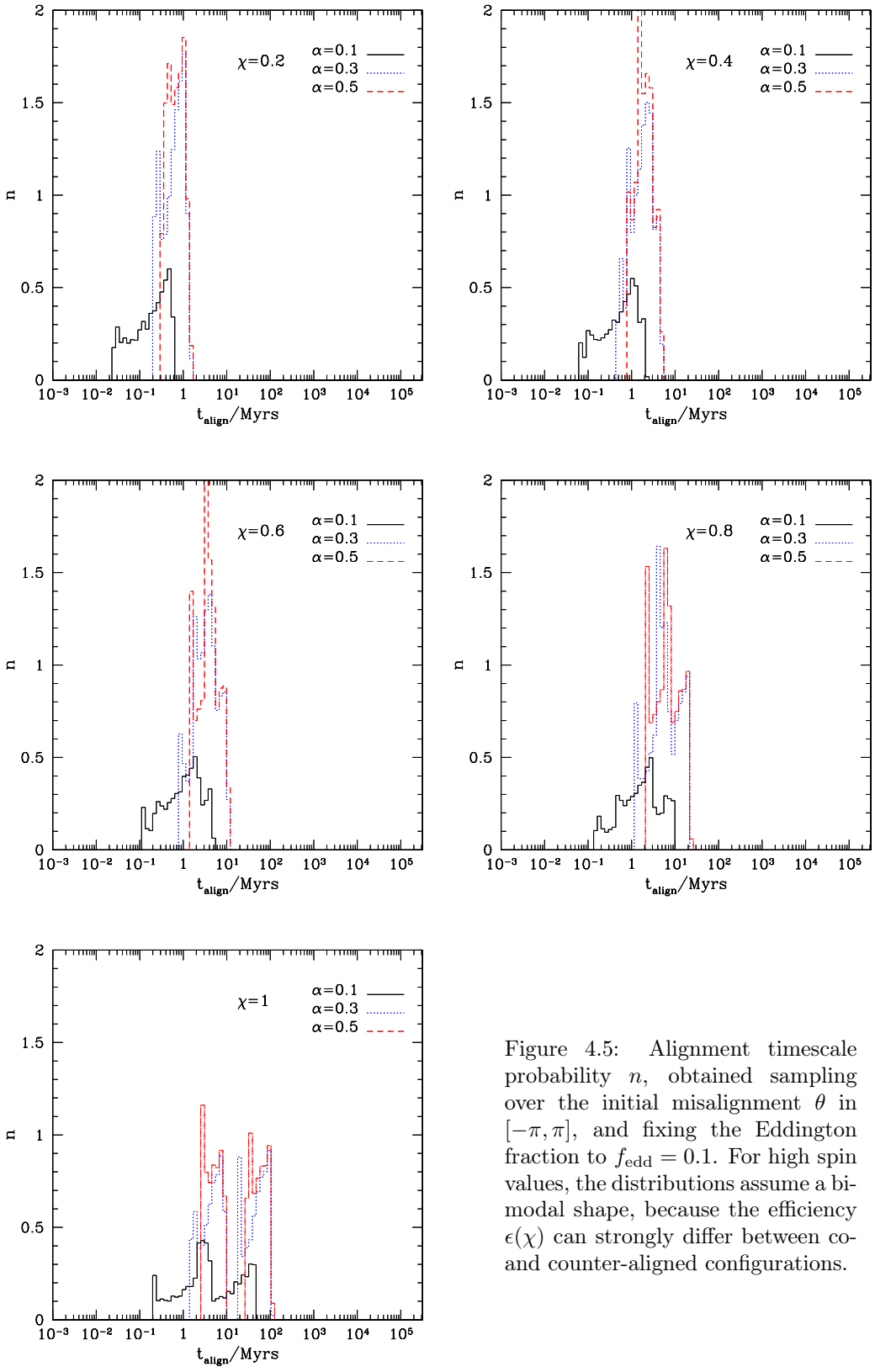

Figure 4.5: Alignment timescale probability n, obtained sampling over the initial misalignment θ in $[-\pi, \pi]$, and fixing the Eddington fraction to $f_{\rm edd} = 0.1$. For high spin values, the distributions assume a bimodal shape, because the efficiency $\epsilon(\chi)$ can strongly differ between co- and counter-aligned configurations.

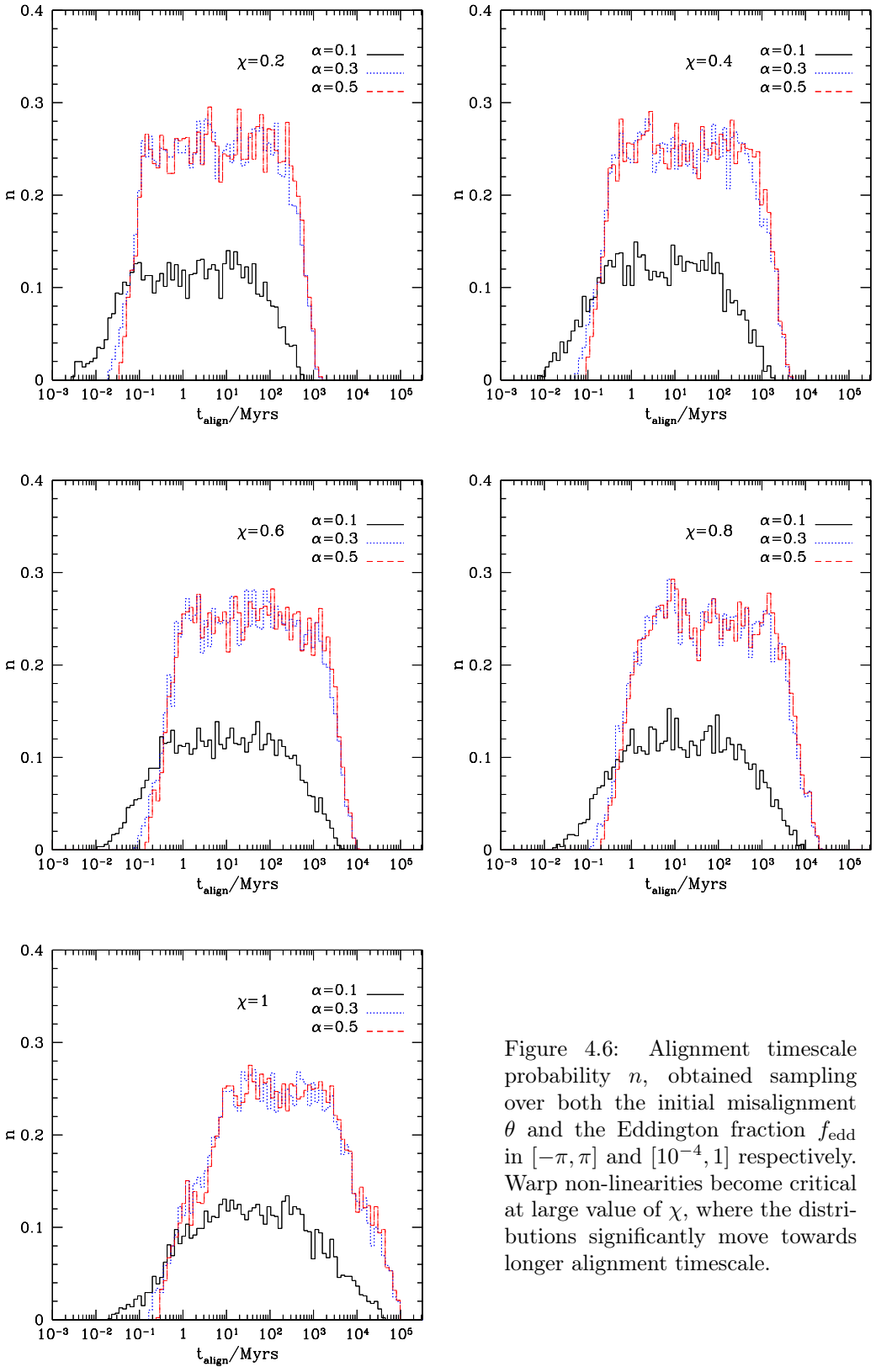

Figure 4.6: Alignment timescale probability n, obtained sampling over both the initial misalignment θ and the Eddington fraction $f_{\rm edd}$ in $[-\pi, \pi]$ and $[10^{-4}, 1]$ respectively. Warp non-linearities become critical at large value of χ, where the distributions significantly move towards longer alignment timescale.

	$\alpha = 0.1$[a]		$\alpha = 0.2$		$\alpha = 0.3$		$\alpha = 0.4$		$\alpha = 0.5$	
$\chi = 0.1$	9.1	(1.2)	26.5	(5.1)	26.7	(10.0)	27.1	(14.2)	28.7	(17.3)
$\chi = 0.2$	25.3	(3.3)	73.3	(14.2)	72.7	(27.8)	74.9	(39.4)	79.3	(48.1)
$\chi = 0.3$	47.1	(5.9)	132.8	(25.6)	131.5	(50.0)	135.3	(71.0)	143.2	(86.7)
$\chi = 0.4$	80.9	(9.8)	219.6	(42.2)	217.3	(82.5)	223.4	(117.1)	236.2	(143.0)
$\chi = 0.5$	110.5	(14.0)	322.5	(62.1)	319.2	(121.2)	328.5	(172.1)	347.4	(210.1)
$\chi = 0.6$	138.2	(17.8)	428.1	(81.0)	422.9	(158.3)	434.9	(224.7)	459.9	(274.3)
$\chi = 0.7$	189.2	(25.7)	586.6	(112.7)	581.2	(220.6)	599.2	(313.2)	634.4	(382.5)
$\chi = 0.8$	285.7	(35.91)	823.9	(158.9)	816.2	(310.4)	840.7	(440.6)	889.7	(538.0)
$\chi = 0.9$	401.3	(51.7)	1149.6	(223.1)	1140.4	(435.8)	1175.8	(618.7)	1244.8	(755.4)
$\chi = 1$	1149.8	(145.1)	3295.9	(632.4)	3263.0	(1235.3)	3359.1	(1753.6)	3553.2	(2141.2)

Table 4.1: Average values of the alignment timescale $t_{\rm align}$ in unit of 10^6yr, computed using the non-linear theory of warp propagation. Both θ and $f_{\rm edd}$ are randomly generated in $[-\pi, \pi]$ and $[10^{-4}, 1]$ respectively. In parenthesis we list the correspondent values calculated using the linear approximation (3.53): the linear theory causes a strong underestimation of the alignment timescale, up to a factor 7 for the low-alpha/high-spin case.

[a] Average values are computed only over ~ 4700 of the 10^4 generated events, because negative viscosity events have been discarded by construction.

theory. In *every* case, the linear theory results in a strong underestimation of the alignment timescale, even up to a factor 7. The largest disagreement occurs for low value of α, because the non-linear estimate of α_2 significantly differs form the linear one (Fig. 3.3); and for large value of χ, where the effect just mentioned is amplified. Since typical merger timescales t_m are of the same order of magnitude of $t_{\rm align}$, a factor 7 can be critical to predict if SMBHs have enough time to reach the aligned configuration before the merger (Sec. 4.4.3).

The probability distributions computed with $\alpha = 0.1$ are quite different from the others, because in this case we remove from the alignment process all the events with negative viscosity coefficient (Sec. 4.3.3). This is clearly evident in Figs. 4.5 and 4.6 where the overall normalization of the $\alpha = 0.1$ case is evidently different from the others. However, even such a strong assumption does not affect significantly the shape of the distributions which is determined by the effects described above. Negative viscosity events have been removed also to computed the average values reported in Table 4.1.

4.4.3 Timescale comparison

Our main result is that the alignment timescale significantly increases for rapidly rotating BHs: they could therefore reach the merger in a misaligned configuration. We detail here a preliminary analysis of the timescale argument presented in Sec. 4.2. A detailed treatment of the shrinking timescale is needed to improve the present result, as sketched in Sec. 4.5.

To predict if SMBHs can be ejected by their galactic bulges after a merger, the alignment timescale should be compared with some estimate of the merger timescale t_m. Here we simply take $t_m = 10$ or $50\,$Myrs, as generally predicted by Escala et al. (2004, 2005); Dotti et al. (2006); Mayer et al. (2007a) and Dotti et al. (2009b).

We show in Fig. 4.7 the probability that the alignment timescale is smaller than $t_m = 10\,$Myrs (top panel) and $t_m = 50\,$Myrs (right panel) as a function of the spin parameter χ, for various choices of α. These plots contains 500 Monte Carlo realization (5 values of α and 100 values of χ) with $N = 10^4$ events each one; both θ and $f_{\rm edd}$ are randomly generated like in Fig. 4.6.

Alignment is efficient for small spin parameters, where we expect most spins to align or counter-align with their discs by the time the binary approaches coalescence. However this is not true for larger spins. In particular, for $\chi > 0.5$ we expect a sizeable fraction of the systems, of the order of 30-40% (or even more for extreme Kerr BHs), to not reach the

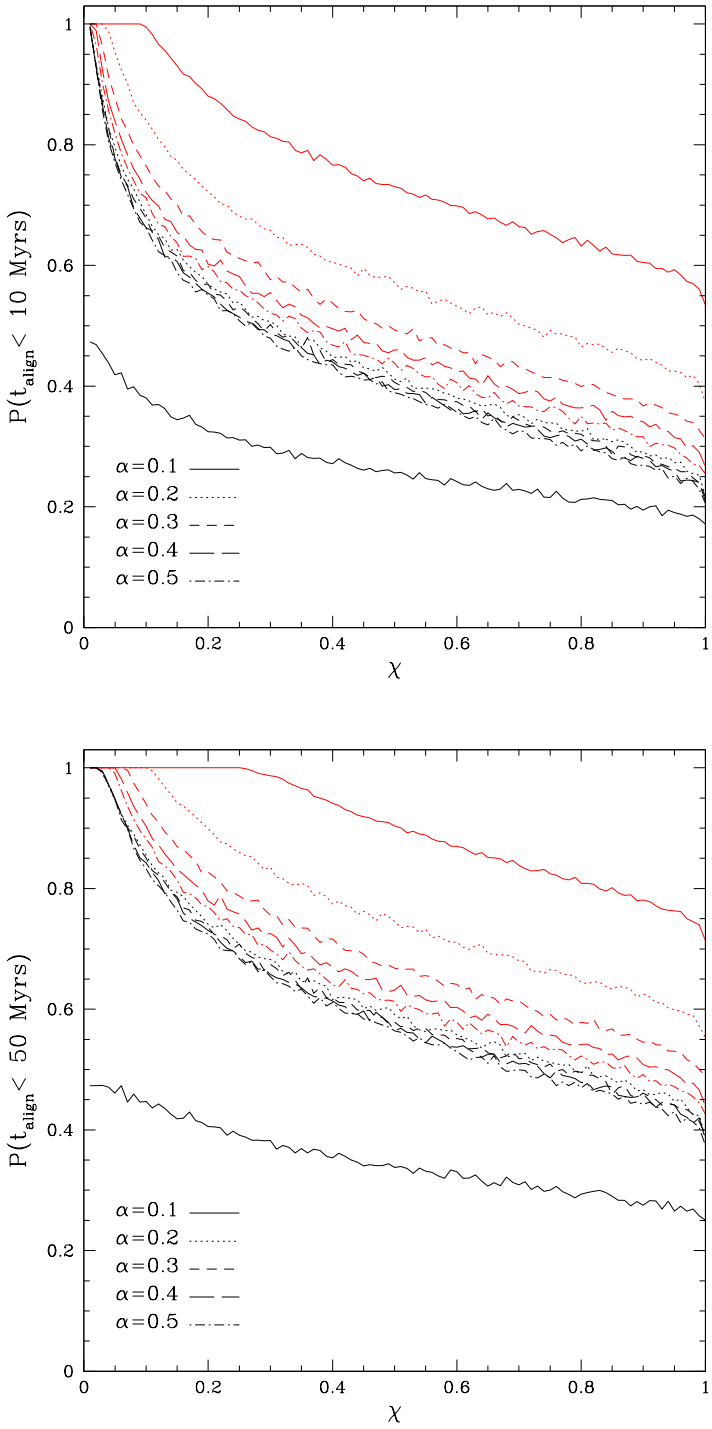

Figure 4.7: Alignment timescale cumulative distributions (Lodato and Gerosa 2013): probability that $t_{\rm align}$ is smaller than 10 Myrs (left panel) or 50 Myrs (right panel), as a function of the spin parameter χ, for various choices of α. For large values of a, a sizeable fraction of systems are likely to have residual spin misalignments after a binary shrinking time. The red lines show the corresponding probabilities in the case where we use the linear approximation (3.53) and we thus do not consider the effect of the warp non-linearities.

aligned configuration after 10 Myrs. The result is still present for 50 Myrs, in which case obviously the BHs have more time to become aligned. However, it can be seen from Fig. 4.7 that our findings are not very sensitive to the proxy chosen (10 or 50 Myrs), ensuring that our results are robust with respect to different choices of the merger timescale.

To emphasize the effect of the warp non-linearity we show the alignment timescale cumulative distributions both including the warp non-linearities (black lines) and considering the small-ψ approximation of Eq. (3.53) (red lines). The effect of the non-linearities is clearly very significant. In particular, it turns out that in the linear case the alignment probability has a much stronger dependence on α. This happens essentially because in the non-linear case the range of values of α_2 as a function of α is much smaller than in the linear case (see Fig. 3.3, where α_2 approach a constant value for large ψ). As noted above, the alignment process is much faster in the non-linear case, especially for low α.

For $\alpha = 0.1$, the probability of alignment does not approach 1 for $\chi \to 0$, even if $t_{\rm al} \to 0$: this result is a consequence of our strong assumption of removing all the events with $\alpha_1 < 0$ from our sample. A more precise treatment of broken discs is needed to overcome this unphysical result (see Sec. 4.3.3). For larger α, the azimuthal viscosity is positive for every event and our results are almost independent on the actual value of α.

Since the alignment timescale is inversely proportional to $\dot{M}$, larger Eddington ratios (such as those assumed by Bogdanović et al. 2007) imply faster alignment. Even in the simpler cases where we keep the Eddington ratio fixed, we find that alignment within 10 Myrs occurs only for $\chi < 0.6$ and $\chi < 0.3$ for $f_{\rm edd} = 0.1$ and $f_{\rm edd} = 0.01$, respectively.

4.4.4 Limitations

Our model is certainly very idealized and could be refined in several ways.

First of all, we have used a uniform logarithmic distribution of the Eddington value without considering in a detailed way how do tidal effects and gap opening (Artymowicz and Lubow 1996) affect the accretion rate on the binary elements. One would expect that the discs surrounding BHs in a binary system might have somewhat smaller accretion rates than in isolation.

A second important limitation of our work comes from the assumption that the length-scale over which the disc inclination varies is comparable with the disc size. This results in the approximation $\psi = \theta$. Our assumption goes in the direction of underestimating the alignment timescale, since if the warp occurs over a short lengthscale even a relatively small initial misalignment might be more difficult to realign. As stressed in Sec. 4.3.1, one would need to explicitly solve for the disc shape to take this effect into account. A self-consistent time-dependent calculation is not available at the moment. As a consequence, we restricted our study to a timescale argument, which prevented us from quantifying the exact degree of misalignment at the end of the merger. Residual misalignment can be estimated only with a detailed time-dependent calculation of the galactic-scale disc dynamics, like in Dotti et al. (2010, 2013). We hope our work may stimulate further generalizations of the present solutions (e.g. Scheuer and Feiler 1996; Martin et al. 2007; Chen et al. 2009) to consider in a self-consistent way the full non-linear theory of warp propagation.

Third, our choice of $t_{\rm m} = 10$ and 50 Myrs as proxies for the shrinking timescale is clearly very simplified, and might in particular be a function of the system parameters, such as the accretion rate and the mass ratio of the binary. Large values of $t_{\rm align}$ can be due to small values of $\dot{M}$ and should therefore be compared with a lower shrinking timescale, suitable for such gas-poorer environments. A possible way to overcome this limitation is presented in Sec. 4.5.

Finally, we have considered only the interaction of the BH spin with the accretion disc. Relativistic effects may modify the spin direction after the decoupling. A PN approach is needed to follow the evolution of the spins at small separations, taking into account the possible role of spin-orbit resonances (Schnittman 2004; Kesden et al. 2010a,b; Berti et al. 2012b). Since resonant locking will be the main subject of the second part of this work, we remind to the related discussion in Chapter 6. Briefly, spin-orbit resonances are triggered

by an asymmetry between the spin misalignment angles at the decoupling. If the BHs that form a binary approach the decoupling with two different residual misalignments, PN resonances can force the two spins to lie in the same plane (*resonant plane locking*). The key effect to introduce a spin asymmetry could be dependance of the accretion rate in $t_{\rm align}$. In binaries with a large mass ratio, where accretion occurs preferentially onto the secondary, the primary might be much harder to align.

4.5 Inspiral timescale

One of the weakest points in our timescale argument is the choice of the merger timescale. In particular, the shrinking timescale may depend on the same parameters of the alignment timescale, such as α and M. Each value of $t_{\rm align}$ should be compared with its own associated value of $t_{\rm m}$, rather than with fixed thresholds like 10 and 50 Myrs. A BH merger is the result of three different phases, where the shrinking is caused by dynamical interactions with stars, viscous interactions with the accretion disc and GW emission (Sec.2.1.2). The bottleneck of the process is the second phase (Fig. 2.2), where even a gas-rich environment may not be efficient enough to decrease the separation in a Hubble time (*final parsec problem*). For this reason, the alignment timescale must be compared with the inspiral timescale in the disc-driven phase, before the decoupling. We do not consider other alignment effects that may arise in the (quick) GW-driven phase. A critical discussion is given in Sec. 4.4.4.

We derive in this Section the inspiral timescale of a BH binary due to interactions with a circumbinary disc. Three regimes can be separated, for different mutual relationships between the BH masses M_1 and M_2 (with $M_1 > M_2$) and the mass of the disc inside the binary orbit $M(a)$. In the first two regimes, the primary mass M_1 is assumed to be larger then both M_2 and $M(a)$, a situation which has been extensively studied in the context of planet formation (e.g Armitage and Rice 2005; Armitage 2010). The third regime instead restricts to comparable-mass BHs.

Type 1 migration. In the Type 1 regime of "planetary" migration, the perturbation caused by the secondary is small enough to not alter the structure of the disc. The torque on the secondary can be computed at the linear level showing that the secondary remains fully embedded within the gas disc, without any gap opening. The migration happens in this regime if viscosity acts quicker than the tidal torque which tends to open the gap. The inspiral occur in this regime if (Armitage 2010)

$$\frac{M_2}{M_1} \lesssim 10^{-5} \left(\frac{H/R}{0.01}\right)^{5/2} \left(\frac{\alpha}{0.1}\right)^{1/2} , \tag{4.20}$$

which not relevant in the SMBH context.

Hydrodynamic simulations of the Type 1 migration in the planetary context have been performed by Miyoshi et al. (1999); D'Angelo et al. (2002, 2003) and Bate et al. (2003); SMBH mergers in this regime are the main subject of Armitage and Natarajan (2002).

Type 2 migration. As the mass of the secondary increases

$$M_1 \gg M(a) \sim M_2 , \tag{4.21}$$

its presence ceases to be a mere perturbation in the disc of the primary. The disc reacts opening a gap around the secondary position, as we described in Sec. 3.4. Angular momentum is transferred from the secondary to the outer disc decreasing the binary separation. The inspiral timescale can be found studying the angular momentum conservation on the outer edge of the gap. The conservation equation (3.15) must be properly modified by the presence of the secondary (Papaloizou and Lin 1984; Lin and Papaloizou 1986a,b; Trilling et al. 1998). In general, a new term appears at the right-hand side of (3.15) to describe

the torque induced by the secondary to the disc. The torque can be easily written down by considering the backreaction of the disc on the secondary $-\partial L_b/\partial t$, where $L_b = M_2 a^2 \Omega$ is the angular momentum of the secondary (Lodato and Clarke 2004; Lodato et al. 2009). The angular momentum conservation of the disc ring just outside the gap reads

$$2\pi R^3 v_R \Sigma \Omega = 2\pi R^3 \nu \Sigma \frac{\partial \Omega}{\partial R} - \frac{\partial}{\partial t} M_2 a^2 \Omega \,. \tag{4.22}$$

The first term in (3.15) can be neglected because it is a first-order quantity in the (infinitesimal) ring width. The three different terms in (4.22) describes angular momentum advection, viscous torque and the torque induce by the secondary, respectively. Since we are considering the edge of the gap opened in the disc at the binary separation, we can set $R = a$, $v_R = \dot{a}$, $\Omega = \Omega(a)$ and $\Sigma = \Sigma(a)$. Assuming keplerian rotation $a^3\Omega^2(a) = GM_1$, we obtain

$$2\pi \Sigma \Omega a^3 \dot{a} = -3\pi \nu \Sigma \Omega a^2 - \frac{1}{2} \Omega M_2 a \dot{a} \,, \tag{4.23}$$

$$\frac{\dot{a}}{a} = -\frac{3}{2} \frac{\nu}{a^2} \frac{4\pi \Sigma a^2}{4\pi \Sigma a^2 + M_2} \,. \tag{4.24}$$

The inspiral timescale is (Syer and Clarke 1995; Ivanov et al. 1999; Lodato et al. 2009)

$$t_m = \frac{a}{|\dot{a}|} \simeq \frac{M_2 + M(a)}{M(a)} t_\nu(a) \,, \tag{4.25}$$

where $t_\nu(a) = a^2/\nu$ is the viscous timescale at the binary separation and we approximated the mass of the inner disc with $M(a) = 4\pi\Sigma(a)$. If the mass of the secondary is negligible $M_2 \ll M(a)$ (but large enough to open the gap), the inspiral timescale reduces to the viscous timescale $t_m \to t_\nu(a)$.

Type 2 migration and gap opening have been studied numerically by many authors, including by Bryden et al. (1999); Nelson et al. (2000); Kley et al. (2001); Papaloizou et al. (2001); D'Angelo et al. (2002, 2003); Bate et al. (2003); Schäfer et al. (2004) and Lufkin et al. (2004). They all assume for simplicity that angular momentum transport in the disc could be represented using a microscopic viscosity. Generalizations to turbulent discs can be found in Winters et al. (2003); Nelson and Papaloizou (2004) and Papaloizou et al. (2004). Nelson and Benz (2003a,b) focus instead on the transition between Type 1 and Type 2 behavior.

High mass ratio. The interaction between the disc and two comparable-mass BHs

$$M_1 \sim M_2 \gg M(a) \,, \tag{4.26}$$

is more complicated because the gravitational potential of the secondary cannot be neglected. The disc reacts opening a cavity of radius $\sim 2a$ around the binary. The process is typically studied by means of numerical simulations, and the inspiral timescale is derived using numerical results (MacFadyen and Milosavljević 2008; Cuadra et al. 2009; Roedig et al. 2011, 2012). To the best of our knowledge, Rafikov (2012) computed the first analytical expression for the inspiral timescale in the regime $M_2/M_1 = q \sim 1$. He presents an analysis of the circumbinary disc properties by reformulating the standard disc equations in terms of the viscous angular momentum flux $G = -2\pi\nu\Sigma R^3 \partial\Omega/\partial R$ instead of Σ. He found for the merger timescale

$$t_m \simeq \frac{1}{(1+q)} \frac{M_2}{M(a)} t_\nu(a) \,, \tag{4.27}$$

which reduces to (4.25) if $q \ll 1$ and $M(a) \ll M_2$.

4.5.1 Guess and improvement

We guess that a possible generalization of the merger timescale formulae could be

$$t_m \simeq \frac{1}{1+q}\frac{M(a)+M_2}{M(a)} t_\nu(a)\,, \tag{4.28}$$

Eq. (4.28) interpolates the previous Eqs. (4.25) and (4.27) in the different regimes. The different merger timescale expressions are plotted in Fig. 4.8 as a function of the mass of the secondary M_2. For simplicity we take $M_1/M(a) = 1000$ and $0.1M(a) < M_2 < M_1$. Our guess agrees with (4.25) (Lodato et al. 2009) in the low-mass-ratio regime, and with (4.27) (Rafikov 2012) when the mass of the two BHs is comparable.

Three main steps are still needed to improve our timescale procedure with a more precise estimate of the merger timescale.

i) Eq. (4.28) needs to be verified analytically, paying particular attention to the right pre factor. This could be done in principle by repeating and improving what presented by Rafikov (2012) and comparing with Haiman et al. (2009).

ii) Two timescale comparisons between $t_{\rm align}$ and $t_{\rm m}$ may be performed, one for each member of the binary. BH Masses and spins might be properly initialized using distributions from SMBH merger tree simulations (e.g. Volonteri et al. 2005, 2009, 2012; Berti and Volonteri 2008; Natarajan and Volonteri 2012), and further assumptions are needed on the disc properties.

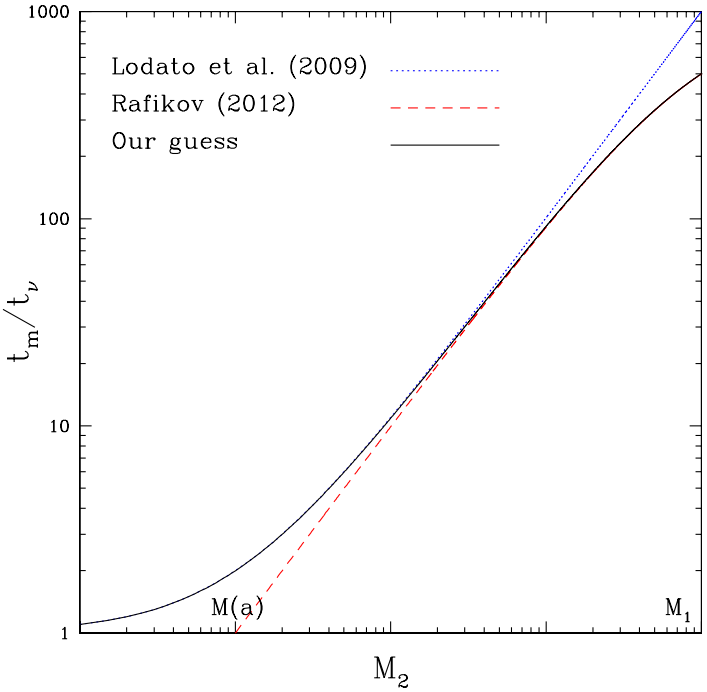

Figure 4.8: Inspiral timescales in unit of the viscous timescale, as a function of the mass of the secondary BH M_2. For simplicity we take $M_1/M(a) = 1000$ and $0.1M(a) < M_2 < M_1$. Dotted blue line shows the inspiral timescale for the Type 2 planetary migration (4.25), dashed red line shows the (4.27) valid in the comparable-mass regime; solid black line shows our guess formula (4.28) which approach the two previous results in their validity regimes.

iii) The difference between cicurmbinary disc and circumprimary/circumsecondary disc may become critical in this context. The accretion rates of the two individual discs enter the alignment timescales (4.11), while the accretion rate of the circumbinary disc may enter in the merger timescale through the viscous timescale. This three accretion rate values cannot be assumed to be independently distributed in a Monte Carlo simulation: they clearly are correlated because the individual discs are fed by the circumbinary disc. We need a coherent prescription to foresee which percentage of the mass from the circumbinary disc will end up accreting onto the primary or onto the secondary BH (see e.g. Artymowicz and Lubow 1996).

4.6 Are supermassive black holes slowly spinning?

We have revisited the arguments suggesting that gas disc are effective in bringing the spins of the two BHs in a merging binary into alignment. In particular, we have improved on every other previous estimates by taking into full consideration the reduction in the warp diffusion coefficient when the misalignment angle becomes large and consequently non-linear terms become important. Our results are consistent, at least within orders of magnitude, with the previous investigation by Perego et al. (2009) and Dotti et al. (2010) (Sec. 4.2): in particular, we find a similar dependence of the alignment timescale with respect to the spin of the BH and the Eddington ratio. Contrary to previous analysis, our estimates show that the alignment timescale is a strong function of the initial misalignment angle. This comes from having considered the full non linear warp propagation theory, instead of restricting to the small amplitude regime: this is a key element, because it allow us to compute a probability for the alignment process, based on the expected distribution of initial misalignments.

We find that if the BH are rapidly spinning ($\chi \gtrsim 0.5$), the system would not end up to be completely aligned, in up to 40% of the cases, at the time at which the two BHs are brought together at distances of the order of 0.01 pc, i.e. after $\sim 10^7$yr. Highly spinning BHs are more likely to be expected to maintain a significant misalignment, which may cause high recoil velocities and even SMBH ejections (Sec. 2.3). The current lack of observational evidence for strongly recoiling BHs (but see the two strong observed candidates in Sec. 2.2) suggests that the *average* BH spin is rather low. Our conclusion regarding the magnitude of the BH spin is related to the average properties of the BH population. Individual SMBH might well have large spins, and observations of broad iron lines (Sec. 1.2.3) would naturally be biased in their favor. On the contrary, if recoiling BHs are found to be more common, such limitation on the magnitude of the BH spin would not apply.

Our work is not the first claim that SMBHs in the Universe could be slowly spinning.

Our predictions clearly support the chaotic accretion picture. King and Pringle (2006, 2007) realize that a series of accretion episodes randomly distributed could explain SMBH formation from stellar-mass BH seeds far better than if SMBH were accreting form a single prograde accretion disc. Chaotic accretion can maintain the BHs to be slowly spinning over the cosmic time, thus allowing a quicker mass growth. The same argument has also been invoked to solve the final parsec problem (Nixon et al. 2011a,b, 2012a,b) and explain the $M - \sigma$ relationship (Nayakshin et al. 2012). Chaotic accretion has also been implemented in galactic scale simulations by Dotti et al. (2013), which however fail to properly consider the warp propagation.

Our finding are also in line with the values predicted by the Soltan argument relating the average SMBH mass to the radiation background of the Universe (Sec. 3.2.4). The totality of background light in the low-redshift Universe is compatible only with black-hole growth with a radiative efficiency $\epsilon \sim 0.1$ and consequently $\chi \sim 0.6$ (Sec. 3.2.1): this is exactly our threshold value to avoid SMBH ejections.

A complete different suggestion that SMBHs could be slowly spinning comes from a timescale analysis performed on AGN jets rather than SMBH merger. Babul et al. (2012) show that gas accretion onto SMBHs in AGNs can modify the spin/jet direction quick enough to fulfill the observational constraints, only if the spin magnitude is as low as $\chi \sim 0.1$. This

could provide an explanation to the *jets reorientation* phenomenon (Gallimore et al. 2006; Dunn et al. 2006; Forman et al. 2007; Wise et al. 2007; Hodges-Kluck et al. 2010). Babul et al. (2012) present also an interesting argument to estimate not only the alignment timescale, but also the residual misalignment. A complete aligned configuration can be reached only if the disc is massive enough to provide a mass flow to the BHs for at least one alignment timescale. They estimate the maximum mass of the disc that could be accreted and therefore the residual misalignment using angular momentum conservation (see also Nixon and King 2013). Unfortunately, the same argument cannot be applied to SMBH merger, where the alignment must be reached before the coalescence.

The cosmological co-evolution of SMBHs and their host galaxies is a significant open problem in our understanding of many high-energy astrophysics and GW topics, such as quasars, AGNs, SMBH binaries and mergers: with this work we outlined how the absence of recoiling BHs can give precious insights on the SMBH spin magnitude distribution.

Part II

Resonant locking in stellar-mass black-hole binaries

By examining the final, smooth black hole, one cannot in any way discover its past history. One cannot discern whether it was created by the coalescence of two smaller holes, or by the direct implosion of a star made of matter, or by the direct implosion of a star made of antimatter. The black hole has no hair *from which to decipher its history. However, the history is not entirely lost. A record has been kept: it has been encoded in the ripples of spacetime curvature that the coalescing holes emitted. Those curvature ripples are much like the sound waves from a symphony. Just as the symphony is encoded in the sound waves' modulations (larger amplitude here, smaller there; higher frequency wiggles here, lower there), so the coalescence history is encoded in modulations of the curvature ripples.*

And just as the sound waves carry their encoded symphony from the orchestra that produces it to the audience, so the curvature ripples carry their encoded history from the coalescing holes to the distant Universe.

K. Thorne, Black Holes and Time Warps:
Einstein's Outrageous Legacy (1994)

Chapter 5

Black-hole binary inspiral

In this second part of the thesis we study the interplay between astrophysics and GR in order to predict the statistical properties of observable stellar-mass BH binaries focusing in particular on the role of the spin orientation angles. We show how a comprehensive model including elements from populations synthesis physics and general-relativistic evolution is needed to model the spin evolution from large separations, where spin directions are determined by astrophysical formation processes, to small separations, where general relativistic spin-orbit couplings become important.

In this Chapter we also review the BH binary evolutionary equations in the GW-driven inspiral at the lowest PN order and we describe the main results obtained by population synthesis studies (in particular the `StarTrack` code) to predict BH binary expected rates.

The goal of the project is twofold: statistical predictions of spin configurations may help GW-data analysts to place templates to increase GW detection efficiency; on the other hand, when detections will be available, the comparison of our predictions with observations could provide precious insights on BH formation processes.

5.1 Preparing for gravitational-wave astronomy

Stellar-mass BH binaries are promising astrophysical sources for future GW detectors. The use of the matched filtering is needed to increase detection rate, but it requires detailed knowledge of the incoming waveform. This depends on the configuration of the binaries when they enters the sensitivity band of the detector. Understanding physical evolutionary processes could therefore help data analysts to place templates in well-defined regions of the parameter space to increase detection efficiency.

5.1.1 Stellar-mass black-hole binaries

Even in the most optimistic scenarios, the merger of extragalactic stellar-mass BH binaries is expected to be unobservable electromagnetically. Unlike mergers involving NSs, where several solar masses of baryons are available to radiate after the collapse, emission from BH binaries will be Eddington limited (Sec. 3.2.2). The Eddington luminosity for several solar mass BHs ($\sim 10^{39}\,\mathrm{erg}$) is small enough to make them very difficult to observe at extragalactic distances, and the expected stellar-mass galactic merger rate is $\sim 0.1\,\mathrm{Myr}^{-1}$ (Belczynski et al. 2007; Table 5.1). The first detection of a double BH will probably come from GW astronomy, and it will probably concern extra-galactic sources.

Observing GWs from BHs, individually or in binaries, will help to test some of the GR predictions in the strongly non-linear regime, as well as to constrain alternative theories of gravity (Press and Thorne 1972; Blanchet and Sathyaprakash 1994, 1995; Sathyaprakash and Schutz 2003, 2009; Horbatsch and Burgess 2012; Berti et al. 2012a). Radiation from

stellar-mass BHs is expected mainly from coalescing binary systems, when one or both of the components is a BH. The larger mass of BH systems makes them visible in GWs from a greater distance than neutron-star binaries: BH events will be much "louder" than those involving neutron stars. Although BHs are formed more rarely than neutron stars, because they require higher-mass progenitor stars, the spatial abundance of binary systems with BHs is amplified relative to neutron-star binaries, because binary systems are much more easily disrupted by NS formation than by BH formation. When a neutron star forms, most of the progenitor star's mass ($6M_\odot$ or more) must be expelled from the system rapidly to produce a $\sim 1.5M_\odot$ object. Due to the stronger gravity of BHs, material is expected to fall back onto the proto-neutron star, which typically reduces the kick received by the newly formed compact object (see Sec. 7.2.5 on SN kicks).

Double-BH systems may also be formed abundantly by capture processes in globular clusters, which could be efficient factories for BH binaries. Being more massive than the average star in a globular cluster, BHs sink towards the center via dynamical friction (Sec. 2.1.2), and this can lead to efficient binary formation (Portegies Zwart and McMillan 2000; Benacquista and Downing 2013).

5.1.2 Gravitational-waves searches for black-hole binaries

The life of a compact binary as a GW source can be divided in three main stages, each of them producing a different GW signal: inspiral, merger and ringdown (an artist representation is given in Fig. 5.1). During the inspiral phase the orbit of the binary decreases due to the emission of gravitational radiation, that carries energy away from the system. The separation can decrease until the BHs merge with each other into a more massive BH. The merger remnant is a highly distorted BH that approaches its final equilibrium configuration (a stationary Kerr solution) by emitting GWs of characteristic frequencies and damping times: this is known as the ringdown phase (e.g. Berti et al. 2006, 2009).

Recent GW searches from double BH binaries with the four detectors of the LIGO/Virgo network are described in Abadie et al. (2011, 2012a) end Aasi et al. (2013). As outlined in Sec. 1.3.5, GW signals are extracted by matched filtering, which consists of computing the cross-correlation between the noisy detector output and a predicted template. Efficient

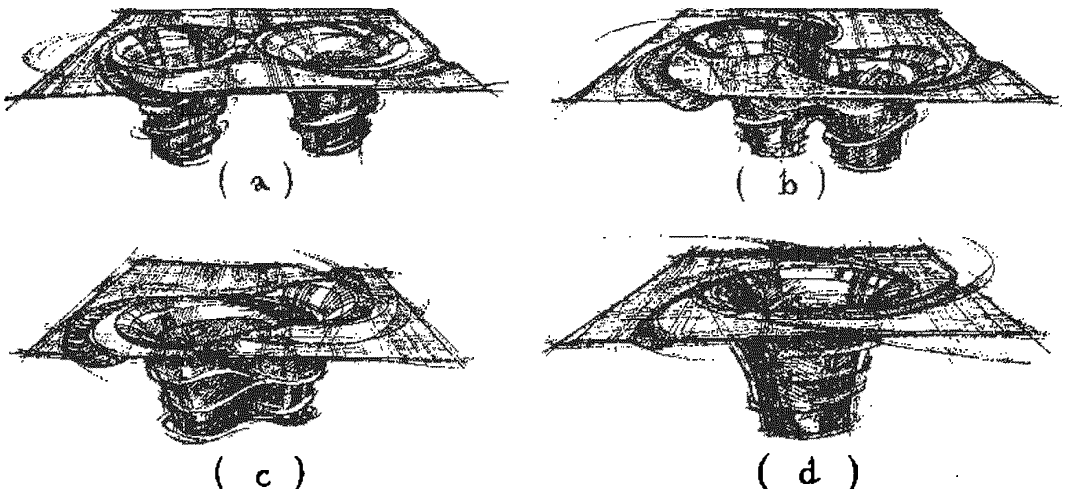

Figure 5.1: Artistic embedding diagrams depicting the curvature of spacetime around two merging BHs (Thorne 1994). The BH event horizons are represented by the circles at the bottom of the pits. Two interacting BHs are present during the inspiral phase (a-b); the horizons merge just before diagram (c) into a deformed BH; this deformation is carried away by GWs in the ringdown phase (d).

detection requires a detailed knowledge of template waveforms which is sensitive to the binary configuration when the GW signal enters the detector sensitivity band. Predicted waveforms are an invaluable tool for GW observations (see the detailed discussion in Cutler et al. 1993; Cutler and Flanagan 1994). The template waveforms currently used in some of the LIGO/Virgo pipelines to search for binary coalescence model the evolution in all the three phases of inspiral, merger and ringdown (IMR); others kind of searches are instead restricted to a single phase. GW emission from the merger phase can only be simulated numerically: IMR waveform models are obtained using numerical relativity simulations as guides to build analytical templates that can be generated more rapidly, sampling a larger range of binary parameters. IMR templates are currently constructed in two main ways. In the effective-one-body approach, the two-body problem is approximated with an effective-one-body description which is then tuned with numerical simulations: a PN-resummed Hamiltonian is provided which can be used to evolve a binary system and predict the GW signal (Buonanno and Damour 1999, 2000; Damour et al. 2000, 2003; Buonanno et al. 2007a,b; Damour et al. 2008a,b; Boyle et al. 2008; Pan et al. 2008, 2011; Damour and Nagar 2009; Damour 2012). In the phenomenological IMR model, the numerical merger waveforms are matched directly to PN inspiral waveforms and used to tune phenomenological parameters in the frequency domain (Ajith et al. 2007, 2008, 2011; Ajith 2008).

The number of observationally distinguishable predicted templates should be extremely large (Owen and Sathyaprakash 1999), both because of the large and strongly mass-dependent number of cycles in each signal and because the emitted waveform depends sensitively on as many as seventeen different parameters. Seven parameters are related just to the relative position of the source and the detector: they consist of the source position (distance, right ascension and declination), two angles defining the orientation of the orbital plane, the phase at coalescence and the time of coalescence. These are "extrinsic" parameters, which are independent of the model of the source. For a BH binary we should obviously add the masses of the BHs, or (equivalently) their total mass and the mass ratio. If the BHs are spinning the signal depends also on the components of each spin vector (or equivalently on the magnitude of each spin and two angles defining the spin orientation). Masses and spins are "intrinsic" parameters, which affect the time evolution of the wave amplitude and phase. The waveform of a circular BH binary has fifteen different parameters, but if we allow the orbit to be eccentric we should add also the eccentricity and one angle defining the orientation of the ellipse on the orbital plane.

Do we really need all these parameters? The difficult task of exploring such a high-dimensional space can be simplified if nature provides physical mechanisms that cause astrophysical binaries to cluster in restricted portions of the parameter space. We will show in the next Section (Peters and Mathews 1963; Peters 1964) that, due to the emission of GWs, the eccentricity of a BH binary is expected to be very small by the time sources enter the sensitivity band of the detectors. This assumption may not be valid if the binary is found in a very dense astrophysical environment, such as a globular cluster, in which three-body interactions can play a leading role in the dynamics (O'Leary et al. 2009).

The question we address here is: *does binary evolution cluster the spin parameters in certain regions of the parameter space?* We address such a possibility by combining astrophysical binary formation models with the PN resonant locking discovered by Schnittman (2004).

5.2 The interplay between astrophysics and relativity

BH binaries enter the sensitivity band of GW detectors during the inspiral phase, which is the main subject of our study. We study the inspiral of a stellar-mass compact binary using three different approaches. At large separations the shrinking is due to interactions with the astrophysical environment. Unlike SMBHs for which exchange of angular momentum with the accretion disc can drive the binary (Sec. 2.1.2), stellar-mass BH shrinking in this phase is typically due to astrophysical mechanisms related to BH formation from stellar

collapse (mainly SN kicks and common-envelope phase, Secs. 5.3.1 and 7.1.1). As in the supermassive case, when the gravitational radiation inspiral timescale becomes smaller than the Hubble time, the dynamics of the binary decouples from the astrophysical environment. At such small separations, the inspiral is driven by GW emission in GR. Unfortunately the two-body problem in GR cannot be completely solved analytically. Following a major breakthrough in 2005 (Pretorius 2005; Baker et al. 2005; Campanelli et al. 2006) numerical relativity can now be used to follow the evolution of the binary during the least few cycles before the merger. These simulations unveiled unexpected consequences of BH mergers, such the superkick phenomenon described in Sec.2.3. Even now, however, these studies are computationally very expensive. Between these two extreme regimes, i.e. when the evolution is dominated by GW emission but GR effects are weak, the evolution can be studied using the PN approximation. Short introduction to the PN approach will be given in Sec. 6.1.

At the PN level, the equilibrium configurations discovered by Schnittman (2004) may lock the spins with well defined orientations. *Do BH binaries keep memory of their formation during the PN resonant locking? Which insight on BH formation from massive star progenitor can be gained with GW observations?*

5.2.1 Gravitational-wave driven inspiral

We briefly derive here the evolutionary equations for the inspiral of BH binaries due to GW emission at the lowest (Newtonian) order, following Buonanno (2007) and Maggiore (2007).

Let us consider a binary system with masses m_1 and m_2, total mass $M = m_1 + m_2$, mass ratio $q = m_2/m_1$ and reduced mass $\mu = m_1\, m_2/(m_1 + m_2)$. We assume for simplicity that the BH far apart (so their orbital dynamics use described by Newtonian physics) and that they move on a circular orbit. Our goal is to compute the traceless quadrupole tensor for this source, and then plug it into the quadrupole formula (Sec. 1.3.2). In a set of coordinates with the z-axis oriented along the orbital angular momentum of the binary, the reduced mass position is defined by

$$\begin{cases} x(t) = a\, \cos \Omega t\,, \\ y(t) = a\, \sin \Omega t\,, \\ z(t) = 0\,, \end{cases} \tag{5.1}$$

where a is the binary separation and Ω is the orbital frequency. The quadrupole traceless mass tensor (1.50) reduces to

$$Q_{ij} = \mu\, x_i x_j - \mu \frac{1}{3}\, \delta_{kl}\, x_k x_l\,. \tag{5.2}$$

The total power radiated in GWs can now be computed using (1.51), and it is equal to the orbital energy variation rate

$$P = -\frac{dE}{dt} = \frac{32}{5} \frac{G\mu^2 a^4 \Omega^6}{c^5}\,. \tag{5.3}$$

At the (dominant) Newtonian order, $E = -G\mu M/2a$ and $\Omega^2 = GM/a^3$, which leads to

$$\frac{da}{dt} = -\frac{64}{5} \frac{G^3 M^3}{c^5 a^3} \frac{q}{(1+q)^2}\,. \tag{5.4}$$

GW emission causes the binary to shrink with a rate scaling as $\dot{a} \sim a^{-3}$, while the inspiral timescale $|a/\dot{a}| \sim a^4$ (cf. also Sec. 2.1.2).

These results can be generalized to eccentric binaries. In this case, two coupled equations describing the evolution of the binary semi-major axis a and eccentricity e drive the dynamics

at the leading, Newtonian order (Peters and Mathews 1963; Peters 1964):

$$\frac{da}{dt} = -\frac{64}{5}\frac{G^3M^3}{c^5a^3}\frac{q}{(1+q)^2}(1-e^2)^{-7/2}\left(1+\frac{73}{24}e^2+\frac{37}{96}e^4\right), \tag{5.5}$$

$$\frac{de}{dt} = -\frac{304}{15}e\frac{G^3M^3}{c^5a^4}\frac{q}{(1+q)^2}(1-e^2)^{-5/2}\left(1+\frac{121}{304}e^2\right). \tag{5.6}$$

For example, from the above equations we have $da/de \sim (12/19)(a/e)$ and consequently $a \sim e^{12/19}$. The eccentricity decreases faster than the separation: deviations from the circular inspiral become smaller and smaller as the separation decreases. Fig. 5.2 shows the merger timescale in the GW-driven phase for BH binaries of total mass $M = 10M_\odot$ and mass ratio $q = 0.8$ (which is the same value used in Chapter 7). The coupled differential equations (5.5) and (5.6) are solved numerically from initial values a_0 and e_0. We plot on a color-coded scale the time necessary[1] to reach $a \simeq 0$. Integrations are performed using the StepperDopr5 routine developed in Press et al. (2002). The merger timescale increases with the initial separation a_0, because a very small amount of energy is emitted when the BHs are far from each other ($P \sim a^{-5}$, from Eq. 5.3). Highly eccentric binaries will merge quicker because less angular momentum has to be emitted (see Eq. 3.1) and more radiation is emitted at periastron because the bodies are closer to each other.

Further PN corrections of these evolutionary equations in the case of elliptic orbits can be found in Damour et al. (2004), Sperhake et al. (2008a) and references therein. In this work we use the standard Peters equations (5.5) and (5.6) to select merging binaries because they give the timescale of the process within the level of accuracy that we require (Sec. 7.1.2). The BH inspiral described in Chapter 6, is modeled in far more detail using higher-order corrections for *circular* orbits.

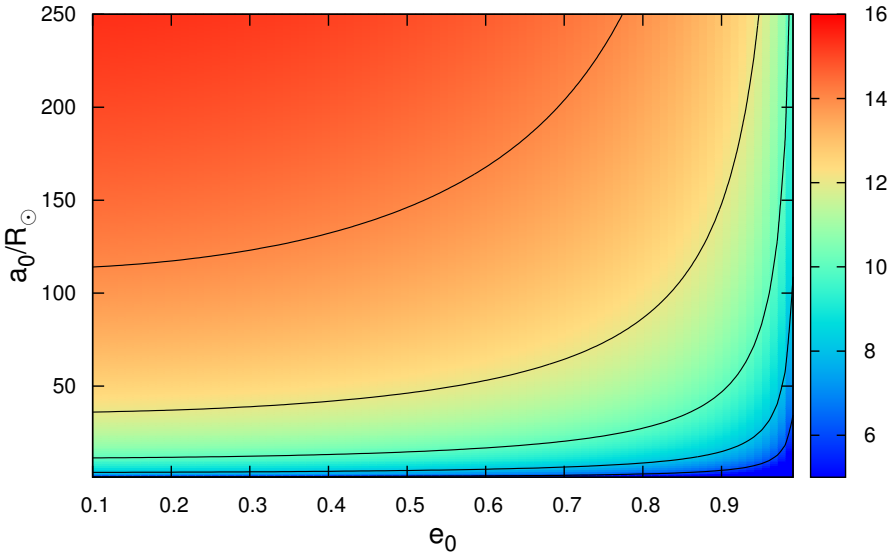

Figure 5.2: Merger timescale in the GW-driven inspiral for BH binaries with $M = 10M_\odot$ and $q = 0.8$. The color-coded map shows (on a logarithmic scale the time needed (in yrs) for a BH binary with semi major axis a_0 and eccentricity e_0 to reach coalescence. Black lines mark $10^6, 10^8, 10^{10}, 10^{12}$ and 10^{14} yrs from bottom to top respectively. The calculation was performed by numerically integrating Eqs. (5.5) and (5.6).

[1]We cannot formally reach the final separation $a = 0$, because the system becomes stiff: in practice we follow the solutions down to fiducial separations $10^{-8}a_0$, which are well outside the range of separations where Eqs. (5.5) and (5.6) are valid.

5.2.2 Length scales

We review here the length scales associated with the formation, inspiral, and merger of BH binaries. The well-defined hierarchy of these length scales demonstrates the necessity of our joint analysis of astrophysics and PN evolution.

GW emission causes a binary with a semimajor axis less than

$$a_{GW} = 45 \left(\frac{M}{10M_\odot}\right)^{3/4} \frac{q^{1/4}}{(1+q)^{1/2}} f^{1/4}(e)\, R_\odot\,. \tag{5.7}$$

to merge on a timescale less than the Hubble time $t_{\rm H} \simeq 10^{10}$yrs (Peters and Mathews 1963; Peters 1964). The function $f(e)$ is defined through Eq. (5.5):

$$f(e) = (1-e^2)^{-7/2}\left(1 + \frac{73}{24}e^2 + \frac{37}{96}e^4\right)\,. \tag{5.8}$$

Astrophysical processes leading to BH formation, include mass transfer, SN explosions and common envelope evolution, and they are required in order to shrink the binary down to separations smaller than $a_{\rm GW}$. GW emission also circularizes the binary at separations comparable to $a_{\rm GW}$. PN spin-orbit couplings become important at much smaller separations (Schnittman 2004; Kesden et al. 2010a)

$$a_{\rm PNi} \sim 10^3 \frac{GM}{c^2} \simeq 10^{-2}\left(\frac{M}{10M_\odot}\right) R_\odot\,, \tag{5.9}$$

below which they can lock binaries into resonant configurations with well defined spin directions (Sec. 6.3). The peak GW frequency emitted from a compact binary is given by twice the orbital frequency:

$$f_{\rm GW} = 2 \times \frac{\Omega}{2\pi} = \left(\frac{GM}{\pi^2 a^3}\right)^{1/2}\,. \tag{5.10}$$

Resonant locking is therefore important at separations above

$$a_{\rm LIGO} \simeq 10^{-3}\left(\frac{M}{10M_\odot}\right)^{1/3}\left(\frac{f_{\rm GW}}{20{\rm Hz}}\right)^{-2/3} R_\odot\,, \tag{5.11}$$

at which the binary reaches the lower limit $f_{\rm GW} \simeq 10 - 20\,{\rm Hz}$ of the Advanced LIGO/Virgo sensitivity band. The third-generation Einstein Telescope is expected to reach even lower frequencies of order $f_{\rm GW} \simeq 1\,{\rm Hz}$. Since these frequencies are well within the regime where PN resonances are important, a unified treatment of the astrophysical initial conditions and of the subsequent PN evolution of the binary is essential to determining which spin configurations are most relevant for GW detectors. Such a treatment is the main goal of this work.

5.3 Astrophysics of black-hole binary formation

Isolated BH binaries do not emit electromagnetically and hence have yet to be observed. Despite this lack of evidence, they are a likely outcome of the evolution of massive stellar binaries. The rate at which they form can be inferred from observations of their progenitors and from systems like binary NSs, that have similar formation channels. Formation rates can also be calculated theoretically using population-synthesis models.

We first describe the main evolutionary stages leading to BH binary formation and then we review the available theoretical predictions, focusing in particular on the `StarTrack`

code. Present model do not keep track of the spin orientation during the formation of a BH binary. In order to fill this gap, we build an astrophysical model that simplifies the standard evolutionary picture to highlight only those physical processes that affect spin directions (Sec. 7.1).

5.3.1 Formation stages

Historically, the evolutionary scenarios for massive binaries were introduced after the discoveries of X-ray binaries (see Sec.1.2.1, van den Heuvel and De Loore 1973), and they are now considered as standard. Following Postnov and Yungelson (2006), the evolution of a massive binary star leading eventually to a compact binary can be divided in ten stages, as summarized in Fig. 5.3. The reader can compare Fig. 5.3 with the analogous Fig. 7.1 of our astrophysical model, which focuses on spin directions.

1) The initial system is composed of two massive binary stars, with both stars on the upper main sequence (O-B type). The duration of this stage is determined by the time the primary spends on the main sequence burning hydrogen, that typically is $\sim 10^6$ yrs. While hydrogen burning proceeds, a central helium core is formed. The expected number of such binaries in the Galaxy is $\sim 10^4$.

2) After exhaustion of the hydrogen in the core, the primary star evolves into a supergiant and leaves the main sequence. During the rapid supergiant expansion, the radius of the primary star may approach the Roche lobe of the system, starting a mass transfer phase onto the secondary (main sequence) star. The mass transfer ends when most of the primary's hydrogen envelope is transferred onto the secondary: a naked helium core is left behind, which can be observed as a Wolf-Rayet star (Nugis and Lamers 2000). The secondary star is expected to acquire large angular momentum due to the infalling material, so that its outer envelope can be spun up. Such massive rapidly rotating stars are observed as Be stars (Porter and Rivinius 2003). During this mass transfer stage, the semimajor axis of the orbit first decreases, reaches a minimum when the masses of the binary components become equal to each other, and then increases. This picture is complicated by stellar wind: mass loss induced by stellar wind removes matter from the binary, thus increasing the binary separation. The duration of the first Roche-Lobe overflow is rather short, of the order of 10^4 yr, so only several dozens such binaries are expected to be in the Galaxy.

3,4) The duration of the helium-burning stage is $\sim 10^5$ yrs, and all the subsequent reactions are completed very quickly. The primary star explodes as a Ib or Ic SN, and a NS or a BH is formed. The inferred Galactic type Ib SN rate is around 10^{-2} per year, and half of the exploding stars may be in binary systems (Postnov and Yungelson 2006). Due to the asymmetry of the SN explosion, a kick is imparted to the newly formed compact object (Sec. 7.2.6), that may unbind the binary. The companion in this case will end up being a runaway OB-star.

5) If the system remains bound after the first SN, it will be formed by a massive main sequence star and a compact object. The orbital eccentricity after the SN explosion may be large enough (cf. Eq. 7.39) that accretion episodes onto the compact object can occur at every periastron passage, reducing the mass of the companion. This can cause further X-ray emission, as observed in ~ 100 Galactic Be/X-ray binaries (Raguzova and Popov 2005). In the NS case, these accretion episodes spin-up the NS rotation, producing a recycled pulsar (Srinivasan 2010). This phase lasts until the secondary's hydrogen is depleted.

6,7) The secondary evolves into a supergiant, reaching a radius that is typically bigger than the binary separation. The *common envelope* stage consists in a helium Wolf-Rayet star and a NS/BH companion surrounded by a single expanding envelope. This phase still presents many uncertainties, such as the efficiency of the process (see Sec. 7.2.4)

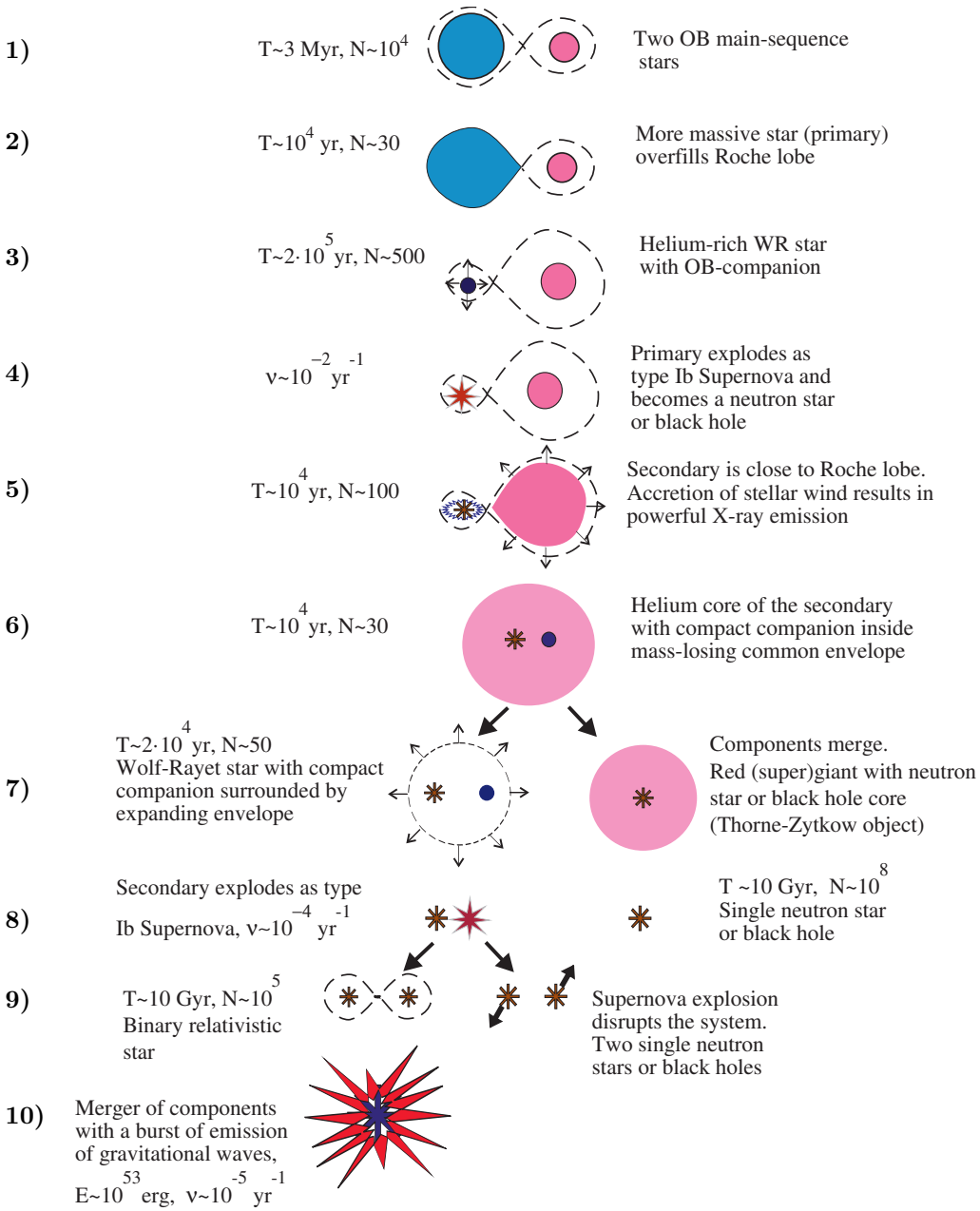

Figure 5.3: Evolution of a binary star leading to formation of a compact binary composed of BHs and/or NSs (Postnov and Yungelson 2006).

and the role of the material accreted from the compact object during this phase. Hyper-Eddington accretion onto a NS is possible in general if the gravitational energy released in accretion is lost by neutrinos (Colgate 1971; Zel'dovich et al. 1972), and this may be the case for the accretion in common envelopes (Chevalier 1993). A predicted consequence is that a NS in this stage may collapse to a BH inside the common envelope. Further complications have been pointed out, because a hyper-Eddington regime may be prevented by the angular momentum of the captured matter and the magnetic field of the NS (Brown et al. 2000). The NS/BH and the helium core may also merge during the common envelope phase to form a (hypothetical) Thorne-Zytkow object (Thorne and Zytkow 1975, 1977).

8,9,10) The secondary star, now reduced to a helium core, explodes as a SN and forms a second compact object. The outcome of the explosion can be a compact binary, or two single compact objects if the system is disrupted by the explosion. For the case of double NS systems, the older NS is expected to have faster rotation velocity than the younger one because of the recycling at the preceding accretion stage. The subsequent orbital evolution of such compact binary systems is due only to GW emission (see Section 5.2.1).

Possible evolutionary channels which produce merging NS and/or BH binaries have been extensively studied in the literature (e.g. Bagot 1997; Wettig and Brown 1996; Dewi and van den Heuvel 2004; Willems and Kalogera 2004). Predictions are currently made using populations synthesis codes (see Sec. 5.3.2). At variance with scenarios involving only NSs, formation models of binaries involving BHs must include different parameters, such as the threshold zero-age main sequence mass necessary to form a BH (van den Heuvel and Habets 1984; Woosley et al. 1995; Portegies Zwart et al. 1997; Fryer 1999), the mass of the forming BHs (Timmes et al. 1996; Bethe and Brown 1998; Fryer 1999; Fryer and Kalogera 2001) and their spins (Sec. 5.3.4).

5.3.2 Population synthesis: rate predictions

The main method used to study the formation and evolution of compact binaries is called *population synthesis*, and it basically consists of Monte-Carlo simulations of samples of binaries spanning a wide range of astrophysical parameters (Kalogera and Belczynski 2001; Popov and Prokhorov 2007).

There are several population synthesis codes used in the literature to model massive binary evolution, which take into account with different degrees of completeness various aspects single and binary stellar physics. We will pay special attention to the `StarTrack` code (Belczynski et al. 2002, 2008a) that is used to build parts of our spin evolution model. Other codes include `BSE` (Hurley et al. 2000, 2002), `Binary_c` (Izzard et al. 2006), `SeBa` (Portegies Zwart and Verbunt 1996; Nelemans et al. 2001a,b; Toonen et al. 2012), a code developed by the Brussels group (De Donder and Vanbeveren 2004; Mennekens et al. 2010) and those used in Tutukov and Yungelson (1993a,b); Lipunov et al. (1997); Portegies Zwart and Yungelson (1998); Voss and Tauris (2003); de Freitas Pacheco et al. (2006).

Some results of population synthesis calculations of compact binary mergers carried out by different groups are presented in Table 5.1, which shows the predicted galactic merger rates for double compact systems. These predictions must be taken with a grain of salt, because of the great number of parameters involved in these Monte Carlo simulations, many of which still poorly constrained (or even unknown) (Eggleton 2006; Paxton et al. 2010, 2011). Population synthesis studies still need to be calibrated against statistically significant samples of observations; and this may only happen when GW astronomy becomes a reality. Some work has been done using binary pulsar statistics in connection with double pulsar observations (Kalogera et al. 2004a,b): the results obtained agree with the population synthesis estimates if SN kicks are in the range $(250-300)$ km s^{-1}, a range which is also considered likely from statistical studies of pulsar proper motion observations (Hobbs et al. 2005; Sec. 7.2.5).

In order to obtain predictions of event rates for GW interferometers, the synthetic merger rates must be converted to detection rates for a given detector/network configuration. The actual detection threshold for a network of GW detectors will depend in general on the positions of the detectors in the network, the characteristics of each detector noise, and the search strategy used (Brady and Fairhurst 2008). Given the galactic merger rate for a compact source $\mathcal{R}$ (i.e. any of the numbers in Table 5.1), the detection rate is given by

$$\dot{N} = \mathcal{R} \times N_G \,, \tag{5.12}$$

where N_G is the number of accessible galaxies in the given experimental configuration. The LIGO/Virgo collaboration (Abadie et al. 2010) provides the following formula as a good approximation to N_G in their detectors, once the galaxy density variations are averaged out at larger distances ($\gtrsim 30$ Mpc):

$$N_G = \frac{4}{3}\pi \left(\frac{D_{\rm horizon}}{\rm Mpc} \right)^3 (2.26)^{-3} (0.0116) \,, \tag{5.13}$$

where $D_{\rm horizon}$ is the "horizon" (maximum observable) distance reached by a given detector configuration as reported in Table 5.2. The factor 1/2.26 in (5.13) is the correction factor used to average over all sky locations and orientations (Finn and Chernoff 1993; Finn 1996); the factor 1.16×10^{-2} Mpc^{-3} is the extrapolated density of galaxies in space (Kopparapu et al. 2008). The final expected rates for the LIGO/Virgo network are reported in Table 5.2, using assumptions that are carefully discussed by (Abadie et al. 2010).

5.3.3 The `StarTrack` code

`StarTrack` is a population synthesis code which builds upon previous analytical studies of single and binary stellar evolution by Hurley et al. (2000, 2002). The main features of the code are described in Belczynski et al. (2002, 2008a). `StarTrack` is meant to be a comprehensive simulation framework for a general stellar environments with special regard to the formation of binaries and the endpoint of binary evolution. The calibration of the parameters used in the code is obtained from available (mainly NS) observations (O'Shaughnessy et al. 2005a,c, 2007, 2008b).

`StarTrack` has been applied and tested on a large variety of astrophysical topics and objects, including statistical comparisons with Chandra observations (Belczynski and Taam 2004b; Sepinsky et al. 2005); predictions of mass ratio (Bulik et al. 2004b), chirp mass (Bulik and Belczyński 2003), and eccentricity (Ihm et al. 2006; Kowalska et al. 2011) distributions in compact binaries; rates (Ruiter et al. 2009; Fryer et al. 2010; Ruiter et al. 2011, 2013) and progenitors (Belczynski et al. 2005) for type Ia SN explosions; compact binaries in globular clusters (Ivanova et al. 2005, 2006; Willems et al. 2007; Ivanova et al. 2008); ultracompact binaries (Belczynski and Taam 2004a); high-redshift X-ray binaries (Belczynski et al. 2010c; Fragos et al. 2013); mass distributions of BHs and NSs (Bulik et al. 2004b; Belczynski et al. 2010b, 2012; Fryer et al. 2012); frequency of BHs in binaries (Belczynski et al. 2004b, 2006b); recycled pulsars (Belczynski et al. 2010d); Be X-ray binaries (Belczynski and Ziolkowski 2009); high-mass X-ray binaries (Linden et al. 2009); ultraluminous X-ray sources (Blecha et al. 2006); short gamma-ray bursts and their connection with double NS mergers (Belczynski et al. 2006a, 2008b; O'Shaughnessy et al. 2008a). The code predictions have also been compared with observations of selected astronomical sources (Belczynski et al. 2004a; Willems and Kalogera 2004; Willems et al. 2006; Fragos et al. 2008, 2009a; Belczynski and Taam 2008; Belczynski et al. 2011, 2013; Luo et al. 2012). Finally, the implications of `StarTrack` synthetic universe for future GW observations have also been extensively addressed (Nutzman et al. 2004; Bulik et al. 2004a; Belczynski et al. 2007, 2010a; O'Shaughnessy et al. 2012).

The last update of `StarTrack` is presented by Dominik et al. (2012), which is the first in a three-paper series. The main goal of the study is a substantial improvement of merger

Authors	NS-NS [yr^{-1}]	NS-BH [yr^{-1}]	BH-BH [yr^{-1}]
Tutukov and Yungelson (1993a,b)	3×10^{-4}	2×10^{-5}	1×10^{-6}
Lipunov et al. (1997)	3×10^{-5}	2×10^{-6}	3×10^{-7}
Portegies Zwart and Yungelson (1998)	2×10^{-5}	1×10^{-6}	
Nelemans et al. (2001a,b)	2×10^{-5}	4×10^{-6}	
Voss and Tauris (2003)	2×10^{-6}	6×10^{-7}	1×10^{-5}
O'Shaughnessy et al. (2005c)	7×10^{-6}	1×10^{-6}	1×10^{-6}
de Freitas Pacheco et al. (2006)	2×10^{-5}		
Belczynski et al. (2007)	1×10^{-5}	9×10^{-7}	9×10^{-7}
Dominik et al. (2012)[a]	2×10^{-5}	2×10^{-6}	8×10^{-6}

Table 5.1: Estimates for Galactic merger rates $\mathcal{R}$ of compact binaries calculated using different population synthesis codes and approaches (updated from Postnov and Yungelson 2006). The values listed are taken from those models indicated by the authors themselves as "likely" or "standard".

Network	Source	D_{horizon} [Mpc]	N_{low} [yr^{-1}]	N_{re} [yr^{-1}]	N_{high} [yr^{-1}]
Initial LIGO/Virgo	NS-NS	33	2×10^{-4}	0.02	0.2
	NS-BH	70	7×10^{-5}	0.004	0.1
	BH-BH	161	2×10^{-4}	0.007	0.5
Advanced LIGO/Virgo	NS-NS	445	0.4	40	400
	NS-BH	927	0.2	10	300
	BH-BH	2187	0.4	20	1000

Table 5.2: Detection rates $\dot{N}$ for compact binary coalescence sources. Columns indicates pessimistic estimates (N_{low}), realistic estimates (N_{re}) and optimistic estimates (N_{high}). Rows indicate different sources: NS-NS, NS-BH and BH-BH (inspiral and) merger. Rates are computed using the procedure detailed in Abadie et al. (2010).

[a]Distributions are publicly available at `www.syntheticuniverse.org` and will be used for a preliminary comparison in Sec. 7.4.2.

rate predictions, by carefully considering all of the main uncertainties in the astrophysics of compact binary formation (and particularly the common envelope phase and the redshift dependance) in order to have precise predictions when Advanced LIGO will start taking data. Simulations were performed varying over many different parameters, and the results are publicly available at `www.syntheticuniverse.org`. The richness of the `StarTrack` evolutionary scenarios is precious for our study, that focuses only on the evolution of the BH spin orientations. Our assumptions build upon prescriptions from the `StarTrack` results that cannot be inferred within our simplified model (e.g. when computing the remnant masses resulting from gravitational collapse as a function of the progenitor masses, Sec. 7.2.1, or in treating the common envelope phase, Sec.. 7.2.4). In Sec. 7.4 we will present a preliminary comparison of our conclusions with the public results from Dominik et al. (2012).

5.3.4 Spin dynamics in black-hole binary formation

Most studies of compact-binary formation do not keep track of the magnitude and orientation of BH spins, and those that do (see e.g. the `StarTrack` papers: O'Shaughnessy et al. 2005b; Belczynski et al. 2008c and Fragos et al. 2010) neglect general-relativistic effects in the late-time evolution of the binary. We showed in Sec. 5.2.2 that a joint analysis of astrophysics

and PN evolution is necessary: one of the goals of our study is to fill this gap.

The present version of the `StarTrack` code assumed that both spins remained aligned with the initial direction of the orbital angular momentum of the BH binary, i.e. the orbital angular momentum with which the binary forms. The evolution of the orbital angular momentum itself is performed by applying energy and angular-momentum conservation when compact objects are formed (and kicked) as a result of gravitational collapse (a procedure also implemented in our model, see Sec. 7.2.6). This approach is suitable for binaries in nonrelativistic orbits, like observed X-ray binaries (Fragos et al. 2010), but it may not be appropriate for merging binaries, that are interesting both as GW sources and as progenitors of short gamma-ray bursts (Belczynski et al. 2008c). Existing BH binary formation models preserve the mutual alignment of the spins with the initial direction, so all BH-BH binaries are formed with the two spin misalignment angles equal to each other ($\theta_1 = \theta_2$ in the notation of the following chapters). Later models of mixed BH X-ray binaries do allow for the possibility of asymmetric spin configurations via accretion (Fragos et al. 2010), but to the best of our knowledge no such studies have been published for the BH-BH case.

In Chapter 6 we will demonstrate that spin-orbit couplings act efficiently whenever a spin angle asymmetry is presents before the onset of GW-driven regime. In Chapter 7, we will develop a slightly more complex (and presumably more realistic) model for spin evolution, allowing for the formation of "asymmetric" BH binaries ($\theta_1 \neq \theta_2$). The model is very simplified and it is not meant to rival the complexity of population synthesis codes like `StarTrack`. Our goal is rather to isolate the physical ingredients that are specifically relevant to BH spin alignment.

Chapter 6

Spin-orbit resonances

The PN approximation is a powerful tool to study Einstein's GR in the limit of small velocities and weak gravitational fields. The evolution equations for spinning BH binaries at the lowest PN order present special equilibrium configurations that turn out to be resonant: if precessional dynamics brings the spin parameters close to one of these solutions, the system can remain locked into resonance. In this Chapter we introduce the PN equation of motions and their resonant solutions for BH binaries. We perform numerical integrations with specify sets of initial conditions to highlight the role of spin asymmetry for resonant locking.

Following common practice in the GR literature, in this Chapter we will typically use geometrical units such that $G = c = 1$, and the Einstein conventions for repeated indices.

6.1 The post-Newtonian approximation

After decoupling from their astrophysical environment, the dynamics of BH binaries in vacuum can be approximated by expanding the Einstein equations in a perturbative PN series, where the perturbative parameter is the ratio v/c of the orbital velocity to the speed of light. For historical reasons (de Sitter 1916a; Einstein et al. 1938), one usually says that a quantity is expanded up to nPN order if all terms up to order $(v/c)^{2n}$ are retained. We present the main ideas of this approximation following the clear presentation given in Damour (1987); an extensive review of the subject can be found in Blanchet (2002).

Newton's and Einstein's gravity. Let us consider a fluid with a given barotropic equation of state linking the mass density ρ and the pressure $p = p(\rho)$. We call $v_i(\mathbf{x}, t)$ the velocity field in cartesian coordinates x^i, with $i = 1, 2, 3$. The equations describing the full dynamics in Newton's gravity are: the continuity equations,

$$\frac{\partial \rho}{\partial t} + \frac{\partial (\rho v^i)}{\partial x^i} = 0 \,, \tag{6.1}$$

which states that the mass of the system is be conserved; the Euler equation for the momentum conservation

$$\rho \left(\frac{\partial v^i}{\partial t} + v^i \frac{\partial v_i}{\partial x^i} \right) = - \frac{\partial p}{\partial x^i} + \rho \frac{\partial \phi}{\partial x^i} \,; \tag{6.2}$$

and the Poisson equation

$$\sum_i \frac{\partial^2 \phi}{\partial x^{i\,2}} = -4\pi G\rho \tag{6.3}$$

for the gravitational potential ϕ.

These Newtonian equations are a special case of by the relativistic equations of motions for a perfect fluid (e.g. Misner et al. 1973). Given the fluid four-velocity u^μ with $\mu = 0, 1, 2, 3$, and the spacetime metric $g^{\mu\nu}$, the stress-energy tensor for a perfect fluid is given by

$$T^{\mu\nu} = (\rho + p)u^\mu u^\nu + pg^{\mu\nu}\,, \tag{6.4}$$

where the parameters ρ and p reduce to mass density and pressure in the Newtonian limit. The Einstein field equations

$$R^{\mu\nu} - \frac{1}{2}Rg^{\mu\nu} = 8\pi T^{\mu\nu}\,, \tag{6.5}$$

describe how the spacetime is curved by the mass-energy content. The Bianchi identies

$$\frac{\partial T^{\mu\nu}}{\partial x^\nu} + \Gamma^\mu_{\nu\rho}T^{\nu\rho} + \Gamma^\nu_{\nu\lambda}T^{\mu\lambda} = 0\,, \tag{6.6}$$

encode the relativistic generalization of the continuity equation

$$\frac{\partial \varepsilon u^\mu}{\partial x^\mu} + \Gamma^\mu_{\mu\rho}\varepsilon u^\rho = 0\,, \tag{6.7}$$

and the Euler equations can be written as

$$(\rho + p)u^\nu \left(\frac{\partial u^\mu}{\partial x^\nu} + \Gamma^\mu_{\nu\rho}u^\rho\right) = -\left(g^{\mu\nu} + u^\mu u^\nu\right)\frac{\partial p}{\partial x^\nu}\,. \tag{6.8}$$

We have introduced a proper rest-mass density ε defined (modulo a constant factor) as

$$\varepsilon = \exp\int \frac{d\rho}{\rho + p(\rho)}\,. \tag{6.9}$$

The Ricci tensor $R^{\mu\nu}$, the Ricci scalar R and the Christoffel symbols $\Gamma^\mu_{\nu\rho}$ all contain with up to second-order derivatives of the metric $g_{\mu\nu}$ (see Eqs. 1.28-1.31). The general problem of motion in GR is therefore described by the second-order partial differential equations (6.5) and (6.6).

The PN approach. The PN approximation seeks to model the solution of the relativistic system (6.5)-(6.6) after the solution of the Newtonian system (6.1)-(6.2)-(6.3). For instance, the continuity equation (6.7) is rewritten as a Newtonian-type equation (6.1)

$$\frac{\partial \tilde{\rho}}{\partial \tilde{t}} + \frac{\partial(\tilde{\rho}\tilde{v}^i)}{\partial \tilde{x}^i} = 0\,, \tag{6.10}$$

where "time", "velocity" and "mass density" are defined respectively as

$$\tilde{t} = \frac{x^0}{c}\,, \qquad \tilde{v}^i = c\frac{u^i}{u^0}\,, \qquad \tilde{\rho} = \varepsilon u^0\sqrt{-\det g_{\alpha\beta}}\,. \tag{6.11}$$

The Einstein equations (6.5) can be cast in a form reminiscent of the Poisson equation (6.3) under weak-field assumptions. First we write the metric as

$$g^{\mu\nu}\sqrt{-\det g_{\alpha\beta}} = \eta^{\mu\nu} + h^{\mu\nu}\,, \tag{6.12}$$

where $\eta^{\mu\nu} = \mathrm{diag}(-1,+1,+1,+1)$ is the (flat) Minkowski metric. Then $h^{\mu\nu}$ is assumed to be small everywhere , thus describing a quasi-Minkowski spacetime where gravitational interactions are weak.

PN expansion series. We assume that the characteristic linear dimension L of the bodies is much smaller than the characteristic separation R between them: $L \ll R$. We call m the typical mass of the bodies involved and v their typical velocity. Three dimensionless parameters can then be introduced to describe a slow-motion/weak-field limit: v/c, Gm/c^2R and GM/c^2L. It is expected that $L \gtrsim Gm/c^2$, where the equality holds only for extremely compact objects such as BHs. By the virial theorem we have $v^2 \sim Gm/R$, which implies together with the above assumption

$$\frac{v^2}{c^2} \sim \frac{Gm}{c^2R} \ll \frac{GM}{c^2L}\,. \tag{6.13}$$

The PN approximation is based on the assumption that the metric $h^{\mu\nu}$ admits an asymptotic expansions in the non-relativistic limit

$$\gamma = \frac{GM}{c^2L} \to 0\,. \tag{6.14}$$

We write

$$h^{\mu\nu}(\mathbf{x},t) = \gamma\, h^{\mu\nu}_{(1\mathrm{PN})}(\mathbf{x},t) + \gamma^{3/2}\, h^{\mu\nu}_{(1.5\mathrm{PN})}(\mathbf{x},t) + \gamma^2\, h^{\mu\nu}_{(2\mathrm{PN})}(\mathbf{x},t) + \dots\,. \tag{6.15}$$

The PN approximation is supposed to get more accurate as more terms in this expansion are retained. At the lowest 1PN order, the zeroth-zeroth component of (6.5) yields

$$\nabla^2\left(\gamma\, h^{00}_{(1\mathrm{PN})}\right) = \frac{16\pi G}{c^2}\varepsilon + O\left(\frac{\gamma^2}{L^2}\right)\,, \tag{6.16}$$

which recalls the Poisson equation of Newtonian gravity. The same approach can be generalized to higher orders in $\gamma^{1/2}$, which leads to a formal hierarchy of Poissons equations for $h^{\mu\nu}_{(n\mathrm{PN})}$. For the n-th order, one finds an equation that schematically looks like

$$\nabla^2\left(\gamma^n h^{\mu\nu}_{(n\mathrm{PN})}\right) = [\text{Terms from } T^{\mu\nu} \text{ in Eq. (6.5)}] + [\text{Terms known from the lower orders}]\,, \tag{6.17}$$

which can be solved, at least in principle, to study the motion at the desired PN level.

6.1.1 Breakdown of the post-Newtonian approach

As firstly realized by Fock (1965), the slow-motion/weak-field limit presented above is not valid throughout the whole spacetime, but only in the *near zone*, which is the region sufficiently far from the horizons that a weak-field approximation is valid, but less than a reduced GW wavelength $\lambda/2\pi$ away from the center of mass of the system, so that retardation effects can be treated perturbatively. Other approaches can be adopted in the *far zone*, i.e. the radiation zone where retardation effects can no longer be treated perturbatively, and in the *inner zone*, very close to the compact objects (see e.g. Thorne 1980; Alvi 2000, 2003; Yunes et al. 2006; Yunes and Tichy 2006; Yunes 2007; Johnson-McDaniel et al. 2009).

When analyzing a BH binary, the PN approximation definitely breaks down when the two BHs eventually become so closely separated that a slow-motion/weak-field description is inappropriate. The problem of the region of validity of the PN approximation can only be addressed when one possesses a different, analytical or numerical, description of the dynamics. In the case of *extreme mass ratio inspirals*, where the presence of a small-mass orbiting body can be treated as a perturbation in the metric of the primary, Poisson (1995, 1997) tested the validity of the 5.5PN theory predictions against analytical results form BH perturbation theory. He found that PN theory is sufficiently accurate provided $v \lesssim 0.2$. BH perturbation theory and PN theory have also been compared for the loss of the binary's binding energy for non-spinning and spinning BH (at 5.5PN and 4PN respectively) by Yunes and Berti (2008, 2011) and Zhang et al. (2011). They found a consistent agreement only if $v \lesssim 0.29$, which corresponds to an orbital separation of $a \gtrsim 11M$. In the comparable-mass regime, PN predictions can only be compared with full numerical relativistic simulations to determine the region of validity of the PN approach (Berti et al. 2008; Hannam et al. 2008a,b, 2010; Santamaría et al. 2010; MacDonald et al. 2011; Sperhake et al. 2011a). Within the NINJA (Numerical INJection Analysis) project, a collaboration between numerical relativists and GW data analysts established that 3PN order gravitational waveforms are sufficiently accurate for use as templates in GW detector provided $v \lesssim 0.33$, i.e. $a \gtrsim 8M$ (see Aylott et al. 2009; Ajith et al. 2012 and references therein). Analytical arguments also seem to indicate that the PN approximation may be more accurate, i.e. valid for even larger velocities, in the comparable-mass regime than for the extreme mass ratio inspirals (Simone et al. 1997; Blanchet 2003; Mora and Will 2004, 2005; Buonanno et al. 2009).

For our goals, we are interested only in the binary configurations as they enter the sensitivity band of GW detectors such as Advanced LIGO/Virgo ($f_{\rm GW} = 20\,{\rm Hz}$) and the Einstein Telescope ($f_{\rm GW} = 1\,{\rm Hz}$), which corresponds to $a \simeq 38M$ and $a \simeq 278M$ respectively. These values are well within the range of validity of the PN approximation, which confirm the validity of our approach. Our simulations formally reach $a = 10M$, which is assumed to be a rough upper limit on the separations at which the PN approach can be consider reliable.

6.2 Post-Newtonian evolutionary equations

The PN equations of motion for spinning BH binaries have been derived by several authors at progressively increasing orders of approximations: see e.g. Papapetrou (1951); Corinaldesi and Papapetrou (1951); Barker and O'Connell (1975a); Thorne and Hartle (1985); Kidder et al. (1993) and Kidder (1995). Previous numerical studies of BH inspirals include Arun et al. (2009, 2011); Kesden et al. (2010a,b); Galley et al. (2010) and Berti et al. (2012b). Buonanno et al. (2003, 2005, 2006) used the PN equations for spinning BHs to build matched-filtering template families for GW detection; a statistical investigation of spinning BH binaries evolutions using Graphical Processing Units has been presented by Herrmann et al. (2010). Lousto et al. (2010b,c) used a slightly different approach, evolving a large sample of spinning BH binaries systems using a non-resummed, PN-expanded Hamiltonian.

We restricted our evolution to circular orbits: we will show in Sec. 7.3.1 that this is a well justified assumption for all binaries in our samples. We denote unit vectors with a hat, and we use subscripts "1" and "2" to indicate the primary and the secondary BH, respectively.

For circular orbits with radius a and orbital velocity $v = (GM/a)^{1/2}$, the *intrinsic* dynamics of a binary system depends on 10 variables: the two masses $m_1 > m_2$, the spins $\mathbf{S_1}$ and $\mathbf{S_2}$ and the direction of the orbital angular momentum $\hat{\mathbf{L}}$. At the PN order we consider both spin magnitudes χ_1 and χ_2 (cf. Eq. 1.5), and the mass ratio $q = m_2/m_1 < 1$ remain fixed during the inspiral. This leaves 7 independent degrees of freedom. Because BHs are vacuum solutions of the Einstein equations, there is only one physical scale in the problem (the total mass of the binary M). Rescaling all quantities relative to the mass M, we are left with 6 *intrinsic* parameters. It is convenient to analyze the precessional dynamics in the frame where the direction of the orbital momentum $\hat{\mathbf{L}}$ lies along the z-axis. If we take (say) the y-axis to be oriented along the projection of $\mathbf{S_2}$ on the orbital plane (see Fig. 6.1),

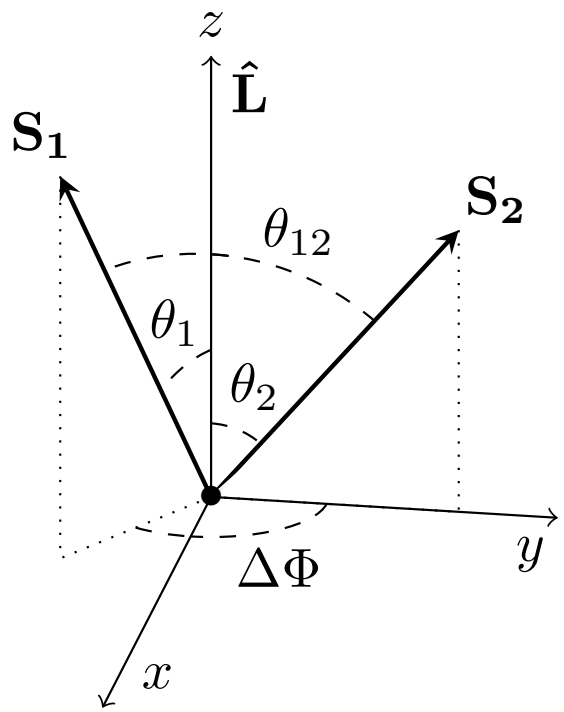

Figure 6.1: Reference system adopted to describe the PN inspiral. The three independent variables in the PN evolution are the angle between the spins and the orbital angular momentum θ_1 and θ_2, and the angle between the projection of the spins on the orbital plane $\Delta\Phi$. We also define θ_{12} to be the angle between the two spins

we are effectively imposing 3 additional constraints just by our choice of the reference frame (2 components of $\hat{\mathbf{L}}$ and 1 component of $\mathbf{S_2}$ are set equal to zero). Then the only 3 variables describing precessional dynamics are the angles θ_1, θ_2 and $\Delta\Phi$, defined to be the angles between the spins and the orbital angular momentum of the binary and the angle between the projections of the two spins on the orbital plane, respectively:

$$\cos\theta_1 = \hat{\mathbf{S}}_\mathbf{1} \cdot \hat{\mathbf{L}}\,, \tag{6.18}$$

$$\cos\theta_2 = \hat{\mathbf{S}}_\mathbf{2} \cdot \hat{\mathbf{L}}\,, \tag{6.19}$$

$$\cos\Delta\Phi = \frac{\hat{\mathbf{S}}_\mathbf{1} \times \hat{\mathbf{L}}}{|\hat{\mathbf{S}}_\mathbf{1} \times \hat{\mathbf{L}}|} \cdot \frac{\hat{\mathbf{S}}_\mathbf{2} \times \hat{\mathbf{L}}}{|\hat{\mathbf{S}}_\mathbf{2} \times \hat{\mathbf{L}}|}\,. \tag{6.20}$$

As shown in Fig. 6.1, θ_1 and θ_2 vary in the range $[0, \pi]$, while $\Delta\Phi \in [-\pi, \pi]$. The angle between the two spins is related to the other independent variables as follows:

$$\cos\theta_{12} = \hat{\mathbf{S}}_\mathbf{1} \cdot \hat{\mathbf{S}}_\mathbf{2} = \sin\theta_1 \sin\theta_2 \cos\Delta\Phi + \cos\theta_1 \cos\theta_2\,. \tag{6.21}$$

In summary, for any given binary with intrinsic parameters (q, χ_1, χ_2), the precessional dynamics is encoded in the variables $(\theta_1, \theta_2, \Delta\Phi)$ as functions of the orbital velocity v or (equivalently) of the orbital frequency $\omega = v^3/M$. These variables can be evolved forward in time by integrating the following PN equations of motion:

$$\frac{d\mathbf{S_1}}{dt} = \mathbf{\Omega_1} \times \mathbf{S_1} \qquad\qquad \frac{d\mathbf{S_2}}{dt} = \mathbf{\Omega_2} \times \mathbf{S_2}\,, \tag{6.22}$$

$$\begin{aligned} M\mathbf{\Omega_1} = \eta v^5 \left(2 + \frac{3q}{2}\right)\hat{\mathbf{L}} + \alpha_1 \frac{v^6}{2M^2}\left[\mathbf{S_2} - 3\left(\hat{\mathbf{L}}\cdot\mathbf{S_2}\right)\hat{\mathbf{L}} - 3q\left(\hat{\mathbf{L}}\cdot\mathbf{S_1}\right)\hat{\mathbf{L}}\right] \\ + \alpha_2 v^7\left[\frac{9}{16} + \frac{5\eta}{4} - \frac{\eta^2}{24} + \frac{\delta m}{M}\left(-\frac{9}{16} + \frac{5\eta}{8}\right)\right]\hat{\mathbf{L}}\,, \end{aligned} \tag{6.23}$$

$$\begin{aligned} M\mathbf{\Omega_2} = \eta v^5 \left(2 + \frac{3}{2q}\right)\hat{\mathbf{L}} + \alpha_1 \frac{v^6}{2M^2}\left[\mathbf{S_1} - 3\left(\hat{\mathbf{L}}\cdot\mathbf{S_1}\right)\hat{\mathbf{L}} - \frac{3}{q}\left(\hat{\mathbf{L}}\cdot\mathbf{S_2}\right)\hat{\mathbf{L}}\right] \\ + \alpha_2 v^7\left[\frac{9}{16} + \frac{5\eta}{4} - \frac{\eta^2}{24} - \frac{\delta m}{M}\left(-\frac{9}{16} + \frac{5\eta}{8}\right)\right]\hat{\mathbf{L}}\,, \end{aligned} \tag{6.24}$$

$$\begin{aligned} \frac{d\hat{\mathbf{L}}}{dt} = -\frac{v}{\eta M^2}\Bigg\{\frac{d\mathbf{S_1}}{dt} + \frac{d\mathbf{S_2}}{dt} - \alpha_2 \frac{2\eta}{M} v^7\left[\eta + \left(\frac{m_2}{M}\right)^2\left(1 + \frac{3}{16}\frac{m_2}{m_1}\right)\right]\left(\hat{\mathbf{L}}\times\mathbf{S_1}\right) \\ - \alpha_2 \frac{2\eta}{M} v^7\left[\eta + \left(\frac{m_1}{M}\right)^2\left(1 + \frac{3}{16}\frac{m_1}{m_2}\right)\right]\left(\hat{\mathbf{L}}\times\mathbf{S_2}\right)\Bigg\}\left[1 + \alpha_2 v^2\left(\frac{3}{2} + \frac{\eta}{6}\right)\right]^{-1}\,, \end{aligned} \tag{6.25}$$

$$\begin{aligned} \frac{dv}{dt} =& \frac{32}{5}\frac{\eta}{M}v^9\Bigg\{1 + v^2\left[-\frac{743}{336} - \frac{11}{4}\eta\right] + v^3\left[4\pi - \sum_{i=1,2}\chi_i(\hat{\mathbf{S}}_\mathbf{i}\cdot\hat{\mathbf{L}})\left(\frac{113}{12}\frac{m_i^2}{M^2} + \frac{25}{4}\eta\right)\right] \\ &+ \alpha_1 v^4\Bigg[\frac{34103}{18144} + \frac{13661}{2016}\eta + \frac{59}{18}\eta^2 + \frac{721}{48}\eta\chi_1\chi_2(\hat{\mathbf{S}}_\mathbf{1}\cdot\hat{\mathbf{L}})(\hat{\mathbf{S}}_\mathbf{2}\cdot\hat{\mathbf{L}}) - \frac{247}{48}\eta\chi_1\chi_2(\hat{\mathbf{S}}_\mathbf{1}\hat{\mathbf{S}}_\mathbf{2}) \\ &+ \sum_{i=1,2}\frac{5}{2}\chi_i^2\left(\frac{m_i}{M}\right)^2\left(3(\hat{\mathbf{S}}_\mathbf{i}\cdot\hat{\mathbf{L}})^2 - 1\right) + \sum_{i=1,2}\frac{1}{96}\chi_i^2\left(\frac{m_i}{M}\right)^2\left(7 - (\hat{\mathbf{S}}_\mathbf{i}\cdot\hat{\mathbf{L}})^2\right)\Bigg] \\ &+ \alpha_1 v^4\Bigg[\left(-\frac{4159}{672} - \frac{189}{8}\eta\right)\pi + \alpha_2\sum_{i=1,2}\chi_i(\hat{\mathbf{S}}_\mathbf{i}\cdot\hat{\mathbf{L}})\left(-\frac{31319}{1008}\frac{m_i^2}{M^2} + \frac{1159}{24}\eta\frac{m_i^2}{M^2}\right. \\ &\left. - \frac{809}{84}\eta + \frac{281}{8}\eta^2\right) - \alpha_2\frac{1}{4}\sum_{i=1,2}\left(\frac{m_i}{M}\right)^3\chi_i(\hat{\mathbf{S}}_\mathbf{i}\cdot\hat{\mathbf{L}})(1 + 3\chi_i^2)\left(1 - \frac{15}{8}\chi_i^2\frac{1 - (\hat{\mathbf{S}}_\mathbf{i}\cdot\hat{\mathbf{L}})^2}{1 + 3\chi_i^2}\right)\Bigg] \\ &+ \alpha_1 v^6\Bigg[\frac{16447322263}{139708800} + \frac{16}{3}\pi^2 - \frac{1712}{105}(\gamma_E + \ln 4v) + \left(-\frac{56198689}{217728} + \frac{451}{48}\pi^2\right)\eta \\ &+ \frac{541}{896}\eta^2 - \frac{5605}{2592}\eta^3\Bigg] + \alpha_1 v^7\pi\left[-\frac{4415}{4032} + \frac{358675}{6048}\eta + \frac{91495}{1512}\eta^2\right]\Bigg\}\,; \end{aligned} \tag{6.26}$$

where $\gamma_E \simeq 0.577$ is Euler's constant and we defined the following combinations of the individual BH masses:

$$M = m_1 + m_2\,, \quad \eta = \frac{m_1 m_2}{M^2}\,, \quad \delta m = m_1 - m_2\,. \tag{6.27}$$

To stress the perturbative structure of the equations, we indicate the expansion parameter v in blue. Red (boolean) variables α_1 and α_2 will be useful in Sec. 6.2.1 to check the relative importance of various PN orders.

The leading 2.5PN terms in Eqs. (6.23)-(6.24) describe precessional motion about the direction of the orbital angular momentum $\hat{\mathbf{L}}$. Spin-orbit couplings appear at 3PN, and they are the reason for the existence of the resonant configurations (Schnittman 2004). These two terms are the generalization of geodetic precession and Lense-Thirring precession, respectively (see Secs. 1.1.4-1.1.5) to the case in which the spacetime curvature induced by the second body is also considered (Kidder 1995). Exactly like in our simple derivation, Lense-Thirring precession appears at a higher PN order than geodetic precession.

From (6.25) we see that the direction of the angular momentum evolves on a precessional timescale $t_p \sim \Omega_{1,2} \propto a^{5/2}$, while Eq. (6.26) implies that its magnitude decreases on the radiation-reaction timescale due to GW emission: $t_{GW} \propto v^{-8} \propto a^4$. Both of them are longer than the dynamical (orbital) time $t_{\rm dyn} \propto a^{3/2}$ in the PN limit for which this analysis is valid:

$$t_{\rm dyn} \ll t_p \ll t_{\rm GW}\,. \tag{6.28}$$

The leading (quadrupolar) order of Eq. (6.26) is equivalent to the circular limit of Eq. (5.5) when we recall that $v^2 = M/a$. The non-spin terms can be found in Blanchet et al. (2002, 2005) and references therein, taking into account the "regularization parameters" that can be found in Blanchet et al. (2004a,b) and Blanchet and Iyer (2005). The 1.5PN spin-orbit interaction has been derived by Kidder et al. (1993) as well as Poisson (1993) and Kidder (1995); calculations for the 2PN spin terms can be found in Kidder et al. (1993); Kidder (1995); Poisson (1998); Laarakkers and Poisson (1999); Gergely (2000) and Mikóczi et al. (2005); while the 2.5PN spin interactions are reported in Blanchet et al. (2006, 2007, 2010).

The 3.5PN terms in (6.23), (6.24) and (6.25) have only recently been computed by Ajith and Favata (2013).

6.2.1 New post-Newtonian terms

To check the importance of the different PN corrections, we insert in the equations two boolean variables α_1 and α_2 (in red in Eqs. 6.22-6.26). Arun et al. (2009, 2011) integrate the PN equation taking $\alpha_1 = \alpha_2 = 0$, while the previous works by Kesden et al. (2010a,b) and Berti et al. (2012b) considered just the terms multiplied by α_1. New higher-order terms, including those recently computed by Ajith and Favata (2013), have been multiplied by α_2 and were included in this study. As a preliminary code test, we performed the integration for two maximally spinning BHs ($\chi_1 = \chi_2 = 1$) starting from an initial separation $a = 100M$ for two different values of the mass ratio $q = 1$ and $q = 1/4$, and two different initial spin configurations at $a = 100M$

(A): $\theta_1 = \pi/2,\ \theta_2 = \pi/2,\ \Delta\Phi = \pi/2\,,$

(B): $\theta_1 = \pi/6,\ \theta_2 = \pi/6,\ \Delta\Phi = 3\pi/4\,.$

We chose these particular values to facilitate comparisons with Arun et al. (2009, 2011). These authors describe the direction of the orbital angular momentum in terms of the spherical coordinate angles (ι, ζ), where ι denotes the angle between the orbital angular momentum and the total angular momentum $\mathbf{J} = \mathbf{L} + \mathbf{S_1} + \mathbf{S_2}$, while ζ is the azimuthal angle in the plane orthogonal to $\mathbf{J}$. The results of our integrations are summarized in

Fig. 6.2, where we show the angle between the orbital angular momentum and the total angular momentum ι as a function of $2M\dot{\Phi}$, where $\dot{\Phi}$ is related to the orbital frequency by

$$\dot{\phi} = \frac{v^3}{M} - cos\left(\iota \frac{d\zeta}{dt}\right) . \tag{6.29}$$

Dashed lines are computed using the same equations as in Arun et al. (2009, 2011) and they exactly reproduce their Fig. 2. The effect of additional PN terms is visible (dotted lines), even for the new small corrections added in the present analysis (solid lines).

Throughout this work we decided to take into account all of the α-terms in Eqs. (6.22-6.26), setting $\alpha_1 = \alpha_2 = 1$. However, we verified that even if the new terms (Alvi 2001; Ajith and Favata 2013) affect the late-time evolution of individual binaries (as shown in Fig. 6.2), they are not statistically significant for the evolution of a whole sample of binaries, leaving the main conclusions of Kesden et al. (2010a,b) and Berti et al. (2012b) unchanged. All of our results about spin angle distributions, locking and alignment are robust to the addition of further PN corrections. The robustness of these statistical properties under the inclusion of higher-order PN terms was already noted in Kesden et al. (2010a,b) and Berti et al. (2012b).

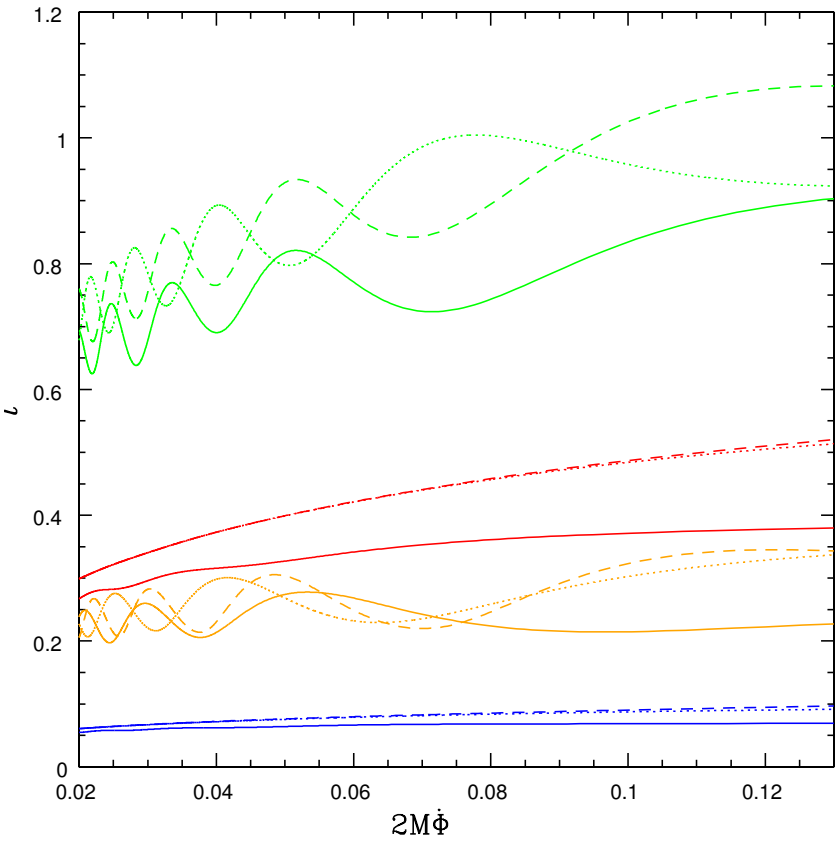

Figure 6.2: Test of the PN spin evolution code. Solid lines are obtained using $\alpha_1 = \alpha_2 = 1$; dotted lines using $\alpha_1 = 1$ and $\alpha_2 = 0$; dashed lines using $\alpha_1 = \alpha_2 = 0$. Red lines are computed with $q = 1$ and spin configuration **(A)**, blue lines with $q = 1$ and spin configuration **(B)**, green lines with $q = 1/4$ and spin configuration **(A)**, and orange lines with $q = 1/4$ and spin configuration **(B)**.

6.2.2 Correlation between $\Delta\Phi$ and θ_{12}

As stressed above, the only three independent variables in the PN evolution of a BH binary are θ_1, θ_2 and $\Delta\Phi$. Here we discuss the statistical correlation between the angles θ_{12} and $\Delta\Phi$ (defined in Eq. 6.20 and 6.21). This will be helpful in the Section below, to decouple the effect of resonances from "simple" precessional evolution.

Let us study a sample of binaries, with given initial distributions $f_1(\cos\theta_1)$ and $f_2(\cos\theta_2)$. The (initial) averaged value of $\cos\theta_{12}$ as a function of $\Delta\Phi$ is

$$\begin{aligned}\langle\cos\theta_{12}\rangle = & \frac{\int f_1(\cos\theta_1)\sin\theta_1\, d\cos\theta_1}{\int f_1(\cos\theta_1)\, d\cos\theta_1}\,\frac{\int f_2(\cos\theta_2)\sin\theta_2\, d\cos\theta_2}{\int f_2(\cos\theta_2)\, d\cos\theta_2}\cos\Delta\Phi \\ & + \frac{\int \cos\theta_1\, f_1\, d\cos\theta_1}{\int f_1\, d\cos\theta_1}\,\frac{\int \cos\theta_2\, f_2\, d\cos\theta_2}{\int f_2\, d\cos\theta_2}\,.\end{aligned} \tag{6.30}$$

Taking uniform (in cosine) distributions between $\bar\theta_i - \delta_i$ and $\bar\theta_i + \delta_i$ $(i = 1, 2)$,

$$f_i(\cos\theta_i) = \begin{cases} 1 & \text{if } \cos(\bar\theta_i + \delta_i) < \cos\theta_i < \cos(\bar\theta_i - \delta_i)\,, \\ 0 & \text{elsewhere;}\end{cases} \tag{6.31}$$

the integrals in (6.30) can be computed analytically, with the result

$$\frac{\int f_i(\cos\theta_i)\sin\theta_i\, d\cos\theta_i}{\int f_i(\cos\theta_i)\, d\cos\theta_i} = \frac{2\delta_i - \cos(2\bar\theta_i)\sin(2\delta_i)}{4\sin\bar\theta_i\sin\delta_i}\,, \tag{6.32}$$

$$\frac{\int f_i(\cos\theta_i)\cos\theta_i\, d\cos\theta_i}{\int f_i(\cos\theta_i)\, d\cos\theta_i} = \cos\theta_i\cos\delta_i\,, \tag{6.33}$$

where we assumed $\delta\theta < \bar\theta$. For distributions f_1 and f_2 that are isotropic in $[0, \pi]$, i.e. $\bar\theta_i = \delta_i = \pi/2$, the average yields instead

$$\langle\cos\theta_{12}\rangle = \frac{\pi^2}{16}\cos\Delta\Phi\,. \tag{6.34}$$

If BH spins evolve precessing on a cone of constant amplitude around the orbital angular momentum (i.e. if we neglect the 3PN spin term in Eq. 6.23 and Eq. 6.24), the evolution should necessary bring the variable $\cos\theta_{12}$ close to the expected value $\langle\cos\theta_{12}\rangle$. Sensible deviations from this behavior indicate that spin-orbit coupling cannot be neglected to analyze the dynamics of the binary.

6.3 Resonant locking

At large separations, only the dominant (2.5PN) term in the precession equations (6.23) and (6.24) is important. The total angular momentum $\mathbf{J} = \mathbf{L} + \mathbf{S_1} + \mathbf{S_2}$ is conserved on the precessional timescale, and at large separations it is $J \sim L \propto a^{1/2}$. During the first phases of the GW-inspiral, the direction of $\mathbf{L}$ can be considered fixed: both spins simply precess about the orbital angular momentum on a precession cone of constant amplitude. However, when the spin-orbit couplings become important the evolution is not trivial. Schnittman (2004) discovered families of equilibrium solution (or *resonances*) that can notably influence the inspiral in this regime. We first review the analytical derivation of the resonant configurations, and then we analyze their main features using numerical time evolutions.

6.3.1 Semi-analytical equilibrium solutions

Schnittman (2004) studied the precession equations (6.22)-(6.24) at 3PN order on the precessional timescale t_p. Since $t_p \ll t_{\rm GW}$, in practice this means that we can neglect every radiation reaction effects ($dv/dt = 0$) and work at some fixed separation a. We look for solutions of the PN equations in which the three independent variables θ_1, θ_2 and $\Delta\Phi$ are constant. Trivial equilibrium examples include the collinear cases with $\cos\theta_1 = \pm 1$ and $\cos\theta_2 = \pm 1$. More interesting cases may occur if solutions are found where S_1 , S_2 , and L are not collinear but they lie in the same plane, precessing together around a fixed axis at a constant rate and remaining at some fixed relative orientation. This is not a necessary condition to find equilibrium solutions: our aim is not to write down *all* possible solutions of the system, but only to show that coplanar solutions exist. We require therefore that $\mathbf{L}$, $\mathbf{S_1}$ and $\mathbf{S_2}$ be coplanar, i.e. $\sin\Delta = 0$ for all times. Since

$$\mathbf{S_2}\cdot(\mathbf{L}\times\mathbf{S_1}) = (m_1^2\chi_1)(m_2^2\chi_2)(\eta M^{3/2}a^{1/2})\sin\theta_1\sin\theta_2\sin\Delta\Phi\,, \tag{6.35}$$

the problem can be solved in practice by finding simultaneous solutions to the equations

$$\mathbf{S_2}\cdot(\mathbf{L}\times\mathbf{S_1}) = 0\,, \tag{6.36}$$

and

$$\frac{d}{dt}\mathbf{S_2}\cdot(\mathbf{L}\times\mathbf{S_1}) = 0\,. \tag{6.37}$$

Beside the collinear case, the first equation is verified for $\Delta\Phi = 0$ or $\Delta\Phi = \pm\pi$; this conditions distinguish between two different families of equilibrium solutions. The second

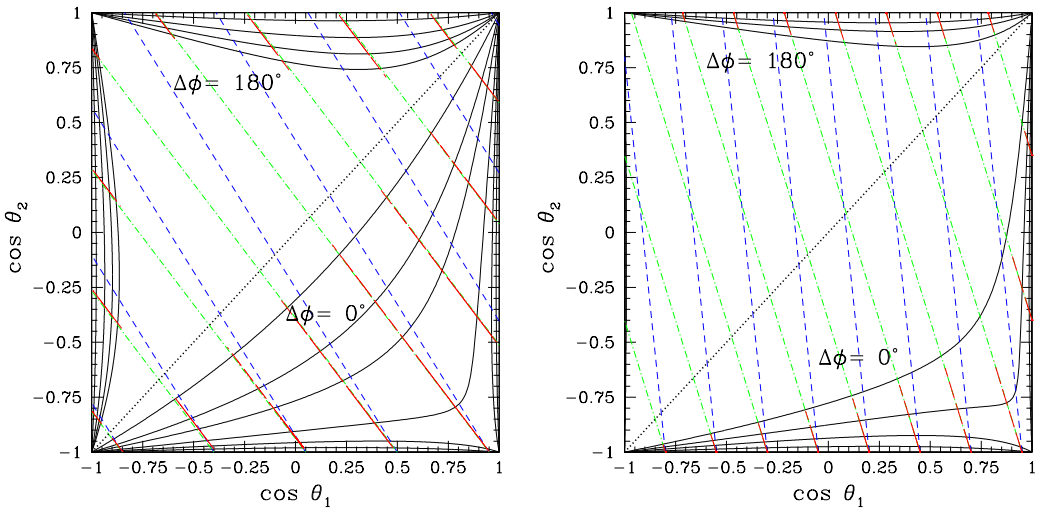

Figure 6.3: Spin-orbit resonances for maximally spinning BH binaries with a mass ratio $q = 9/11$ (left panel) and $q = 1/3$ (right panel) (Kesden et al. 2010a). Solid black curves show the one-parameter families of equilibrium solutions different fixed binary separations. Approaching the diagonal from below, these curves correspond to the $\Delta\Phi = 0$ resonances at separations $a = 1000M$, $500M$, $250M$, $100M$, $50M$, $10M$. The curves approaching from above correspond to the $\Delta\Phi = \pm\pi$ resonances with $a = 250M$, $50M$, $20M$, $10M$. Dashed red curves show how these solutions evolves during the inspiral from $a = 1000M$ to $a = 10M$. $(\mathbf{S_1}+\mathbf{S_2})\cdot\mathbf{L}$ is constant along the dashed blue lines, $\mathbf{S_0}\cdot\mathbf{L}$ is constant along the dotted green lines.

equation is equivalent to

$$(\mathbf{\Omega_1} \times \mathbf{S_1}) \cdot [\mathbf{S_2} \times (\mathbf{L} + \mathbf{S_1})] = (\mathbf{\Omega_2} \times \mathbf{S_2}) \cdot [\mathbf{S_2} \times (\mathbf{L} + \mathbf{S_2})] \,, \tag{6.38}$$

that can be easily solved numerically for both $\Delta\Phi = 0$ and $\Delta\Phi = \pm\pi$ to find the equilibrium values of θ_1 and θ_2. The results are two one-parameter families of equilibrium solutions. The resonant values θ_1 and θ_2 are different for any fixed binary separation a. This is crucial, as otherwise resonances would affect only a small portion of the three-dimensional parameter space $(\theta_1, \theta_2, \Delta\Phi)$ through which generic binaries evolve. As GWs slowly extract energy and angular momentum from the binary on the radiation time t_{GW}, the resonances sweep through a significant portion of the (θ_1, θ_2) plane. The variable $\Delta\Phi$ of a generic BH binary varies on the much shorter precession timescale t_p, and thus has a significant chance to closely approach the resonant values $\Delta\Phi = 0, \pm\pi$ at some point during the inspiral.

We illustrate resonant coplanar solutions in Fig.6.3, assuming for simplicity maximally spinning BHs ($\chi_1 = \chi_2 = 1$) and two values of the mass ratio ($q = 9/11$ and $q = 1/3$). Black curves show the resonant values for different binary separations. Two families of equilibrium solutions are present: the $\Delta\Phi = 0$ solutions always have $\theta_1 < \theta_2$, and thus appear below the diagonal in the plot; the $\Delta\Phi = \pm\pi$ solution can only be found in the $\theta_2 < \theta_1$ region. In the limit $a \to \infty$, the resonant configurations have either $\mathbf{S_1}$ or $\mathbf{S_2}$ (anti)aligned with $\mathbf{L}$, which corresponds to the four borders of the plot in Fig. 6.3. As the inspiral proceeds, i.e. as a decreases, the one-parameter families of resonant configurations approach the diagonal $\theta_1 = \theta_2$, and formally reach it if $a \to 0$. Red lines show the evolution of a resonant configuration during the inspiral, illustrating the dependence on a in Eq. (6.38). The projection $(\mathbf{S_1} + \mathbf{S_2}) \cdot \mathbf{L}$ of the total spin on the orbital angular momentum is constant along the dashed blue lines. These blue lines have steeper slopes than the red lines along which the resonant configurations evolve. This implies that the total spin becomes antialigned (aligned) with the orbital angular momentum for resonant cofigurations with $\Delta\Phi = 0(\pm\pi)$ leading to smaller (larger) final spins (Kesden et al. 2010a). Evolutionary red lines are almost coincident with dotted green lines, along with the projection $\mathbf{S_0} \cdot \mathbf{L}$ of the effective-one-body spin (Damour 2001)

$$\mathbf{S_0} = (1+q)\mathbf{S_1} + \left(1 + \frac{1}{q}\right)\mathbf{S_2} \tag{6.39}$$

is constant. The quantity $\mathbf{S_0} \cdot \mathbf{L}$ is a constant of motion at 2PN order: this follows directly from (6.22)-(6.25) (see also Racine 2008). In our evolutionary 3.5PN equations, $\mathbf{S_0} \cdot \mathbf{L}$ can only be considered as an approximate constant of motion.

Is it particularly interesting to study the resonant evolution of the angle θ_{12}. While the system evolves towards $\theta_1 = \theta_2$, the angle between the two spins (6.21) tends to

$$\cos\theta_{12} \to \cos\Delta\Phi + \cos^2\theta_1 \,(1 - \cos\Delta\Phi) \,. \tag{6.40}$$

In the same limit, since $\mathbf{S_0} \cdot \mathbf{L}$ is an (approximate) constant of motion, we have

$$\mathbf{S_0} \cdot \mathbf{L} \to \cos\theta_1 \frac{M^2(\chi_1 + q\chi_2)}{1+q} \,, \tag{6.41}$$

and therefore

$$\cos\theta_{12} \to \cos\Delta\Phi + \left[\frac{(1+q)(\mathbf{S_0} \cdot \mathbf{L})}{M^2(\chi_1 + q\chi_2)}\right]^2 (1 - \cos\Delta\Phi) \,. \tag{6.42}$$

From this results we see that while the $\Delta\Phi = 0$ resonance tends to align the two spins with each other ($\theta_{12} \to 0$), the $\Delta\Phi = \pm\pi$ resonance has a tendency towards the anti-alignment of the spins, that however cannot be reached completely. The actual misalignment in this

case depends on the initial conditions of the PN inspiral, which set the value of $\mathbf{S_0}\cdot\mathbf{L}$. The intrinsic asymmetry between the two resonances can also be seen in Fig.6.3: the family of resonances with $\Delta\Phi = 0$ (below the diagonal) approach the diagonal $\theta_1 = \theta_2$ more closely than the other. This also implies that spin-spin alignment may be more effective than spin-spin anti-alignment.

The influence of the mass ratio q can be studied by comparing the two panels in Fig. 6.3, where resonances are shown for $q = 9/11$ and $q = 1/3$, respectively. As the mass ratio decreases, the equilibrium solutions affect only a smaller portion of the (θ_1, θ_2) plane: binaries will be less affected by the resonances as they sweep through the plane. Binaries which are already in a resonant configuration will also be less affected, since the resonant curves do not approach the diagonal as closely. Therefore, spin-orbit resonances are more important for mass ratio close to one, but *not exactly* equal to 1. Symmetry implies that the PN spin alignment must vanish for equal-mass binaries, since the labeling of the BHs is arbitrary for $q = 1$ and it is therefore impossible to distinguish $\theta_1 < \theta_2$ from $\theta_2 < \theta_1$ (Berti et al. 2012b). As we will see in Sec. 6.3.3, the asymmetry of the binary is the key element to trigger PN resonant dynamics.

Here we presented results assuming maximally spinning BHs, i.e. $\chi_1 = \chi_2 = 1$. The importance of spin resonances obviously decreases if lower spin magnitudes are considered. Numerical experiments reported by Kesden et al. (2010b,a) show that resonances remain influential provided $q \gtrsim 0.4$ and $\chi_1, \chi_2 \gtrsim 0.5$.

We can summarize the resonant behavior as follows:

$$\theta_1 < \theta_2\,, \qquad \Delta\Phi \to 0\,, \qquad \cos\theta_{12} \to \cos(\theta_1 - \theta_2) \to 0\,; \tag{6.43}$$

$$\theta_1 < \theta_2\,, \qquad \Delta\Phi \to \pm\pi\,, \qquad \cos\theta_{12} \to \cos(\theta_1 + \theta_2) \to 2\left[\frac{(1+q)(\mathbf{S_0}\cdot\mathbf{L})}{M^2(\chi_1 + q\chi_2)}\right]^2 - 1\,. \tag{6.44}$$

If the more massive BH (primary) is initially more aligned with the orbital angular momentum ($\theta_1 < \theta_2$), the system can remain locked in the $\Delta\Phi = 0$ resonance, which may cause a complete spin-spin alignment ($\cos\theta_{12} \to 0$). If the less massive BH (secondary) is initially more aligned with the orbital angular momentum ($\theta_2 < \theta_1$), the system can remain locked in the $\Delta\Phi = \pm\pi$ resonance, which presents a tendency to anti-align the two spins which each other: further anti-alignment is prevented by the initial condition (through the approximate conserved quantity $\mathbf{S_0}\cdot\mathbf{L}$).

6.3.2 Numerical setup

Precession and GW radiation reaction may bring the binary configurations close to the resonant solutions, causing a resonant locking. When resonant locking occurs, the PN evolution proceeds by displaying oscillations around the coplanar equilibrium solutions along the red lines in Fig. 6.3. However, while equilibrium solutions can be found by the (semi-)analytical argument just presented, PN locking can only be studied numerically, since it involves radiation reaction.

We perform numerical integration of the ten ordinary differential equations (6.22)-(6.26) in the reference frame reported in Fig. 6.1. Previous numerical experiments (Kesden et al. 2010b,a; Berti et al. 2012b) showed that a relatively long PN evolution is needed to fully capture the resonant behavior. In fact, resonant behavior was not detected by Lousto et al. (2010b), who initialize their simulations at $a = 50M$. We started our simulations at $a = 1000M$, adopting the prescription extensively tested by Kesden et al. (2010a). Integration is performed down to $a = 10M$, where the PN approximation breaks down and numerical relativity becomes necessary to follow the inspiral (Sec. 6.1.1).

Monte Carlo simulations are performed evolving 10^3 BH binaries for each sample, using the adaptive stepsize integrator StepperdopR5 in C++ (Press et al. 2002). To monitor the variables along the whole evolution, we output all quantities using a constant logarithmic spacing in the orbital frequency at low frequencies ($a > 100M$), and the stepsize as used

in the integrator at high frequencies ($a > 100M$). Typically this results in ~ 64000 points in the range $10M < a < 1000M$. Numerical attempts indicate that a tolerance parameter 2×10^8 in the adaptive stepsize integrator is sufficient for an accuracy of order 1% or better in the final quantities. Integration and output for 10^3 binaries typically take $\sim 10-12$ hours on a quad-core machine with 800 Mhz CPUs, owned by the Gravity Group at the University of Mississippi.

6.3.3 Spin asymmetry and resonant evolution

To show the influence of resonant effects on the binary dynamics, we first performed several test runs under well controlled initial conditions. Precious insight on the main resonant features can be gained from these simple simulations . These hints will be very valuable to understood the PN evolution of astrophysically predicted samples of BH binaries in the next Chapter.

We first choose isotropic distributions of $\cos\theta_1$, $\cos\theta_2$ (in $[-1,1]$) and $\Delta\Phi$ (in $[-\pi,\pi]$), following Kesden et al. (2010a). We assume maximally spinning BHs and two different values for the mass ratio ($q = 9/11$ and $q = 1/3$). Fig. 6.4 shows different snapshots of the evolution from $a = 1000M$ to $a = 10M$. To stress the role of the two different resonances, binaries are colored with respect to their *initial* value of θ_1 and θ_2: red binaries have $\theta_1 \leq \theta_2$ at $a = 1000M$, while blue binaries are initialized with $\theta_2 < \theta_1$. The PN evolution is shown in both the $(\cos\theta_1, \cos\theta_2)$ plane and the $(\Delta\Phi, \cos\theta_{12})$ plane. We also show the *initial* correlation computed integrating (6.21) over the distributions of θ_1 and θ_2 at $a = 1000M$ (see Sec. 6.2.2). While the distributions remain isotropic in the $(\cos\theta_1, \cos\theta_2)$ plane (as already noted by Bogdanović et al. 2007), the presence of resonant configurations causes a clear segregation of the sample in the $(\Delta\Phi, \cos\theta_{12})$ plane, which are the relevant variables to understand resonant evolution (Kesden et al. 2010a). If the more massive BH is more aligned with the orbital angular momentum than the less massive one ($\theta_1 < \theta_2$, red points) the evolution is strongly influenced by the $\Delta\Phi = 0$ resonance, and it will generally align the two spins with each other ($\cos\theta_{12} \to 1$); if instead the less massive BH is initially more aligned ($\theta_1 > \theta_2$, blue points), then the $\Delta\Phi = \pi$ resonance forces the spins of the locked binaries to get closer to anti-aligned configurations (see Eq. 6.44). BH precession alone cannot describe the observed evolution: the average value of $\cos\theta_{12}$ moves away from the non-resonant value computed in Sec. 6.2.2. At small separations, binaries lie above (below) the correlation line in the $\Delta\Phi = 0\,(\pm\pi)$ region.

These same results are still valid, but to a lesser extent for isotropic samples with lower values of q. A comparison between the top and bottom panels of Fig. 6.4 shows that spin-orbit couplings are not so critical in the inspiral of lower-mass-ratio binaries.

We also studied three controlled configurations in order to understand the role of the asymmetry of the initial spin misalignments. As in the previous runs, we keep both the mass ratio and the spin magnitudes fixed to $q = 9/11, 1/3$ and $\chi_1 = \chi_2 = 1$. Here we show only the results obtained assuming $q = 9/11$, since plots with $q = 1/3$ are qualitatively similar but less instructive, because resonances are weaker. The angle $\Delta\Phi$ varies on the short precession timescale, while the separation a evolves on the longer inspiral timescale. Because of the timescale hierarchy (6.28), binaries are found at $a = 1000M$ (i.e. where we initialize the PN evolution) at a random point of their precessional motion. For this reason we always choose $\Delta\Phi$ uniformly in $[-\pi,\pi]$ at the beginning of the simulations. As for the initial distributions of θ_1 and θ_2, our configurations are:

$(10-10)$: both spins are misaligned on average by the same angle with respect to the orbital angular momentum: θ_1 and θ_2 are uniformly drawn in cosine in the range $[10^\circ - 3^\circ, 10^\circ + 3^\circ]$;

$(10-0)$: the secondary BH is almost aligned with the orbital angular momentum: θ_1 is uniformly drawn in cosine in the range $[10^\circ - 3^\circ, 10^\circ + 3^\circ]$ and θ_2 in $[0^\circ, 3^\circ]$;

$(0-10)$: the primary BH is almost aligned with the orbital angular momentum: θ_1 is uniformly drawn in cosine in the range $[0°, 3°]$ and θ_2 in $[10° - 3°, 10° + 3°]$.

In the $(10-0)$ and $(0-10)$ configurations, an asymmetry in the spin misalignments is assumed at $a = 1000M$, while binaries in the $(10-10)$ configuration approach the PN regime with symmetric spin angle distributions. Fig. 6.5 shows snapshots of the PN evolution with the same conventions used in the previous figures for each different run. In the $(10-10)$ run there is no efficient locking into PN resonances. The number of binaries which freely precess is always bigger that the number of binaries locked in a resonant configuration. Resonances still exist, as they remain solutions of the PN equations, but their effect is statistically almost irrelevant. If we decided to stop the evolution at $R = 10M$ or $R = 20M$ (which is quite arbitrary, see Sec. 6.1.1) the points would lie in very different regions of the $(\Delta\Phi, \cos\theta_{12})$ plane, indicating that the binaries are not librating around any resonant configuration. On the other hand, the locking is extremely efficient in both the $(10-0)$ and the $(0-10)$ runs: almost all binaries are locked around $\Delta\Phi = 0$ or $\Delta\Phi = \pi$. The samples are almost perfectly segregated by the PN evolutions. We can also see that binaries depart from the expected correlation line during the PN evolution, that in this regime cannot be described without properly taking into account spin-orbit interactions. Depending on whether the initial spin angle distributions are symmetric or asymmetric, the evolution can shift from almost free precession to almost perfect resonant locking. The isotropic case of Fig. 6.4 is somewhat in between.

To illustrate the efficiency of resonant locking, in Fig. 6.6 we followed the evolution of some relevant variables during the inspiral. For each simulation we track the properties of all binaries in the sample (black line) and of the two subsamples for which the primary is initially more/less aligned than the secondary (red/blue lines). In all plots the separation decreases on the x-axis from $a = 1000M$ to $a = 10M$ as the binary shrinks. The first column shows the difference between the number of binaries with $\cos\theta_2 > \cos\theta_1$ ($N_{\rm up}$) and the number of binaries with $\cos\theta_1 < \cos\theta_2$ ($N_{\rm down}$), normalized to the dimension of each (sub)sample; the second and the third columns show the evolution the averaged parameters $\langle|\Delta\Phi|\rangle$ and $\langle\cos\theta_{12}\rangle$[1]. All variables show quick oscillations on the precessional timescale, and slower trends on the inspiral timescale. In the isotropic case, during the inspiral more and more binaries get locked into a resonant configuration, evolving towards the diagonal in the $(\cos\theta_1, \cos\theta_2)$ plane (see Fig. 6.3), and they are attracted by either $\Delta\Phi = 0$ or $\Delta\Phi = \pi$. The same trends are even more evident in both the $(10-0)$ and the $(0-10)$ run, where $|\Delta\Phi|$ reaches a mean value of $150°$ and $30°$, respectively. If both spins start equally misaligned on average, as in the $(10-10)$ run, these features are still present, but strong precessional oscillations make their effect irrelevant. In this configuration the binaries spend the same amount of time with $\cos\theta_1 > \cos\theta_2$ as they do with $\cos\theta_2 < \cos\theta_1$, and they are therefore attracted by both resonances.

[1] Note than here we are averaging numerically over all three variables θ_1, θ_2 and $\Delta\Phi$. In Sec. 6.2.2, the expected correlation is computed by averaging analytically over θ_1 and θ_2 only.

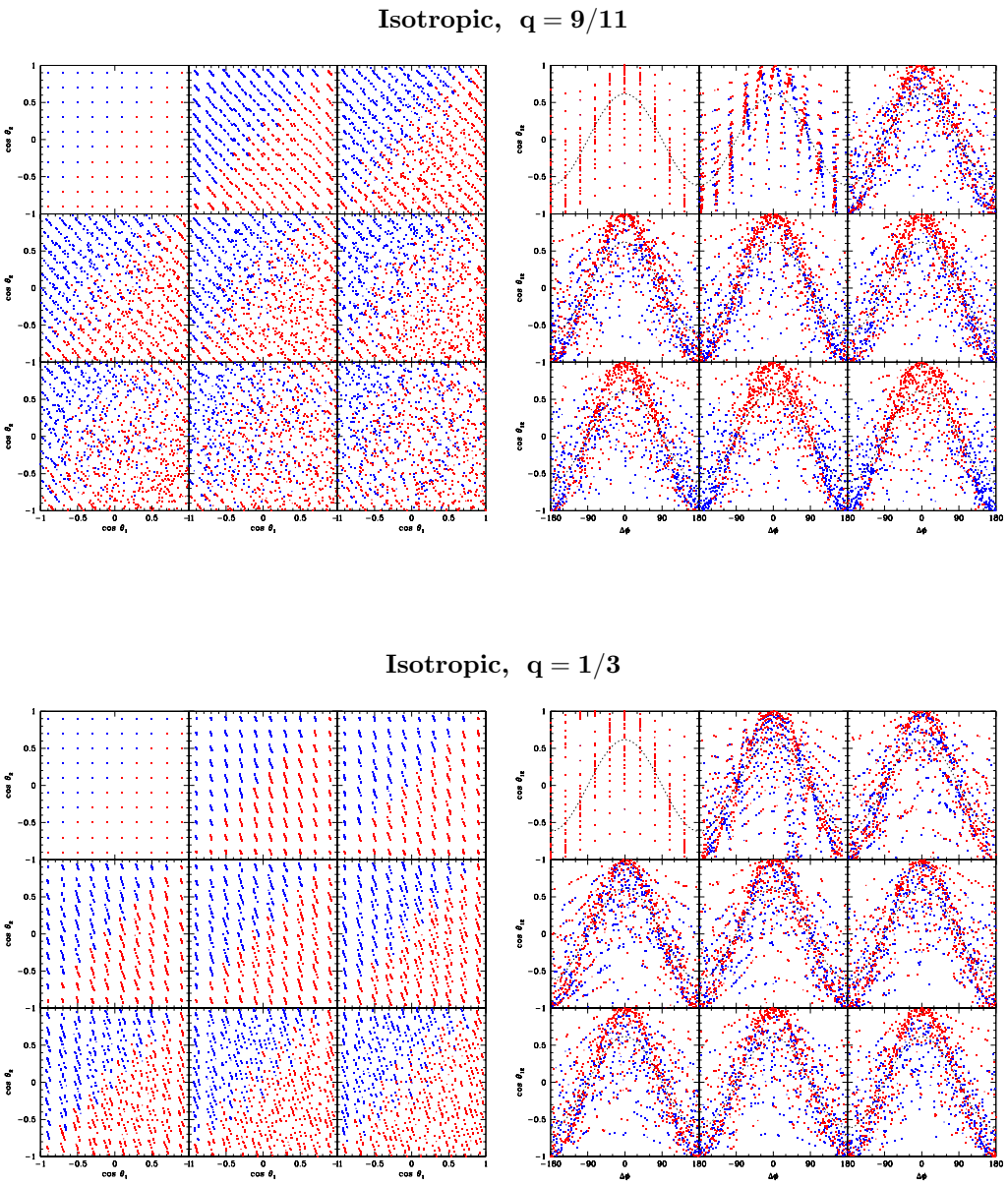

Figure 6.4: Distribution of $(\cos\theta_1, \cos\theta_2)$, left panels, and $(\Delta\Phi, \cos\theta_{12})$, right panels, for an isotropic sample of maximally spinning BH binaries with $q = 9/11$, top panels, and $q = 1/3$, bottom panels. In each panel the evolution is plotted for different separations: from right to left and from top to bottom, at $a = 1000M$ (initial conditions), $1000M$ (slightly after the beginning of the PN evolution), $750M$, $500M$, $250M$, $100M$, $50M$, $20M$ and $10M$. Red points start with $\cos\theta_1 > \cos\theta_2$, blue points start with $\cos\theta_1 < \cos\theta_2$; the black dotted line is the expected correlation between $\cos\theta_{12}$ and $\Delta\Phi$

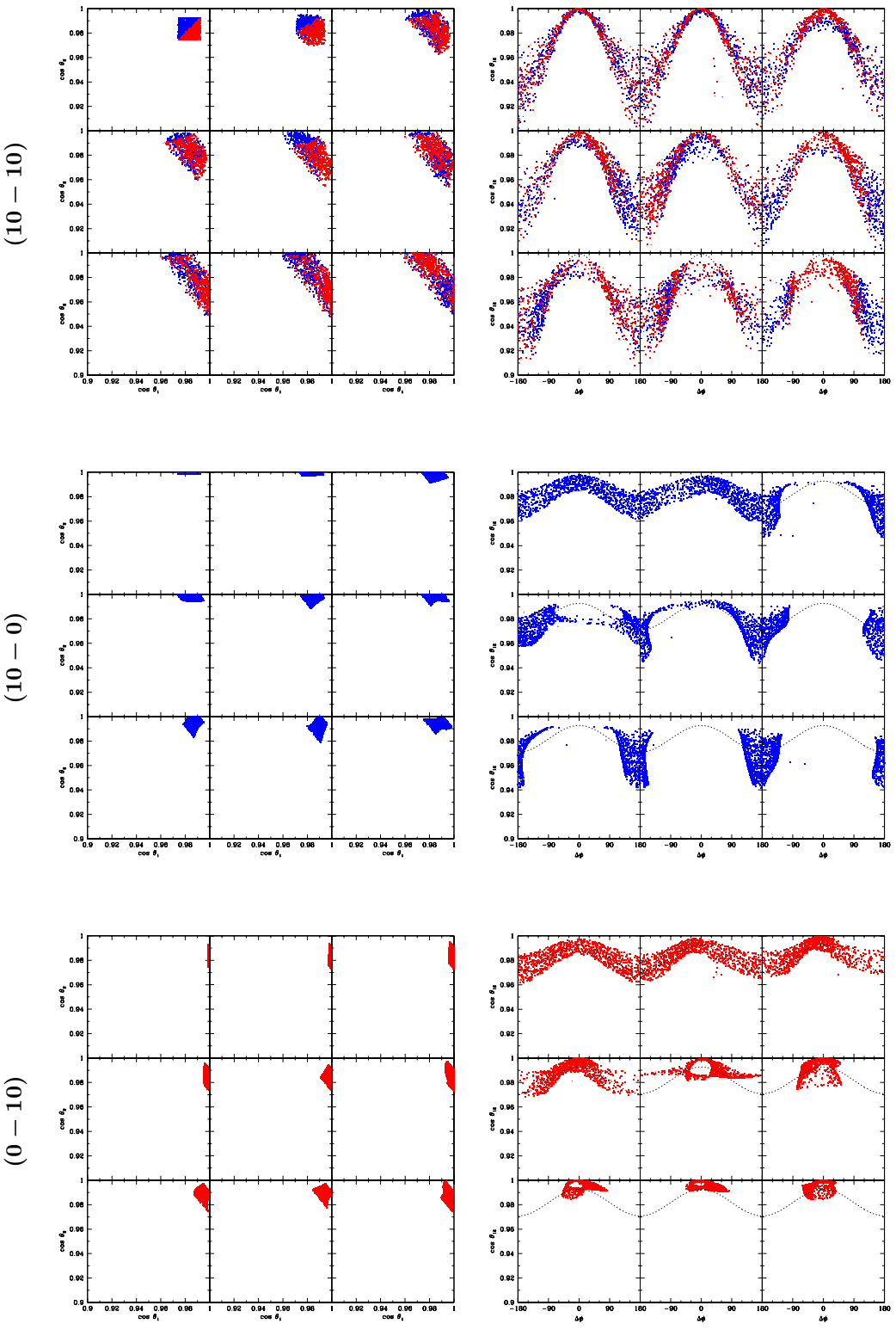

Figure 6.5: Distribution of $(\cos\theta_1, \cos\theta_2)$, left panels, and $(\Delta\Phi, \cos\theta_{12})$, right panels, for our three test (a)symmetric samples of maximally spinning BH binaries with $q = 9/11$: (10-10), (10-0) and (0-10). In each panel the evolution is plotted for different separations: from right to left and from top to bottom, at $a = 1000M$ (initial conditions), $1000M$ (slightly after the beginning of the PN evolution), $750M$, $500M$, $250M$, $100M$, $50M$, $20M$ and $10M$. Red points start with $\cos\theta_1 > \cos\theta_2$, blue points start with $\cos\theta_1 < \cos\theta_2$; the black dotted line is the expected correlation between $\cos\theta_{12}$ and $\Delta\Phi$

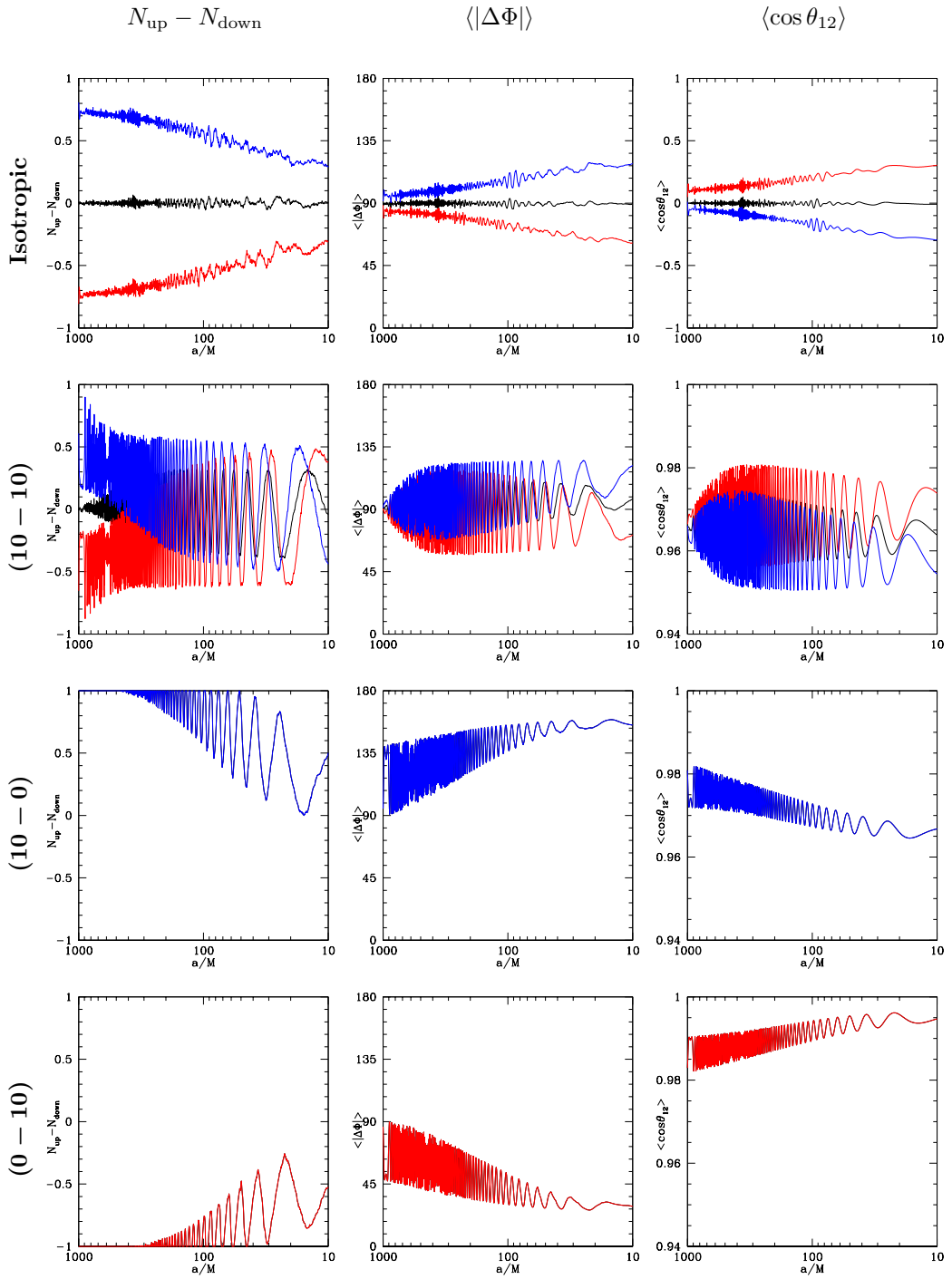

Figure 6.6: Efficiency of the resonant locking. The three columns show, from left to right, the difference between the number of binaries above and below the diagonal in the $(\cos\theta_1, \cos\theta_2)$ plane, the average of the absolute value of $\Delta\Phi$ and the average of $\cos\theta_{12}$. All the values are plotted as function of a from $1000M$ to $10M$. In the four rows, from top to bottom, we show the results for our different simulations with $q = 9/11$: isotropic, $(10 - 10)$, $(10 - 0)$ and $(0 - 10)$. The black lines contains all binaries in the sample; the red lines, just the ones starting with $\cos\theta_1 < \cos\theta_2$; the blues lines the ones starting with $\cos\theta_2 < \cos\theta_1$.

Chapter 7

Linking formation and evolution

In this Chapter we present a simple astrophysical model of spinning BH binary formation and evolution. We first introduce the main ideas behind the model, deferring details of the implementation to a dedicated Section. Spin distributions following from our astrophysical model are then evolved in the PN regime to predict binary configurations as the GW signal enters the sensitivity band of second- and third-generation detectors. Resonant-plane locking and complete spin-spin alignment may occur in the PN regime and are linked to specific formation mechanisms, namely tidal interactions and mass transfer events. The Chapter ends with a preliminary comparison of our predictions with existing population-synthesis models.

7.1 Spin evolution modeling

We develop a BH binary formation model which focuses on the spin orientations, and in particular on mechanisms that could produce a spin asymmetry leading to resonant locking (Sec. 6.3.3). Fig. 7.1 summarizes the critical stages of binary evolution in our model. We first introduce the main ideas of the model; more details can be found in Sec. 7.2.

We will loosely use the term "supernova" to indicate the core collapse of massive stars, even when such events are not luminous.

7.1.1 Fiducial scenarios for binary evolution

In order to highlight the effects of spin orientation during the PN inspiral of BH binaries, we fix the BH binary mass ratio to a fiducual value $q = 0.8$ (cf. Dominik et al. 2012). Due to the strong dependence of the PN evolution on the binary mass ratio (cf. e.g. Fig. 6.4), the importance of the different astrophysical mechanisms is less evident if wide distributions are considered. By fixing the mass ratio we can perform a *controlled experiment* to understand which formation channels are likely to produce spin-orbit resonant locking. This is a significant limitations of our model, and it will be extensively discussed in Sec. 7.4.1.

Two scenarios are possible to form BH binaries with the same mass ratio because in interacting binaries the mass ratio can be reversed by mass transfer events. Since the main-sequence lifetime of a star is a decreasing function of its mass, the initially more massive star in a binary is expected to collapse first. If mass transfer from this star to its less massive companion is small, which we will refer to as the *standard mass ratio* (SMR) scenario, the initially more massive star will go on to form the more massive member of the BH binary. We cannot however rule out the possibility that prior to the first SN, the initially more massive star overflows its Roche lobe and donates mass to its initially lighter, longer-lived companion. This mass transfer may produce a mass-ratio reversal, so that the heavier BH in the binary forms second: we will call this the *reversed mass ratio* (RMR) scenario. According

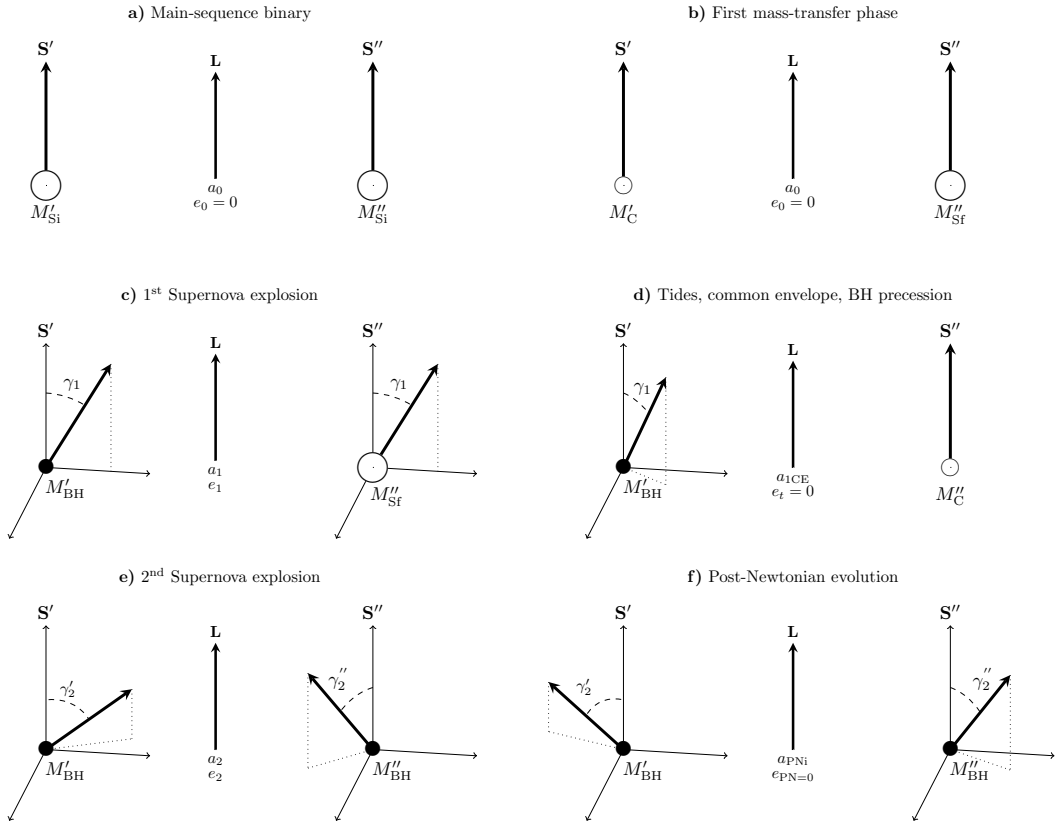

Figure 7.1: A schematic representation of our model for BH binary formation and spin evolution (Gerosa et al. 2013). Empty circles represent stars, filled circles represent BHs. The first phase (**a**) shows the initial main-sequence stellar binary. Mass transfer from the primary to the secondary (**b**) leads to a possible mass-ratio reversal. The first SN kick tilts the angle between the spins and the orbital plane (**c**). Tidal interactions can realign the stellar member of the binary (**d**). The second SN kick tilts the orbital plane again (**e**). Gravitational radiation shrinks and circularizes the binary before our explicit PN evolution begins (**f**).

to population-synthesis models, mass-ratio reversal happens for a sizable fraction (typically from $\sim 10\%$ to 50%) of the total number of BH binaries (cf. Dominik et al. 2012 and Table 7.4 below). To ensure that a final mass ratio $q = 0.8$ is obtained, the initial stellar masses of the binaries can be fixed to $(M'_{Si}, M''_{Si}) = (35M_\odot, 16.75M_\odot)$ in the SMR scenario, or $(30M_\odot, 24M_\odot)$ in the RMR scenario. Sec. 7.2.1 shows how this choice of initial masses leads to BHs of the desired final masses. Throughout the rest of this Chapter, we use a single prime to identify the initially more massive stellar progenitor or "primary", and a double prime to denote the initially less massive progenitor or "secondary" ($M'_{Si} > M''_{Si}$). As in the previous chapters, we use subscripts 1 and 2 to indicate the primary and the secondary BH, respectively ($m_1 > m_2$).

The initial main-sequence stage of the evolution is shown as phase **a** in Fig. 7.1. Binaries are assumed to form on circular orbits with initial semimajor axes a_0 drawn from the distribution described in Sec. 7.2.2, where we also show that our results do not depend on the initial eccentricity. We assume that the spins of the primary $\mathbf{S}'$ and secondary $\mathbf{S}''$ are initially aligned with the orbital angular momentum $\mathbf{L}$.

As the primary evolves, its envelope expands until it fills its Roche lobe, initiating stable mass transfer to the secondary (phase **b** in Fig. 7.1). We assume that this mass transfer continues until the primary has depleted its hydrogen envelope, leaving behind a helium

core of mass $M'_C = 8.5M_\odot$ ($M'_C = 8M_\odot$) in the SMR (RMR) scenario (Belczynski et al. 2008a). Following Dominik et al. (2012), we assume semi-conservative mass transfer: the secondary accretes half of the mass lost by the primary, growing to a mass $M''_{Sf} = 30M_\odot$ ($M''_{Sf} = 35M_\odot$) in the SMR (RMR) scenario at the end of the mass-transfer episode. In principle mass transfer should also change the orbital separation, but we neglect this change as it is smaller than the width of the distribution of initial separations, as well as subsequent changes in the separation during the CE phase.

Following the end of mass transfer, the primary explodes in a SN (phase **c** in Fig. 7.1) producing a BH of mass $M'_{BH} = 7.5\ M_\odot$ ($M'_{BH} = 6\ M_\odot$) in the SMR (RMR) scenario (Belczynski et al. 2008a). For simplicity, in our simulations the spin of this newly born BH is assumed to be maximal[1] and aligned with its stellar progenitor. The SN ejecta are generally emitted asymmetrically, imparting a recoil velocity to the BH because of linear momentum conservation. When a BH is formed, his typical kick velocity $v_{\rm BH}$ is usually parametrized as a fraction of the recoil velocities for protoneutron stars $v_{\rm pNS}$:

$$v_{\rm BH} \simeq (1 - f_{\rm fb}) v_{\rm pNS}\,, \tag{7.1}$$

where $f_{\rm fb} \in [0,\ 1]$ is the "fallback parameter" (cf. Sec. 7.2.5). The stronger gravity of BHs is expected to reduce the amount of mass ejected, and thus kicks are expected to be weaker than those imparted to NSs . The recoil tilts the orbital plane by an angle γ_1, and changes the semimajor axis and eccentricity to a_1 and e_1, respectively. These orbital changes depend on both the kick and the mass lost during the SN, as described in Sec. 7.2.6. We assume the kick direction to be confined in a double cone of amplitude θ_b about the spin direction.

After the SN explosion of the primary, the secondary evolves and expands. The primary raises tides on the swollen secondary, and dissipation may allow these tides to both circularize the orbit (so that the final eccentricity is $e_t \simeq 0$) and align the spin $\mathbf{S''}$ of the secondary with the orbital angular momentum $\mathbf{L}$, as shown in phase **d** of Fig. 7.1. This tidal alignment is described in greater detail in Sec. 7.2.7. Given the uncertainty in the efficiency of tidal alignment, we explore both extreme possibilities: complete circularization and alignment of $\mathbf{S''}$ ("Tides" runs), as well as no circularization and no alignment at all ("No Tides" runs). As the secondary expands further, it fills its Roche lobe initiating a second phase of mass transfer. However, unlike the first mass-transfer event, this second mass-transfer phase will be highly unstable (Soberman et al. 1997; Ge et al. 2010; Clausen et al. 2012). Instead of being accreted by the primary, most of this gas will expand into a common envelope about both members of the binary. Energy will be transferred from the binary's orbit to the common envelope, ultimately unbinding it from the system. This energy loss shrinks the semimajor axis of the binary from a_1 to $a_{1\rm CE}$ (Dominik et al. 2012), as shown in phase **d** of Fig. 7.1 (see Sec. 7.2.4). After the secondary loses its hydrogen envelope, the remaining helium core has a mass $M''_C = 8M_\odot$ ($M''_C = 8.5M_\odot$) in the SMR (RMR) scenario (Belczynski et al. 2008a).

After the end of common-envelope evolution, the naked helium core of the secondary rapidly completes its stellar evolution and explodes as a SN, as shown in phase **e** of Fig. 7.1. This explosion produces a BH of mass $M''_{\rm BH} = 6M_\odot$ ($M''_{\rm BH} = 7.5M_\odot$) in the SMR (RMR) scenario (Belczynski et al. 2008a), as listed in Table 7.2. For simplicity, we assume that this BH has a maximal spin that is aligned with the spin $\mathbf{S''}$ of its stellar progenitor, as we did for the primary. The SN leads to mass loss and a hydrodynamical recoil that change the semimajor axis and eccentricity of the binary to a_2 and e_2, respectively. It also tilts the orbital plane by an angle Θ, that can be calculated using the same procedure as given for the first SN in Sec. 7.2.6. This tilt changes the angles between $\mathbf{L}$ and the spins $\mathbf{S'}$ and $\mathbf{S''}$ to γ'_2 and γ''_2, respectively. If tides efficiently align $\mathbf{S''}$ with $\mathbf{L}$ prior to the second SN, these

[1]Note that spin-orbit resonances are effective provided that the dimensionless spins $\chi_i \gtrsim 0.5$ Kesden et al. (2010a).

angles are given by

$$\cos\gamma_2' = \cos\gamma_1\cos\Theta + \cos\varphi'\sin\gamma_1\sin\Theta\,, \tag{7.2}$$

$$\cos\gamma_2'' = \cos\Theta\ , \quad \text{(tides)} \tag{7.3}$$

where φ' is the angle between the projection of $\mathbf{S}'$ in the orbital plane before the SN and the projection of the change in $\mathbf{L}$ into this same initial orbital plane. If φ' is uniformly distributed (i.e. the direction of the SN kick of the secondary is uncorrelated with the spin of the primary), the second term on the right-hand side of Eq. (7.2) averages to zero, implying that $\gamma_2' > \gamma_2''$ for most binaries. This is the mechanism for creating a binary BH population preferentially attracted to the $\Delta\Phi = \pm 180^\circ$ family of spin-orbit resonances in the SMR scenario and the $\Delta\Phi = 0^\circ$ family of resonances in the RMR scenario. We expect results qualitatively similar to the bottom and lower panel of Fig. 6.5.

If tides are inefficient, γ_2'' is instead given by

$$\cos\gamma_2'' = \cos\xi = \cos\gamma_1\cos\Theta - \sin\varpi\sin\gamma_1\sin\Theta\,, \quad \text{(no tides)} \tag{7.4}$$

where ξ is the angle between $\mathbf{S}''$ and the post-SN angular momentum (cf. Eq. 7.41), and ϖ is the angle between the projection of $\mathbf{S}''$ into the orbital plane before the second SN and the separation vector between the members of the binary. We can assume ϖ to be independent of φ' and uniformly distributed: the second term on the right-hand side of Eq. (7.4) also averages to zero, implying that $\gamma_2' \simeq \gamma_2''$ for most binaries. We expect therefore that binaries will not be preferentially attracted by either family of resonances in the "No Tides" scenario, like we saw in the top panel of Fig. 6.5. The assumption that ϖ is independent of φ' and uniformly distributed is well justified, because the primary and secondary spins precess at different rates ($\Omega_1 \neq \Omega_2$ from Eqs. 6.23 and 6.24) and the precession timescale

$$t_{\rm p} \sim \Omega_{1,2}^{-1} \sim \frac{GM}{c^3}\left(\frac{v}{c}\right)^{-5} \sim 0.5\left(\frac{M}{M_\odot}\right)^{-3/2}\left(\frac{a}{R_\odot}\right)^{5/2}\ {\rm yr} \tag{7.5}$$

is short compared to the time $t_{\rm SN} \sim 10^6\,{\rm yr}$ between SN events.

After the second SN, the BH binary is left in a non-relativistic orbit that gradually decays through the emission of gravitational radiation, as shown in phase **f** of Fig. 7.1. We calculate how this orbital decay reduces the semimajor axis and eccentricity using (5.5) and (5.6). To an excellent approximation, the BH spins simply precess about $\mathbf{L}$ during this stage of the evolution, leaving γ_2' and γ_2'' fixed to their values after the second SN. Once the semimajor axis reaches a value $a_{\rm PNi} = 1000M$ (in units where $G = c = 1$), we integrate higher-order PN equations of motion as described in Sec. 6.2 to carefully model how the orbit and spins evolve. We assume that radiation reaction circularizes the orbit ($e_{\rm PN} = 0$) by the time we start integrating the higher-order PN equations describing the precessional dynamics of the BH binary. This assumption is fully justified, as we will show by explicit integration in Sec. 7.3.1 below.

7.1.2 Synthetic black-hole binary populations

We consider fiducial scenarios for the formation of BH binaries characterized by three choices:

i) stable mass transfer prior to the first SN can preserve (SMR) or reverse (RMR) the mass ratio of the binary;

ii) hydrodynamic kicks generated by the SN can have a polar ($\theta_b = 10^\circ$) or isotropic ($\theta_b = 90^\circ$) distribution with respect to the exploding star's spin;

iii) tides do or do not circularize the orbit and align the spin $\mathbf{S}''$ of the secondary with the orbital angular momentum $\mathbf{L}$ prior to the second SN.

In this Section, we construct synthetic populations of BH binaries for the 8 different scenarios determined by the three binary choices listed above. To generate members of these synthetic populations, we perform Monte Carlo simulations of 10^8 binary progenitors[2] in which random values determine

i) the initial semimajor axis a_0 (Sec. 7.2.2),

ii) the magnitude and direction of the kick produced in the first SN (Sec. 7.2.5),

iii) the magnitude and direction of the kick produced in the second SN (Sec. 7.2.5),

iv) the angles φ' and ϖ specifying the directions of the spins $\mathbf{S}'$ and $\mathbf{S}''$ before the second SN (Sec. 7.1.1),

v) the angle $\Delta\Phi$ between the projections of the BH spins in the orbital plane at separation $a_{\rm PNi}$ (Sec. 6.3.3).

The angles φ', ϖ, and $\Delta\Phi$ in items iv) and v) above are uniformly distributed in the range $[0, 2\pi]$. The synthetic populations generated via this procedure determine the initial conditions for the PN equations of motion, as described in Sec. 7.3.1.

A binary-star system can *fail* to produce a merging BH binary for one of the following reasons:

i) it is unbound by the first SN ($e_1 > 1$);

ii) it merges during the common-envelope evolution between the two SN ($a_{1CE} < a_{\rm mCE}$);

iii) it is unbound by the second SN ($e_2 > 1$);

iv) the time $t_{\rm GW}$ required for gravitational radiation to shrink the semimajor axis from a_2 to $a_{\rm PNi}$, found by solving the coupled PN equations (5.5) and (5.6), exceeds the Hubble time $t_{\rm H} \simeq 10^{10}$ Gyr.

Table 7.1 lists the fraction of 10^8 simulated binaries $\nu_{\rm SN1}$, $\nu_{\rm mCE}$, $\nu_{\rm SN2}$, and ν_H that fail to produce merging BH binaries for reasons i) through iv) listed above, as well as the fraction $\nu_{\rm BH} = 1 - (\nu_{\rm SN1} + \nu_{\rm mCE} + \nu_{\rm SN2} + \nu_{\rm H})$ that *do* evolve into such binaries.

Kicks	Tides	Transfer	$\nu_{\rm SN1}(\%)$	$\nu_{\rm mCE}(\%)$	$\nu_{\rm SN2}(\%)$	$\nu_{\rm H}(\%)$	$\nu_{\rm BH}(\%)$
Isotropic	On	SMR	32.50 (80.50)	26.53 (12.24)	2.66 (0.51)	0.04 (0.00)	38.27 (6.74)
Isotropic	On	RMR	32.55 (80.28)	34.86 (14.91)	2.97 (0.30)	0.04 (0.00)	29.59 (4.50)
Isotropic	Off	SMR	32.50 (80.50)	26.53 (12.24)	2.93 (0.60)	0.04 (0.01)	38.01 (6.65)
Isotropic	Off	RMR	32.55 (80.28)	34.86 (14.91)	3.01 (0.35)	0.04 (0.00)	29.54 (4.46)
Polar	On	SMR	31.84 (83.14)	26.68 (9.40)	3.29 (0.24)	0.01 (0.01)	38.18 (7.21)
Polar	On	RMR	31.86 (82.97)	34.88 (12.10)	3.65 (0.24)	0.02 (0.00)	29.58 (4.70)
Polar	Off	SMR	31.81 (83.16)	26.65 (9.38)	3.35 (0.52)	0.03 (0.01)	38.15 (6.93)
Polar	Off	RMR	31.84 (82.98)	34.89 (12.09)	3.65 (0.33)	0.04 (0.00)	29.59 (4.60)

Table 7.1: Fraction of binaries ν (in percentage) that satisfy the following conditions, each of which successively *prevent* the formation of a merging BH binary: i) are unbound by the first SN ($\nu_{\rm SN1}$), ii) merge during the CE phase ($\nu_{\rm mCE}$), iii) are unbound by the second SN ($\nu_{\rm SN2}$), iv) do not merge within a Hubble time due to gravitational-radiation reaction ($\nu_{\rm H}$). The final column is the fraction $\nu_{\rm BH} = 1 - (\nu_{\rm SN1} + \nu_{\rm mCE} + \nu_{\rm SN2} + \nu_{\rm H})$ of all simulated binaries that form merging BH binaries. In parentheses we list the corresponding fractions if SN kicks are not suppressed by fallback, i.e. if we set $f_{\rm fb} = 0$ rather than $f_{\rm fb} = 0.8$. Statistical errors are $\pm 0.01\%$.

[2]Each panel of Fig. 7.2 only shows a subsample of 10^4 progenitors to avoid cluttering.

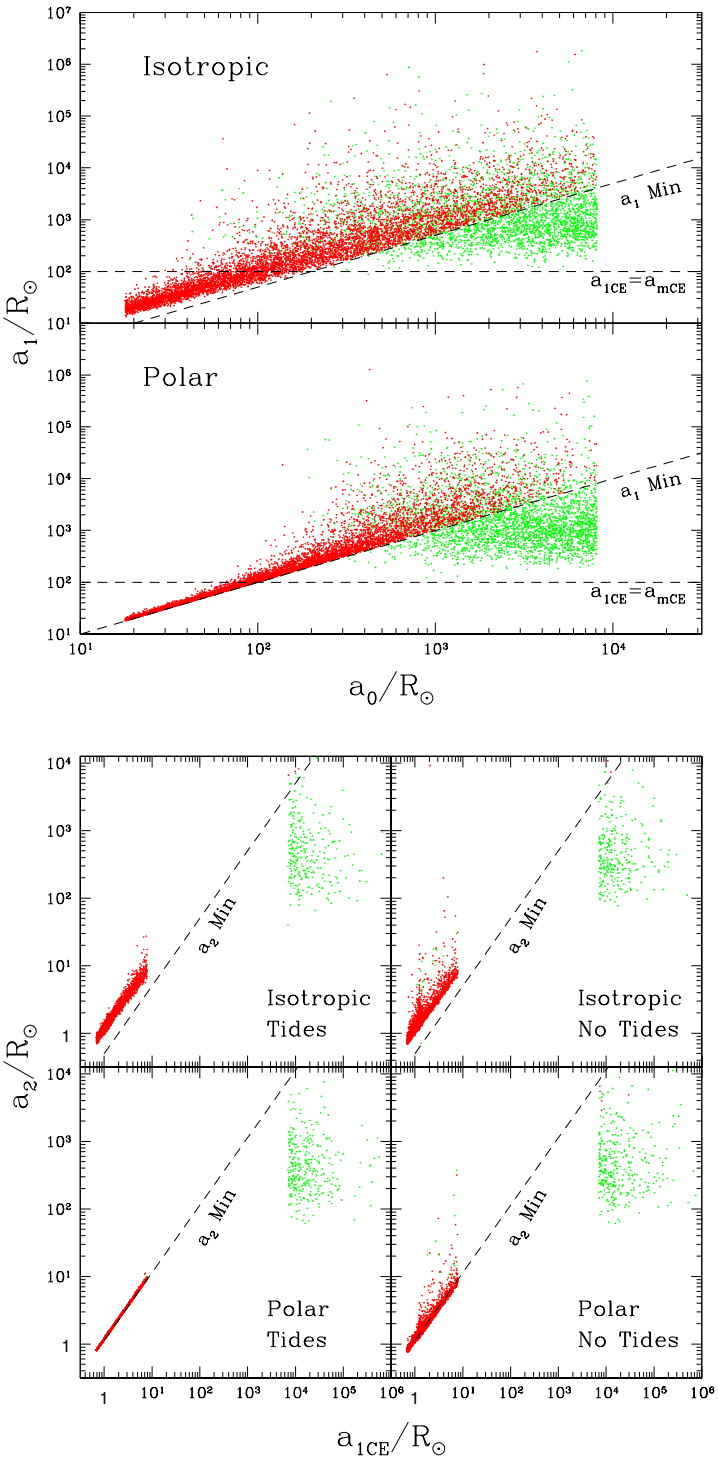

Figure 7.2: Scatter plot showing the change in the semimajor axis due to the first (top panel: $a_0 \to a_1$) and second (bottom panel: $a_{1\mathrm{CE}} \to a_2$) SN (Gerosa et al. 2013). All plots refer to the SMR scenario, but the behavior in the RMR scenario is very similar. Red dots represent binaries that remain bound after each explosion, while green dots correspond to binaries that are unbound. Dashed lines show the minimum post-SN semimajor axis $a_{f,\mathrm{Min}}$ given by Eq. (7.43) and the critical semimajor axis a_{mCE} given by Eq. (7.20) below which binaries merge during common-envelope evolution. Kicks are too small to saturate the isotropic limit $a_{f,\mathrm{Min}}$ for $a_i \lesssim 10^2 R_\odot$.

The failure fractions indicate the relative importance of different physical phenomena. To emphasize the sensitivity of our results to the highly uncertain SN kicks, we also show how these fractions change when the BH kick $v_{\rm BH}$ fully equals that imparted to the protoneutron star $v_{\rm pNS}$, i.e. taking $f_{\rm fb} = 0$ rather than our canonical choice $f_{\rm fb} = 0.8$ (Sec. 7.2.5). Stronger kicks unbind more binaries during the first SN, increasing $\nu_{\rm SN1}$ and thereby reducing the overall fraction $\nu_{\rm BH}$ of binaries that survive to form BH binaries. This qualitatively agrees with results of detailed population-synthesis models (see variations 0, 8, and 9 in Table 7.4). We adopt $f_{\rm fb} = 0.8$ in the remainder of our study.

Fig. 7.2 shows how the choices that define our fiducial scenarios affect whether SN kicks unbind the binaries. One result apparent from this plot (and supported by the failure fractions $\nu_{\rm SN}$ listed in Table 7.1) is that the probability of unbinding the system depends only weakly on whether the SN kicks are isotropic or polar. This is consistent with the findings of Postnov and Kuranov (2008), which suggest mild sensitivity to θ_b. Fig. 7.2 also shows the effect of tides on the fraction $\nu_{\rm BH}$ of BH binaries produced. In the absence of tidal dissipation ("No Tides"), the binaries have nonzero eccentricity ($e_i \neq 0$) when the second SN occurs. Eq. (7.35) shows that the final semimajor axis a_f has additional dependence on the true anomaly ψ_i in this limit, broadening the distribution of a_f, as can be seen in the right panel of Fig. 7.2. The kicks can add coherently to the large orbital velocities near pericenter of highly eccentric orbits, allowing binaries to become unbound even after CE evolution has reduced the semimajor axis, as shown by the handful of green points with $a_{1CE} \lesssim 10 R_\odot$ in the right panel of Fig. 7.2. This increases the fraction $\nu_{\rm SN2}$ of binaries unbound in the second SN when tides are "Off" in Table 7.1.

The importance of common-envelope evolution can be seen as well: virtually all binaries that fail to form a common envelope ($a_{1CE} \gtrsim 10^4 R_\odot$) are unbound by the second SN. Binaries bound tightly enough to survive the second SN almost always manage to merge through GW emission in less than a Hubble time ($\nu_{\rm H} \ll 1$). As the disc-driven phase in the case of SMBH (Sec. 2.1.2), the common-envelope evolution can shrink the orbit of stellar-mass BH down to separations where GW can finally lead the inspiral in a Hubble time.

7.2 Astrophysical spin evolution

We use population-synthesis models, and in particular results from the `StarTrack` code, to justify and put into context the simple procedure adopted in this work to follow the spin evolution. The simple model and fiducial scenarios considered do not account for a thorough exploration of the parameter space, but they illustrate the essential physics and demonstrate that PN resonance locking can be the preferred outcome of astrophysically motivated BH binary formation channels.

We describe here the necessary prescriptions to implement our astrophysical model: stellar physics formulae; choice of initial orbital parameter; treatment of stable mass transfer phase, common-envelope evolution, SN kicks and tidal alignment. Table 7.2 provides numerical values for the masses and radii of both the primary and secondary throughout the evolution in both our SMR and RMR scenarios.

7.2.1 Single stellar evolution

Here we provide the relevant information about the evolution of isolated stars implemented in our model. Main-sequence stars born with a mass M_S have a radius (Demircan and Kahraman 1991)

$$\frac{R_S}{R_\odot} \simeq 1.33 \left(\frac{M_S}{M_\odot}\right)^{0.555} . \tag{7.6}$$

Massive, metal-rich main-sequence stars lose a substantial amount of mass via winds prior to going SN, but we neglect this mass loss for simplicity. The inclusion of wind mass loss

	SMR	RMR		SMR	RMR
$M'_{\rm Si}$	$35M_\odot$	$30M_\odot$	$R'_{\rm Si}$	$9.57R_\odot$	$8.78R_\odot$
$M''_{\rm Si}$	$16.75M_\odot$	$24M_\odot$	$R''_{\rm Si}$	$6.36R_\odot$	$7.76R_\odot$
$M''_{\rm Sf}$	$30M_\odot$	$35M_\odot$	$R''_{\rm Sf}$	$8.78R_\odot$	$9.57R_\odot$
$M'_{\rm C}$	$8.5M_\odot$	$8M_\odot$	$R'_{\rm C}$	$0.26R_\odot$	$0.26R_\odot$
$M''_{\rm C}$	$8M_\odot$	$8.5M_\odot$	$R''_{\rm C}$	$0.27R_\odot$	$0.27R_\odot$
$M'_{\rm BH}$	$7.5M_\odot$	$6M_\odot$	$R'_{\rm G}$	$3608R_\odot$	$3500R_\odot$
$M''_{\rm BH}$	$6M_\odot$	$7.5M_\odot$	$R''_{\rm G}$	$3500R_\odot$	$3608R_\odot$
$a_{\rm min}$	$17.9R_\odot$	$18.8R_\odot$	$a_{\rm noCE}$	$6981R_\odot$	$6758R_\odot$
$a_{\rm max}$	$8128R_\odot$	$8787R_\odot$	$a_{\rm mCE}$	$0.69R_\odot$	$0.63R_\odot$

Table 7.2: Masses and length scales at various stages of the binary evolution in our SMR and RMR scenarios (Gerosa et al. 2013). The only independent parameters are the main-sequence masses $M'_{\rm Si}$ and $M''_{\rm Si}$, which have been tuned to study final BH binaries with mass ratio $q = 0.8$. The other values are defined in the main text, and they are obtained using the analytical prescriptions presented in Sec. 7.2.

in our model would reduce the mass of the hydrogen envelope available to be transferred to the secondary during the first mass-transfer event (cf. Sec. 5.3.1). While neglecting this mass loss quantitatively changes the binary evolution, it does not qualitatively alter our conclusions. Larger (and appropriately chosen) initial stellar masses would lead to final BH binaries with masses comparable to those considered in our model even in the presence of winds (Hurley et al. 2000, 2002).

Stars with main-sequence masses in the range $25M_\odot \leq M_S \leq 40M_\odot$ evolve into supergiants with helium-core masses well approximated by (top panel of Fig. 14 of Belczynski et al. 2008a)

$$M_C \simeq 0.1M_S + 5M_\odot\,, \tag{7.7}$$

and radii (Rappaport et al. 1995)

$$\frac{R_G}{R_\odot} \simeq 4950\frac{(M_C/M_\odot)^{4.5}}{1+4(M_C/M_\odot)^4} + 0.5\,. \tag{7.8}$$

Once the hydrogen envelopes have been lost, the naked helium cores have radii (Fryer and Woosley 1998)

$$\log\left(\frac{R_C}{R_\odot}\right) \simeq -0.699 + 0.0557\left(\log\frac{M_C}{M_\odot} - 0.172\right)^{-2.5}\,. \tag{7.9}$$

We neglect further evolution of the naked helium star before SN. For the large masses typical of BH progenitors, the naked helium cores have radiative envelopes and do not expand substantially during subsequent shell burning (Ivanova et al. 2003; Belczynski et al. 2008a). After going SN, a main-sequence star leaves behind a BH of mass (bottom panel of Fig. 14 of Belczynski et al. 2008a)

$$M_{\rm BH} \simeq 0.3M_S - 3M_\odot\,. \tag{7.10}$$

7.2.2 Initial orbital parameters

The initial binary separation a_0 is drawn from a uniform logarithmic distribution in the range $[a_{\rm min}, a_{\rm max}]$ (Öpik 1924; Abt 1983; Poveda et al. 2007; Belczynski et al. 2008a). The upper limit $a_{\rm max}$ is chosen to ensure that the primary fills its Roche lobe during its supergiant phase, while the lower limit $a_{\rm min}$ is chosen so that the secondary does *not* fill its Roche lobe

after receiving mass from the primary. The Roche-lobe radius R_L of a star of mass m_α in an orbit of semimajor axis a about a companion of mass m_β is (Eggleton 1983)

$$R_L(a, m_\alpha, m_\beta) \simeq \frac{0.49Q^{2/3}}{0.6Q^{2/3} + \ln(1 + Q^{1/3})} a \,, \tag{7.11}$$

where $Q \equiv m_\alpha/m_\beta$, so the above limits are determined by the constraints

$$R_L(a_{\max}, M'_{Si}, M''_{Si}) = R'_G \,, \tag{7.12}$$

$$R_L(a_{\min}, M''_{Sf}, M'_C) = R''_{Sf} \,. \tag{7.13}$$

These limits are somewhat arbitrary, but different choices would not affect our results. In fact, binaries that do not go through mass transfer ($a > a_{\max}$) are so widely separated that they are easily unbound by the first SN, while binaries where mass is transferred back to the primary prior to this SN ($a < a_{\min}$) will merge in the CE phase. In other words, we are not losing binaries from our final sample by our choice of the initial separation boundaries.

As for the initial eccentricity e_0, we decided to restrict our study to circular orbits. We verified that the actual value of e_0 has minimal effect: we have repeated our PN simulations using an initially thermal distribution of eccentricities of the form $f(e_0) = 2e_0$ (Heggie 1975), and we observed no significant difference in the final distribution of $\Delta\Phi$ and θ_{12}.

7.2.3 Stable mass transfer

When a star fills its Roche lobe, gas will either be stably transferred to its companion or form a common envelope about both members of the binary. Stable mass transfer is discussed in this Section, while common-envelope evolution is discussed in Sec. 7.2.4. In general, the stability of mass transfer depends on the donor star, the accreting star, and the mass ejected to infinity; as a first approximation, stability criteria are usually implemented by simple thresholds on the binary mass ratio, as summarized by e.g. Clausen et al. (2012) and references therein. For most of the BH-BH binary progenitors (Belczynski et al. 2008a; Dominik et al. 2012), mass transfer from the primary to the secondary prior to the first SN will be stable, while mass transfer from the secondary to the primary between the two SN events will lead to the formation of a common envelope.

A fraction f_a of the mass lost by the primary in the first mass-transfer event will be accreted by the secondary, increasing its mass to

$$M''_{Sf} = M''_{Si} + f_a(M'_{Si} - M'_C) \,. \tag{7.14}$$

Fully conservative mass transfer ($f_a = 1$) preserves the total mass of the system, while all of the mass lost by the donor is ejected from the system in fully non-conservative mass transfer ($f_a = 0$). We assume that stable mass transfer is semiconservative ($f_a = 1/2$), in agreement with the standard model of Dominik et al. (2012). Larger values of f_a during this first mass-transfer event will tend to favor the RMR scenario over the SMR scenario. Since f_a is directly tied to the fraction of binaries that undergo mass-ratio reversal in a given mass and mass-ratio range, our model suggests that it is potentially measurable via GW observations (Sec. 7.4.2).

For simplicity, we assume that tides and the mass transfer itself efficiently circularize the orbit, but we prevent any circularization when tides are taken to be inefficient (for recent investigations of mass transfer and circularization in eccentric binaries, see Sepinsky et al. 2009, 2010).

7.2.4 Common-envelope evolution

If the semimajor axis a_1 of the binary following the first SN is greater than $a_{\rm noCE}$, as determined from the constraint

$$R_L(a_{\rm noCE}, M''_{Sf}, M'_{\rm BH}) = R''_G\,, \tag{7.15}$$

with R''_G given by Eq. (7.8), the secondary does not fill its Roche lobe and no common-envelope evolution occurs. For smaller values of a_1, a common-envelope phase does occur and the envelope binding energy is converted to gravitational energy. We use conservation of energy to determine how much the binary's orbit shrinks during common-envelope evolution (Webbink 1984, 2008). The gravitational binding energy of the common envelope can be expressed as

$$E_b = -\frac{GM''_{Sf}\left(M''_{Sf} - M''_C\right)}{\lambda\mathcal{R}}\,, \tag{7.16}$$

where M''_{Sf} is the mass of the secondary at the onset of common-envelope evolution, $M''_{Sf} - M''_C$ is the mass lost by the secondary during this evolution, $\mathcal{R} = R_L(a_1, M''_{Sf}, M'_{\rm BH})$ is the Roche-lobe radius of the secondary at the onset of common-envelope evolution, and λ is a dimensionless parameter of order unity that depends on the mass and structure of the secondary, notably the location of the core-envelope boundary. Full stellar-evolution codes can be used to calculate the appropriate value of λ for our BH progenitors (Xu and Li 2010a,b; Loveridge et al. 2011; for a different approach see De Marco et al. 2011). We adopt an analytic fit to Fig. 3 of Dominik et al. (2012), which summarizes the results of these calculations:

$$\lambda = ae^{-b\,\mathcal{R}/R_\odot} + c\,, \tag{7.17}$$

where $a = 0.358$, $b = 7.19\times10^{-3}$, and $c = 0.05$. Conservation of energy during CE evolution implies

$$-\frac{GM'_{\rm BH}M''_{Sf}}{2a_1} + E_b = -\frac{GM'_{\rm BH}M''_C}{2a_{1CE}}\,; \tag{7.18}$$

solving for a_{1CE} yields

$$a_{1CE} = a_1\frac{M''_{\rm C}}{M''_{\rm Sf}}\left(1 + \frac{2}{\lambda}\frac{a_1}{\mathcal{R}}\frac{M''_{\rm Sf} - M''_{\rm C}}{M'_{\rm BH}}\right)^{-1}\,. \tag{7.19}$$

If a_{1CE} is less than $a_{\rm mCE}$, as determined from the constraint

$$R_L(a_{\rm mCE}, M''_C, M'_{\rm BH}) = R''_C\,, \tag{7.20}$$

with R''_C given by Eq. (7.9), the helium core of the secondary itself fills its Roche lobe before the end of common-envelope evolution. This leads to a prompt merger, preventing the eventual formation of a BH binary. Our final prescription for a_{1CE} as a function of a_1 is shown in Fig. 7.3. Common-envelope evolution shrinks the semimajor axis by a factor $\sim 10^3$ and thereby allowing the eventual BH binary to merge in less than a Hubble time.

Motivated by previous hydrodynamical simulations (Ricker and Taam 2008, 2012; Passy et al. 2012), we neglect accretion onto the primary BH during common-envelope evolution. These studies suggest that the BH accretes at substantially less than the Bondi-Hoyle accretion rate (Hoyle and Lyttleton 1941; Bondi and Hoyle 1944) during the evolution, accumulating $\lesssim 0.1M_\odot$ in mass. Given this small change in mass, we are justified in ignoring any resulting changes in the BH spin (King and Kolb 1999). As noted in Sec. 7.2.1, we also neglect the expansion of naked helium stars, and therefore explicitly forbid a helium-star common-envelope phase (Ivanova et al. 2003).

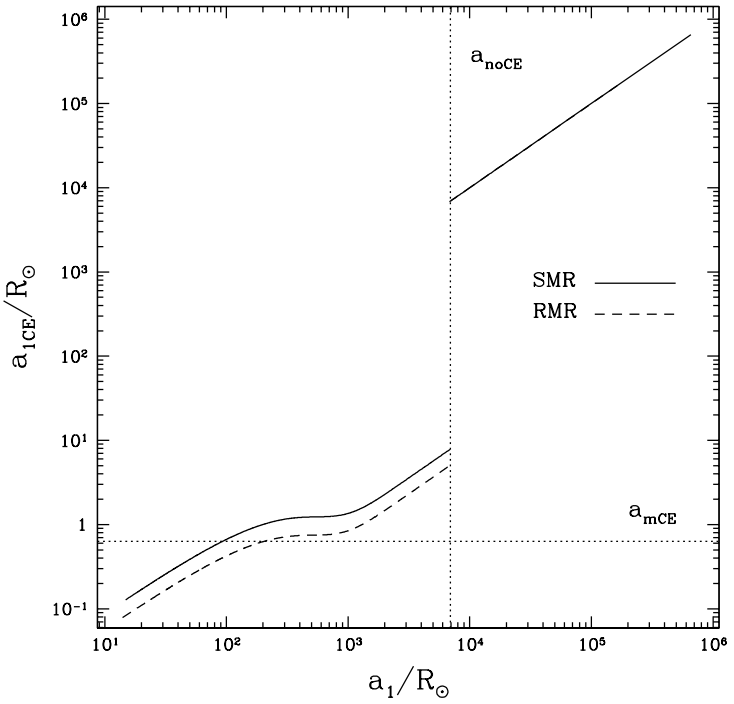

Figure 7.3: The semimajor axis a_{1CE} at the end of common-envelope evolution as a function of its initial value a_1 in both the SMR and RMR scenarios (Gerosa et al. 2013). If $a_1 > a_{\rm noCE}$, as given implicitly by Eq. (7.15), the secondary fails to fill its Roche lobe, no common-envelope evolution occurs, and $a_{1CE} = a_1$. If $a_{1CE} < a_{\rm mCE}$, as given implicitly by Eq. (7.20), the helium core of the secondary fills its Roche lobe prior to the end of the common envelope and the binary merges, failing to eventual form a BH binary. The nonlinear relationship between the semimajor axis before and after the common-envelope phase when $a_1 < a_{\rm noCE}$ results from the nontrivial dependence of the common-envelope efficiency parameter λ on a_1, as given by Eq. (7.17).

7.2.5 Supernova kicks: magnitude and direction

Asymmetric SN events impart hydrodynamical recoils to the newly formed protoneutron stars (Hills 1983; Brandt and Podsiadlowski 1995; Belczynski et al. 2008c; Nordhaus et al. 2012). We calibrate the magnitude of this primordial kick using observed proper motions of young pulsars: each protoneutron star is kicked with a velocity $v_{\rm pNS}$ drawn from a single Maxwellian with parameter $\sigma = 265$ km/s (Hobbs et al. 2005). A fraction $f_{\rm fb}$ of this asymmetrically ejected material falls back onto the protoneutron star and is accreted as it collapses into a BH. This fallback suppresses the magnitude of the final kick imparted to the BH to $v_{\rm BH} \simeq (1 - f_{\rm fb})v_{\rm pNS}$. For BHs with masses $M_{\rm BH} = (6M_\odot, 7.5M_\odot)$, as in our fiducial scenarios, core-collapse simulations by Fryer (1999) and Fryer and Kalogera (2001) suggest $f_{\rm fb} \simeq 0.8$. This BH kick distribution is consistent with the observed proper motions of galactic X-ray binaries hosting BHs (Fragos et al. 2009b; Wong et al. 2012). Although our results are not extremely sensitive to the precise magnitude of the BH kicks, the existence of such kicks is crucial in our model, as they are the only observationally well motivated mechanism to introduce misalignment between the compact binary spins and the orbital plane.

We assume that the BH kicks are distributed in a double cone of opening angle θ_b about the BH spin and consider two extreme scenarios: isotropic ($\theta_b = 90°$) or polar ($\theta_b = 10°$) kicks. There is some observational (Wang et al. 2006a; Noutsos et al. 2013) and theoretical

(Spruit and Phinney 1998; Lai et al. 2001) support for the polar model. However we examine both possibilities because this choice has a significant effect on the resulting binary orbits. Our choice of $\theta_b = 10^\circ$ in the polar model was partly motivated by a comparable observed misalignment between the spin and proper motion of the Crab pulsar (Kaplan et al. 2008).

7.2.6 Supernova kicks: influence on the orbit

In this Section, we describe how SN kicks are implemented in our Monte Carlo calculations. The expressions provided below have been published previously either under more restrictive assumptions (Kalogera 1996, 2000) or using different notation (Hurley et al. 2002). Each SN reduces the mass of the binary and imparts a kick to the newly produced compact remnant. We calculate how these effects change the Keplerian orbital elements by applying energy and angular-momentum conservation to the binary before and after the SN. As the duration of the SN explosion is short compared to the other stages of binary evolution, we assume that this orbital modification occurs instantaneously.

In our simulations we assume that the binary is on a circular orbit ($e_i = 0$) and that the stellar spins are aligned with the orbital angular momentum ($\gamma_i = 0$) when the first SN occurs (we have actually relaxed the circularity assumption in additional simulations not presented here, and we verified that this has a negligible impact on our conclusions: cf. Sec. 7.2.2. If tides are inefficient, both of these simplifying assumptions will not hold, in general, for the second SN. Therefore here we present general expressions for the post-SN orbital elements.

True anomaly. The binary separation r for a Keplerian orbit with initial semimajor axis a_i and eccentricity e_i can be expressed as

$$r = \frac{a_i(1-e_i^2)}{1+e_i\cos\psi_i}\,, \tag{7.21}$$

where ψ_i is the true anomaly. Values for the true anomaly at the time of the SN are chosen by assuming that the explosion is equally likely to occur at any given time. The time t after the binary reaches pericenter is given by

$$\frac{2\pi}{P}t = E - e_i\sin E\,, \tag{7.22}$$

where

$$P = 2\pi\left(\frac{a_i^3}{GM_i}\right)^{1/2} \tag{7.23}$$

is the period of a binary of total mass M_i. The eccentric anomaly E is related to the true anomaly ψ_i by (see e.g. Chobotov 1991; Goldstein et al. 2002)

$$\cos\psi_i = \frac{\cos E - e_i}{1-e_i\cos E}\,. \tag{7.24}$$

We assume that t is uniformly distributed in the range $[0, P]$ and derive the corresponding values of ψ_i from these relations.

Reference frame. Let us consider the orthonormal basis ($\hat{\mathbf{r}}$, $\hat{\mathbf{L}}_\mathbf{i}$, $\hat{\mathbf{r}}\times\hat{\mathbf{L}}_\mathbf{i}$), where $\hat{\mathbf{r}}$ is a unit vector along the line of separation between the members of the binary and $\mathbf{L_i}$ is the orbital angular momentum of the binary before the kick, as shown in Fig. 7.4.

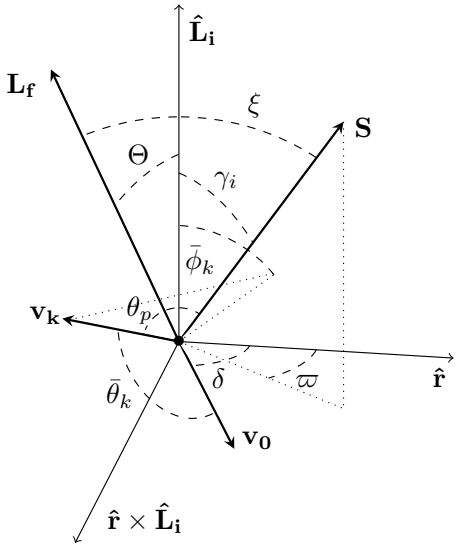

Figure 7.4: Reference frame adopted to study SN kicks, centered on the exploding star. The spin $\mathbf{S}$, the pre-SN velocity $\mathbf{v_0}$, the kick velocity $\mathbf{v_k}$ and the final orbital angular momentum $\mathbf{L_f}$ are shown in the basis $(\hat{\mathbf{r}}, \hat{\mathbf{L}}_\mathbf{i}, \hat{\mathbf{r}} \times \hat{\mathbf{L}}_\mathbf{i})$, where $\hat{\mathbf{r}}$ points toward the companion star and $\mathbf{L_i}$ is the orbital angular momentum before the explosion.

The position of the collapsing star with respect to its companion is

$$\mathbf{r} = -r\,\hat{\mathbf{r}}\,, \tag{7.25}$$

where the separation r is given by (7.21). The direction of the spin $\mathbf{S}$ of the star is specified by the angle γ_i between $\mathbf{S}$ and $\mathbf{L_i}$ and the angle ϖ between the projection of $\mathbf{S}$ in the orbital plane and $\hat{\mathbf{r}}$:

$$\mathbf{S} = S\sin\gamma_i\cos\varpi\,\hat{\mathbf{r}} + S\cos\gamma_i\,\hat{\mathbf{L}}_\mathbf{i} + S\sin\gamma_i\sin\varpi\,\hat{\mathbf{r}}\times\hat{\mathbf{L}}_\mathbf{i}\,. \tag{7.26}$$

The velocity of the collapsing star before the kick $\mathbf{v_0}$ is given by the standard expression for a Keplerian orbit

$$\mathbf{v_0} = -v_0\cos\delta\,\hat{\mathbf{r}} + v_0\sin\delta\,\hat{\mathbf{r}}\times\hat{\mathbf{L}}_\mathbf{i}\,, \tag{7.27}$$

where

$$v_0^2 = \frac{GM}{a_0}\frac{1+2e_i\cos\psi_i+e_i^2}{(1-e_i)^2}\,, \qquad \cos\delta = \frac{e_i\sin\psi_i}{(1+2e_i\cos\psi_i+e_i^2)^{1/2}}\,. \tag{7.28}$$

The direction of the kick velocity $\mathbf{v_k}$ is defined by a polar angle $\bar{\theta}_k$ and an azimuthal angle $\bar{\phi}_k$. Here $\bar{\theta}_k$ is the angle between $\mathbf{v_k}$ and the pre-SN orbital velocity $\mathbf{v_0}$, and the axis defined by $\bar{\phi}_k = 0$ is chosen to be parallel to the orbital angular momentum $\mathbf{L_i}$:

$$\mathbf{v_k} = v_k\cos\bar{\theta}_k\,\hat{\mathbf{v}}_\mathbf{0} + v_k\sin\bar{\theta}_k\cos\bar{\phi}_k\,\hat{\mathbf{L}}_\mathbf{i} + v_k\sin\bar{\theta}_k\sin\bar{\phi}_k\,\hat{\mathbf{v}}_\mathbf{0}\times\hat{\mathbf{L}}_\mathbf{i} \tag{7.29}$$

$$\begin{aligned} &= -\,v_k(\cos\bar{\theta}_k\cos\delta + \sin\bar{\theta}_k\sin\bar{\phi}_k\sin\delta)\,\hat{\mathbf{r}} \\ &\quad + v_k(\cos\bar{\theta}_k\sin\delta - \sin\bar{\theta}_k\sin\bar{\phi}_k\cos\delta)\,\hat{\mathbf{r}}\times\hat{\mathbf{L}}_\mathbf{i} + v_k\sin\bar{\theta}_k\cos\bar{\phi}_k\,\hat{\mathbf{L}}_\mathbf{i}\,. \end{aligned} \tag{7.30}$$

The kick magnitude v_k is chosen using the prescription presented in Sec. 7.2.5. In terms of these angles, the angle θ_p between $\mathbf{S}$ and $\mathbf{v_k}$ is given by

$$\cos\theta_p = \frac{\mathbf{v_k}\cdot\mathbf{S}}{v_k\,S} = -\left(\sin\bar{\theta}_k\sin\bar{\phi}_k\sin\delta + \cos\bar{\theta}_k\cos\delta\right)\cos\varpi\sin\gamma_i + \left(\cos\bar{\theta}_k\sin\delta - \sin\bar{\theta}_k\sin\bar{\phi}_k\cos\delta\right)\sin\varpi\sin\gamma_i + \sin\bar{\theta}_k\cos\bar{\phi}_k\cos\gamma_i\ . \tag{7.31}$$

In our Monte Carlo simulations, kick directions are drawn from uniform distributions in $\bar{\phi}_k$, $\cos\bar{\theta}_k$, and ϖ. Kicks confined to within an angle θ_b of the stellar spin $\mathbf{S}$ are therefore implemented by repeated draws from this distribution such that

$$\theta_p \le \theta_b \qquad \text{or} \qquad \theta_p \ge \pi - \theta_b\,. \tag{7.32}$$

The SN reduces the total mass of the binary from M_i to M_f and changes the velocity of the exploding star from $\mathbf{v_0}$ to $\mathbf{v_0}+\mathbf{v_k}$. The final semimajor axis a_f and eccentricity e_f can be found applying energy and angular-momentum conservation to the binary after the SN explosion.

Energy conservation. After the explosion the total (specific) energy of the binary is given by the Keplerian expression (cf. Eq. 3.1)

$$E = -\frac{GM_f}{2a_f}\,. \tag{7.33}$$

The energy at the explosion can also be found as the sum of kinetic and potential energy

$$E = \frac{(\mathbf{v_0}+\mathbf{v_k})^2}{2} - \frac{GM_i}{r}\,. \tag{7.34}$$

Conservation of energy requires for the final semimajor axis:

$$a_f = a_i\,\beta\left[2\,(\beta-1)\,\frac{1+e_i\cos\psi_i}{1-e_i^2} + 1 - u_k^2 - 2u_k\left(\frac{1+2e_i\cos\psi_i+e_i^2}{1-e_i^2}\right)^{1/2}\cos\bar{\theta}_k\right]^{-1}, \tag{7.35}$$

where $\beta = M_f/M_i$ and u_k is the magnitude of the kick velocity normalized to the circular orbital velocity before the explosion, i.e.

$$u_k = v_k\sqrt{\frac{a_i}{GM_i}}\,. \tag{7.36}$$

Angular-momentum conservation. When the star receives the kick, the (specific) orbital angular momentum is given by

$$\mathbf{L_f} = \mathbf{r}\times(\mathbf{v_0}+\mathbf{v_k}) = \sqrt{GM_ia_i(1-e_i^2)}\left\{\left[1+u_k\left(\frac{1-e_i^2}{1+2e_i\cos\psi_i+e_i^2}\right)^{1/2} \times\left(\cos\bar{\theta}_k - \frac{e_i\sin\psi_i\sin\bar{\theta}_k\sin\bar{\phi}_k}{1+e_i\cos\psi_0}\right)\right]\hat{\mathbf{L}}_\mathbf{i} - \left[u_k\sin\bar{\theta}_k\cos\bar{\phi}_k\frac{(1-e_i^2)^{1/2}}{1+e_i\cos\psi_i}\right]\hat{\mathbf{r}}\times\hat{\mathbf{L}}_\mathbf{i}\right\}. \tag{7.37}$$

When the new orbit forms, the angular momentum has the Keplerian expression (cf. Eq. 3.1)

$$\mathbf{L_f}^2 = GM_f a_f (1 - e_f^2)\,. \tag{7.38}$$

Conservation of angular momentum can thus be used to compute the final eccentricity e_f:

$$\begin{aligned} 1 - e_f^2 = \frac{1 - e_i^2}{\beta^2} \Bigg\{ \left[1 + u_k \left(\frac{1 - e_i^2}{1 + 2e_i \cos\psi_i + e_i^2} \right)^{1/2} \left(\cos\bar{\theta}_k - \frac{e_i \sin\psi_i \sin\bar{\theta}_k \sin\bar{\phi}_k}{1 + e_i \cos\psi_0} \right) \right]^2 \\ + (1 - e_i^2) \left(\frac{u_k \sin\bar{\theta}_k \cos\bar{\phi}_k}{1 + e_i \cos\psi_i} \right)^2 \Bigg\} \\ \times \left[2(\beta - 1) \frac{1 + e_i \cos\psi_i}{1 - e_i^2} + 1 - u_k^2 - 2u_k \left(\frac{1 + 2e_i \cos\psi_i + e_i^2}{1 - e_i^2} \right)^{1/2} \cos\bar{\theta}_k \right]. \end{aligned} \tag{7.39}$$

If the right-hand side of Eq. (7.39) is negative, $e_f > 1$ and the SN has unbound the binary. For binaries that remain bound, the orbital plane is tilted by an angle Θ such that

$$\begin{aligned} \cos\Theta = \frac{\mathbf{L_i} \cdot \mathbf{L}_f}{L_i\, L_f} = \left[1 + u_k \left(\frac{1 - e_i^2}{1 + 2e_i \cos\psi_i + e_i^2} \right)^{1/2} \left(\cos\bar{\theta}_k - \frac{e_i \sin\psi_i \sin\bar{\theta}_k \sin\bar{\phi}_k}{1 + e_i \cos\psi_i} \right) \right] \\ \times \Bigg\{ \left[1 + u_k \left(\frac{1 - e_i^2}{1 + 2e_i \cos\psi_i + e_i^2} \right)^{1/2} \left(\cos\bar{\theta}_k - \frac{e_i \sin\psi_i \sin\bar{\theta}_k \sin\bar{\phi}_k}{1 + e_i \cos\psi_i} \right) \right]^2 \\ + (1 - e_i^2) \left(\frac{u_k \sin\bar{\theta}_k \cos\bar{\phi}_k}{1 + e_i \cos\psi_i} \right)^2 \Bigg\}^{-1/2}, \end{aligned} \tag{7.40}$$

and the angle between $\mathbf{S}$ and the orbital angular momentum is changed from γ_i to ξ, where

$$\begin{aligned} \cos\xi = \frac{\mathbf{S} \cdot \mathbf{L}_f}{S\, L_f} = \Bigg\{ \left[1 + u_k \left(\frac{1 - e_i^2}{1 + 2e_i \cos\psi_i + e_i^2} \right)^{1/2} \left(\cos\bar{\theta}_k - \frac{e_i \sin\psi_i \sin\bar{\theta}_k \sin\bar{\phi}_k}{1 + e_i \cos\psi_i} \right) \right] \cos\gamma_i \\ - u_k \frac{\sqrt{1 - e_i^2}}{1 + e_i \cos\psi_i} \sin\bar{\theta}_k \cos\bar{\phi}_k \sin\gamma_i \sin\varpi \Bigg\} \times \Bigg\{ \left[1 + u_k \left(\frac{1 - e_i^2}{1 + 2e_i \cos\psi_i + e_i^2} \right)^{1/2} \\ \times \left(\cos\bar{\theta}_k - \frac{e_i \sin\psi_i \sin\bar{\theta}_k \sin\bar{\phi}_k}{1 + e_i \cos\psi_i} \right) \right]^2 + (1 - e_i^2) \left(\frac{u_k \sin\bar{\theta}_k \cos\bar{\phi}_k}{1 + e_i \cos\psi_i} \right)^2 \Bigg\}^{-1/2}. \end{aligned} \tag{7.41}$$

When $\mathbf{S}$ is aligned with $\mathbf{L}$ before the SN ($\gamma_i = 0$), the tilt of the orbital plane equals the misalignment of the exploding star's spin ($\xi = \Theta$).

Circular and aligned binaries. The above expressions greatly simplify for initially circular binaries. For example, the SN will disrupt the binary if

$$u_k^2 + 2u_k \cos\bar{\theta}_k + 1 - 2\beta > 0 \quad (e_i = 0). \tag{7.42}$$

The equations simplify even further if **S** and **L** are initially aligned ($\gamma_i = 0$), in which case exactly polar kicks are given by $\bar{\theta}_k = \pi/2, \bar{\phi}_k = 0$. Exactly polar kicks larger than $u_k > \sqrt{2\beta - 1}$ always unbind the binary, while for isotropic kicks a bound tail of the distribution remains provided $u_k < 1 + \sqrt{2\beta}$. If kicks are confined to cones within an angle θ_b of $\mathbf{L_i}$, the minimum final semimajor axis is

$$a_{f,\mathrm{Min}} = \frac{a_i \beta}{2\beta - \cos^2 \theta_b} \quad (e_i = 0, \gamma_i = 0); \tag{7.43}$$

exactly polar kicks ($\theta_b = 0$) can only increase the semimajor axis ($a_{f,\mathrm{Min}} > a_1$), while isotropic kicks ($\theta_b = 90°$) can reduce the semimajor axis by at most a factor of 2 ($a_{f,\mathrm{Min}} = a_1/2$). Exactly polar kicks also add a significant component of angular momentum perpendicular to the initial orbital plane, leading to a strong spin tilt:

$$\cos \Theta = \frac{1}{\sqrt{1 + u_k^2}} \quad (e_i = 0, \gamma_i = 0). \tag{7.44}$$

However, the maximum tilt that polar kicks can produce while the binary remains bound is

$$\Theta = \cos^{-1}(2\beta)^{-1/2}\,. \tag{7.45}$$

By contrast, isotropic kicks can make the binary more tightly bound, allowing greater latitude for kicks to produce bound systems with large spin misalignments.

7.2.7 Tidal alignment

As discussed in Sec. 7.1.1, tidal dissipation can circularize the orbit of the binary and align the spin of the secondary with the orbital angular momentum between the two SN explosions (Kopal 1959; Brouwer and Clemence 1961; Alexander 1973; Zahn 1975; Lecar et al. 1976; Hut 1981; Hurley et al. 2002). Tidal friction is a dissipative process which converts the kinetic energy on the deformation induced by tidal gravity into heat, while conserving the angular momentum. Tidal interactions are operating in the Earth-Moon binary system, slowing down the Earth's rotation and driving the Moon outwards.

A detailed treatment of the theory of tidal damping in massive stars is far beyond the scope of the present work. We therefore only consider the two extreme possibilities: tides can either fully circularize the binary and align the spin of the secondary, or they are completely inefficient. We provide order-of-magnitude estimates for tidal processes below; the full derivation of the equations can be found in Hut (1981) and Eggleton (2006).

Tides should generally act on both members of the binary. However tidal effects on the BH can safely be ignored, given its small size. We therefore focus on tidal effects on the secondary between the two SN (phase **d** of the evolutionary scenario presented in Fig. 7.1). If the secondary is fully convective, as expected for the core of a BH progenitor, convection causes internal damping on the viscous timescale

$$t_V \simeq \frac{3^{1/3}}{\gamma} \left(\frac{M_S}{M_\odot}\right)^{1/3} \left(\frac{R_S}{R_\odot}\right)^{2/3} \left(\frac{L_S}{L_\odot}\right)^{-1/3}, \tag{7.46}$$

where M_S, R_S and L_S are the mass, radius and luminosity of the secondary, and γ is a prefactor that depends on details of the stellar structure (Eggleton and Kiseleva-Eggleton

2001). The orbit evolves on the tidal-friction timescale (Eggleton 2006)

$$t_{\rm tid} \simeq \tilde{k}\,\frac{t_V}{9}\,\frac{M_{\rm S}^2}{(M_{\rm BH}+M_S)M_{\rm BH}}\left(\frac{a}{R_S}\right)^8 \tag{7.47}$$

$$\simeq 4\times10^{-3}\,\tilde{k}\gamma\,\frac{1}{Q(1+Q)}\left(\frac{M_{\rm S}}{10M_\odot}\right)^{1/3}\left(\frac{R_{\rm S}}{10R_\odot}\right)^{2/3}\left(\frac{L_{\rm S}}{10^4L_\odot}\right)^{-1/3}\left(\frac{a}{R_{\rm S}}\right)^8 {\rm yr}\,, \tag{7.48}$$

where $M_{\rm BH}$ is the mass of the primary, $Q = M_{\rm BH}/M_S$ is the mass ratio at this stage of the evolution, and $\tilde{k}$ is a constant related to the quadrupole mass moment of the secondary, thus depending on its shape[3]. Values of γ and $\tilde{k}$ can be computed exactly for polytropic stars, i.e. self-gravitating, spherically symmetric solutions of the fluid equations (6.1)-(6.3) with a power-law equation of state $P \propto \rho^{1+1/n}$ (Table 7.3). Convective stars are well approximated by $n = 1.5$ polytropes (e.g. Prialnik 2009), for which $\tilde{k}\gamma \simeq 0.2$ is of order unity.

Even though the details depend on the initial stellar spin, tidal friction should synchronize and align the spin of the secondary with the now circular orbit on this same timescale (Eggleton and Kiseleva-Eggleton 2001). The most notable feature of the tidal-friction timescale $t_{\rm tid}$ given by Eq. (7.47) is its extremely steep dependence on the ratio a/R_S. While the secondary remains on the main sequence with a radius given by Eq. (7.6), this ratio is typically 100 or greater for binaries that avoid merging during CE evolution. This implies that tidal alignment occurs on timescales much longer than the Hubble time $t_H \simeq 10^{10}$ yrs. However, once the secondary evolves to fill its Roche lobe, its radius is given by Eq. (7.11) and the ratio a/R_S becomes of order unity. This reduces the tidal-friction timescale well below typical stellar-evolution timescales of a few million years (hydrogen-core burning) or even the briefer time

$$t_{\rm HG} \simeq 2.7\times10^4\left(\frac{M_{\rm C}}{10M_\odot}\right)^2\left(\frac{R_{\rm C}}{10R_\odot}\right)^{-1}\left(\frac{L_{\rm S}}{10^4L_\odot}\right)^{-1}{\rm yrs} \tag{7.49}$$

that the secondary spends on the Hertzsprung gap after exhausting the hydrogen in its core (i.e., the Kelvin-Helmholtz timescale of the core). Since our fiducial scenarios require the secondary to fill its Roche lobe prior to the second SN, one might expect tidal alignment to always be efficient. Substantial uncertainties remain in the model however. Stars with partially radiative envelopes may have longer tidal-friction timescales (Eggleton 2006; Belczynski et al. 2008a), and the stellar core may not efficiently couple to its envelope, as suggested by recent Kepler observations of core-rotation rates (Beck et al. 2012). Therefore, for completeness, we also explore the "extreme" alternative scenario of completely inefficient tidal alignment. Being dissipative in nature, tidal interactions decrease the semimajor axis in addition to circularizing the orbit. This change is small compared to that induced by common-envelope evolution, and can therefore be neglected along with the orbital changes produced by other phenomena (e.g. magnetic braking and mass transfer).

n	0	1	1.5	3	3.5	4
γ	1.00	0.610	0.339	0.0122	0.0020	0.00018
$\tilde{k}$	0.160	0.433	0.604	0.944	0.979	0.995

Table 7.3: Constants relevant to tidal interactions in the case of polytropic stars. We list the values of the constants γ and $\tilde{k}$ (which enter in Eq. 7.48) for polytropic solutions of the stellar-structure equations as a function of the polytropic index n. Details can be found in Eggleton (2006).

[3]In the notation of Eggleton (2006): $\tilde{k} = (1 - Q^2)$, where Q is the dimensionless quadrupole moment

7.3 Spin directions: a unified treatment

We finally present here our main results. The PN evolutionary equations described in Chapter 6 are initialized with our astrophysical predictions, presented in Sec. 7.1, to predict the spin configurations by the time the gravitational radiate from BH binaries enters the sensitivity band of GW detectors.

7.3.1 Initial data for the post-Newtonian inspiral

By construction, all of the merging BH binaries produced in Sec. 7.1 have $M = 13.5 M_{\odot}$, $q = 0.8$, and $\chi_1 = \chi_2 = 1$. For this mass ratio and these spin magnitudes, binaries become attracted towards resonances ("resonant locking") at separations $a \lesssim 100M$. As tested in Chapter 6, in order to fully capture the resonant behavior it is sufficient follow binaries from the initial separation $a_{\rm PNi} = 1000M$ (large enough so that we can neglect spin-spin coupling at greater separations) down to $a_{\rm PNf} = 10M$. Recall that the mass ratio was defined such that $q \equiv m_2/m_1 \leq 1$, and the angles θ_1, θ_2 and $\Delta\Phi$ are defined through (6.18)-(6.20).

In the SMR scenario, the primary yields the larger BH ($M'_{\rm BH} > M''_{\rm BH}$), so the angles are initialized to be

$$\theta_1 = \gamma'_2, \qquad \theta_2 = \gamma''_2 \,. \tag{7.50}$$

where γ'_2 is given in (7.2), and γ''_2 is given in (7.3) and (7.4) for the "Tides" and the "No Tides" runs, respectively. In the RMR case, the primary transfers so much mass to the secondary prior to the first SN that it actually produces the smaller BH ($M'_{\rm BH} < M''_{\rm BH}$), implying that we must reverse our initialization:

$$\theta_1 = \gamma''_2, \qquad \theta_2 = \gamma'_2 \,. \tag{7.51}$$

By neglecting spin-spin couplings for $a > a_{\rm PNi}$ we are allowed to initialize θ_i in this manner, but the lower-order spin-orbit coupling allows $\Delta\Phi$ to evolve on the precessional timescale, which is short compared to the time it takes to inspiral from a_2 to $a_{\rm PNi}$. We can therefore choose $\Delta\Phi$ at $a_{\rm PNi}$ to be uniformly distributed in the range $[-180^\circ, +180^\circ]$.

Finally, since gravitational radiation is very efficient at circularizing the orbit (to leading order $e \propto a^{19/12}$; see Eqs. 5.5-5.6), we assume that all BH binaries have circularized by the time they reach $a_{\rm PNi}$. We checked this assumption by numerically integrating (5.5) and (5.6) from a_2 to $a_{\rm PNi}$ after initializing it with the values e_2 predicted following the second SN; the residual eccentricity at $a_{\rm PNi}$ was less than 10^{-4} for all BH binaries in our samples.

7.3.2 Resonant-plane locking and spin-alignment

We evolved 10^3 BH binaries for each of the 8 different fiducial astrophysical scenarios described in Sec. 7.1.2 with the numerical setup presented in Sec. 6.3.2. The results for our eight runs are shown in Figs. 7.5-7.8, where we show the evolution of the dynamical variables $(\theta_1, \theta_2, \Delta\Phi)$. Here we plot θ_1, θ_2 and θ_{12} instead of their cosines, at variance with Figs. 6.4-6.5, in order to emphasize the details of the distributions for low values of the misalignment angles.

In Fig. 7.5 we show our results for both the SMR (red points) and RMR (green points) scenarios with efficient tides and isotropic kicks. Efficient tidal interactions lead to spin orientations that are strongly affected by spin-orbit resonances. When binaries are brought close enough to resonant configurations by precessional motion and gravitational-radiation reaction, they no longer precess freely through all values of $\Delta\Phi$, but instead oscillate about the resonant configurations. In the SMR scenario, the initial orientation of the spins is such that $\theta_1 > \theta_2$ (cf. our $(10-0)$ run in Sec. 6.3.3), and the binaries lock into resonances with $\Delta\Phi = \pm 180^\circ$. In contrast, in the RMR scenario the initial spins have $\theta_1 < \theta_2$ (as in the $(0-10)$ run of Sec. 6.3.3) and the binaries lock into resonances with $\Delta\Phi = 0^\circ$. Once the binaries are trapped near resonances, they evolve toward the diagonal in the (θ_1, θ_2) plane,

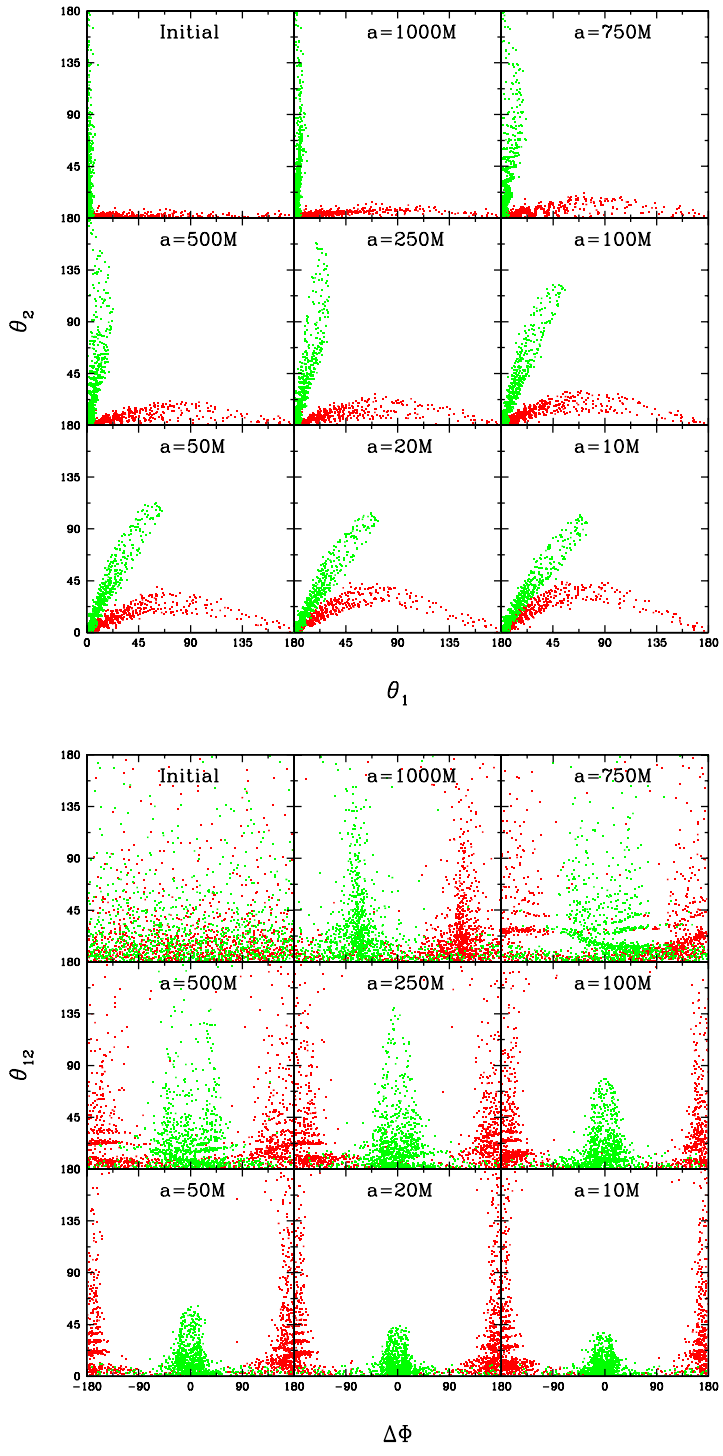

Figure 7.5: Scatter plots of the PN inspiral of maximally spinning BH binaries with mass ratio $q = 0.8$ from an initial separation $a_{\rm PNi}$ just above $1000M$ to a final separation $a_{\rm PNf} = 10M$. The top panel shows this evolution in the (θ_1, θ_2) plane and the bottom panel shows the evolution in the $(\Delta\Phi, \theta_{12})$ plane. Red and green dots refer to the SMR and RMR scenarios, respectively. The initial distribution for these Monte Carlo simulations was constructed from an astrophysical model with **efficient tides** and **isotropic kicks** (Gerosa et al. 2013).

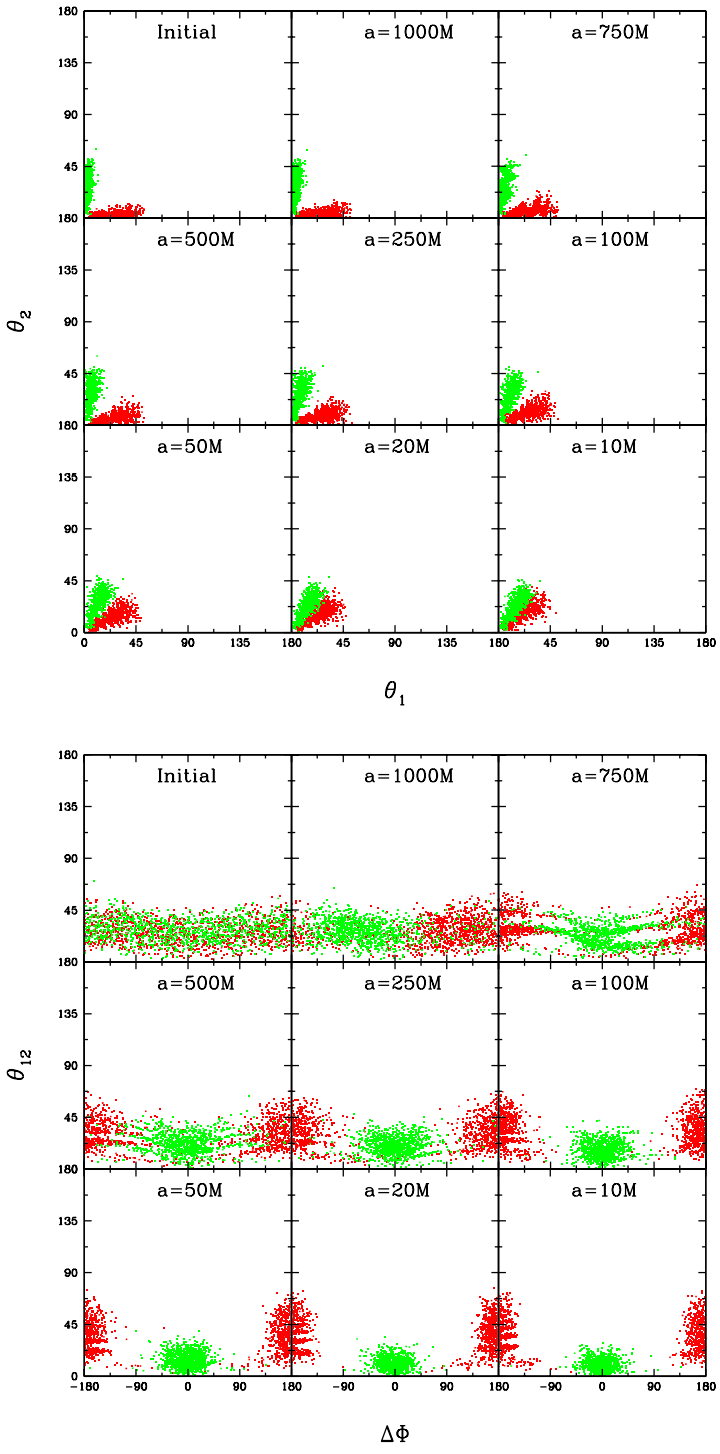

Figure 7.6: Scatter plots of the PN inspiral of maximally spinning BH binaries with mass ratio $q = 0.8$ from an initial separation $a_{\rm PNi}$ just above $1000M$ to a final separation $a_{\rm PNf} = 10M$. The top panel shows this evolution in the (θ_1, θ_2) plane and the bottom panel shows the evolution in the $(\Delta\Phi, \theta_{12})$ plane. Red and green dots refer to the SMR and RMR scenarios, respectively. The initial distribution for these Monte Carlo simulations was constructed from an astrophysical model with **efficient tides** and **polar kicks** (Gerosa et al. 2013).

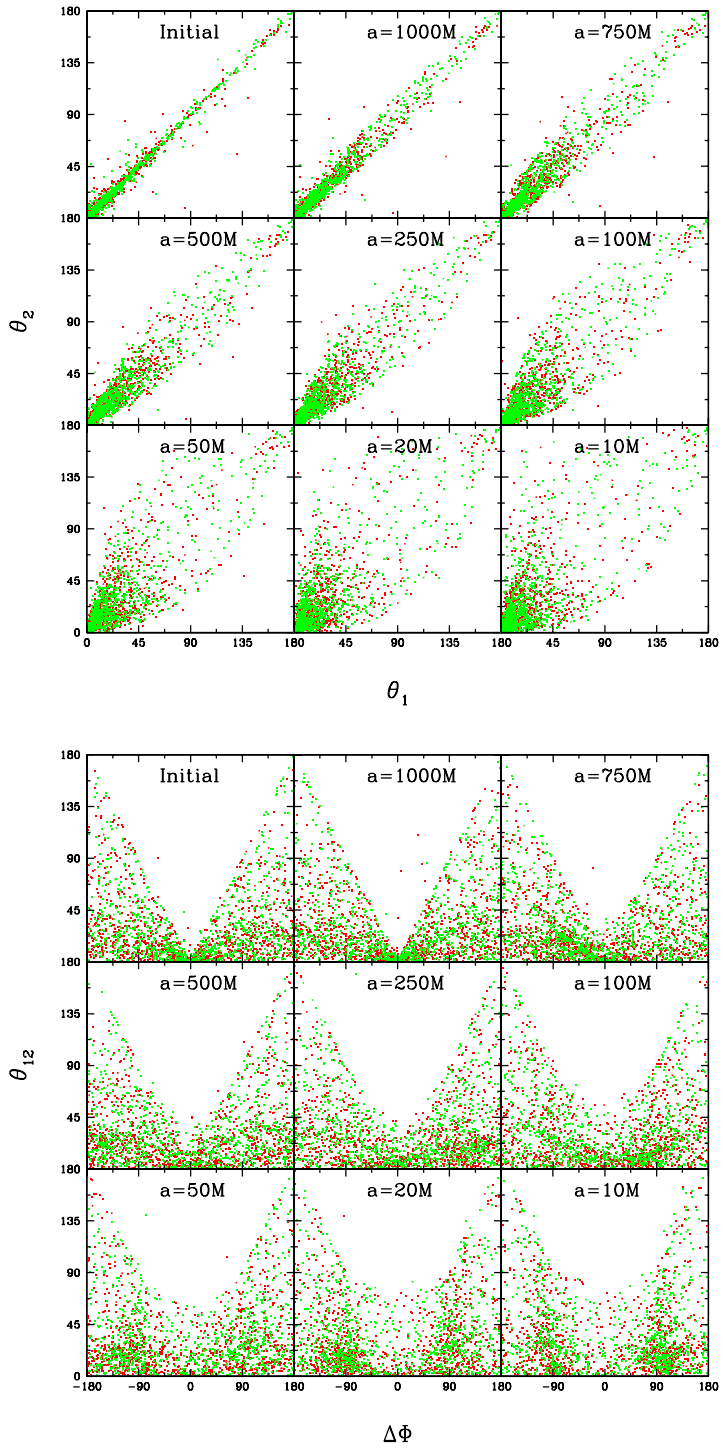

Figure 7.7: Scatter plots of the PN inspiral of maximally spinning BH binaries with mass ratio $q = 0.8$ from an initial separation $a_{\rm PNi}$ just above $1000M$ to a final separation $a_{\rm PNf} = 10M$. The top panel shows this evolution in the (θ_1, θ_2) plane and the bottom panel shows the evolution in the $(\Delta\Phi, \theta_{12})$ plane. Red and green dots refer to the SMR and RMR scenarios, respectively. The initial distribution for these Monte Carlo simulations was constructed from an astrophysical model with **inefficient tides** and **isotropic kicks** (Gerosa et al. 2013).

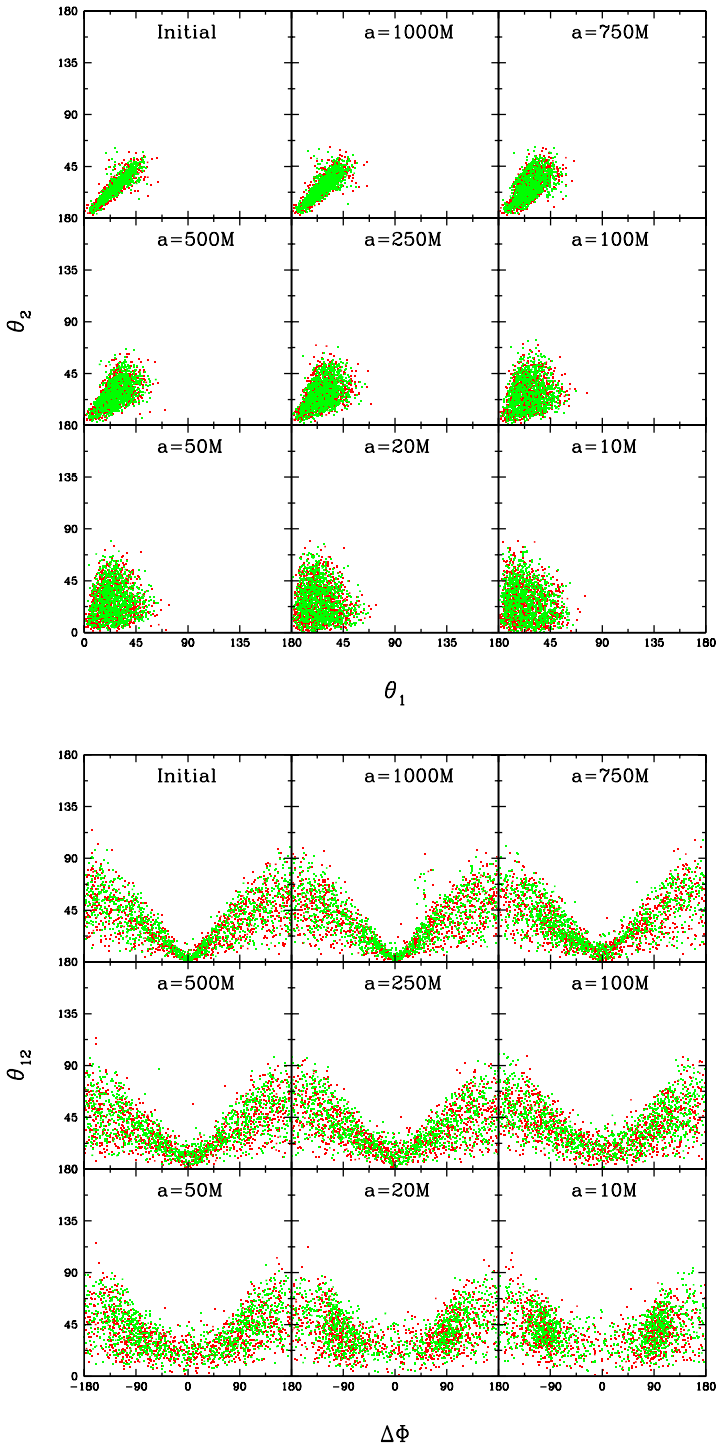

Figure 7.8: Scatter plots of the PN inspiral of maximally spinning BH binaries with mass ratio $q = 0.8$ from an initial separation $a_{\rm PNi}$ just above $1000M$ to a final separation $a_{\rm PNf} = 10M$. The top panel shows this evolution in the (θ_1, θ_2) plane and the bottom panel shows the evolution in the $(\Delta\Phi, \theta_{12})$ plane. Red and green dots refer to the SMR and RMR scenarios, respectively. The initial distribution for these Monte Carlo simulations was constructed from an astrophysical model with **inefficient tides** and **polar kicks** (Gerosa et al. 2013).

as seen in the top panel of Fig. 7.5. This corresponds to $\theta_{12} \to 0^\circ$ for binaries near the $\Delta\Phi = 0^\circ$ family of resonances (RMR scenario). As seen in the bottom panel of Fig. 7.5, there is a much broader range of final values for θ_{12} in the SMR scenario, because these final values depend on the initial astrophysical distribution of $\mathbf{S_0} \cdot \hat{\mathbf{L}}$ according to Eq. (6.44).

Fig. 7.6 shows that spin-orbit resonances can have an even stronger effect on BH binaries when SN kicks are polar (aligned within $\theta_b = 10^\circ$ of the stellar spin, Sec. 7.2.5). As discussed in Sec. 7.2.6, exactly polar kicks tilt the orbital plane by an angle Θ given by (7.44), which can only attain a maximum value $\cos^{-1}(2\beta)^{-1/2}$ (where $\beta = M_f/M_i$ is the ratio of the total binary mass before and after the SN) without unbinding the binary. For $\beta \simeq 0.9$, as in our SMR and RMR scenarios, $\Theta \lesssim 40^\circ$, and kicks are rarely large enough even to saturate this limit. This explains the much narrower distribution of initial values of θ_i in the left panel of Fig. 7.6 compared to Fig. 7.5. Binaries with these smaller initial misalignments are more easily captured into resonances, as can be seen from the near total segregation of the SMR and RMR populations in $\Delta\Phi$ by the time the binaries reach $a_{\rm PNf} = 10M$ in the bottom panel of Fig. 7.6.

In our model, two physical mechanisms are responsible for changing BH spin orientations: SN kicks and tidal alignment. Both mechanisms are critical: kicks generate misalignments between the spins and the orbital angular momentum, but only tides can introduce the asymmetry between these misalignments that causes one family of spin-orbit resonances (the $\Delta\Phi = \pm 180^\circ$ family in the SMR scenario, the $\Delta\Phi = 0^\circ$ family in the RMR scenario) to be favored over the other. When tidal effects are removed, as shown in Figs. 7.7 and 7.8, BH binaries are formed with $\theta_1 \simeq \theta_2$ on average. Being symmetric under exchange of the two BHs, the evolution in the SMR and RMR scenarios is almost identical. As expected (cf. the $(10-10)$ test run presented in Sec. 6.3.3), binaries do not lock into resonant configurations, instead precessing freely during the whole inspiral. In the late stages of inspiral, the binaries tend to pile up at $\Delta\Phi = \pm 90^\circ$, i.e. they spend more time in configurations where the projections of the two spins on the orbital plane are orthogonal to each other. Unlike the spin-orbit resonances, configurations with $\Delta\Phi = \pm 90^\circ$ are not steady-state solutions to the spin-evolution equations in the absence of radiation reaction (Schnittman 2004). The pile up at these configurations however is an essential complement to the spin-orbit resonances for preserving the well known result that initially isotropic spin distributions remain isotropic: see e.g. Bogdanović et al. (2007), as well as our "Isotropic" runs in Sec. 6.3.3. A first attempt at understanding the physical origin of this phenomenon is presented in Sec. 7.3.3.

The $a = 1000M$ snapshots in Figs. 7.5-7.8 are taken shortly after the beginning of the PN evolution. The angle $\Delta\Phi$ varies on the precessional timescale and can therefore change quite rapidly before the separation decreases appreciably on the longer inspiral timescale. The initial clustering in $\Delta\Phi$ visible in the top-top panels of Figs. 7.5 and 7.6 is *not* a resonant effect, as the binaries continue to sweep through all values of $\Delta\Phi$ at these large separations. It results instead from the different rates at which binaries in the SMR and RMR populations precess, segregating the groups from each other during the first few precessional cycles.

7.3.3 Pile-up configurations

As we observed in the previous Section, the pile up at $\Delta\Phi = \pm\pi/2$ observed in the "No Tides" simulations is *not* a resonant effect: it is due instead to a combination of the precessional motion of the spins about $\mathbf{L}$ and of the change in direction of $\hat{\mathbf{L}}$, which is necessary to preserve the conservation of the total angular momentum $\mathbf{J}$ on precessional timescales. Evolutions performed removing the 3PN spin-orbit couplings in Eqs. (6.23)-(6.24) show the same qualitative behavior. Binaries are not librating around any equilibrium solution. They evolve spanning the whole range in $\Delta\Phi$, but their precessional motion slows down when $\Delta\Phi \sim \pi/2$, and therefore they spend more time in these configurations.

To further investigate the pile-up behavior, we compute the time derivative of $\Delta\Phi$ on the precessional timescale. This can be done directly from the definition of $\Delta\Phi$ reported in

(6.20), using (6.23)-(6.24) but taking $dv/dt = 0$. We find:

$$M\frac{d\Delta\Phi}{dt} = v^5\frac{3}{2}\frac{1-q}{1+q} - v^6\frac{1}{(1+q)^2}\left\{\left[\left(1-\frac{3q}{2}\right)\chi_1\cos\theta_1 - q^2\left(1-\frac{3}{2q}\right)\chi_2\cos\theta_2\right] + \frac{1}{2}\cos\Delta\Phi\left(\chi_1\frac{\sin\theta_1}{\tan\theta_2} - q^2\chi_2\frac{\sin\theta_2}{\tan\theta_1}\right)\right\}. \tag{7.52}$$

The analytical formula (7.52) describes, at least qualitatively, the observed pile up. The 3PN term proportional to $\cos\Delta\Phi$ vanishes for $\Delta\Phi \to \pm\pi/2$: when binaries approach these regions, the rate of change of $\Delta\Phi$ generally decreases. Moreover, this term is a subleasing PN correction to the leading 2.5PN order term, thus explaining why the effect is more pronounced in the late inspiral (see Figs. 7.7-7.8)

The previous argument is only qualitative in nature. Both θ_1 and θ_2 in (7.52) are not constant on the precessional timescale, even if we ignore all spin-orbit couplings. The direction of the angular momentum changes on the precessional timescale due to (6.25). This causes a variation of θ_1, θ_2 and $\Delta\Phi$, because these angles are all defined in the reference frame reported in Fig. 6.1, with $\hat{\mathbf{L}}$ along the z-axis. For this reason, both θ_1 and θ_2 in that formula depend in a subtle way on $\Delta\Phi$. Further investigations are required to fully understand the origin of the pile-up effect.

7.3.4 Black-hole binaries in the sensitivity band

SN kicks tilt the orbit, producing a misalignment between the orbital angular momentum and the orientation of the spins of the binary members. As a result, the main factors determining the spin alignment of a BH binary are the magnitude of SN kicks and the possibility that other physical effects may realign the spins with the orbital angular momentum in between SN events. Dominant among these physical effects (aside from the SN kick itself) are the efficiency of tidal interactions and the possibility of a mass-ratio reversal due to mass transfer from the initially more massive, faster evolving progenitor.

Tides affect the binary in two significant ways: they align the spins of stellar BH progenitors with the orbital angular momentum and they reduce the binary eccentricity. Additionally, tides force stars to rotate synchronously with the orbit, increasing the likelihood of a large BH spin at collapse and implying that our results will depend only mildly (if at all) on the initial stellar spin. Consider the evolution of the system between the two SN events, when the binary consists of a BH and a non-degenerate star. If tidal interactions are efficient (a reasonable assumption, as we argued in Sec. 7.2.7) they tend to align the star (but not the BH) with the orbital angular momentum. This introduces an asymmetry in the angles (θ_1, θ_2) which is critical to determining the spin configuration at the end of the inspiral. Mass transfer can change the mass ratio of interacting binaries. In particular this may produce a mass-ratio reversal, so that the heavier BH is formed by the (initially) lighter star. Since BHs are relatively immune to the effects of tides, the spin of the first BH to form will be more misaligned than the spin of the second BH, as this misalignment will have accumulated due to the kicks generated during *both* SN events. Therefore, in the SMR scenario BH binaries will have $\theta_1 > \theta_2$ at formation, and thus $\Delta\Phi \simeq \pm 180^\circ$ by the time they enter the GW-detection band. On the other hand, in the RMR scenario BH binaries initially have $\theta_1 < \theta_2$, so that by late in the inspiral $\Delta\Phi \simeq 0^\circ$, and furthermore the spins are nearly aligned with each other (i.e., $\theta_{12} \simeq 0$). In summary, whenever tidal interactions are efficient, our model predicts that BH spins should preferentially lie in a "resonant plane" (identified by the conditions $\Delta\Phi = 0^\circ$ in the RMR scenario, and $\Delta\Phi = \pm 180^\circ$ in the SMR scenario) when they become detectable by GW interferometers. A third (more unlikely) possibility is that tidal interactions are not efficient. In this case our simulations show that binaries will preferentially have $\Delta\Phi \simeq \pm 90^\circ$. *Because the most likely values of* $\Delta\Phi$ *in the three scenarios (RMR, SMR and no tides) are mutually exclusive, GW measurements of a*

statistically significant sample of values of $\Delta\Phi$ will provide important astrophysical information on compact-binary formation scenarios. In particular, they will tell us whether tidal interactions are efficient, and (if so) whether mass transfer can produce mass-ratio reversals.

Fig. 7.9 makes these conclusions more quantitative by showing three histograms of $\Delta\Phi$ (top) and θ_{12} (bottom), corresponding to snapshots taken at different times during the inspiral, and correspondingly to different GW frequency $f_{\rm GW}$ (see Eq. 5.10). To reduce the Poisson noise, we evolved larger samples of 10^4 BH binaries to produce these figures. All simulations shown in this figure assume that kick directions are isotropically distributed. The "No Tides" panels contain both SMR and RMR events.

The distribution of $\Delta\Phi$ is flat at large separations (blue dotted lines, corresponding to early times and small orbital frequency) because spin-spin couplings are weak, and the BH spins simply precess about the orbital angular momentum. If tidal alignment is efficient, in the late inspiral the BH spins lock into equilibrium configurations with either $\Delta\Phi = 0^\circ$ or $\Delta\Phi = \pm 180^\circ$. This effect is clearly visible at GW frequencies $f_{\rm GW} = 1$ Hz (red dashed lines), roughly corresponding to the lowest cutoff frequency of third-generation detectors like the Einstein Telescope, and it is even more pronounced when the binaries enter the Advanced LIGO/Virgo band at $f_{\rm GW} \simeq 20$ Hz (black solid lines). If tides are artificially removed, free precession during the late stages of the inspiral slows down the evolution of $\Delta\Phi$ when the components of the spin orthogonal to the orbital angular momentum are also orthogonal to each other, causing binaries that are not locked into resonance to pile up at $\Delta\Phi = \pm 90^\circ$.

Let us stress again that the statistical effect of resonances is clearly visible at $f_{\rm GW} = 20\,$Hz, i.e. when BH binaries enter the Advanced LIGO/Virgo band. Therefore GW measurements of $\Delta\Phi$ could be used to constrain uncertainties in BH binary-formation scenarios. The inclusion of resonant effects in population-synthesis models (combined with a statistically significant sample of GW measurements of $\Delta\Phi$) has the potential to constrain some of the main uncertainties in the models, such as tidal timescales, the efficiency of common-envelope evolution, and the SN engine mechanism.

7.4 A diagnostic for compact-binary formation

If the angles $\Delta\Phi$ and θ_{12} are measurable with GW observations, our model predicts that they will carry a strong signature of BH binary formation processes. In this Section we discuss the limitations of the present study and the improvements that will be necessary to model the spin evolution more accurately. We also present a preliminary comparison with population-synthesis predictions.

7.4.1 Model limitations

In our study we chose to follow the evolution of two binary progenitors (SMR and RMR) in detail, using a specific formation channel. The resulting BH binaries resemble at least qualitatively the low-mass BH binaries that can be formed through a wide range of compact object formation scenarios at a range of metallicities: see e.g. Dominik et al. (2012).

An important assumption made in this study is that of negligible mass loss. Current calculations suggest that the progenitors of the most commonly detected BH binaries will in fact have low metallicity and strongly suppressed mass loss (Dominik et al. 2012). The advantage of our approach is that by neglecting mass loss and focusing on a pair of fiducial binaries we can perform a "controlled experiment" to highlight how different physical phenomena influence the efficiency of PN resonance locking. Variations in the range of initial binary masses, wind mass loss and other mass transfer modes will affect the mass distribution of the binaries and the initial distribution of the misalignment angles $(\theta_1\,, \theta_2)$, but not our main qualitative predictions, that should be rather robust.

This study included what we believe to be the most important physical mechanisms that could trap binaries in resonant configurations, but it is certainly possible that additional ingredients overlooked in our model could complicate our simple interpretation of the results.

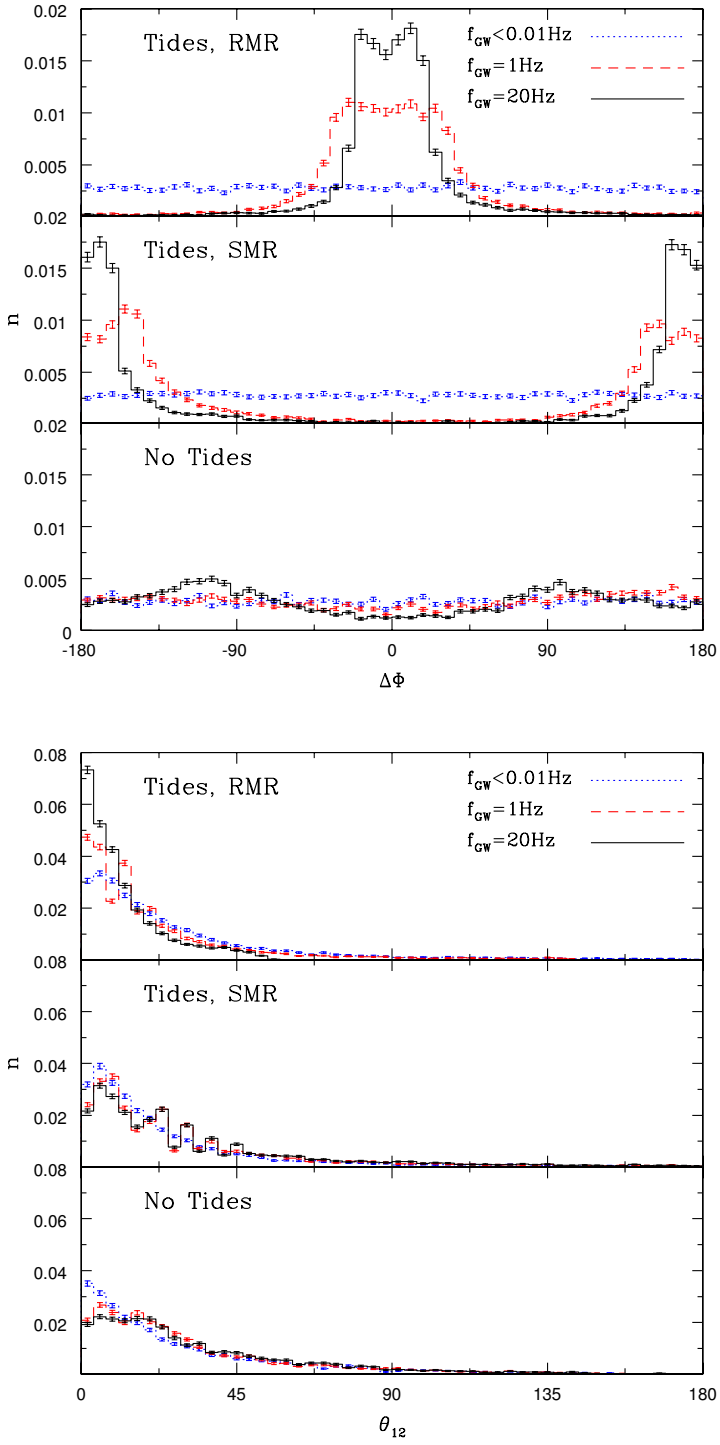

Figure 7.9: Probability distribution of the angle $\Delta\Phi$ (top) and θ_{12} (bottom) for different emitted GW frequencies $f_{\rm GW}$, assuming statistical Poisson noise. Under the effect of tides the PN evolution brings the spins in the same plane ($\Delta\Phi \to 0°, \pm 180°$), in both the RMR and the SMR scenario. When tidal effects are removed the spins precess freely and pile up at $\Delta\Phi = \pm 90°$. In the RMR scenario the spins end up being almost completely aligned with each other, i.e. most binaries have $\theta_{12} \simeq 0°$. In the SMR scenario and in the absence of tides, a long tail at large values of θ_{12} remains even in the late inspiral.

For example, our argument relies on a universal and deterministic relationship between stellar masses and compact remnants. By contrast, some studies suggest that the relationship between the initial and final mass may depend sensitively on interior structure (Ugliano et al. 2012), rotation, or conceivably even stochastically on the specific turbulent realization just prior to explosion. Likewise, our argument makes the sensible assumption that BH spins are aligned with the spin of their stellar progenitor, but neutron star observations suggest that the protoneutron star's spin axis may be perturbed in a SN (Farr et al. 2011).

Our case studies of binary evolution omit by construction many of the complexities present in more fully developed population-synthesis models (it is instructive in this sense to compare Fig. 7.1 and Fig. 5.3). The inclusion of additional physics presents interesting opportunities for a more detailed understanding of the connection between poorly constrained assumptions in population-synthesis models and GW observations. Some of the limitations we imposed on our model – and therefore, interesting opportunities for follow-up studies – are listed below:

i) we follow the formation and evolution of only two progenitor binaries, rather than monitoring a distribution of masses;

ii) we only consider maximally spinning BHs, while we should consider astrophysically motivated spin magnitude distributions;

iii) we adopt very simple prescriptions for mass transfer and evolution, which have minimal feedback onto the structure and evolution of each star;

iv) we employ an extreme "all or nothing" limit for tidal interactions;

v) we assume that BHs are kicked with a specific fraction of the overall SN kick strength;

vi) we neglect stellar mass loss, magnetic braking and other phenomena that can occur in different formation scenarios.

In summary: while our fiducial scenario provides a representative environment to explore the physics of PN resonances, the specific mass distribution and the quantitative distribution of the misalignment angles at the beginning of the PN-driven inspiral will depend on detailed binary-evolution physics which is neglected by construction in our toy model. It will be interesting to initialize our Monte Carlo simulations using more comprehensive binary-evolution models that include a distribution of progenitor masses, track tidal backreaction on the spins and orbit, and model in more detail mass transfer and the modifications it introduces to core and stellar evolution.

7.4.2 Comparison with population-synthesis results

Let us provide a specific example to illustrate these uncertainties and their potential observational payoff by combining our predictions with results obtained with the `StarTrack` code (see Sec. 5.3.3). Our fiducial model assumed relatively low-mass BHs. These systems receive strong SN kicks (due to small fallback) and are more significantly influenced by common-envelope contraction (because of the greater relative effect of the envelope binding energy). By contrast, more massive BHs in the `StarTrack` sample will accrete a significantly higher fraction of their pre-SN mass, which drastically suppresses the typical kick magnitude. As a result, massive BH binaries can be expected to have BH spins more aligned with the orbital angular momentum.

This sort of qualitative difference between low- and high-mass BH binaries presents an opportunity for GW detectors. The most easily measurable quantity in GW observations is the "chirp mass" $M_{\rm chirp} = \eta^{3/5} M$, where $M = m_1 + m_2$ is the total binary mass and $\eta = m_1 m_2 / M^2$ is the symmetric mass ratio (see e.g. Cutler and Flanagan 1994; Poisson and Will 1995). Therefore, even though current simulations suggest that the detected sample will be dominated by high-mass, nearly aligned BH binaries, observations can clearly identify the

low-mass sample, which should exhibit significant initial misalignment and more interesting precessional dynamics. Given the significant uncertainties in population-synthesis models, even upper limits on the spin-orbit misalignment for high-mass BH binaries would be extremely valuable, either to corroborate the expectation of strong alignment or to demonstrate the significance of SN kicks for high-mass BHs.

Based on our prototype study, let us assume that each PN resonance is an unambiguous indicator of a specific fomation scenario: hypothetical GW measurements of angles $\Delta\Phi \sim \pm 180^\circ$ mean efficient tides in the "standard mass ratio" (SMR) scenario; measurements of $\Delta\Phi \sim 0^\circ$ mean that mass reversal also occurred (RMR); finally, $\Delta\Phi \sim \pm 90^\circ$ is an indication that tidal effects were inefficient (cf. Fig. 7.9). Under these assumptions, statistically significant measurements of $\Delta\Phi$ could directly identify how often each of the three formation channels (efficient tides, SMR; efficient tides, RMR; inefficient tides) occurs, for each binary mass.

To illustrate how informative these measurements might be, Fig. 7.10 shows the relative number of merging binaries that undergo mass-ratio reversal as a function of chirp mass, as derived from the most recent `StarTrack` binary-evolution models (Dominik et al. 2012). The figure (which is meant to be purely illustrative) refers to "Subvariation A" of the "standard model" of Dominik et al. (2012). Each panel shows the chirp-mass distribution of binaries that either do (RMR, dashed blue histograms) or do not (SMR, red solid histograms) undergo mass-ratio reversal. This distribution has characteristic "peaks" at specific values of the chirp mass at any given Z and it depends very strongly on composition, as we can see by comparing the two panels (which refer to $Z/Z_\odot = 1$ and $Z/Z_\odot = 0.1$, respectively). According to our model, measurements of $\Delta\Phi$ for a large enough sample of binaries would

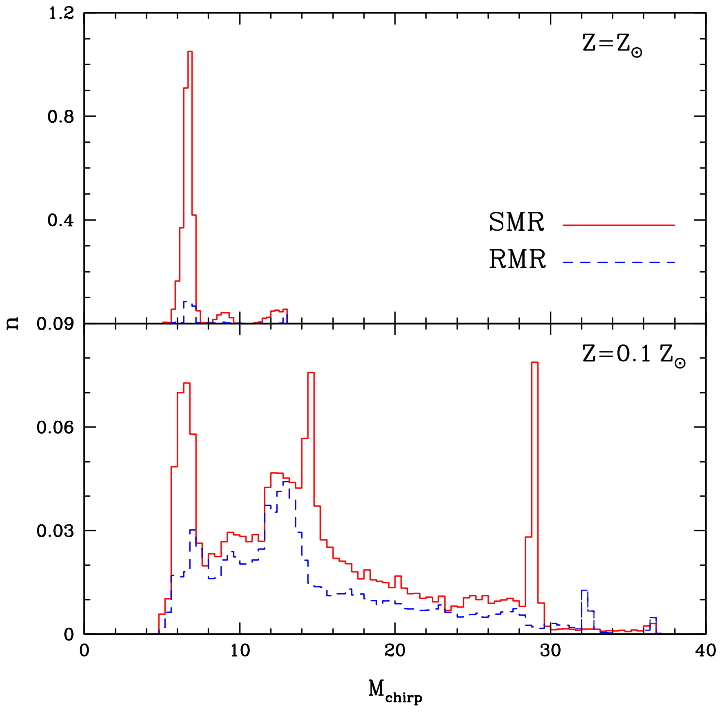

Figure 7.10: Histograms of binaries that do (RMR) or do not (SMR) undergo mass-ratio reversal as a function of chirp mass, according to the publicly available `StarTrack` data (`www.syntheticuniverse.org`). For illustration, here we choose "Subvariation A" of the "standard model", in the terminology of Dominik et al. (2012). A comparison of the upper and lower panels shows the striking differences in the chirp-mass distribution resulting from different choices for the metallicity Z .

allow us to reconstruct the shape of these histograms as a function of chirp mass, potentially enabling new high-precision tests of binary evolution, above and beyond the information provided by the mass distribution alone.

A preliminary assessment of the main features of population-synthesis models that could be probed by these measurements can be inferred from Table 7.4. There we list the overall fraction of BH binary systems that undergo mass-ratio reversal for several different binary-evolution scenarios explored in Dominik et al. (2012). The most dramatic difference is due to composition: with few exceptions, models with solar composition ($Z/Z_\odot = 1$) almost exclusively produce SMR binaries, while models with subsolar composition ($Z/Z_\odot = 0.1$) produce comparable proportions of SMR and RMR binaries. Furthermore there are clear trends in the ratio RMR/SMR as a function of the envelope-binding-energy parameter λ discussed in Sec. 7.2.4 (compare variations 1 to 4); the strength of SN kicks (variations 8 and 9); and the amount of mass loss through winds (variation 11). These parameters are also well known to significantly influence the overall number and mass distribution of merging binaries.

In conclusion, while our model needs further testing and scrutiny against more complete population-synthesis calculations, it strongly indicates that GW measurements of $\Delta\Phi$ and θ_{12} will provide a useful diagnostic of compact binary formation, complementary to the more familiar mass and spin measurements.

7.4.3 Discussion

The spin-orbit resonances discovered by Schnittman (2004) tend to lock the spin in a resonant plane if the binary has mass ratio $q \gtrsim 0.4$ and the dimensionless spin magnitudes $\chi_i \gtrsim 0.5$ as long as there is an initial asymmetry in the relative orientation of the spins with respect to the orbital angular momentum, i.e. $\theta_1 \neq \theta_2$ (Kesden et al. 2010a,b; Berti et al. 2012b and Sec. 6.3.3) We built a toy model for BH binary formation focusing on the main physical ingredients that can produce such an asymmetry: SN kicks (that tilt the orbital plane every time a BH is formed), tidal interactions (that tend to realign the spin of the star that collapses later with the orbital angular momentum) and mass transfer (that can produce mass-ratio reversal, so that the heaviest BH corresponds to the lighter stellar progenitor). We showed that for stellar-mass compact objects formed at the endpoint of isolated binary evolution the required conditions should ubiquitously occur.

Perhaps more interestingly, we demonstrated that the angle $\Delta\Phi$ between the components of the BH spins in the plane orthogonal to the orbital angular momentum is in one-to-one correspondence with the BH formation channel that gave birth to the BH binary: if tides are efficient the PN evolution attracts the spins to the resonant plane with $\Delta\Phi \simeq 0^\circ$ ($\Delta\Phi \simeq \pm 180^\circ$) if mass reversal does (does not) occur. When tidal effects are inefficient the spins precess freely, and they pile up at $\Delta\Phi = \pm 90^\circ$ by the time the binary enters the band of advanced GW detectors. A preliminary comparison with detailed population-synthesis calculations suggests that the fraction of binaries in each family of resonant configurations, both overall and as a function of (chirp) mass, should provide a highly informative diagnostic of some of the main uncertainties involved in binary-evolution physics (metallicity, binding energy of the CE, magnitude of BH kicks) *as long as that fraction can be reliably measured.*

Our initial study merits detailed follow-ups to assess (i) the potential accuracy of GW measurements of the precessional parameters, and (ii) the information that can be extracted by comparison with population-synthesis models.

Detailed studies are required from the point of view of GW data analysis. We have assumed for simplicity that each PN resonance can be easily and unambigously distinguished. In practice, accurate matched-filtering measurements of the angles $\Delta\Phi$ and θ_{12} will need more work on the GW source-modeling front. Relevant issues here include the construction of gravitational-waveform templates adapted to resonant configurations, the development of specialized parameter-estimation strategies and the understanding of systematic (as opposed to statistical) errors for second- and third-generation detectors. Spin modulations are known to influence both the amplitude and phase of the emitted radiation, and while there are

several preliminary investigations of parameter estimation from spinning, precessing binaries, the direct measurement of parameters characterizing the spin-orbit resonances may require the inclusion of higher-order spin terms and/or higher harmonics in the waveform models.

From an astrophysical standpoint, the observable distribution of binary systems as they enter the detector band should be calculated (more realistically) by applying our PN evolution to initial data derived from state-of-the-art binary population-synthesis models. In addition to corroborating our results, such a study will establish a comprehensive library of reference models that can be compared to observational data using Bayesian or other model-selection strategies: see e.g. O'Shaughnessy et al. (2008b, 2010); Mandel and O'Shaughnessy (2010); Mandel (2010); Sesana et al. (2011); Gair et al. (2011); O'Shaughnessy (2012) for previous efforts in this direction. Such a study is necessary also to make contact with other observables, such as as the rate and mass distribution of compact binaries. Only with a comprehensive and self-consistent set of predictions can we quantify how much the information provided by PN resonances complements information available through other observable quantities.

In conclusion, the direct observation of resonant locking will be challenging from a GW data-analysis standpoint. However the relatively transparent astrophysical interpretation of PN resonances makes such an investigation worthwhile. Even if only observationally accessible for the loudest signals, these resonances will enable unique insights into the evolutionary channels that produce merging compact binaries. In our opinion, more detailed studies of resonant locking in connection with population-synthesis models will offer a great observational opportunity for GW astronomy.

Variation	Subvariation A $Z/Z_\odot = 0.1$			Subvariation B $Z/Z_\odot = 0.1$		
	SMR	RMR	#	SMR	RMR	#
0: Standard	63.2%	36.8%	32496	66.8%	33.2%	17038
1: $\lambda = 0.01$	67.9%	32.1%	12368	67.4%	32.6%	11401
2: $\lambda = 0.1$	62.7%	37.3%	27698	65.2%	34.8%	16885
3: $\lambda = 1$	54.2%	45.8%	51806	65.7%	34.3%	19415
4: $\lambda = 10$	50.1%	49.9%	50884	62.9%	37.1%	17939
5: $M_{\rm NS} = 3M_\odot$	62.5%	37.5%	32236	66.2%	33.8%	16868
6: $M_{\rm NS} = 2M_\odot$	62.3%	37.7%	32535	65.9%	34.1%	16804
7: $\sigma = 132.5$km/s	58.2%	41.8%	36546	63.1%	36.9%	18935
8: $v_{\rm BH} = v_{\rm pNS}$	56.2%	43.8%	948	72.5%	27.5%	207
9: $v_{\rm BH} = 0$	56.3%	43.7%	52832	58.8%	41.2%	34569
10: Delayed SN	61.4%	38.6%	27310	66.3%	33.7%	13841
11: Weak winds	58.4%	41.6%	33872	63.6%	36.4%	17765

Variation	Subvariation A $Z/Z_\odot = 1$			Subvariation B $Z/Z_\odot = 1$		
	SMR	RMR	#	SMR	RMR	#
0: Standard	91.9%	8.1%	10160	92.9%	7.1%	8795
1: $\lambda = 0.01$	93.6%	6.4%	8171	93.6%	6.4%	8171
2: $\lambda = 0.1$	88.9%	11.1%	11977	92.1%	7.9%	8577
3: $\lambda = 1$	79.1%	20.9%	15820	91.6%	8.4%	8442
4: $\lambda = 10$	73.2%	26.8%	14425	91.6%	8.4%	8321
5: $M_{\rm NS} = 3M_\odot$	91.6%	8.4%	9972	92.8%	7.2%	8589
6: $M_{\rm NS} = 2M_\odot$	91.5%	8.5%	9922	92.5%	7.5%	8590
7: $\sigma = 132.5$km/s	88.9%	11.1%	11099	89.6%	10.4%	9334
8: $v_{\rm BH} = v_{\rm pNS}$	56.2%	43.8%	16	0%	100%	2
9: $v_{\rm BH} = 0$	66.3%	33.7%	35267	65.2%	34.8%	32547
10: Delayed SN	81.5%	18.5%	1032	81.2%	18.8%	881
11: Weak winds	70.5%	29.5%	21786	64.2%	35.8%	16182

Table 7.4: BH binary rates predicted by `StarTrack` using data publicly available from `www.syntheticuniverse.org` (Gerosa et al. 2013). RMR (SMR) is the percentage of binaries that do (not) experience mass-ratio reversal due to mass transfer; # indicates the total number of BH binaries in the sample. Each row refers to a different variation over the "standard model". The variations illustrate the effect of changing one parameter (common-envelope binding energy λ, maximum NS mass $M_{\rm NS}$, kick magnitude σ, fallback parameter, etcetera) with respect to the "best guesses" of the standard model. Each row also shows the effect of changing the metallicity Z and the Hertzsprung-gap donor prescription (Subvariations A and B): see Dominik et al. (2012) for details.

Outlook

In this thesis we modeled the interplay between astrophysics and GR, to predict what information can be gained from statistical observations of spin directions in BH binaries. In both the stellar-mass and the supermassive range, the life of a BH binary can be divided in two phases: at large separation the evolution is due to interactions with the astrophysical environment, while at small separation the inspiral is mainly driven by GW emission. We provided theoretical models to link these two regimes. Some memory of the early astrophysical evolution is still present in the GW-driven inspiral and the subsequent merger, so this astrophysical evolution can be reconstructed with future specific measurements.

We focused on two important issues in BH binary modeling: we updated the alignment timescale between the spin of a SMBH and its surrounding accretion disc using the non-linear theory of warp propagation; and we performed a joint analysis of stellar-mass BH binary formation and PN evolution to predict the spin configurations when binaries become detectable by GW interferometers.

i) *On galactic scales*, the spin orientation of SMBHs is critically modified by the presence of gas in the form of accretions discs. If large spin-orbit misalignments are retained after the disc-driven phase, numerical relativity simulations predict that the BH resulting from the merger could receive a strong recoil and be expelled from the galaxy. The interaction between the BH spin and the orbital angular momentum of the disc must be modeled in detail to predict whether SMBH ejections are likely. BH spin and accretion disc interact with each other through the Bardeen–Petterson effect, which is a notable phenomenon where astrophysical fluid dynamics and GR both contribute to the final behavior of the system. General-relativistic frame dragging triggers the exchange of angular momentum between the disc and the hole. Lense–Thirring precession quickly (i.e., on the viscous timescale) induces a non-planar configuration of the disc: angular momentum can then be transmitted within the disc through the propagation of warps. To conserve angular momentum, the system tends to a planar configuration, thus aligning the BH spin with the orbital angular momentum of the (outer) disc. We found that warps must be treated properly to fully describe the alignment process. If the non-linear theory of warp propagation is considered, the alignment timescale between the spin of each BH and the orbital angular momentum of the circumbinary disc is sensibly larger. By updating the alignment timescale, we found that it may become comparable with typical estimates of the merger timescale. Assuming that the disc angular momentum is parallel to the orbital angular momentum of the binary, we compared the alignment timescale and the merger timescale to predict the likelihood of large recoil velocities. We found that the average magnitude of SMBH spins must be low to avoid frequent ejections.

   The evolution of the system during the disc-driven phase determines whether the disc is efficient enough to modify the spin orientation, and can be combined with numerical relativity predictions to predict recoil velocity distributions. Future detections of GW signals with planned space-based detectors and observations of electromagnetic signatures of recoiling BHs could provide precious information on the statistical properties of spinning SMBHs and their gaseous environments.

ii) *On smaller scales*, stellar-mass BH mergers are particularly relevant because they are expected to be detected soon as GW sources by ground-based interferometers. Even if obtained by solving the equations of GR in vacuum, the PN evolution is strongly dependent on the (astrophysical) initial conditions. If some asymmetry between the two spin-orbit misalignment angles is present in the early inspiral, resonant evolution quickly becomes dominant and completely determines the behavior of the system. Binaries lock into configurations identified by a resonant plane, shared by the two spins and the binary orbital angular momentum. We therefore focused on those astrophysical formation processes that can both introduce a spin-orbit misalignment and cause the necessary asymmetry. To end its life as a BH binary, a massive binary star must go through two SN explosions. SN kicks tilt the orbital plane, thus modifying the relative directions of the spins and of the orbital angular momentum. When the physical dimensions of the members of the binary are intrinsically asymmetric, i.e. when the system is formed by a BH and a star, tidal friction can transfer this asymmetry to the spin orientations. In fact, tidal interaction consists in angular momentum exchange, which depends on the characteristic lenghtscales of the objects involved. On the other hand, mass transfer efficiency sets the "direction" of this asymmetry by determining which BH forms firstly. If mass transfer reverses the binary mass ratio, the fistly formed BH (which has the initially heavier stellar progenitor) may be the secondary member of the binary, rather than the primary. Mass transfer events determine which of the two resonant families will be relevant in the binary inspiral. Asymmetry induced in the astrophysics-dominated phase results in resonant locking in the PN regime, creating a one-to-one correspondence between the spin angles at the end of the inspiral and different binary formation scenarios.

   The consequences of the existence of the resonant plane should be explored further. More templates could be placed in the resonant plane region to increase GW detection rates. The measurability of the resonant angles is worthy of further investigations, because of the relatively clean interpretation of their distributions. When statistical samples of GW observations will be available, distributions of the spin orientation angles may constrain poorly known astrophysical mechanisms that are responsible for the formation of BH binary systems.

The PN evolution should be applied to the inspiral of SMBHs as well. The role of resonances in this regime is not fully understood yet. Our study shows, that warp non-linearities must be modeled in detail, especially when the initial misalignments are large. However, solutions of the disc structure in the non-linear regime are not available in the literature. Self-consistent solutions in the general case would allow to predict residual misalignments after the disc-driven phase. The resulting spin angle distributions could then be evolved in the PN regime, using the same numerical procedure applied here in the stellar-mass range. In gas-rich mergers, the smaller BH may accrete more gas from the circumbinary disc, becoming more aligned with the orbital angular momentum. This may be the necessary mechanism to introduce the critical spin asymmetry in SMBH binaries, analogous to tidal friction for stellar-mass BH binaries. A joint analysis of disc physics and PN evolution in SMBH binaries could provide new insights in BH astrophysics and the role of GR on galactic scales.

Bibliography

Aasi J., Abadie J., Abbott B.P., Abbott R., Abbott T.D., Abernathy M., Accadia T., Acernese F., Adams C., Adams T., et al. (2013). "Search for gravitational waves from binary black hole inspiral, merger, and ringdown in LIGO-Virgo data from 2009-2010". *Physical Review D*, **87**(2):022002. [ADS].

Abadie J., Abbott B.P., Abbott R., Abbott T.D., Abernathy M., Accadia T., Acernese F., Adams C., Adhikari R., Affeldt C., et al. (2012a). "Search for gravitational waves from low mass compact binary coalescence in LIGO's sixth science run and Virgo's science runs 2 and 3". *Physical Review D*, **85**(8):082002. [ADS].

Abadie J., Abbott B.P., Abbott R., Abbott T.D., Abernathy M., Accadia T., Acernese F., Adams C., Adhikari R.X., Affeldt C., et al. (2012b). "Search for Gravitational Waves Associated with Gamma-Ray Bursts during LIGO Science Run 6 and Virgo Science Runs 2 and 3". *Astrophysical Journal*, **760**:12. [ADS].

Abadie J., Abbott B.P., Abbott R., Abbott T.D., Abernathy M., Accadia T., Acernese F., Adams C., Adhikari R.X., Affeldt C., et al. (2012c). "Sensitivity Achieved by the LIGO and Virgo Gravitational Wave Detectors during LIGO's Sixth and Virgo's Second and Third Science Runs". *ArXiv*, (1203.2674). [ADS].

Abadie J., Abbott B.P., Abbott R., Abernathy M., Accadia T., Acernese F., Adams C., Adhikari R., Ajith P., Allen B., et al. (2010). "TOPICAL REVIEW: Predictions for the rates of compact binary coalescences observable by ground-based gravitational-wave detectors". *Classical and Quantum Gravity*, **27**(17):173001. [ADS].

Abadie J., Abbott B.P., Abbott R., Abernathy M., Accadia T., Acernese F., Adams C., Adhikari R., Ajith P., Allen B., et al. (2011). "Search for gravitational waves from binary black hole inspiral, merger, and ringdown". *Physical Review D*, **83**(12):122005. [ADS].

Abbott B.P., Abbott R., Adhikari R., Ajith P., Allen B., Allen G., Amin R.S., Anderson S.B., Anderson W.G., Arain M.A., et al. (2009). "LIGO: the Laser Interferometer Gravitational-Wave Observatory". *Reports on Progress in Physics*, **72**(7):076901. [ADS].

Abel T., Bryan G.L., Norman M.L. (2000). "The Formation and Fragmentation of Primordial Molecular Clouds". *Astrophysical Journal*, **540**:39–44. [ADS].

Abramovici A., Althouse W.E., Drever R.W.P., Gursel Y., Kawamura S., Raab F.J., Shoemaker D., Sievers L., Spero R.E., Thorne K.S. (1992). "LIGO - The Laser Interferometer Gravitational-Wave Observatory". *Science*, **256**:325–333. [ADS].

Abramowicz M.A., Fragile P.C. (2013). "Foundations of Black Hole Accretion Disk Theory". *Living Reviews in Relativity*, **16**:1. [ADS].

Abramowicz M.A., Kluźniak W. (2001). "A precise determination of black hole spin in GRO J1655-40". *Astronomy and Astrophysics*, **374**:L19–L20. [ADS].

Abt H.A. (1983). "Normal and abnormal binary frequencies". *Annual Review of Astronomy and Astrophysics*, **21**:343–372. [ADS].

Acernese F., Amico P., Al-Shourbagy M., Aoudia S., Avino S., Babusci D., Ballardin G., Barillé R., Barone F., Barsotti L., et al. (2005). "Status of Virgo". *Classical and Quantum Gravity*, **22**:869. [ADS].

Ajith P. (2008). "Gravitational-wave data analysis using binary black-hole waveforms". *Classical and Quantum Gravity*, **25**(11):114033. [ADS].

Ajith P., Babak S., Chen Y., Hewitson M., Krishnan B., Sintes A.M., Whelan J.T., Brügmann B., Diener P., Dorband N., et al. (2008). "Template bank for gravitational waveforms from coalescing binary black holes: Nonspinning binaries". *Physical Review D*, **77**(10):104017. [ADS].

Ajith P., Babak S., Chen Y., Hewitson M., Krishnan B., Whelan J.T., Brügmann B., Diener P., Gonzalez J., Hannam M., et al. (2007). "A phenomenological template family for black-hole coalescence waveforms". *Classical and Quantum Gravity*, **24**:689. [ADS].

Ajith P., Boyle M., Brown D.A., Brügmann B., Buchman L.T., Cadonati L., Campanelli M., Chu T., Etienne Z.B., Fairhurst S., et al. (2012). "The NINJA-2 catalog of hybrid post-Newtonian/numerical-relativity waveforms for non-precessing black-hole binaries". *Classical and Quantum Gravity*, **29**(12):124001. [ADS].

Ajith P., Favata M. (2013). *In preparation.*

Ajith P., Hannam M., Husa S., Chen Y., Brügmann B., Dorband N., Müller D., Ohme F., Pollney D., Reisswig C., et al. (2011). "Inspiral-Merger-Ringdown Waveforms for Black-Hole Binaries with Nonprecessing Spins". *Physical Review Letters*, **106**(24):241101. [ADS].

Alexander M.E. (1973). "The Weak Friction Approximation and Tidal Evolution in Close Binary Systems". *Astrophysics and Space Science*, **23**:459–510. [ADS].

Alvi K. (2000). "Approximate binary-black-hole metric". *Physical Review D*, **61**(12):124013. [ADS].

Alvi K. (2001). "Energy and angular momentum flow into a black hole in a binary". *Physical Review D*, **64**(10):104020. [ADS].

Alvi K. (2003). "Note on ingoing coordinates for binary black holes". *Physical Review D*, **67**(10):104006. [ADS].

Armitage P.J. (2010). *Astrophysics of Planet Formation*. pp. 294. ISBN 978-0-521-88745-8 (hardback). Cambridge, UK: Cambridge University Press, 2010. [ADS].

Armitage P.J., Natarajan P. (1999). "The Blandford-Znajek Mechanism and the Emission from Isolated Accreting Black Holes". *Astrophysical Journal, Letters*, **523**:L7–L10. [ADS].

Armitage P.J., Natarajan P. (2002). "Accretion during the Merger of Supermassive Black Holes". *Astrophysical Journal*, **567**:L9–L12. [ADS].

Armitage P.J., Natarajan P. (2005). "Eccentricity of Supermassive Black Hole Binaries Coalescing from Gas-rich Mergers". *Astrophysical Journal*, **634**:921–927. [ADS].

Armitage P.J., Rice W.K.M. (2005). "Planetary migration". *ArXiv*, (0507492). [ADS].

Armstrong J.W. (2006). "Low-Frequency Gravitational Wave Searches Using Spacecraft Doppler Tracking". *Living Reviews in Relativity*, **9**:1. [ADS].

Artymowicz P., Lubow S.H. (1994). "Dynamics of binary-disk interaction. 1: Resonances and disk gap sizes". *Astrophysical Journal*, **421**:651–667. [ADS].

Artymowicz P., Lubow S.H. (1996). "Mass Flow through Gaps in Circumbinary Disks". *Astrophysical Journal, Letters*, **467**:L77. [ADS].

Arun K.G., Buonanno A., Faye G., Ochsner E. (2009). "Higher-order spin effects in the amplitude and phase of gravitational waveforms emitted by inspiraling compact binaries: Ready-to-use gravitational waveforms". *Physical Review D*, **79**(10):104023. [ADS].

Arun K.G., Buonanno A., Faye G., Ochsner E. (2011). "Erratum: Higher-order spin effects in the amplitude and phase of gravitational waveforms emitted by inspiraling compact binaries: Ready-to-use gravitational waveforms [Phys. Rev. D 79, 104023 (2009)]". *Physical Review D*, **84**(4):049901. [ADS].

Astone P., Babusci D., Baggio L., Bassan M., Bignotto M., Bonaldi M., Camarda M., Carelli P., Cavallari G., Cerdonio M., et al. (2007). "Results of the IGEC-2 search for gravitational wave bursts during 2005". *Physical Review D*, **76**(10):102001. [ADS].

Astone P., Baggio L., Bassan M., Bignotto M., Bonaldi M., Bonifazi P., Cavallari G., Cerdonio M., Coccia E., Conti L., et al. (2010). "IGEC2: A 17-month search for gravitational wave bursts in 2005-2007". *Physical Review D*, **82**(2):022003. [ADS].

Aylott B., Baker J.G., Boggs W.D., Boyle M., Brady P.R., Brown D.A., Brügmann B., Buchman L.T., Buonanno A., Cadonati L., et al. (2009). "Testing gravitational-wave searches with numerical relativity waveforms: results from the first Numerical INJection Analysis (NINJA) project". *Classical and Quantum Gravity*, **26**(16):165008. [ADS].

Babul A., Sharma P., Reynolds C.S. (2012). "Isotropic Heating of Galaxy Cluster Cores via Rapidly Reorienting AGN Jets". *ArXiv*, (1209.5748). [ADS].

Backer D.C., Jaffe A.H., Lommen A.N. (2004). "Massive Black Holes, Gravitational Waves and Pulsars". *Coevolution of Black Holes and Galaxies*, page 438. [ADS].

Bagot P. (1997). "On the progenitors of double neutron star systems." *Astronomy and Astrophysics*, **322**:533–544. [ADS].

Baker J.G., Boggs W.D., Centrella J., Kelly B.J., McWilliams S.T., Miller M.C., van Meter J.R. (2008). "Modeling Kicks from the Merger of Generic Black Hole Binaries". *Astrophysical Journal, Letters*, **682**:L29–L32. [ADS].

Baker J.G., Centrella J.M., Choi D.I., Koppitz M., van Meter J.R. (2005). "Modeling Gravitational Radiation Waveforms from Black Hole Mergers." In *American Astronomical Society Meeting Abstracts*, volume 37 of *Bulletin of the American Astronomical Society*, page 143.03. [ADS].

Balbus S.A., Hawley J.F. (1991). "A powerful local shear instability in weakly magnetized disks. I - Linear analysis. II - Nonlinear evolution". *Astrophysical Journal*, **376**:214–233. [ADS].

Balick B., Brown R.L. (1974). "Intense sub-arcsecond structure in the galactic center". *Astrophysical Journal*, **194**:265–270. [ADS].

Bardeen J.M. (1970). "Kerr Metric Black Holes". *Nature*, **226**:64–65. [ADS].

Bardeen J.M. (1973). "Timelike and null geodesics in the Kerr metric." In *Black Holes (Les Astres Occlus)*, edited by C. Dewitt, B.S. Dewitt, pages 215–239. [ADS].

Bardeen J.M., Petterson J.A. (1975). "The Lense-Thirring Effect and Accretion Disks around Kerr Black Holes". *Astrophysical Journal, Letters*, **195**:L65. [ADS].

Bardeen J.M., Press W.H., Teukolsky S.A. (1972). "Rotating Black Holes: Locally Nonrotating Frames, Energy Extraction, and Scalar Synchrotron Radiation". *Astrophysical Journal*, **178**:347–370. [ADS].

Barish B.C., Weiss R. (1999). "LIGO and the detection of gravitational waves." *Physics Today*, **52**:44–50. [ADS].

Barker B.M., O'Connell R.F. (1975a). "Gravitational two-body problem with arbitrary masses, spins, and quadrupole moments". *Physical Review D*, **12**:329–335. [ADS].

Barker B.M., O'Connell R.F. (1975b). "Relativistic effects in the binary pulsar PSR 1913+16". *Astrophysical Journal, Letters*, **199**:L25. [ADS].

Barnes J.E., Hernquist L. (1992). "Dynamics of interacting galaxies". *Annual Review of Astronomy and Astrophysics*, **30**:705–742. [ADS].

Barth A.J., Bentz M.C., Greene J.E., Ho L.C. (2008). "An Offset Seyfert 2 Nucleus in the Minor Merger System NGC 3341". *Astrophysical Journal, Letters*, **683**:L119–L122. [ADS].

Baruteau C., Ramirez-Ruiz E., Masset F. (2012). "No snowplough mechanism during the rapid hardening of supermassive black hole binaries". *Monthly Notices of the Royal Astronomical Society*, **423**:L65–L69. [ADS].

Bate M.R., Lubow S.H., Ogilvie G.I., Miller K.A. (2003). "Three-dimensional calculations of high- and low-mass planets embedded in protoplanetary discs". *Monthly Notices of the Royal Astronomical Society*, **341**:213–229. [ADS].

Beck P.G., Montalban J., Kallinger T., De Ridder J., Aerts C., García R.A., Hekker S., Dupret M.A., Mosser B., Eggenberger P., et al. (2012). "Fast core rotation in red-giant stars as revealed by gravity-dominated mixed modes". *Nature*, **481**:55–57. [ADS].

Begelman M.C., Blandford R.D., Rees M.J. (1980). "Massive black hole binaries in active galactic nuclei". *Nature*, **287**:307–309. [ADS].

Begelman M.C., Blandford R.D., Rees M.J. (1984). "Theory of extragalactic radio sources". *Reviews of Modern Physics*, **56**:255–351. [ADS].

Begelman M.C., Volonteri M., Rees M.J. (2006). "Formation of supermassive black holes by direct collapse in pre-galactic haloes". *Monthly Notices of the Royal Astronomical Society*, **370**:289–298. [ADS].

Belczynski K., Benacquista M., Bulik T. (2010a). "Double Compact Objects as Low-frequency Gravitational Wave Sources". *Astrophysical Journal*, **725**:816–823. [ADS].

Belczynski K., Bulik T., Bailyn C. (2011). "The Fate of Cyg X-1: An Empirical Lower Limit on Black-hole-Neutron-star Merger Rate". *Astrophysical Journal, Letters*, **742**:L2. [ADS].

Belczynski K., Bulik T., Fryer C.L., Ruiter A., Valsecchi F., Vink J.S., Hurley J.R. (2010b). "On the Maximum Mass of Stellar Black Holes". *Astrophysical Journal*, **714**:1217–1226. [ADS].

Belczynski K., Bulik T., Mandel I., Sathyaprakash B.S., Zdziarski A.A., Mikołajewska J. (2013). "Cyg X-3: A Galactic Double Black Hole or Black-hole-Neutron-star Progenitor". *Astrophysical Journal*, **764**:96. [ADS].

Belczynski K., Bulik T., Ruiter A.J. (2005). "New Constraints on Type Ia Supernova Progenitor Models". *Astrophysical Journal*, **629**:915–921. [ADS].

Belczynski K., Holz D.E., Fryer C.L., Berger E., Hartmann D.H., O'Shea B. (2010c). "On the Origin of the Highest Redshift Gamma-Ray Bursts". *Astrophysical Journal*, **708**:117–126. [ADS].

Belczynski K., Kalogera V., Bulik T. (2002). "A Comprehensive Study of Binary Compact Objects as Gravitational Wave Sources: Evolutionary Channels, Rates, and Physical Properties". *Astrophysical Journal*, **572**:407–431. [ADS].

Belczynski K., Kalogera V., Rasio F.A., Taam R.E., Zezas A., Bulik T., Maccarone T.J., Ivanova N. (2008a). "Compact Object Modeling with the StarTrack Population Synthesis Code". *Astrophysical Journal, Supplement*, **174**:223–260. [ADS].

Belczynski K., Kalogera V., Zezas A., Fabbiano G. (2004a). "X-Ray Binary Populations: The Luminosity Function of NGC 1569". *Astrophysical Journal, Letters*, **601**:L147–L150. [ADS].

Belczynski K., Lorimer D.R., Ridley J.P., Curran S.J. (2010d). "Double and single recycled pulsars: an evolutionary puzzle?" *Monthly Notices of the Royal Astronomical Society*, **407**:1245–1254. [ADS].

Belczynski K., O'Shaughnessy R., Kalogera V., Rasio F., Taam R.E., Bulik T. (2008b). "The Lowest-Mass Stellar Black Holes: Catastrophic Death of Neutron Stars in Gamma-Ray Bursts". *Astrophysical Journal, Letters*, **680**:L129–L132. [ADS].

Belczynski K., Perna R., Bulik T., Kalogera V., Ivanova N., Lamb D.Q. (2006a). "A Study of Compact Object Mergers as Short Gamma-Ray Burst Progenitors". *Astrophysical Journal*, **648**:1110–1116. [ADS].

Belczynski K., Sadowski A., Rasio F.A. (2004b). "A Comprehensive Study of Young Black Hole Populations". *Astrophysical Journal*, **611**:1068–1079. [ADS].

Belczynski K., Sadowski A., Rasio F.A., Bulik T. (2006b). "Initial Populations of Black Holes in Star Clusters". *Astrophysical Journal*, **650**:303–325. [ADS].

Belczynski K., Taam R.E. (2004a). "Galactic Populations of Ultracompact Binaries". *Astrophysical Journal*, **603**:690–696. [ADS].

Belczynski K., Taam R.E. (2004b). "On the Chandra X-Ray Sources in the Galactic Center". *Astrophysical Journal*, **616**:1159–1166. [ADS].

Belczynski K., Taam R.E. (2008). "The Most Massive Progenitors of Neutron Stars: CXO J164710.2-455216". *Astrophysical Journal*, **685**:400–405. [ADS].

Belczynski K., Taam R.E., Kalogera V., Rasio F.A., Bulik T. (2007). "On the Rarity of Double Black Hole Binaries: Consequences for Gravitational Wave Detection". *Astrophysical Journal*, **662**:504–511. [ADS].

Belczynski K., Taam R.E., Rantsiou E., van der Sluys M. (2008c). "Black Hole Spin Evolution: Implications for Short-Hard Gamma-Ray Bursts and Gravitational Wave Detection". *Astrophysical Journal*, **682**:474–486. [ADS].

Belczynski K., Wiktorowicz G., Fryer C.L., Holz D.E., Kalogera V. (2012). "Missing Black Holes Unveil the Supernova Explosion Mechanism". *Astrophysical Journal*, **757**:91. [ADS].

Belczynski K., Ziolkowski J. (2009). "On the Apparent Lack of Be X-Ray Binaries with Black Holes". *Astrophysical Journal*, **707**:870–877. [ADS].

Benacquista M.J., Downing J.M.B. (2013). "Relativistic Binaries in Globular Clusters". *Living Reviews in Relativity*, **16**:4. [ADS].

Bennert V.N., Auger M.W., Treu T., Woo J.H., Malkan M.A. (2011). "A Local Baseline of the Black Hole Mass Scaling Relations for Active Galaxies. I. Methodology and Results of Pilot Study". *Astrophysical Journal*, **726**:59. [ADS].

Bennett C.L., Larson D., Weiland J.L., Jarosik N., Hinshaw G., Odegard N., Smith K.M., Hill R.S., Gold B., Halpern M., et al. (2012). "Nine-Year Wilkinson Microwave Anisotropy Probe (WMAP) Observations: Final Maps and Results". *ArXiv*, (1212.5225). [ADS].

Berti E., Cardoso V., Starinets A.O. (2009). "TOPICAL REVIEW: Quasinormal modes of black holes and black branes". *Classical and Quantum Gravity*, **26**(16):163001. [ADS].

Berti E., Cardoso V., Will C.M. (2006). "Gravitational-wave spectroscopy of massive black holes with the space interferometer LISA". *Physical Review D*, **73**(6):064030. [ADS].

Berti E., Gualtieri L., Horbatsch M., Alsing J. (2012a). "Light scalar field constraints from gravitational-wave observations of compact binaries". *Physical Review D*, **85**(12):122005. [ADS].

Berti E., Iyer S., Will C.M. (2008). "Post-Newtonian diagnosis of quasiequilibrium configurations of neutron star neutron star and neutron star black hole binaries". *Physical Review D*, **77**(2):024019. [ADS].

Berti E., Kesden M., Sperhake U. (2012b). "Effects of post-Newtonian spin alignment on the distribution of black-hole recoils". *Physical Review D*, **85**(12):124049. [ADS].

Berti E., Volonteri M. (2008). "Cosmological Black Hole Spin Evolution by Mergers and Accretion". *Astrophysical Journal*, **684**:822–828. [ADS].

Bertin G. (2000). *Dynamics of Galaxies*. pp. 430. ISBN 0521472628. Cambridge, UK: Cambridge University Press, June 2000. [ADS].

Bethe H.A., Brown G.E. (1998). "Evolution of Binary Compact Objects That Merge". *Astrophysical Journal*, **506**:780–789. [ADS].

Bianchi S., Chiaberge M., Piconcelli E., Guainazzi M., Matt G. (2008). "Chandra unveils a binary active galactic nucleus in Mrk 463". *Monthly Notices of the Royal Astronomical Society*, **386**:105–110. [ADS].

Binggeli B., Jerjen H. (1998). "Is the shape of the luminosity profile of dwarf elliptical galaxies an useful distance indicator?" *Astronomy and Astrophysics*, **333**:17–26. [ADS].

Birkhoff G.D., Langer R.E. (1923). *Relativity and modern physics*. Cambridge, Harvard University Press; [etc., etc.] 1923. [ADS].

Blanchet L. (2002). "Gravitational Radiation from Post-Newtonian Sources and Inspiralling Compact Binaries". *Living Reviews in Relativity*, **5**:3. [ADS].

Blanchet L. (2003). "On the Accuracy of the Post-Newtonian Approximation". In *2001: A Relativistic Spacetime Odyssey*, edited by I. Ciufolini, D. Dominici, L. Lusanna, pages 411–430. [ADS].

Blanchet L., Buonanno A., Faye G. (2006). "Higher-order spin effects in the dynamics of compact binaries. II. Radiation field". *Physical Review D*, **74**(10):104034. [ADS].

Blanchet L., Buonanno A., Faye G. (2007). "Erratum: Higher-order spin effects in the dynamics of compact binaries. II. Radiation field [Phys. Rev. D 74, 104034 (2006)]". *Physical Review D*, **75**(4):049903. [ADS].

Blanchet L., Buonanno A., Faye G. (2010). "Erratum: Higher-order spin effects in the dynamics of compact binaries. II. Radiation field [Phys. Rev. D 74, 104034 (2006)]". *Physical Review D*, **81**(8):089901. [ADS].

Blanchet L., Damour T., Esposito-Farèse G. (2004a). "Dimensional regularization of the third post-Newtonian dynamics of point particles in harmonic coordinates". *Physical Review D*, **69**(12):124007. [ADS].

Blanchet L., Damour T., Esposito-Farèse G., Iyer B.R. (2004b). "Gravitational Radiation from Inspiralling Compact Binaries Completed at the Third Post-Newtonian Order". *Physical Review Letters*, **93**(9):091101. [ADS].

Blanchet L., Faye G., Iyer B.R., Joguet B. (2002). "Gravitational-wave inspiral of compact binary systems to 7/2 post-Newtonian order". *Physical Review D*, **65**(6):061501. [ADS].

Blanchet L., Faye G., Iyer B.R., Joguet B. (2005). "Erratum: Gravitational-wave inspiral of compact binary systems to 7/2 post-Newtonian order [Phys. Rev. D 65, 061501(R) (2002)]". *Physical Review D*, **71**(12):129902. [ADS].

Blanchet L., Iyer B.R. (2005). "Hadamard regularization of the third post-Newtonian gravitational wave generation of two point masses". *Physical Review D*, **71**(2):024004. [ADS].

Blanchet L., Sathyaprakash B.S. (1994). "Signal analysis of gravitational wave tails". *Classical and Quantum Gravity*, **11**:2807–2831. [ADS].

Blanchet L., Sathyaprakash B.S. (1995). "Detecting a Tail Effect in Gravitational-Wave Experiments". *Physical Review Letters*, **74**:1067–1070. [ADS].

Blandford R.D. (1987). *Astrophysical black holes.*, pages 277–329. Three Hundred Years of Gravitation. [ADS].

Blandford R.D., Payne D.G. (1982). "Hydromagnetic flows from accretion discs and the production of radio jets". *Monthly Notices of the Royal Astronomical Society*, **199**:883–903. [ADS].

Blandford R.D., Znajek R.L. (1977). "Electromagnetic extraction of energy from Kerr black holes". *Monthly Notices of the Royal Astronomical Society*, **179**:433–456. [ADS].

Blecha L., Civano F., Elvis M., Loeb A. (2013). "Constraints on the nature of CID-42: recoil kick or supermassive black hole pair?" *Monthly Notices of the Royal Astronomical Society*, **428**:1341–1350. [ADS].

Blecha L., Ivanova N., Kalogera V., Belczynski K., Fregeau J., Rasio F. (2006). "Close Binary Interactions of Intermediate-Mass Black Holes: Possible Ultraluminous X-Ray Sources?" *Astrophysical Journal*, **642**:427–437. [ADS].

Blecha L., Loeb A. (2008). "Effects of gravitational-wave recoil on the dynamics and growth of supermassive black holes". *Monthly Notices of the Royal Astronomical Society*, **390**:1311–1325. [ADS].

Bode T., Bogdanović T., Haas R., Healy J., Laguna P., Shoemaker D. (2012). "Mergers of Supermassive Black Holes in Astrophysical Environments". *Astrophysical Journal*, **744**:45. [ADS].

Bogdanović T., Eracleous M., Sigurdsson S. (2009). "SDSS J092712.65+294344.0: Recoiling Black Hole or a Subparsec Binary Candidate?" *Astrophysical Journal*, **697**:288–292. [ADS].

Bogdanović T., Reynolds C.S., Miller M.C. (2007). "Alignment of the Spins of Supermassive Black Holes Prior to Coalescence". *Astrophysical Journal, Letters*, **661**:L147–L150. [ADS].

Bolton C.T. (1972). "Identification of Cygnus X-1 with HDE 226868". *Nature*, **235**:271–273. [ADS].

Bondi H. (1952). "On spherically symmetrical accretion". *Monthly Notices of the Royal Astronomical Society*, **112**:195. [ADS].

Bondi H., Hoyle F. (1944). "On the mechanism of accretion by stars". *Monthly Notices of the Royal Astronomical Society*, **104**:273. [ADS].

Bonning E.W., Shields G.A., Salviander S. (2007). "Recoiling Black Holes in Quasars". *Astrophysical Journal, Letters*, **666**:L13–L16. [ADS].

Bower G.C., Falcke H., Herrnstein R.M., Zhao J.H., Goss W.M., Backer D.C. (2004). "Detection of the Intrinsic Size of Sagittarius A* Through Closure Amplitude Imaging". *Science*, **304**:704–708. [ADS].

Bower G.C., Goss W.M., Falcke H., Backer D.C., Lithwick Y. (2006). "The Intrinsic Size of Sagittarius A* from 0.35 to 6 cm". *Astrophysical Journal, Letters*, **648**:L127–L130. [ADS].

Boyer R.H., Lindquist R.W. (1967). "Maximal Analytic Extension of the Kerr Metric". *Journal of Mathematical Physics*, **8**:265–281. [ADS].

Boyle M., Buonanno A., Kidder L.E., Mroué A.H., Pan Y., Pfeiffer H.P., Scheel M.A. (2008). "High-accuracy numerical simulation of black-hole binaries: Computation of the gravitational-wave energy flux and comparisons with post-Newtonian approximants". *Physical Review D*, **78**(10):104020. [ADS].

Brady P.R., Fairhurst S. (2008). "Interpreting the results of searches for gravitational waves from coalescing binaries". *Classical and Quantum Gravity*, **25**(10):105002. [ADS].

Brandt N., Podsiadlowski P. (1995). "The effects of high-velocity supernova kicks on the orbital properties and sky distributions of neutron-star binaries". *Monthly Notices of the Royal Astronomical Society*, **274**:461–484. [ADS].

Brenneman L.W., Reynolds C.S. (2006). "Constraining Black Hole Spin via X-Ray Spectroscopy". *Astrophysical Journal*, **652**:1028–1043. [ADS].

Brenneman L.W., Reynolds C.S., Nowak M.A., Reis R.C., Trippe M., Fabian A.C., Iwasawa K., Lee J.C., Miller J.M., Mushotzky R.F., et al. (2011). "The Spin of the Supermassive Black Hole in NGC 3783". *Astrophysical Journal*, **736**:103. [ADS].

Broderick A.E., Loeb A., Narayan R. (2009). "The Event Horizon of Sagittarius A*". *Astrophysical Journal*, **701**:1357–1366. [ADS].

Broderick A.E., Narayan R. (2006). "On the Nature of the Compact Dark Mass at the Galactic Center". *Astrophysical Journal, Letters*, **638**:L21–L24. [ADS].

Bromley B.C., Miller W.A., Pariev V.I. (1998). "The inner edge of the accretion disk around a supermassive black hole". *Nature*, **391**:54. [ADS].

Bromley J.M., Somerville R.S., Fabian A.C. (2004). "High-redshift quasars and the supermassive black hole mass budget: constraints on quasar formation models". *Monthly Notices of the Royal Astronomical Society*, **350**:456–472. [ADS].

Bromm V., Coppi P.S., Larson R.B. (2002). "The Formation of the First Stars. I. The Primordial Star-forming Cloud". *Astrophysical Journal*, **564**:23–51. [ADS].

Brouwer D., Clemence G.M. (1961). *Methods of celestial mechanics*. New York: Academic Press, 1961. [ADS].

Brown G.E., Bethe H.A. (1994). "A Scenario for a Large Number of Low-Mass Black Holes in the Galaxy". *Astrophysical Journal*, **423**:659. [ADS].

Brown G.E., Lee C.H., Wijers R.A.M.J., Bethe H.A. (2000). "Evolution of black holes in the galaxy". *Physics Reports*, **333**:471–504. [ADS].

Bryden G., Chen X., Lin D.N.C., Nelson R.P., Papaloizou J.C.B. (1999). "Tidally Induced Gap Formation in Protostellar Disks: Gap Clearing and Suppression of Protoplanetary Growth". *Astrophysical Journal*, **514**:344–367. [ADS].

Bulik T., Belczyński K. (2003). "Constraints on the Binary Evolution from Chirp Mass Measurements". *Astrophysical Journal, Letters*, **589**:L37–L40. [ADS].

Bulik T., Belczyński K., Rudak B. (2004a). "Astrophysical significance of the detection of coalescing binaries with gravitational waves". *Astronomy and Astrophysics*, **415**:407–414. [ADS].

Bulik T., Gondek-Rosinska D., Belczynski K. (2004b). "Expected masses of merging compact object binaries observed in gravitational waves". *Monthly Notices of the Royal Astronomical Society*, **352**:1372–1380. [ADS].

Buonanno A. (2007). "Gravitational waves". *ArXiv*, (0709.4682). [ADS].

Buonanno A., Chen Y., Pan Y., Tagoshi H., Vallisneri M. (2005). "Detecting gravitational waves from precessing binaries of spinning compact objects. II. Search implementation for low-mass binaries". *Physical Review D*, **72**(8):084027. [ADS].

Buonanno A., Chen Y., Vallisneri M. (2003). "Detecting gravitational waves from precessing binaries of spinning compact objects: Adiabatic limit". *Physical Review D*, **67**(10):104025. [ADS].

Buonanno A., Chen Y., Vallisneri M. (2006). "Erratum: Detecting gravitational waves from precessing binaries of spinning compact objects: Adiabatic limit [Phys. Rev. D 67, 104025 (2003)]". *Physical Review D*, **74**(2):029904. [ADS].

Buonanno A., Cook G.B., Pretorius F. (2007a). "Inspiral, merger, and ring-down of equal-mass black-hole binaries". *Physical Review D*, **75**(12):124018. [ADS].

Buonanno A., Damour T. (1999). "Effective one-body approach to general relativistic two-body dynamics". *Physical Review D*, **59**(8):084006. [ADS].

Buonanno A., Damour T. (2000). "Transition from inspiral to plunge in binary black hole coalescences". *Physical Review D*, **62**(6):064015. [ADS].

Buonanno A., Iyer B.R., Ochsner E., Pan Y., Sathyaprakash B.S. (2009). "Comparison of post-Newtonian templates for compact binary inspiral signals in gravitational-wave detectors". *Physical Review D*, **80**(8):084043. [ADS].

Buonanno A., Pan Y., Baker J.G., Centrella J., Kelly B.J., McWilliams S.T., van Meter J.R. (2007b). "Approaching faithful templates for nonspinning binary black holes using the effective-one-body approach". *Physical Review D*, **76**(10):104049. [ADS].

Campanelli M., Lousto C., Zlochower Y., Merritt D. (2007a). "Large Merger Recoils and Spin Flips from Generic Black Hole Binaries". *Astrophysical Journal, Letters*, **659**:L5–L8. [ADS].

Campanelli M., Lousto C.O., Marronetti P., Zlochower Y. (2006). "Accurate Evolutions of Orbiting Black-Hole Binaries without Excision". *Physical Review Letters*, **96**(11):111101. [ADS].

Campanelli M., Lousto C.O., Zlochower Y., Merritt D. (2007b). "Maximum Gravitational Recoil". *Physical Review Letters*, **98**(23):231102. [ADS].

Cantrell A.G., Bailyn C.D., Orosz J.A., McClintock J.E., Remillard R.A., Froning C.S., Neilsen J., Gelino D.M., Gou L. (2010). "The Inclination of the Soft X-Ray Transient A0620-00 and the Mass of its Black Hole". *Astrophysical Journal*, **710**:1127–1141. [ADS].

Caproni A., Abraham Z., Livio M., Mosquera Cuesta H.J. (2007). "Is the Bardeen-Petterson effect responsible for the warping and precession in NGC4258?" *Monthly Notices of the Royal Astronomical Society*, **379**:135–142. [ADS].

Caproni A., Abraham Z., Mosquera Cuesta H.J. (2006a). "Bardeen-Petterson Effect and the Disk Structure of the Seyfert Galaxy NGC 1068". *Astrophysical Journal*, **638**:120–124. [ADS].

Caproni A., Livio M., Abraham Z., Mosquera Cuesta H.J. (2006b). "Warping and Precession in Galactic and Extragalactic Accretion Disks". *Astrophysical Journal*, **653**:112–126. [ADS].

Carr B.J. (2005). "Primordial Black Holes - Recent Developments". In *22nd Texas Symposium on Relativistic Astrophysics*, edited by P. Chen, E. Bloom, G. Madejski, V. Patrosian, pages 89–100. [ADS].

Carroll S.M. (1997). "Lecture Notes on General Relativity". *ArXiv*, (9712019). [ADS].

Casares J. (2007). "Observational evidence for stellar-mass black holes". In *IAU Symposium*, edited by V. Karas, G. Matt, volume 238 of *IAU Symposium*, pages 3–12. [ADS].

Celotti A., Miller J.C., Sciama D.W. (1999). "Astrophysical evidence for the existence of black holes". *Classical and Quantum Gravity*, **16**:A3–A21. [ADS].

Chandrasekhar S. (1943). "Dynamical Friction. I. General Considerations: the Coefficient of Dynamical Friction." *Astrophysical Journal*, **97**:255. [ADS].

Chandrasekhar S. (1987). *Truth and beauty. Aesthetics and motivations in science*. Chicago: University of Chicago Press, 1987. [ADS].

Chang P., Strubbe L.E., Menou K., Quataert E. (2010). "Fossil gas and the electromagnetic precursor of supermassive binary black hole mergers". *Monthly Notices of the Royal Astronomical Society*, **407**:2007–2016. [ADS].

Chen L., Wu S., Yuan F. (2009). "A steady-state solution for warped accretion discs". *Monthly Notices of the Royal Astronomical Society*, **398**:1900–1904. [ADS].

Chevalier R.A. (1993). "Neutron star accretion in a stellar envelope". *Astrophysical Journal, Letters*, **411**:L33–L36. [ADS].

Chobotov V.A. (1991). "Orbital mechanics". Technical report. [ADS].

Christodoulou D. (1970). "Reversible and Irreversible Transformations in Black-Hole Physics". *Physical Review Letters*, **25**:1596–1597. [ADS].

Ciufolini I., Pavlis E.C. (2004). "A confirmation of the general relativistic prediction of the Lense-Thirring effect". *Nature*, **431**:958–960. [ADS].

Civano F., Elvis M., Lanzuisi G., Aldcroft T., Trichas M., Bongiorno A., Brusa M., Blecha L., Comastri A., Loeb A., et al. (2012). "Chandra High-resolution observations of CID-42, a Candidate Recoiling Supermassive Black Hole". *Astrophysical Journal*, **752**:49. [ADS].

Civano F., Elvis M., Lanzuisi G., Jahnke K., Zamorani G., Blecha L., Bongiorno A., Brusa M., Comastri A., Hao H., et al. (2010). "A Runaway Black Hole in COSMOS: Gravitational Wave or Slingshot Recoil?" *Astrophysical Journal*, **717**:209–222. [ADS].

Clausen D., Wade R.A., Kopparapu R.K., O'Shaughnessy R. (2012). "Population Synthesis of Hot Subdwarfs: A Parameter Study". *Astrophysical Journal*, **746**:186. [ADS].

Colgate S.A. (1971). "Neutron-Star Formation, Thermonuclear Supernovae, and Heavy-Element Reimplosion". *Astrophysical Journal*, **163**:221. [ADS].

Collin-Souffrin S., Dumont A.M. (1990). "Line and continuum emission from the outer regions of accretion discs in active galactic nuclei. II - Radial structure of the disc." *Astronomy and Astrophysics*, **229**:292–328. [ADS].

Colpi M., Dotti M. (2009). "Massive Binary Black Holes in the Cosmic Landscape". *ArXiv*, (0906.4339). [ADS].

Comerford J.M., Griffith R.L., Gerke B.F., Cooper M.C., Newman J.A., Davis M., Stern D. (2009). "1.75 h $^{-1}$ kpc Separation Dual Active Galactic Nuclei at z = 0.36 in the Cosmos Field". *Astrophysical Journal, Letters*, **702**:L82–L86. [ADS].

Conselice C.J. (2007). "Galaxy Mergers and Interactions at High Redshift". In *IAU Symposium*, edited by F. Combes, J. Palouš, volume 235 of *IAU Symposium*, pages 381–384. [ADS].

Corinaldesi E., Papapetrou A. (1951). "Spinning Test-Particles in General Relativity. II". *Royal Society of London Proceedings Series A*, **209**:259–268. [ADS].

Corrales L.R., Haiman Z., MacFadyen A. (2010). "Hydrodynamical response of a circumbinary gas disc to black hole recoil and mass loss". *Monthly Notices of the Royal Astronomical Society*, **404**:947–962. [ADS].

Cuadra J., Armitage P.J., Alexander R.D., Begelman M.C. (2009). "Massive black hole binary mergers within subparsec scale gas discs". *Monthly Notices of the Royal Astronomical Society*, **393**:1423–1432. [ADS].

Cui W., Zhang S.N., Chen W. (1998). "Evidence for Frame Dragging around Spinning Black Holes in X-Ray Binaries". *Astrophysical Journal, Letters*, **492**:L53. [ADS].

Cutler C., Apostolatos T.A., Bildsten L., Finn L.S., Flanagan E.E., Kennefick D., Markovic D.M., Ori A., Poisson E., Sussman G.J. (1993). "The last three minutes - Issues in gravitational-wave measurements of coalescing compact binaries". *Physical Review Letters*, **70**:2984–2987. [ADS].

Cutler C., Flanagan É.E. (1994). "Gravitational waves from merging compact binaries: How accurately can one extract the binary's parameters from the inspiral waveform\?" *Physical Review D*, **49**:2658–2697. [ADS].

Damour T. (1987). *The problem of motion in Newtonian and Einsteinian gravity.*, pages 128–198. Three Hundred Years of Gravitation. [ADS].

Damour T. (2001). "Coalescence of two spinning black holes: An effective one-body approach". *Physical Review D*, **64**(12):124013. [ADS].

Damour T. (2012). "The General Relativistic Two Body Problem and the Effective One Body Formalism". *ArXiv*, (1212.3169). [ADS].

Damour T., Gopakumar A., Iyer B.R. (2004). "Phasing of gravitational waves from inspiralling eccentric binaries". *Physical Review D*, **70**(6):064028. [ADS].

Damour T., Iyer B.R., Jaranowski P., Sathyaprakash B.S. (2003). "Gravitational waves from black hole binary inspiral and merger: The span of third post-Newtonian effective-one-body templates". *Physical Review D*, **67**(6):064028. [ADS].

Damour T., Jaranowski P., Schäfer G. (2000). "Determination of the last stable orbit for circular general relativistic binaries at the third post-Newtonian approximation". *Physical Review D*, **62**(8):084011. [ADS].

Damour T., Nagar A. (2009). "Improved analytical description of inspiralling and coalescing black-hole binaries". *Physical Review D*, **79**(8):081503. [ADS].

Damour T., Nagar A., Dorband E.N., Pollney D., Rezzolla L. (2008a). "Faithful effective-one-body waveforms of equal-mass coalescing black-hole binaries". *Physical Review D*, **77**(8):084017. [ADS].

Damour T., Nagar A., Hannam M., Husa S., Brügmann B. (2008b). "Accurate effective-one-body waveforms of inspiralling and coalescing black-hole binaries". *Physical Review D*, **78**(4):044039. [ADS].

Damour T., Taylor J.H. (1991). "On the orbital period change of the binary pulsar PSR 1913 + 16". *Astrophysical Journal*, **366**:501–511. [ADS].

D'Angelo G., Henning T., Kley W. (2002). "Nested-grid calculations of disk-planet interaction". *Astronomy and Astrophysics*, **385**:647–670. [ADS].

D'Angelo G., Kley W., Henning T. (2003). "Orbital Migration and Mass Accretion of Protoplanets in Three-dimensional Global Computations with Nested Grids". *Astrophysical Journal*, **586**:540–561. [ADS].

Davis S.W., Done C., Blaes O.M. (2006). "Testing Accretion Disk Theory in Black Hole X-Ray Binaries". *Astrophysical Journal*, **647**:525–538. [ADS].

De Donder E., Vanbeveren D. (2004). "The influence of binaries on galactic chemical evolution". *New Astronomy Review*, **48**:861–975. [ADS].

de Freitas Pacheco J.A., Regimbau T., Vincent S., Spallicci A. (2006). "Expected Coalescence Rates of Ns-Ns Binaries for Laser Beam Interferometers". *International Journal of Modern Physics D*, **15**:235–249. [ADS].

De Marco O., Passy J.C., Moe M., Herwig F., Mac Low M.M., Paxton B. (2011). "On the α formalism for the common envelope interaction". *Monthly Notices of the Royal Astronomical Society*, **411**:2277–2292. [ADS].

de Sitter W. (1916a). "Einstein's theory of gravitation and its astronomical consequences". *Monthly Notices of the Royal Astronomical Society*, **76**:699–728. [ADS].

de Sitter W. (1916b). "On Einstein's theory of gravitation and its astronomical consequences. Second paper". *Monthly Notices of the Royal Astronomical Society*, **77**:155–184. [ADS].

Demircan O., Kahraman G. (1991). "Stellar mass-luminosity and mass-radius relations". *Astrophysics and Space Science*, **181**:313–322. [ADS].

Demorest P.B., Ferdman R.D., Gonzalez M.E., Nice D., Ransom S., Stairs I.H., Arzoumanian Z., Brazier A., Burke-Spolaor S., Chamberlin S.J., et al. (2013). "Limits on the Stochastic Gravitational Wave Background from the North American Nanohertz Observatory for Gravitational Waves". *Astrophysical Journal*, **762**:94. [ADS].

Dewi J.D.M., van den Heuvel E.P.J. (2004). "The formation of the double neutron star pulsar J0737 - 3039". *Monthly Notices of the Royal Astronomical Society*, **349**:169–172. [ADS].

Di Matteo T., Croft R.A.C., Springel V., Hernquist L. (2003). "Black Hole Growth and Activity in a Λ Cold Dark Matter Universe". *Astrophysical Journal*, **593**:56–68. [ADS].

Di Matteo T., Springel V., Hernquist L. (2005). "Energy input from quasars regulates the growth and activity of black holes and their host galaxies". *Nature*, **433**:604–607. [ADS].

Doeleman S.S., Weintroub J., Rogers A.E.E., Plambeck R., Freund R., Tilanus R.P.J., Friberg P., Ziurys L.M., Moran J.M., Corey B., et al. (2008). "Event-horizon-scale structure in the supermassive black hole candidate at the Galactic Centre". *Nature*, **455**:78–80. [ADS].

Dominik M., Belczynski K., Fryer C., Holz D.E., Berti E., Bulik T., Mandel I., O'Shaughnessy R. (2012). "Double Compact Objects. I. The Significance of the Common Envelope on Merger Rates". *Astrophysical Journal*, **759**:52. [ADS].

Dotti M., Colpi M., Haardt F. (2006). "Laser Interferometer Space Antenna double black holes: dynamics in gaseous nuclear discs". *Monthly Notices of the Royal Astronomical Society*, **367**:103–112. [ADS].

Dotti M., Colpi M., Pallini S., Perego A., Volonteri M. (2013). "On the Orientation and Magnitude of the Black Hole Spin in Galactic Nuclei". *Astrophysical Journal*, **762**:68. [ADS].

Dotti M., Montuori C., Decarli R., Volonteri M., Colpi M., Haardt F. (2009a). "SDSSJ092712.65+294344.0: a candidate massive black hole binary". *Monthly Notices of the Royal Astronomical Society*, **398**:L73–L77. [ADS].

Dotti M., Ruszkowski M., Paredi L., Colpi M., Volonteri M., Haardt F. (2009b). "Dual black holes in merger remnants - I. Linking accretion to dynamics". *Monthly Notices of the Royal Astronomical Society*, **396**:1640–1646. [ADS].

Dotti M., Sesana A., Decarli R. (2012). "Massive Black Hole Binaries: Dynamical Evolution and Observational Signatures". *Advances in Astronomy*, **2012**:940568. [ADS].

Dotti M., Volonteri M., Perego A., Colpi M., Ruszkowski M., Haardt F. (2010). "Dual black holes in merger remnants - II. Spin evolution and gravitational recoil". *Monthly Notices of the Royal Astronomical Society*, **402**:682–690. [ADS].

Dunn R.J.H., Fabian A.C., Sanders J.S. (2006). "Precession of the super-massive black hole in NGC 1275 (3C 84)?" *Monthly Notices of the Royal Astronomical Society*, **366**:758–766. [ADS].

Eddington A.S. (1926). *The Internal Constitution of the Stars*. Cambridge: Cambridge University Press, 1926. ISBN 9780521337083. [ADS].

Eggleton P. (2006). *Evolutionary Processes in Binary and Multiple Stars*. pp. . ISBN 0521855578. Cambridge, UK: Cambridge University Press, 2006. [ADS].

Eggleton P.P. (1983). "Approximations to the radii of Roche lobes". *Astrophysical Journal*, **268**:368. [ADS].

Eggleton P.P., Kiseleva-Eggleton L. (2001). "Orbital Evolution in Binary and Triple Stars, with an Application to SS Lacertae". *Astrophysical Journal*, **562**:1012–1030. [ADS].

Einstein A. (1916). "Näherungsweise Integration der Feldgleichungen der Gravitation". *Sitzungsberichte der Königlich Preußischen Akademie der Wissenschaften (Berlin), Seite 688-696.*, pages 688–696. [ADS].

Einstein A., Infeld L., Hoffmann B. (1938). "The Gravitational Equations and the Problem of Motion". *Annals of Mathematics*, **39**:65–100. [ADS].

Eisenhauer F., Genzel R., Alexander T., Abuter R., Paumard T., Ott T., Gilbert A., Gillessen S., Horrobin M., Trippe S., et al. (2005). "SINFONI in the Galactic Center: Young Stars and Infrared Flares in the Central Light-Month". *Astrophysical Journal*, **628**:246–259. [ADS].

Ekers R.D., Goss W.M., Schwarz U.J., Downes D., Rogstad D.H. (1975). "A full synthesis map of Sgr A at 5 GHz." *Astronomy and Astrophysics*, **43**:159–166. [ADS].

Escala A., Larson R.B., Coppi P.S., Mardones D. (2004). "The Role of Gas in the Merging of Massive Black Holes in Galactic Nuclei. I. Black Hole Merging in a Spherical Gas Cloud". *Astrophysical Journal*, **607**:765–777. [ADS].

Escala A., Larson R.B., Coppi P.S., Mardones D. (2005). "The Role of Gas in the Merging of Massive Black Holes in Galactic Nuclei. II. Black Hole Merging in a Nuclear Gas Disk". *Astrophysical Journal*, **630**:152–166. [ADS].

Esposito L.W., Harrison E.R. (1975). "Properties of the Hulse-Taylor binary pulsar system". *Astrophysical Journal, Letters*, **196**:L1. [ADS].

Everitt C.W.F., Debra D.B., Parkinson B.W., Turneaure J.P., Conklin J.W., Heifetz M.I., Keiser G.M., Silbergleit A.S., Holmes T., Kolodziejczak J., et al. (2011). "Gravity Probe B: Final Results of a Space Experiment to Test General Relativity". *Physical Review Letters*, **106**(22):221101. [ADS].

Faber S.M., Tremaine S., Ajhar E.A., Byun Y.I., Dressler A., Gebhardt K., Grillmair C., Kormendy J., Lauer T.R., Richstone D. (1997). "The Centers of Early-Type Galaxies with HST. IV. Central Parameter Relations." *Astronomical Journal*, **114**:1771. [ADS].

Fabian A.C. (2002). "X-rays from active galactic nuclei: relativistically broadened emission lines". *Royal Society of London Philosophical Transactions Series A*, **360**:2035. [ADS].

Fabian A.C., Iwasawa K., Reynolds C.S., Young A.J. (2000). "Broad Iron Lines in Active Galactic Nuclei". *Publications of the ASP*, **112**:1145–1161. [ADS].

Fabian A.C., Kara E., Walton D.J., Wilkins D.R., Ross R.R., Lozanov K., Uttley P., Gallo L.C., Zoghbi A., Miniutti G., et al. (2013). "Long XMM observation of the narrow-line Seyfert 1 galaxy IRAS 13224-3809: rapid variability, high spin and a soft lag". *Monthly Notices of the Royal Astronomical Society*, **429**:2917–2923. [ADS].

Fabian A.C., Nandra K., Reynolds C.S., Brandt W.N., Otani C., Tanaka Y., Inoue H., Iwasawa K. (1995). "On broad iron Kalpha lines in Seyfert 1 galaxies". *Monthly Notices of the Royal Astronomical Society*, **277**:L11–L15. [ADS].

Fabian A.C., Rees M.J., Stella L., White N.E. (1989). "X-ray fluorescence from the inner disc in Cygnus X-1". *Monthly Notices of the Royal Astronomical Society*, **238**:729–736. [ADS].

Fabian A.C., Wilkins D.R., Miller J.M., Reis R.C., Reynolds C.S., Cackett E.M., Nowak M.A., Pooley G.G., Pottschmidt K., Sanders J.S., et al. (2012). "On the determination of the spin of the black hole in Cyg X-1 from X-ray reflection spectra". *Monthly Notices of the Royal Astronomical Society*, **424**:217–223. [ADS].

Falceta-Gonçalves D., Caproni A., Abraham Z., Teixeira D.M., de Gouveia Dal Pino E.M. (2010). "Precessing Jets and X-ray Bubbles from NGC 1275 (3C 84) in the Perseus Galaxy Cluster: A View from Three-dimensional Numerical Simulations". *Astrophysical Journal, Letters*, **713**:L74–L78. [ADS].

Fan X., Hennawi J.F., Richards G.T., Strauss M.A., Schneider D.P., Donley J.L., Young J.E., Annis J., Lin H., Lampeitl H., et al. (2004). "A Survey of z>5.7 Quasars in the Sloan Digital Sky Survey. III. Discovery of Five Additional Quasars". *Astronomical Journal*, **128**:515–522. [ADS].

Fan X., Narayanan V.K., Lupton R.H., Strauss M.A., Knapp G.R., Becker R.H., White R.L., Pentericci L., Leggett S.K., Haiman Z., et al. (2001). "A Survey of z>5.8 Quasars in the Sloan Digital Sky Survey. I. Discovery of Three New Quasars and the Spatial Density of Luminous Quasars at z˜6". *Astronomical Journal*, **122**:2833–2849. [ADS].

Fan X., Strauss M.A., Richards G.T., Hennawi J.F., Becker R.H., White R.L., Diamond-Stanic A.M., Donley J.L., Jiang L., Kim J.S., et al. (2006). "A Survey of z>5.7 Quasars in the Sloan Digital Sky Survey. IV. Discovery of Seven Additional Quasars". *Astronomical Journal*, **131**:1203–1209. [ADS].

Fan X., Strauss M.A., Schneider D.P., Becker R.H., White R.L., Haiman Z., Gregg M., Pentericci L., Grebel E.K., Narayanan V.K., et al. (2003). "A Survey of z>5.7 Quasars in the Sloan Digital Sky Survey. II. Discovery of Three Additional Quasars at z>6". *Astronomical Journal*, **125**:1649–1659. [ADS].

Fanton C., Calvani M., de Felice F., Cadez A. (1997). "Detecting Accretion Disks in Active Galactic Nuclei". *Publications of the ASJ*, **49**:159–169. [ADS].

Farr W.M., Kremer K., Lyutikov M., Kalogera V. (2011). "Spin Tilts in the Double Pulsar Reveal Supernova Spin Angular-momentum Production". *Astrophysical Journal*, **742**:81. [ADS].

Favata M., Hughes S.A., Holz D.E. (2004). "How Black Holes Get Their Kicks: Gravitational Radiation Recoil Revisited". *Astrophysical Journal*, **607**:L5–L8. [ADS].

Ferrarese L., Ford H. (2005). "Supermassive Black Holes in Galactic Nuclei: Past, Present and Future Research". *Space Science Reviews*, **116**:523–624. [ADS].

Ferrarese L., Merritt D. (2000). "A Fundamental Relation between Supermassive Black Holes and Their Host Galaxies". *Astrophysical Journal, Letters*, **539**:L9–L12. [ADS].

Ferrarese L., Pogge R.W., Peterson B.M., Merritt D., Wandel A., Joseph C.L. (2001). "Supermassive Black Holes in Active Galactic Nuclei. I. The Consistency of Black Hole Masses in Quiescent and Active Galaxies". *Astrophysical Journal, Letters*, **555**:L79–L82. [ADS].

Finn L.S. (1996). "Binary inspiral, gravitational radiation, and cosmology". *Physical Review D*, **53**:2878–2894. [ADS].

Finn L.S., Chernoff D.F. (1993). "Observing binary inspiral in gravitational radiation: One interferometer". *Physical Review D*, **47**:2198–2219. [ADS].

Fitchett M.J. (1983). "The influence of gravitational wave momentum losses on the centre of mass motion of a Newtonian binary system". *Monthly Notices of the Royal Astronomical Society*, **203**:1049–1062. [ADS].

Fock V. (1965). "The Theory of Space, Time and Gravitation". *American Journal of Physics*, **33**:248–249. [ADS].

Forman W., Jones C., Churazov E., Markevitch M., Nulsen P., Vikhlinin A., Begelman M., Böhringer H., Eilek J., Heinz S., et al. (2007). "Filaments, Bubbles, and Weak Shocks in the Gaseous Atmosphere of M87". *Astrophysical Journal*, **665**:1057–1066. [ADS].

Fragile P.C., Anninos P. (2005). "Hydrodynamic Simulations of Tilted Thick-Disk Accretion onto a Kerr Black Hole". *Astrophysical Journal*, **623**:347–361. [ADS].

Fragile P.C., Blaes O.M., Anninos P., Salmonson J.D. (2007). "Global General Relativistic Magnetohydrodynamic Simulation of a Tilted Black Hole Accretion Disk". *Astrophysical Journal*, **668**:417–429. [ADS].

Fragile P.C., Mathews G.J., Wilson J.R. (2001). "Bardeen-Petterson Effect and Quasi-periodic Oscillations in X-Ray Binaries". *Astrophysical Journal*, **553**:955–959. [ADS].

Fragos T., Kalogera V., Belczynski K., Fabbiano G., Kim D.W., Brassington N.J., Angelini L., Davies R.L., Gallagher J.S., King A.R., et al. (2008). "Models for Low-Mass X-Ray Binaries in the Elliptical Galaxies NGC 3379 and NGC 4278: Comparison with Observations". *Astrophysical Journal*, **683**:346–356. [ADS].

Fragos T., Kalogera V., Willems B., Belczynski K., Fabbiano G., Brassington N.J., Kim D.W., Angelini L., Davies R.L., Gallagher J.S., et al. (2009a). "Transient Low-mass X-ray Binary Populations in Elliptical Galaxies NGC 3379 and NGC 4278". *Astrophysical Journal, Letters*, **702**:L143–L147. [ADS].

Fragos T., Lehmer B., Tremmel M., Tzanavaris P., Basu-Zych A., Belczynski K., Hornschemeier A., Jenkins L., Kalogera V., Ptak A., et al. (2013). "X-Ray Binary Evolution Across Cosmic Time". *Astrophysical Journal*, **764**:41. [ADS].

Fragos T., Tremmel M., Rantsiou E., Belczynski K. (2010). "Black Hole Spin-Orbit Misalignment in Galactic X-ray Binaries". *Astrophysical Journal, Letters*, **719**:L79–L83. [ADS].

Fragos T., Willems B., Kalogera V., Ivanova N., Rockefeller G., Fryer C.L., Young P.A. (2009b). "Understanding Compact Object Formation and Natal Kicks. II. The Case of XTE J1118 + 480". *Astrophysical Journal*, **697**:1057–1070. [ADS].

Frank J., King A., Raine D.J. (2002). *Accretion Power in Astrophysics: Third Edition*. pp. 398. ISBN 0521620538. Cambridge, UK: Cambridge University Press, February 2002. [ADS].

Frank J., Rees M.J. (1976). "Effects of massive central black holes on dense stellar systems". *Monthly Notices of the Royal Astronomical Society*, **176**:633–647. [ADS].

Freise A., Strain K. (2010). "Interferometer Techniques for Gravitational-Wave Detection". *Living Reviews in Relativity*, **13**:1. [ADS].

Fryer C.L. (1999). "Mass Limits For Black Hole Formation". *Astrophysical Journal*, **522**:413–418. [ADS].

Fryer C.L., Belczynski K., Wiktorowicz G., Dominik M., Kalogera V., Holz D.E. (2012). "Compact Remnant Mass Function: Dependence on the Explosion Mechanism and Metallicity". *Astrophysical Journal*, **749**:91. [ADS].

Fryer C.L., Kalogera V. (2001). "Theoretical Black Hole Mass Distributions". *Astrophysical Journal*, **554**:548–560. [ADS].

Fryer C.L., Ruiter A.J., Belczynski K., Brown P.J., Bufano F., Diehl S., Fontes C.J., Frey L.H., Holland S.T., Hungerford A.L., et al. (2010). "Spectra of Type Ia Supernovae from Double Degenerate Mergers". *Astrophysical Journal*, **725**:296–308. [ADS].

Fryer C.L., Woosley S.E. (1998). "Helium Star/Black Hole Mergers: A New Gamma-Ray Burst Model". *Astrophysical Journal, Letters*, **502**:L9. [ADS].

Gair J.R., Sesana A., Berti E., Volonteri M. (2011). "Constraining properties of the black hole population using LISA". *Classical and Quantum Gravity*, **28**(9):094018. [ADS].

Galley C.R., Herrmann F., Silberholz J., Tiglio M., Guerberoff G. (2010). "Statistical constraints on binary black hole inspiral dynamics". *Classical and Quantum Gravity*, **27**(24):245007. [ADS].

Gallimore J.F., Axon D.J., O'Dea C.P., Baum S.A., Pedlar A. (2006). "A Survey of Kiloparsec-Scale Radio Outflows in Radio-Quiet Active Galactic Nuclei". *Astronomical Journal*, **132**:546–569. [ADS].

Gallo L.C., Miniutti G., Miller J.M., Brenneman L.W., Fabian A.C., Guainazzi M., Reynolds C.S. (2011). "Multi-epoch X-ray observations of the Seyfert 1.2 galaxy Mrk 79: bulk motion of the illuminating X-ray source". *Monthly Notices of the Royal Astronomical Society*, **411**:607–619. [ADS].

Ge H., Webbink R.F., Han Z., Chen X. (2010). "Stellar adiabatic mass loss model and applications". *Astrophysics and Space Science*, **329**:243–248. [ADS].

Gebhardt K., Bender R., Bower G., Dressler A., Faber S.M., Filippenko A.V., Green R., Grillmair C., Ho L.C., Kormendy J., et al. (2000). "A Relationship between Nuclear Black Hole Mass and Galaxy Velocity Dispersion". *Astrophysical Journal*, **539**:L13–L16. [ADS].

Genzel R. (2007). "The power of new experimental techniques in astronomy: zooming in on the black hole in the Center of the Milky Way". *Highlights of Astronomy*, **14**:63–76. [ADS].

Genzel R., Eisenhauer F., Gillessen S. (2010). "The Galactic Center massive black hole and nuclear star cluster". *Reviews of Modern Physics*, **82**:3121–3195. [ADS].

Genzel R., Thatte N., Krabbe A., Kroker H., Tacconi-Garman L.E. (1996). "The Dark Mass Concentration in the Central Parsec of the Milky Way". *Astrophysical Journal*, **472**:153. [ADS].

Gergely L.Á. (2000). "Spin-spin effects in radiating compact binaries". *Physical Review D*, **61**(2):024035. [ADS].

Gerosa D., Kesden M., Berti E., O'Shaughnessy R., Sperhake U. (2013). "Resonant-plane locking and spin alignment in stellar-mass black-hole binaries: a diagnostic of compact-binary formation". *ArXiv*, (1302.4442). [ADS].

Ghez A.M., Duchêne G., Matthews K., Hornstein S.D., Tanner A., Larkin J., Morris M., Becklin E.E., Salim S., Kremenek T., et al. (2003). "The First Measurement of Spectral Lines in a Short-Period Star Bound to the Galaxy's Central Black Hole: A Paradox of Youth". *Astrophysical Journal, Letters*, **586**:L127–L131. [ADS].

Ghez A.M., Salim S., Hornstein S.D., Tanner A., Lu J.R., Morris M., Becklin E.E., Duchêne G. (2005). "Stellar Orbits around the Galactic Center Black Hole". *Astrophysical Journal*, **620**:744–757. [ADS].

Ghez A.M., Salim S., Weinberg N.N., Lu J.R., Do T., Dunn J.K., Matthews K., Morris M.R., Yelda S., Becklin E.E., et al. (2008). "Measuring Distance and Properties of the Milky Way's Central Supermassive Black Hole with Stellar Orbits". *Astrophysical Journal*, **689**:1044–1062. [ADS].

Gillessen S., Eisenhauer F., Fritz T.K., Bartko H., Dodds-Eden K., Pfuhl O., Ott T., Genzel R. (2009a). "The Orbit of the Star S2 Around SGR A* from Very Large Telescope and Keck Data". *Astrophysical Journal, Letters*, **707**:L114–L117. [ADS].

Gillessen S., Eisenhauer F., Trippe S., Alexander T., Genzel R., Martins F., Ott T. (2009b). "Monitoring Stellar Orbits Around the Massive Black Hole in the Galactic Center". *Astrophysical Journal*, **692**:1075–1109. [ADS].

Goldstein H., Poole C., Safko J. (2002). *Classical mechanics*. (3rd ed.) San Francisco: Addison-Wesley, 2002. [ADS].

González J.A., Hannam M., Sperhake U., Brügmann B., Husa S. (2007a). "Supermassive Recoil Velocities for Binary Black-Hole Mergers with Antialigned Spins". *Physical Review Letters*, **98**(23):231101. [ADS].

González J.A., Sperhake U., Brügmann B., Hannam M., Husa S. (2007b). "Maximum Kick from Nonspinning Black-Hole Binary Inspiral". *Physical Review Letters*, **98**(9):091101. [ADS].

González-Martín O., Vaughan S. (2012). "X-ray variability of 104 active galactic nuclei. XMM-Newton power-spectrum density profiles". *Astronomy and Astrophysics*, **544**:A80. [ADS].

Green P.J., Myers A.D., Barkhouse W.A., Mulchaey J.S., Bennert V.N., Cox T.J., Aldcroft T.L. (2010a). "SDSS J1254+0846: A Binary Quasar Caught in the Act of Merging". *Astrophysical Journal*, **710**:1578–1588. [ADS].

Green P.J., Myers A.D., Barkhouse W.A., Mulchaey J.S., Bennert V.N., Cox T.J., Aldcroft T.L., Wrobel J.M. (2010b). "ERRATUM: "SDSS J1254+0846: A Binary Quasar Caught in the Act of Merging"". *Astrophysical Journal*, **712**:762. [ADS].

Gualandris A., Merritt D. (2008). "Ejection of Supermassive Black Holes from Galaxy Cores". *Astrophysical Journal*, **678**:780–797. [ADS].

Guedes J., Madau P., Mayer L., Callegari S. (2011). "Recoiling Massive Black Holes in Gas-rich Galaxy Mergers". *Astrophysical Journal*, **729**:125. [ADS].

Gültekin K., Richstone D.O., Gebhardt K., Lauer T.R., Tremaine S., Aller M.C., Bender R., Dressler A., Faber S.M., Filippenko A.V., et al. (2009). "The M-σ and M-L Relations in Galactic Bulges, and Determinations of Their Intrinsic Scatter". *Astrophysical Journal*, **698**:198–221. [ADS].

Günther R., Kley W. (2002). "Circumbinary disk evolution". *Astronomy and Astrophysics*, **387**:550–559. [ADS].

Haiman Z., Kocsis B., Menou K. (2009). "The Population of Viscosity- and Gravitational Wave-driven Supermassive Black Hole Binaries Among Luminous Active Galactic Nuclei". *Astrophysical Journal*, **700**:1952–1969. [ADS].

Haiman Z., Loeb A. (1998). "Observational Signatures of the First Quasars". *Astrophysical Journal*, **503**:505. [ADS].

Haller J.W., Rieke M.J., Rieke G.H., Tamblyn P., Close L., Melia F. (1996a). "Stellar Kinematics and the Black Hole in the Galactic Center". *Astrophysical Journal*, **456**:194. [ADS].

Haller J.W., Rieke M.J., Rieke G.H., Tamblyn P., Close L., Melia F. (1996b). "Stellar Kinematics and the Black Hole in the Galactic Center: Erratum". *Astrophysical Journal*, **468**:955. [ADS].

Hannam M., Husa S., Brügmann B., Gopakumar A. (2008a). "Comparison between numerical-relativity and post-Newtonian waveforms from spinning binaries: The orbital hang-up case". *Physical Review D*, **78**(10):104007. [ADS].

Hannam M., Husa S., González J.A., Sperhake U., Brügmann B. (2008b). "Where post-Newtonian and numerical-relativity waveforms meet". *Physical Review D*, **77**(4):044020. [ADS].

Hannam M., Husa S., Ohme F., Müller D., Brügmann B. (2010). "Simulations of black-hole binaries with unequal masses or nonprecessing spins: Accuracy, physical properties, and comparison with post-Newtonian results". *Physical Review D*, **82**(12):124008. [ADS].

Häring N., Rix H.W. (2004). "On the Black Hole Mass-Bulge Mass Relation". *Astrophysical Journal*, **604**:L89–L92. [ADS].

Harry G.M. (2010). "Advanced LIGO: the next generation of gravitational wave detectors". *Classical and Quantum Gravity*, **27**(8):084006. [ADS].

Hartle J.B. (2003). *Gravity : an introduction to Einstein's general relativity*. San Francisco, CA, USA: Addison Wesley, ISBN 0-8053-8662-9, 2003, XXII + 582 pp. [ADS].

Hawking S.W., Ellis G.F.R. (1973). *The large-scale structure of space-time*. Cambridge (UK): Cambridge University Press, 11 + 391 p. [ADS].

Healy J., Herrmann F., Hinder I., Shoemaker D.M., Laguna P., Matzner R.A. (2009). "Superkicks in Hyperbolic Encounters of Binary Black Holes". *Physical Review Letters*, **102**(4):041101. [ADS].

Heckman T.M., Krolik J.H., Moran S.M., Schnittman J., Gezari S. (2009). "SDSSJ092712.65+294344.0: NGC 1275 at z = 0.7?" *Astrophysical Journal*, **695**:363–367. [ADS].

Heggie D.C. (1975). "Binary evolution in stellar dynamics". *Monthly Notices of the Royal Astronomical Society*, **173**:729–787. [ADS].

Herrmann F., Hinder I., Shoemaker D.M., Laguna P., Matzner R.A. (2007). "Binary black holes: Spin dynamics and gravitational recoil". *Physical Review D*, **76**(8):084032. [ADS].

Herrmann F., Silberholz J., Bellone M., Guerberoff G., Tiglio M. (2010). "FAST TRACK COMMUNICATION: Integrating post-Newtonian equations on graphics processing units". *Classical and Quantum Gravity*, **27**(3):032001. [ADS].

Hills J.G. (1983). "The effects of sudden mass loss and a random kick velocity produced in a supernova explosion on the dynamics of a binary star of arbitrary orbital eccentricity - Applications to X-ray binaries and to the binary pulsars". *Astrophysical Journal*, **267**:322–333. [ADS].

Hinshaw G., Larson D., Komatsu E., Spergel D.N., Bennett C.L., Dunkley J., Nolta M.R., Halpern M., Hill R.S., Odegard N., et al. (2012). "Nine-Year Wilkinson Microwave Anisotropy Probe (WMAP) Observations: Cosmological Parameter Results". *ArXiv*, (1212.5226). [ADS].

Hobbs G., Archibald A., Arzoumanian Z., Backer D., Bailes M., Bhat N.D.R., Burgay M., Burke-Spolaor S., Champion D., Cognard I., et al. (2010). "The International Pulsar Timing Array project: using pulsars as a gravitational wave detector". *Classical and Quantum Gravity*, **27**(8):084013. [ADS].

Hobbs G., Lorimer D.R., Lyne A.G., Kramer M. (2005). "A statistical study of 233 pulsar proper motions". *Monthly Notices of the Royal Astronomical Society*, **360**:974–992. [ADS].

Hodges-Kluck E.J., Reynolds C.S., Miller M.C., Cheung C.C. (2010). "A Deep Chandra Observation of the X-shaped Radio Galaxy 4C +00.58: A Candidate for Merger-induced Reorientation?" *Astrophysical Journal, Letters*, **717**:L37–L41. [ADS].

Hopkins P.F., Richards G.T., Hernquist L. (2007). "An Observational Determination of the Bolometric Quasar Luminosity Function". *Astrophysical Journal*, **654**:731–753. [ADS].

Horbatsch M.W., Burgess C.P. (2012). "Cosmic black-hole hair growth and quasar OJ287". *Journal of Cosmology and Astroparticle Physics*, **5**:010. [ADS].

Hoyle F., Lyttleton R.A. (1941). "On the accretion theory of stellar evolution". *Monthly Notices of the Royal Astronomical Society*, **101**:227. [ADS].

Hudson D.S., Reiprich T.H., Clarke T.E., Sarazin C.L. (2006). "X-ray detection of the proto supermassive binary black hole at the centre of Abell 400". *Astronomy and Astrophysics*, **453**:433–446. [ADS].

Hughes S.A., Blandford R.D. (2003). "Black Hole Mass and Spin Coevolution by Mergers". *Astrophysical Journal, Letters*, **585**:L101–L104. [ADS].

Hulse R.A., Taylor J.H. (1975). "Discovery of a pulsar in a binary system". *Astrophysical Journal, Letters*, **195**:L51–L53. [ADS].

Hurley J.R., Pols O.R., Tout C.A. (2000). "Comprehensive analytic formulae for stellar evolution as a function of mass and metallicity". *Monthly Notices of the Royal Astronomical Society*, **315**:543–569. [ADS].

Hurley J.R., Tout C.A., Pols O.R. (2002). "Evolution of binary stars and the effect of tides on binary populations". *Monthly Notices of the Royal Astronomical Society*, **329**:897–928. [ADS].

Hut P. (1981). "Tidal evolution in close binary systems". *Astronomy and Astrophysics*, **99**:126–140. [ADS].

Ihm C.M., Kalogera V., Belczynski K. (2006). "Eccentricities of Double Neutron Star Binaries". *Astrophysical Journal*, **652**:540–547. [ADS].

Israel W. (1967). "Event Horizons in Static Vacuum Space-Times". *Physical Review*, **164**:1776–1779. [ADS].

Ivanov P.B., Illarionov A.F. (1997). "The oscillatory shape of the stationary twisted disc around a Kerr black hole". *Monthly Notices of the Royal Astronomical Society*, **285**:394–402. [ADS].

Ivanov P.B., Papaloizou J.C.B., Polnarev A.G. (1999). "The evolution of a supermassive binary caused by an accretion disc". *Monthly Notices of the Royal Astronomical Society*, **307**:79–90. [ADS].

Ivanova N., Belczynski K., Fregeau J.M., Rasio F.A. (2005). "The evolution of binary fractions in globular clusters". *Monthly Notices of the Royal Astronomical Society*, **358**:572–584. [ADS].

Ivanova N., Belczynski K., Kalogera V., Rasio F.A., Taam R.E. (2003). "The Role of Helium Stars in the Formation of Double Neutron Stars". *Astrophysical Journal*, **592**:475–485. [ADS].

Ivanova N., Heinke C.O., Rasio F.A., Belczynski K., Fregeau J.M. (2008). "Formation and evolution of compact binaries in globular clusters - II. Binaries with neutron stars". *Monthly Notices of the Royal Astronomical Society*, **386**:553–576. [ADS].

Ivanova N., Heinke C.O., Rasio F.A., Taam R.E., Belczynski K., Fregeau J. (2006). "Formation and evolution of compact binaries in globular clusters - I. Binaries with white dwarfs". *Monthly Notices of the Royal Astronomical Society*, **372**:1043–1059. [ADS].

Izzard R.G., Dray L.M., Karakas A.I., Lugaro M., Tout C.A. (2006). "Population nucleosynthesis in single and binary stars. I. Model". *Astronomy and Astrophysics*, **460**:565–572. [ADS].

Janssen G.H., Stappers B.W., Kramer M., Purver M., Jessner A., Cognard I. (2008). "European Pulsar Timing Array". In *40 Years of Pulsars: Millisecond Pulsars, Magnetars and More*, edited by C. Bassa, Z. Wang, A. Cumming, V.M. Kaspi, volume 983 of *American Institute of Physics Conference Series*, pages 633–635. [ADS].

Jenet F., Finn L.S., Lazio J., Lommen A., McLaughlin M., Stairs I., Stinebring D., Verbiest J., Archibald A., Arzoumanian Z., et al. (2009). "The North American Nanohertz Observatory for Gravitational Waves". *ArXiv*, (0909.1058). [ADS].

Johnson J.L., Whalen D.J., Li H., Holz D.E. (2012). "Supermassive Seeds for Supermassive Black Holes". *ArXiv*, (1211.0548). [ADS].

Johnson-McDaniel N.K., Yunes N., Tichy W., Owen B.J. (2009). "Conformally curved binary black hole initial data including tidal deformations and outgoing radiation". *Physical Review D*, **80**(12):124039. [ADS].

Junker W., Schaefer G. (1992). "Binary systems - Higher order gravitational radiation damping and wave emission". *Monthly Notices of the Royal Astronomical Society*, **254**:146–164. [ADS].

Kalogera V. (1996). "Orbital Characteristics of Binary Systems after Asymmetric Supernova Explosions". *Astrophysical Journal*, **471**:352. [ADS].

Kalogera V. (2000). "Spin-Orbit Misalignment in Close Binaries with Two Compact Objects". *Astrophysical Journal*, **541**:319–328. [ADS].

Kalogera V., Belczynski K. (2001). "Binary Population Synthesis: Methods, Normalization and Surprises". In *The Influence of Binaries on Stellar Population Studies*, edited by D. Vanbeveren, volume 264 of *Astrophysics and Space Science Library*, page 447. [ADS].

Kalogera V., Kim C., Lorimer D.R., Burgay M., D'Amico N., Possenti A., Manchester R.N., Lyne A.G., Joshi B.C., McLaughlin M.A., et al. (2004a). "Erratum: "The Cosmic Coalescence Rates for Double Neutron Star Binaries" ApJ, 601, L179". *Astrophysical Journal, Letters*, **614**:L137–L138. [ADS].

Kalogera V., Kim C., Lorimer D.R., Burgay M., D'Amico N., Possenti A., Manchester R.N., Lyne A.G., Joshi B.C., McLaughlin M.A., et al. (2004b). "The Cosmic Coalescence Rates for Double Neutron Star Binaries". *Astrophysical Journal, Letters*, **601**:L179–L182. [ADS].

Kaplan D.L., Chatterjee S., Gaensler B.M., Anderson J. (2008). "A Precise Proper Motion for the Crab Pulsar, and the Difficulty of Testing Spin-Kick Alignment for Young Neutron Stars". *Astrophysical Journal*, **677**:1201–1215. [ADS].

Karas V., Czerny B., Abrassart A., Abramowicz M.A. (2000). "A cloud model of active galactic nuclei: the iron Kα line diagnostics". *Monthly Notices of the Royal Astronomical Society*, **318**:547–560. [ADS].

Kauffmann G., Haehnelt M. (2000). "A unified model for the evolution of galaxies and quasars". *Monthly Notices of the Royal Astronomical Society*, **311**:576–588. [ADS].

Kennicutt Jr. R.C., Schweizer F., Barnes J.E. (1996). *Galaxies: Interactions and Induced Star Formation.* Saas-Fee Advanced Course 26 Lecture Notes 1996. Kennicutt, R.C., Jr.; Schweizer, F.; Barnes, J.E. [ADS].

Kerr R.P. (1963). "Gravitational Field of a Spinning Mass as an Example of Algebraically Special Metrics". *Physical Review Letters*, **11**:237–238. [ADS].

Kesden M., Sperhake U., Berti E. (2010a). "Final spins from the merger of precessing binary black holes". *Physical Review D*, **81**(8):084054. [ADS].

Kesden M., Sperhake U., Berti E. (2010b). "Relativistic Suppression of Black Hole Recoils". *Astrophysical Journal*, **715**:1006–1011. [ADS].

Kidder L.E. (1995). "Coalescing binary systems of compact objects to (post)$^{5/2}$-Newtonian order. V. Spin effects". *Physical Review D*, **52**:821–847. [ADS].

Kidder L.E., Will C.M., Wiseman A.G. (1993). "Spin effects in the inspiral of coalescing compact binaries". *Physical Review D*, **47**:4183. [ADS].

King A.R., Kolb U. (1999). "The evolution of black hole mass and angular momentum". *Monthly Notices of the Royal Astronomical Society*, **305**:654–660. [ADS].

King A.R., Livio M., Lubow S.H., Pringle J.E. (2013). "Accretion disc viscosity: what do warped discs tell us?" *Monthly Notices of the Royal Astronomical Society*. [ADS].

King A.R., Lubow S.H., Ogilvie G.I., Pringle J.E. (2005). "Aligning spinning black holes and accretion discs". *Monthly Notices of the Royal Astronomical Society*, **363**:49–56. [ADS].

King A.R., Pringle J.E. (2006). "Growing supermassive black holes by chaotic accretion". *Monthly Notices of the Royal Astronomical Society*, **373**:L90–L92. [ADS].

King A.R., Pringle J.E. (2007). "Fuelling active galactic nuclei". *Monthly Notices of the Royal Astronomical Society*, **377**:L25–L28. [ADS].

King A.R., Pringle J.E., Hofmann J.A. (2008). "The evolution of black hole mass and spin in active galactic nuclei". *Monthly Notices of the Royal Astronomical Society*, **385**:1621–1627. [ADS].

King A.R., Pringle J.E., Livio M. (2007). "Accretion disc viscosity: how big is alpha?" *Monthly Notices of the Royal Astronomical Society*, **376**:1740–1746. [ADS].

Kinney A.L., Schmitt H.R., Clarke C.J., Pringle J.E., Ulvestad J.S., Antonucci R.R.J. (2000). "Jet Directions in Seyfert Galaxies". *Astrophysical Journal*, **537**:152–177. [ADS].

Klessen R.S., Spaans M., Jappsen A.K. (2007). "The stellar mass spectrum in warm and dusty gas: deviations from Salpeter in the Galactic centre and in circumnuclear starburst regions". *Monthly Notices of the Royal Astronomical Society*, **374**:L29–L33. [ADS].

Kley W., D'Angelo G., Henning T. (2001). "Three-dimensional Simulations of a Planet Embedded in a Protoplanetary Disk". *Astrophysical Journal*, **547**:457–464. [ADS].

Komossa S. (2012). "Recoiling Black Holes: Electromagnetic Signatures, Candidates, and Astrophysical Implications". *Advances in Astronomy*, **2012**:364973. [ADS].

Komossa S., Burwitz V., Hasinger G., Predehl P., Kaastra J.S., Ikebe Y. (2003). "Discovery of a Binary Active Galactic Nucleus in the Ultraluminous Infrared Galaxy NGC 6240 Using Chandra". *Astrophysical Journal, Letters*, **582**:L15–L19. [ADS].

Komossa S., Merritt D. (2008). "Tidal Disruption Flares from Recoiling Supermassive Black Holes". *Astrophysical Journal, Letters*, **683**:L21–L24. [ADS].

Komossa S., Zhou H., Lu H. (2008). "A Recoiling Supermassive Black Hole in the Quasar SDSS J092712.65+294344.0?" *Astrophysical Journal, Letters*, **678**:L81–L84. [ADS].

Kondratko P.T., Greenhill L.J., Moran J.M. (2005). "Evidence for a Geometrically Thick Self-Gravitating Accretion Disk in NGC 3079". *Astrophysical Journal*, **618**:618–634. [ADS].

Kopal Z. (1959). *Close binary systems*. The International Astrophysics Series, London: Chapman Hall, 1959. [ADS].

Kopparapu R.K., Hanna C., Kalogera V., O'Shaughnessy R., González G., Brady P.R., Fairhurst S. (2008). "Host Galaxies Catalog Used in LIGO Searches for Compact Binary Coalescence Events". *Astrophysical Journal*, **675**:1459–1467. [ADS].

Kormendy J., Richstone D. (1995). "Inward Bound—The Search For Supermassive Black Holes In Galactic Nuclei". *Annual Review of Astronomy and Astrophysics*, **33**:581. [ADS].

Kotko I., Lasota J.P. (2012). "The viscosity parameter α and the properties of accretion disc outbursts in close binaries". *Astronomy and Astrophysics*, **545**:A115. [ADS].

Kowalska I., Bulik T., Belczynski K., Dominik M., Gondek-Rosinska D. (2011). "The eccentricity distribution of compact binaries". *Astronomy and Astrophysics*, **527**:A70. [ADS].

Kramer M. (1998). "Determination of the Geometry of the PSR B1913+16 System by Geodetic Precession". *Astrophysical Journal*, **509**:856–860. [ADS].

Krolik J.H. (1999). *Active galactic nuclei : from the central black hole to the galactic environment*. Princeton, N. J. : Princeton University Press, c1999. [ADS].

Kruskal M.D. (1960). "Maximal Extension of Schwarzschild Metric". *Physical Review*, **119**:1743–1745. [ADS].

Kumar S., Pringle J.E. (1985). "Twisted accretion discs - The Bardeen-Petterson effect". *Monthly Notices of the Royal Astronomical Society*, **213**:435–442. [ADS].

Kyrian K., Semerák O. (2007). "Spinning test particles in a Kerr field - II". *Monthly Notices of the Royal Astronomical Society*, **382**:1922–1932. [ADS].

Laarakkers W.G., Poisson E. (1999). "Quadrupole Moments of Rotating Neutron Stars". *Astrophysical Journal*, **512**:282–287. [ADS].

Lacey C., Cole S. (1993). "Merger rates in hierarchical models of galaxy formation". *Monthly Notices of the Royal Astronomical Society*, **262**:627–649. [ADS].

Lacy J.H., Townes C.H., Geballe T.R., Hollenbach D.J. (1980). "Observations of the motion and distribution of the ionized gas in the central parsec of the Galaxy. II". *Astrophysical Journal*, **241**:132–146. [ADS].

Lacy J.H., Townes C.H., Hollenbach D.J. (1982). "The nature of the central parsec of the Galaxy". *Astrophysical Journal*, **262**:120–134. [ADS].

Lai D., Chernoff D.F., Cordes J.M. (2001). "Pulsar Jets: Implications for Neutron Star Kicks and Initial Spins". *Astrophysical Journal*, **549**:1111–1118. [ADS].

Lang R.N., Hughes S.A. (2006). "Measuring coalescing massive binary black holes with gravitational waves: The impact of spin-induced precession". *Physical Review D*, **74**(12):122001. [ADS].

Lang R.N., Hughes S.A. (2008). "Erratum: Measuring coalescing massive binary black holes with gravitational waves: The impact of spin-induced precession [Phys. Rev. D 74, 122001 (2006)]". *Physical Review D*, **77**(10):109901. [ADS].

Laor A. (1991). "Line profiles from a disk around a rotating black hole". *Astrophysical Journal*, **376**:90–94. [ADS].

Larwood J.D., Papaloizou J.C.B. (1997). "The hydrodynamical response of a tilted circumbinary disc: linear theory and non-linear numerical simulations". *Monthly Notices of the Royal Astronomical Society*, **285**:288–302. [ADS].

Lasota J.P. (2001). "The disc instability model of dwarf novae and low-mass X-ray binary transients". *New Astronomy Review*, **45**:449–508. [ADS].

Lecar M., Wheeler J.C., McKee C.F. (1976). "Tidal circularization of the binary X-ray sources Hercules X-1 and Centaurus X-3". *Astrophysical Journal*, **205**:556–562. [ADS].

Lei W.H., Zhang B., Gao H. (2013). "Frame Dragging, Disk Warping, Jet Precessing, and Dipped X-Ray Light Curve of Sw J1644+57". *Astrophysical Journal*, **762**:98. [ADS].

Lense J., Thirring H. (1918). "Über den Einfluß der Eigenrotation der Zentralkörper auf die Bewegung der Planeten und Monde nach der Einsteinschen Gravitationstheorie". *Physikalische Zeitschrift*, **19**:156. [ADS].

Li L.X., Narayan R., McClintock J.E. (2009). "Inferring the Inclination of a Black Hole Accretion Disk from Observations of its Polarized Continuum Radiation". *Astrophysical Journal*, **691**:847–865. [ADS].

Lin D.N.C., Papaloizou J. (1979). "Tidal torques on accretion discs in binary systems with extreme mass ratios". *Monthly Notices of the Royal Astronomical Society*, **186**:799–812. [ADS].

Lin D.N.C., Papaloizou J. (1986a). "On the tidal interaction between protoplanets and the primordial solar nebula. II - Self-consistent nonlinear interaction". *Astrophysical Journal*, **307**:395–409. [ADS].

Lin D.N.C., Papaloizou J. (1986b). "On the tidal interaction between protoplanets and the protoplanetary disk. III - Orbital migration of protoplanets". *Astrophysical Journal*, **309**:846–857. [ADS].

Linden T., Sepinsky J.F., Kalogera V., Belczynski K. (2009). "Probing Electron-Capture Supernovae: X-Ray Binaries in Starbursts". *Astrophysical Journal*, **699**:1573–1577. [ADS].

Lippai Z., Frei Z., Haiman Z. (2008). "Prompt Shocks in the Gas Disk around a Recoiling Supermassive Black Hole Binary". *Astrophysical Journal, Letters*, **676**:L5–L8. [ADS].

Lipunov V.M., Postnov K.A., Prokhorov M.E. (1997). "Formation and coalescence of relativistic binary stars: the effect of kick velocity". *Monthly Notices of the Royal Astronomical Society*, **288**:245–259. [ADS].

Livio M., Ogilvie G.I., Pringle J.E. (1999). "Extracting Energy from Black Holes: The Relative Importance of the Blandford-Znajek Mechanism". *Astrophysical Journal*, **512**:100–104. [ADS].

Lo K.Y., Schilizzi R.T., Cohen M.H., Ross H.N. (1975). "VLBI observations of the compact radio source in the center of the Galaxy". *Astrophysical Journal, Letters*, **202**:L63–L65. [ADS].

Lodato G. (2007). "Self-gravitating accretion discs". *Nuovo Cimento Rivista Serie*, **30**:293. [ADS].

Lodato G. (2008). "Classical disc physics". *New Astronomy Review*, **52**:21–41. [ADS].

Lodato G., Clarke C.J. (2004). "Massive planets in FU Orionis discs: implications for thermal instability models". *Monthly Notices of the Royal Astronomical Society*, **353**:841–852. [ADS].

Lodato G., Gerosa D. (2013). "Black hole mergers: do gas discs lead to spin alignment?" *Monthly Notices of the Royal Astronomical Society*, **429**:L30–L34. [ADS].

Lodato G., Natarajan P. (2006). "Supermassive black hole formation during the assembly of pre-galactic discs". *Monthly Notices of the Royal Astronomical Society*, **371**:1813–1823. [ADS].

Lodato G., Natarajan P. (2007). "The mass function of high-redshift seed black holes". *Monthly Notices of the Royal Astronomical Society*, **377**:L64–L68. [ADS].

Lodato G., Nayakshin S., King A.R., Pringle J.E. (2009). "Black hole mergers: can gas discs solve the 'final parsec' problem?" *Monthly Notices of the Royal Astronomical Society*, **398**:1392–1402. [ADS].

Lodato G., Price D.J. (2010). "On the diffusive propagation of warps in thin accretion discs". *Monthly Notices of the Royal Astronomical Society*, **405**:1212–1226. [ADS].

Lodato G., Pringle J.E. (2006). "The evolution of misaligned accretion discs and spinning black holes". *Monthly Notices of the Royal Astronomical Society*, **368**:1196–1208. [ADS].

Lodato G., Pringle J.E. (2007). "Warp diffusion in accretion discs: a numerical investigation". *Monthly Notices of the Royal Astronomical Society*, **381**:1287–1300. [ADS].

Lodato G., Rice W.K.M. (2004). "Testing the locality of transport in self-gravitating accretion discs". *Monthly Notices of the Royal Astronomical Society*, **351**:630–642. [ADS].

Loeb A. (2007). "Observable Signatures of a Black Hole Ejected by Gravitational-Radiation Recoil in a Galaxy Merger". *Physical Review Letters*, **99**(4):041103. [ADS].

Lohfink A.M., Reynolds C.S., Miller J.M., Brenneman L.W., Mushotzky R.F., Nowak M.A., Fabian A.C. (2012). "The Black Hole Spin and Soft X-Ray Excess of the Luminous Seyfert Galaxy Fairall 9". *Astrophysical Journal*, **758**:67. [ADS].

Longair M.S. (2008). *Galaxy Formation*. Berlin: Springer, 2008. ISBN 978-3-540-73477-2. [ADS].

Longair M.S. (2011). *High Energy Astrophysics*. Cambridge, UK: Cambridge University Press, 2011. [ADS].

Lorimer D.R. (2008). "Binary and Millisecond Pulsars". *Living Reviews in Relativity*, **11**:8. [ADS].

Lousto C.O., Campanelli M., Zlochower Y., Nakano H. (2010a). "Remnant masses, spins and recoils from the merger of generic black hole binaries". *Classical and Quantum Gravity*, **27**(11):114006. [ADS].

Lousto C.O., Nakano H., Zlochower Y., Campanelli M. (2010b). "Erratum: Statistical studies of spinning black-hole binaries [Phys. Rev. DPRVDAQ1550-7998 81, 084023 (2010)]". *Physical Review D*, **82**(12):129902. [ADS].

Lousto C.O., Nakano H., Zlochower Y., Campanelli M. (2010c). "Statistical studies of spinning black-hole binaries". *Physical Review D*, **81**(8):084023. [ADS].

Lousto C.O., Zlochower Y. (2008). "Further insight into gravitational recoil". *Physical Review D*, **77**(4):044028. [ADS].

Lousto C.O., Zlochower Y. (2009). "Modeling gravitational recoil from precessing highly spinning unequal-mass black-hole binaries". *Physical Review D*, **79**(6):064018. [ADS].

Lousto C.O., Zlochower Y. (2011). "Hangup Kicks: Still Larger Recoils by Partial Spin-Orbit Alignment of Black-Hole Binaries". *Physical Review Letters*, **107**(23):231102. [ADS].

Lousto C.O., Zlochower Y. (2012). "Nonlinear Gravitational Recoil from the Mergers of Precessing Black-Hole Binaries". *ArXiv*, (1211.7099). [ADS].

Lousto C.O., Zlochower Y., Dotti M., Volonteri M. (2012). "Gravitational recoil from accretion-aligned black-hole binaries". *Physical Review D*, **85**(8):084015. [ADS].

Loveridge A.J., van der Sluys M.V., Kalogera V. (2011). "Analytical Expressions for the Envelope Binding Energy of Giants as a Function of Basic Stellar Parameters". *Astrophysical Journal*, **743**:49. [ADS].

Lubow S.H., Ogilvie G.I., Pringle J.E. (2002). "The evolution of a warped disc around a Kerr black hole". *Monthly Notices of the Royal Astronomical Society*, **337**:706–712. [ADS].

Lufkin G., Quinn T., Wadsley J., Stadel J., Governato F. (2004). "Simulations of gaseous disc-embedded planet interaction". *Monthly Notices of the Royal Astronomical Society*, **347**:421–429. [ADS].

Luo B., Fabbiano G., Fragos T., Kim D.W., Belczynski K., Brassington N.J., Pellegrini S., Tzanavaris P., Wang J., Zezas A. (2012). "Probing the X-Ray Binary Populations of the Ring Galaxy NGC 1291". *Astrophysical Journal*, **749**:130. [ADS].

Maccarone T.J. (2002). "On the misalignment of jets in microquasars". *Monthly Notices of the Royal Astronomical Society*, **336**:1371–1376. [ADS].

MacDonald I., Nissanke S., Pfeiffer H.P. (2011). "Suitability of post-Newtonian/numerical-relativity hybrid waveforms for gravitational wave detectors". *Classical and Quantum Gravity*, **28**(13):134002. [ADS].

MacFadyen A.I., Milosavljević M. (2008). "An Eccentric Circumbinary Accretion Disk and the Detection of Binary Massive Black Holes". *Astrophysical Journal*, **672**:83–93. [ADS].

Madau P., Quataert E. (2004). "The Effect of Gravitational-Wave Recoil on the Demography of Massive Black Holes". *Astrophysical Journal, Letters*, **606**:L17–L20. [ADS].

Maggiore M. (2007). *Gravitational Waves. Vol. 1: Theory and Experiments*. Oxford University Press, October 2007. 572p. (ISBN-13: 978-0-19-857074-5).

Magorrian J., Tremaine S., Richstone D., Bender R., Bower G., Dressler A., Faber S.M., Gebhardt K., Green R., Grillmair C., et al. (1998). "The Demography of Massive Dark Objects in Galaxy Centers". *Astronomical Journal*, **115**:2285–2305. [ADS].

Malizia A., Bassani L., Bird A.J., Landi R., Masetti N., de Rosa A., Panessa F., Molina M., Dean A.J., Perri M., et al. (2008). "First high-energy observations of narrow-line Seyfert 1s with INTEGRAL/IBIS". *Monthly Notices of the Royal Astronomical Society*, **389**:1360–1366. [ADS].

Manchester R.N. (2008). "The Parkes Pulsar Timing Array Project". In *40 Years of Pulsars: Millisecond Pulsars, Magnetars and More*, edited by C. Bassa, Z. Wang, A. Cumming, V.M. Kaspi, volume 983 of *American Institute of Physics Conference Series*, pages 584–592. [ADS].

Mandel I. (2010). "Parameter estimation on gravitational waves from multiple coalescing binaries". *Physical Review D*, **81**(8):084029. [ADS].

Mandel I., O'Shaughnessy R. (2010). "Compact binary coalescences in the band of ground-based gravitational-wave detectors". *Classical and Quantum Gravity*, **27**(11):114007–+. [ADS].

Maness H.L., Taylor G.B., Zavala R.T., Peck A.B., Pollack L.K. (2004). "Breaking All the Rules: The Compact Symmetric Object 0402+379". *Astrophysical Journal*, **602**:123–134. [ADS].

Marconi A., Hunt L.K. (2003). "The Relation between Black Hole Mass, Bulge Mass, and Near-Infrared Luminosity". *Astrophysical Journal, Letters*, **589**:L21–L24. [ADS].

Marconi A., Risaliti G., Gilli R., Hunt L.K., Maiolino R., Salvati M. (2004). "Local supermassive black holes, relics of active galactic nuclei and the X-ray background". *Monthly Notices of the Royal Astronomical Society*, **351**:169–185. [ADS].

Marsh T.R., Horne K. (1988). "Images of accretion discs. II - Doppler tomography". *Monthly Notices of the Royal Astronomical Society*, **235**:269–286. [ADS].

Martin R.G. (2008). "The warped disc of NGC 4258". *Monthly Notices of the Royal Astronomical Society*, **387**:830–838. [ADS].

Martin R.G., Pringle J.E., Tout C.A. (2007). "Alignment and precession of a black hole with a warped accretion disc". *Monthly Notices of the Royal Astronomical Society*, **381**:1617–1624. [ADS].

Martin R.G., Pringle J.E., Tout C.A. (2009). "The shape of an accretion disc in a misaligned black hole binary". *Monthly Notices of the Royal Astronomical Society*, **400**:383–391. [ADS].

Martin R.G., Reis R.C., Pringle J.E. (2008). "Misalignment of the microquasar V4641 Sgr (SAX J1819.3-2525)". *Monthly Notices of the Royal Astronomical Society*, **391**:L15–L18. [ADS].

Martocchia A., Karas V., Matt G. (2000). "Effects of Kerr space-time on spectral features from X-ray illuminated accretion discs". *Monthly Notices of the Royal Astronomical Society*, **312**:817–826. [ADS].

Mateo M.L. (1998). "Dwarf Galaxies of the Local Group". *Annual Review of Astronomy and Astrophysics*, **36**:435–506. [ADS].

Mayer L., Kazantzidis S., Madau P., Colpi M., Quinn T., Wadsley J. (2007a). "Multi-Scale Simulations of Merging Galaxies with Supermassive Black Holes". In *Relativistic Astrophysics Legacy and Cosmology - Einstein's Legacy*, edited by B. Aschenbach, V. Burwitz, G. Hasinger, B. Leibundgut, page 152. [ADS].

Mayer L., Kazantzidis S., Madau P., Colpi M., Quinn T., Wadsley J. (2007b). "Rapid Formation of Supermassive Black Hole Binaries in Galaxy Mergers with Gas". *Science*, **316**:1874–. [ADS].

McClintock J.E., Narayan R., Davis S.W., Gou L., Kulkarni A., Orosz J.A., Penna R.F., Remillard R.A., Steiner J.F. (2011). "Measuring the spins of accreting black holes". *Classical and Quantum Gravity*, **28**(11):114009. [ADS].

McClintock J.E., Shafee R., Narayan R., Remillard R.A., Davis S.W., Li L.X. (2006). "The Spin of the Near-Extreme Kerr Black Hole GRS 1915+105". *Astrophysical Journal*, **652**:518–539. [ADS].

McHardy I.M., Gunn K.F., Uttley P., Goad M.R. (2005). "MCG-6-30-15: long time-scale X-ray variability, black hole mass and active galactic nuclei high states". *Monthly Notices of the Royal Astronomical Society*, **359**:1469–1480. [ADS].

Megevand M., Anderson M., Frank J., Hirschmann E.W., Lehner L., Liebling S.L., Motl P.M., Neilsen D. (2009). "Perturbed disks get shocked: Binary black hole merger effects on accretion disks". *Physical Review D*, **80**(2):024012. [ADS].

Melia F. (2003). *The edge of infinity. Supermassive black holes in the universe*. Cambridge: Cambridge University Press. ISBN 0-521-81405-7, 2003, IX + 148 pp. [ADS].

Melia F., Falcke H. (2001). "The Supermassive Black Hole at the Galactic Center". *Annual Review of Astronomy and Astrophysics*, **39**:309–352. [ADS].

Mennekens N., Vanbeveren D., De Greve J.P., De Donder E. (2010). "The delay-time distribution of Type Ia supernovae: a comparison between theory and observation". *Astronomy and Astrophysics*, **515**:A89. [ADS].

Merloni A., Vietri M., Stella L., Bini D. (1999). "On gravitomagnetic precession around black holes". *Monthly Notices of the Royal Astronomical Society*, **304**:155–159. [ADS].

Merritt D., Milosavljević M. (2005). "Massive Black Hole Binary Evolution". *Living Reviews in Relativity*, **8**:8. [ADS].

Merritt D., Milosavljević M., Favata M., Hughes S.A., Holz D.E. (2004). "Consequences of Gravitational Radiation Recoil". *Astrophysical Journal*, **607**:L9–L12. [ADS].

Merritt D., Schnittman J.D., Komossa S. (2009). "Hypercompact Stellar Systems Around Recoiling Supermassive Black Holes". *Astrophysical Journal*, **699**:1690–1710. [ADS].

Michelson P.F., Taber R.C. (1984). "Can a resonant-mass gravitational-wave detector have wideband sensitivity?" *Physical Review D*, **29**:2149–2157. [ADS].

Middleton M., Done C., Gierliński M., Davis S.W. (2006). "Black hole spin in GRS 1915+105". *Monthly Notices of the Royal Astronomical Society*, **373**:1004–1012. [ADS].

Mikóczi B., Vasúth M., Gergely L.Á. (2005). "Self-interaction spin effects in inspiralling compact binaries". *Physical Review D*, **71**(12):124043. [ADS].

Miller J.M., Fabian A.C., Reynolds C.S., Nowak M.A., Homan J., Freyberg M.J., Ehle M., Belloni T., Wijnands R., van der Klis M., et al. (2004). "Evidence of Black Hole Spin in GX 339-4: XMM-Newton/EPIC-pn and RXTE Spectroscopy of the Very High State". *Astrophysical Journal, Letters*, **606**:L131–L134. [ADS].

Miller J.M., Fabian A.C., Wijnands R., Reynolds C.S., Ehle M., Freyberg M.J., van der Klis M., Lewin W.H.G., Sanchez-Fernandez C., Castro-Tirado A.J. (2002). "Evidence of Spin and Energy Extraction in a Galactic Black Hole Candidate: The XMM-Newton/EPIC-pn Spectrum of XTE J1650-500". *Astrophysical Journal, Letters*, **570**:L69–L73. [ADS].

Miller J.M., Reynolds C.S., Fabian A.C., Miniutti G., Gallo L.C. (2009). "Stellar-Mass Black Hole Spin Constraints from Disk Reflection and Continuum Modeling". *Astrophysical Journal*, **697**:900–912. [ADS].

Miller M.C., Colbert E.J.M. (2004). "Intermediate-Mass Black Holes". *International Journal of Modern Physics D*, **13**:1–64. [ADS].

Milosavljević M., Merritt D. (2001). "Formation of Galactic Nuclei". *Astrophysical Journal*, **563**:34–62. [ADS].

Milosavljević M., Merritt D. (2003). "The Final Parsec Problem". In *The Astrophysics of Gravitational Wave Sources*, edited by J.M. Centrella, volume 686 of *American Institute of Physics Conference Series*, pages 201–210. [ADS].

Milosavljević M., Phinney E.S. (2005). "The Afterglow of Massive Black Hole Coalescence". *Astrophysical Journal, Letters*, **622**:L93–L96. [ADS].

Miniutti G., Panessa F., de Rosa A., Fabian A.C., Malizia A., Molina M., Miller J.M., Vaughan S. (2009). "An intermediate black hole spin in the NLS1 galaxy SWIFT J2127.4+5654: chaotic accretion or spin energy extraction?" *Monthly Notices of the Royal Astronomical Society*, **398**:255–262. [ADS].

Misner C.W., Thorne K.S., Wheeler J.A. (1973). *Gravitation*. San Francisco: W.H. Freeman and Co., 1973. [ADS].

Misra R., Sutaria F.K. (1999). "Comparisons of Various Model FITS to the Iron Line Profile in MCG -6-30-15". *Astrophysical Journal*, **517**:661–667. [ADS].

Miyoshi K., Takeuchi T., Tanaka H., Ida S. (1999). "Gravitational Interaction between a Protoplanet and a Protoplanetary Disk. I. Local Three-Dimensional Simulations". *Astrophysical Journal*, **516**:451–464. [ADS].

Montuori C., Dotti M., Colpi M., Decarli R., Haardt F. (2011). "Search for sub-parsec massive binary black holes through line diagnosis". *Monthly Notices of the Royal Astronomical Society*, **412**:26–32. [ADS].

Montuori C., Dotti M., Haardt F., Colpi M., Decarli R. (2012). "Search for sub-parsec massive binary black holes through line diagnosis - II". *Monthly Notices of the Royal Astronomical Society*, **425**:1633–1639. [ADS].

Mora T., Will C.M. (2004). "Post-Newtonian diagnostic of quasiequilibrium binary configurations of compact objects". *Physical Review D*, **69**(10):104021. [ADS].

Mora T., Will C.M. (2005). "Erratum: Post-Newtonian diagnostic of quasiequilibrium binary configurations of compact objects [Phys. Rev. D 69, 104021 (2004)]". *Physical Review D*, **71**(12):129901. [ADS].

Mortlock D.J., Warren S.J., Venemans B.P., Patel M., Hewett P.C., McMahon R.G., Simpson C., Theuns T., Gonzáles-Solares E.A., Adamson A., et al. (2011). "A luminous quasar at a redshift of z = 7.085". *Nature*, **474**:616–619. [ADS].

Nagar N.M., Wilson A.S. (1999). "The Relative Orientation of Nuclear Accretion and Galaxy Stellar Disks in Seyfert Galaxies". *Astrophysical Journal*, **516**:97–113. [ADS].

Narayan R. (2005). "Black holes in astrophysics". *New Journal of Physics*, **7**:199. [ADS].

Natarajan P., Armitage P.J. (1999). "Warped discs and the directional stability of jets in active galactic nuclei". *Monthly Notices of the Royal Astronomical Society*, **309**:961–968. [ADS].

Natarajan P., Pringle J.E. (1998). "The Alignment of Disk and Black Hole Spins in Active Galactic Nuclei". *Astrophysical Journal*, **506**:L97–L100. [ADS].

Natarajan P., Volonteri M. (2012). "The mass function of black holes $1<z<4.5$: comparison of models with observations". *Monthly Notices of the Royal Astronomical Society*, **422**:2051–2057. [ADS].

Navarro J.F., Frenk C.S., White S.D.M. (1996). "The Structure of Cold Dark Matter Halos". *Astrophysical Journal*, **462**:563. [ADS].

Nayakshin S., Power C., King A.R. (2012). "The Observed M-σ Relations Imply That Super-massive Black Holes Grow by Cold Chaotic Accretion". *Astrophysical Journal*, **753**:15. [ADS].

Nelemans G., Portegies Zwart S.F., Verbunt F., Yungelson L.R. (2001a). "Population synthesis for double white dwarfs. II. Semi-detached systems: AM CVn stars". *Astronomy and Astrophysics*, **368**:939–949. [ADS].

Nelemans G., Yungelson L.R., Portegies Zwart S.F., Verbunt F. (2001b). "Population synthesis for double white dwarfs . I. Close detached systems". *Astronomy and Astrophysics*, **365**:491–507. [ADS].

Nelson A.F., Benz W. (2003a). "On the Early Evolution of Forming Jovian Planets. I. Initial Conditions, Systematics, and Qualitative Comparisons to Theory". *Astrophysical Journal*, **589**:556–577. [ADS].

Nelson A.F., Benz W. (2003b). "On the Early Evolution of Forming Jovian Planets. II. Analysis of Accretion and Gravitational Torques". *Astrophysical Journal*, **589**:578–604. [ADS].

Nelson R.P., Papaloizou J.C.B. (1999). "Hydrodynamic simulations of propagating WARPS and bending waves in accretion discs". *Monthly Notices of the Royal Astronomical Society*, **309**:929–940. [ADS].

Nelson R.P., Papaloizou J.C.B. (2000). "Hydrodynamic simulations of the Bardeen-Petterson effect". *Monthly Notices of the Royal Astronomical Society*, **315**:570–586. [ADS].

Nelson R.P., Papaloizou J.C.B. (2004). "The interaction of giant planets with a disc with MHD turbulence - IV. Migration rates of embedded protoplanets". *Monthly Notices of the Royal Astronomical Society*, **350**:849–864. [ADS].

Nelson R.P., Papaloizou J.C.B., Masset F., Kley W. (2000). "The migration and growth of protoplanets in protostellar discs". *Monthly Notices of the Royal Astronomical Society*, **318**:18–36. [ADS].

Nixon C., King A. (2013). "Do Jets Precess... or Even Move at All?" *Astrophysical Journal, Letters*, **765**:L7. [ADS].

Nixon C., King A., Price D., Frank J. (2012a). "Tearing up the Disk: How Black Holes Accrete". *Astrophysical Journal, Letters*, **757**:L24. [ADS].

Nixon C.J. (2012). "Stable counteralignment of a circumbinary disc". *Monthly Notices of the Royal Astronomical Society*, **423**:2597–2600. [ADS].

Nixon C.J., Cossins P.J., King A.R., Pringle J.E. (2011a). "Retrograde accretion and merging supermassive black holes". *Monthly Notices of the Royal Astronomical Society*, **412**:1591–1598. [ADS].

Nixon C.J., King A.R. (2012). "Broken discs: warp propagation in accretion discs". *Monthly Notices of the Royal Astronomical Society*, **421**:1201–1208. [ADS].

Nixon C.J., King A.R., Price D.J. (2012b). "Rapid AGN accretion from counter-rotating discs". *Monthly Notices of the Royal Astronomical Society*, **422**:2547–2552. [ADS].

Nixon C.J., King A.R., Pringle J.E. (2011b). "The final parsec problem: aligning a binary with an external accretion disc". *Monthly Notices of the Royal Astronomical Society*, **417**:L66–L69. [ADS].

Noble S.C., Mundim B.C., Nakano H., Krolik J.H., Campanelli M., Zlochower Y., Yunes N. (2012). "Circumbinary Magnetohydrodynamic Accretion into Inspiraling Binary Black Holes". *Astrophysical Journal*, **755**:51. [ADS].

Nordhaus J., Brandt T.D., Burrows A., Almgren A. (2012). "The hydrodynamic origin of neutron star kicks". *Monthly Notices of the Royal Astronomical Society*, **423**:1805–1812. [ADS].

Noutsos A., Schnitzeler D.H.F.M., Keane E.F., Kramer M., Johnston S. (2013). "Pulsar spin-velocity alignment: kinematic ages, birth periods and braking indices". *Monthly Notices of the Royal Astronomical Society*. [ADS].

Novikov I.D., Thorne K.S. (1973). "Astrophysics of black holes." In *Black Holes (Les Astres Occlus)*, edited by C. Dewitt, B.S. Dewitt, pages 343–450. [ADS].

Nugis T., Lamers H.J.G.L.M. (2000). "Mass-loss rates of Wolf-Rayet stars as a function of stellar parameters". *Astronomy and Astrophysics*, **360**:227–244. [ADS].

Nutzman P., Kalogera V., Finn L.S., Hendrickson C., Belczynski K. (2004). "Gravitational Waves from Extragalactic Inspiraling Binaries: Selection Effects and Expected Detection Rates". *Astrophysical Journal*, **612**:364–374. [ADS].

Ogilvie G.I. (1999). "The non-linear fluid dynamics of a warped accretion disc". *Monthly Notices of the Royal Astronomical Society*, **304**:557–578. [ADS].

Ogilvie G.I. (2000). "An alpha theory of time-dependent warped accretion discs". *Monthly Notices of the Royal Astronomical Society*, **317**:607–622. [ADS].

Ogilvie G.I., Dubus G. (2001). "Precessing warped accretion discs in X-ray binaries". *Monthly Notices of the Royal Astronomical Society*, **320**:485–503. [ADS].

Ogilvie G.I., Latter H.N. (2013a). "Hydrodynamic instability in warped astrophysical discs". *ArXiv*, (1303.0264). [ADS].

Ogilvie G.I., Latter H.N. (2013b). "Local and global dynamics of warped astrophysical discs". *ArXiv*, (1303.0263). [ADS].

O'Leary R.M., Kocsis B., Loeb A. (2009). "Gravitational waves from scattering of stellar-mass black holes in galactic nuclei". *Monthly Notices of the Royal Astronomical Society*, **395**:2127–2146. [ADS].

Öpik E. (1924). "Statistical Studies of Double Stars: On the Distribution of Relative Luminosities and Distances of Double Stars in the Harvard Revised Photometry North of Declination -31°". *Publications of the Tartu Astrofizica Observatory*, **25**:1. [ADS].

Orosz J.A., McClintock J.E., Narayan R., Bailyn C.D., Hartman J.D., Macri L., Liu J., Pietsch W., Remillard R.A., Shporer A., et al. (2007). "A 15.65-solar-mass black hole in an eclipsing binary in the nearby spiral galaxy M 33". *Nature*, **449**:872–875. [ADS].

Orosz J.A., Steeghs D., McClintock J.E., Torres M.A.P., Bochkov I., Gou L., Narayan R., Blaschak M., Levine A.M., Remillard R.A., et al. (2009). "A New Dynamical Model for the Black Hole Binary LMC X-1". *Astrophysical Journal*, **697**:573–591. [ADS].

Orosz J.A., Steiner J.F., McClintock J.E., Torres M.A.P., Remillard R.A., Bailyn C.D., Miller J.M. (2011). "An Improved Dynamical Model for the Microquasar XTE J1550-564". *Astrophysical Journal*, **730**:75. [ADS].

O'Shaughnessy R. (2012). "Comparing compact binary parameter distributions I: Methods". *ArXiv*, (1204.3117). [ADS].

O'Shaughnessy R., Belczynski K., Kalogera V. (2008a). "Short Gamma-Ray Bursts and Binary Mergers in Spiral and Elliptical Galaxies: Redshift Distribution and Hosts". *Astrophysical Journal*, **675**:566–585. [ADS].

O'Shaughnessy R., Kalogera V., Belczynski K. (2005a). "Mapping Inspiral Rates on Population Synthesis Parameters". *Astrophysical Journal*, **620**:385–389. [ADS].

O'Shaughnessy R., Kalogera V., Belczynski K. (2007). "Mapping Population Synthesis Event Rates on Model Parameters. II. Convergence and Accuracy of Multidimensional Fits". *Astrophysical Journal*, **667**:1048–1058. [ADS].

O'Shaughnessy R., Kalogera V., Belczynski K. (2010). "Binary Compact Object Coalescence Rates: The Role of Elliptical Galaxies". *Astrophysical Journal*, **716**:615–633. [ADS].

O'Shaughnessy R., Kaplan J., Kalogera V., Belczynski K. (2005b). "Bounds on Expected Black Hole Spins in Inspiraling Binaries". *Astrophysical Journal*, **632**:1035–1041. [ADS].

O'Shaughnessy R., Kim C., Fragos T., Kalogera V., Belczynski K. (2005c). "Constraining Population Synthesis Models via the Binary Neutron Star Population". *Astrophysical Journal*, **633**:1076–1084. [ADS].

O'Shaughnessy R., Kim C., Kalogera V., Belczynski K. (2008b). "Constraining Population Synthesis Models via Empirical Binary Compact Object Merger and Supernova Rates". *Astrophysical Journal*, **672**:479–488. [ADS].

O'Shaughnessy R., Kopparapu R.K., Belczynski K. (2012). "Impact of star formation inhomogeneities on merger rates and interpretation of LIGO results". *Classical and Quantum Gravity*, **29**(14):145011. [ADS].

Owen B.J., Sathyaprakash B.S. (1999). "Matched filtering of gravitational waves from inspiraling compact binaries: Computational cost and template placement". *Physical Review D*, **60**(2):022002. [ADS].

Özel F., Psaltis D., Narayan R., McClintock J.E. (2010). "The Black Hole Mass Distribution in the Galaxy". *Astrophysical Journal*, **725**:1918–1927. [ADS].

Pan Y., Buonanno A., Baker J.G., Centrella J., Kelly B.J., McWilliams S.T., Pretorius F., van Meter J.R. (2008). "Data-analysis driven comparison of analytic and numerical coalescing binary waveforms: Nonspinning case". *Physical Review D*, **77**(2):024014. [ADS].

Pan Y., Buonanno A., Boyle M., Buchman L.T., Kidder L.E., Pfeiffer H.P., Scheel M.A. (2011). "Inspiral-merger-ringdown multipolar waveforms of nonspinning black-hole binaries using the effective-one-body formalism". *Physical Review D*, **84**(12):124052. [ADS].

Pani P., Barausse E., Berti E., Cardoso V. (2010). "Gravitational instabilities of superspinars". *Physical Review D*, **82**(4):044009. [ADS].

Papaloizou J., Lin D.N.C. (1984). "On the tidal interaction between protoplanets and the primordial solar nebula. I - Linear calculation of the role of angular momentum exchange". *Astrophysical Journal*, **285**:818–834. [ADS].

Papaloizou J.C.B., Lin D.N.C. (1995). "Theory Of Accretion Disks I: Angular Momentum Transport Processes". *Annual Review of Astronomy and Astrophysics*, **33**:505–540. [ADS].

Papaloizou J.C.B., Nelson R.P., Masset F. (2001). "Orbital eccentricity growth through disc-companion tidal interaction". *Astronomy and Astrophysics*, **366**:263–275. [ADS].

Papaloizou J.C.B., Nelson R.P., Snellgrove M.D. (2004). "The interaction of giant planets with a disc with MHD turbulence - III. Flow morphology and conditions for gap formation in local and global simulations". *Monthly Notices of the Royal Astronomical Society*, **350**:829–848. [ADS].

Papaloizou J.C.B., Pringle J.E. (1983). "The time-dependence of non-planar accretion discs". *Monthly Notices of the Royal Astronomical Society*, **202**:1181–1194. [ADS].

Papapetrou A. (1951). "Spinning Test-Particles in General Relativity. I". *Royal Society of London Proceedings Series A*, **209**:248–258. [ADS].

Passy J.C., De Marco O., Fryer C.L., Herwig F., Diehl S., Oishi J.S., Mac Low M.M., Bryan G.L., Rockefeller G. (2012). "Simulating the Common Envelope Phase of a Red Giant Using Smoothed-particle Hydrodynamics and Uniform-grid Codes". *Astrophysical Journal*, **744**:52. [ADS].

Patrick A.R., Reeves J.N., Porquet D., Markowitz A.G., Braito V., Lobban A.P. (2012). "A Suzaku survey of Fe K lines in Seyfert 1 active galactic nuclei". *Monthly Notices of the Royal Astronomical Society*, **426**:2522–2565. [ADS].

Paxton B., Bildsten L., Dotter A., Herwig F., Lesaffre P., Timmes F. (2010). "MESA: Modules for Experiments in Stellar Astrophysics". [ADS]. Astrophysics Source Code Library.

Paxton B., Bildsten L., Dotter A., Herwig F., Lesaffre P., Timmes F. (2011). "Modules for Experiments in Stellar Astrophysics (MESA)". *Astrophysical Journal, Supplement*, **192**:3. [ADS].

Penrose R. (1969). "Gravitational Collapse: the Role of General Relativity". *Nuovo Cimento Rivista Serie*, **1**:252. [ADS].

Penrose R., Floyd R.M. (1971). "Extraction of Rotational Energy from a Black Hole". *Nature Physical Science*, **229**:177–179. [ADS].

Perego A., Dotti M., Colpi M., Volonteri M. (2009). "Mass and spin co-evolution during the alignment of a black hole in a warped accretion disc". *Monthly Notices of the Royal Astronomical Society*, **399**:2249–2263. [ADS].

Peters P.C. (1964). "Gravitational Radiation and the Motion of Two Point Masses". *Physical Review*, **136**:1224–1232. [ADS].

Peters P.C., Mathews J. (1963). "Gravitational Radiation from Point Masses in a Keplerian Orbit". *Physical Review*, **131**:435–440. [ADS].

Peterson B.M., Ferrarese L., Gilbert K.M., Kaspi S., Malkan M.A., Maoz D., Merritt D., Netzer H., Onken C.A., Pogge R.W., et al. (2004). "Central Masses and Broad-Line Region Sizes of Active Galactic Nuclei. II. A Homogeneous Analysis of a Large Reverberation-Mapping Database". *Astrophysical Journal*, **613**:682–699. [ADS].

Petterson J.A. (1977a). "Twisted accretion disks. I - Derivation of the basic equations". *Astrophysical Journal*, **214**:550–559. [ADS].

Petterson J.A. (1977b). "Twisted accretion disks. II - Applications to X-ray binary systems". *Astrophysical Journal*, **216**:827–837. [ADS].

Petterson J.A. (1978). "Twisted accretion disks. III - The time-dependent equations". *Astrophysical Journal*, **226**:253–263. [ADS].

Pitkin M., Reid S., Rowan S., Hough J. (2011). "Gravitational Wave Detection by Interferometry (Ground and Space)". *Living Reviews in Relativity*, **14**:5. [ADS].

Poisson E. (1993). "Gravitational radiation from a particle in circular orbit around a black hole. IV. Analytical results for the slowly rotating case". *Physical Review D*, **48**:1860–1863. [ADS].

Poisson E. (1995). "Gravitational radiation from a particle in circular orbit around a black hole. VI. Accuracy of the post-Newtonian expansion". *Physical Review D*, **52**:5719–5723. [ADS].

Poisson E. (1997). "Erratum and Addendum: Gravitational radiation from a particle in circular orbit around a black hole. VI. Accuracy of the post-Newtonian expansion". *Physical Review D*, **55**:7980–7981. [ADS].

Poisson E. (1998). "Gravitational waves from inspiraling compact binaries: The quadrupole-moment term". *Physical Review D*, **57**:5287–5290. [ADS].

Poisson E., Will C.M. (1995). "Gravitational waves from inspiraling compact binaries: Parameter estimation using second-post-Newtonian waveforms". *Physical Review D*, **52**:848–855. [ADS].

Ponce M., Faber J.A., Lombardi J.C. (2012). "Accretion Disks around Kicked Black Holes: Post-kick Dynamics". *Astrophysical Journal*, **745**:71. [ADS].

Popov S.B., Prokhorov M.E. (2007). "REVIEWS OF TOPICAL PROBLEMS: Population synthesis in astrophysics". *Physics Uspekhi*, **50**:1123–1146. [ADS].

Portegies Zwart S.F., McMillan S.L.W. (2000). "Black Hole Mergers in the Universe". *Astrophysical Journal, Letters*, **528**:L17–L20. [ADS].

Portegies Zwart S.F., Verbunt F. (1996). "Population synthesis of high-mass binaries." *Astronomy and Astrophysics*, **309**:179–196. [ADS].

Portegies Zwart S.F., Verbunt F., Ergma E. (1997). "The formation of black-holes in low-mass X-ray binaries." *Astronomy and Astrophysics*, **321**:207–212. [ADS].

Portegies Zwart S.F., Yungelson L.R. (1998). "Formation and evolution of binary neutron stars". *Astronomy and Astrophysics*, **332**:173–188. [ADS].

Porter J.M., Rivinius T. (2003). "Classical Be Stars". *Publications of the ASP*, **115**:1153–1170. [ADS].

Postnov K.A., Kuranov A.G. (2008). "Neutron star spin-kick velocity correlation effect on binary neutron star coalescence rates and spin-orbit misalignment of the components". *Monthly Notices of the Royal Astronomical Society*, **384**:1393–1398. [ADS].

Postnov K.A., Yungelson L.R. (2006). "The Evolution of Compact Binary Star Systems". *Living Reviews in Relativity*, **9**:6. [ADS].

Poveda A., Allen C., Hernández-Alcántara A. (2007). "The Frequency Distribution of Semi-major Axes of Wide Binaries: Cosmogony and Dynamical Evolution". In *IAU Symposium*, edited by W.I. Hartkopf, P. Harmanec, E.F. Guinan, volume 240 of *IAU Symposium*, pages 417–425. [ADS].

Press W.H., Schechter P. (1974). "Formation of Galaxies and Clusters of Galaxies by Self-Similar Gravitational Condensation". *Astrophysical Journal*, **187**:425–438. [ADS].

Press W.H., Teukolsky S.A., Vetterling W.T., Flannery B.P. (2002). *Numerical recipes in C++ : the art of scientific computing.* xxviii, 1,002 p. : ill. ; 26 cm. Includes bibliographical references and index. ISBN : 0521750334. [ADS].

Press W.H., Thorne K.S. (1972). "Gravitational-Wave Astronomy". *Annual Review of Astronomy and Astrophysics*, **10**:335. [ADS].

Pretorius F. (2005). "Evolution of Binary Black-Hole Spacetimes". *Physical Review Letters*, **95**(12):121101. [ADS].

Prialnik D. (2009). *An Introduction to the Theory of Stellar Structure and Evolution.* ambridge University Press, 2009. ISBN: 9780521866040. [ADS].

Pringle J.E. (1981). "Accretion discs in astrophysics". *Annual Review of Astronomy and Astrophysics*, **19**:137–162. [ADS].

Pringle J.E. (1992). "A simple approach to the evolution of twisted accretion discs". *Monthly Notices of the Royal Astronomical Society*, **258**:811–818. [ADS].

Pringle J.E. (1996). "Self-induced warping of accretion discs". *Monthly Notices of the Royal Astronomical Society*, **281**:357–361. [ADS].

Psaltis D. (2006). *Accreting neutron stars and black holes: a decade of discoveries*, pages 1–38. Compact stellar X-ray sources. [ADS].

Racine É. (2008). "Analysis of spin precession in binary black hole systems including quadrupole-monopole interaction". *Physical Review D*, **78**(4):044021. [ADS].

Rafikov R.R. (2012). "Structure and evolution of circumbinary disks around supermassive black hole (SMBH) binaries". *ArXiv*, (1205.5017). [ADS].

Raguzova N.V., Popov S.B. (2005). "Be X-ray binaries and candidates". *Astronomical and Astrophysical Transactions*, **24**:151–185. [ADS].

Rappaport S., Podsiadlowski P., Joss P.C., Di Stefano R., Han Z. (1995). "The relation between white dwarf mass and orbital period in wide binary radio pulsars". *Monthly Notices of the Royal Astronomical Society*, **273**:731–741. [ADS].

Rawlings S., Saunders R. (1991). "Evidence for a common central-engine mechanism in all extragalactic radio sources". *Nature*, **349**:138–140. [ADS].

Rees M.J. (1978). "Relativistic jets and beams in radio galaxies". *Nature*, **275**:516. [ADS].

Reid M.J. (2009). "Is There a Supermassive Black Hole at the Center of the Milky Way?" *International Journal of Modern Physics D*, **18**:889–910. [ADS].

Reipurth B., Heathcote S. (1997). "50 Years of Herbig-Haro Research. From discovery to HST". In *Herbig-Haro Flows and the Birth of Stars*, edited by B. Reipurth, C. Bertout, volume 182 of *IAU Symposium*, pages 3–18. [ADS].

Remillard R.A., McClintock J.E. (2006). "X-Ray Properties of Black-Hole Binaries". *Annual Review of Astronomy and Astrophysics*, **44**:49–92. [ADS].

Remillard R.A., Muno M.P., McClintock J.E., Orosz J.A. (2002). "Evidence for Harmonic Relationships in the High-Frequency Quasi-periodic Oscillations of XTE J1550-564 and GRO J1655-40". *Astrophysical Journal*, **580**:1030–1042. [ADS].

Reynolds C.S. (2013). "Measuring Black Hole Spin using X-ray Reflection Spectroscopy". *ArXiv*, (1302.3260). [ADS].

Reynolds C.S., Fabian A.C. (2008). "Broad Iron-Kα Emission Lines as a Diagnostic of Black Hole Spin". *Astrophysical Journal*, **675**:1048–1056. [ADS].

Rezzolla L. (2009). "Modelling the final state from binary black-hole coalescences". *Classical and Quantum Gravity*, **26**(9):094023. [ADS].

Rhoades C.E., Ruffini R. (1974). "Maximum Mass of a Neutron Star". *Physical Review Letters*, **32**:324–327. [ADS].

Ricker P.M., Taam R.E. (2008). "The Interaction of Stellar Objects within a Common Envelope". *Astrophysical Journal, Letters*, **672**:L41–L44. [ADS].

Ricker P.M., Taam R.E. (2012). "An AMR Study of the Common-envelope Phase of Binary Evolution". *Astrophysical Journal*, **746**:74. [ADS].

Riles K. (2013). "Gravitational waves: Sources, detectors and searches". *Progress in Particle and Nuclear Physics*, **68**:1–54. [ADS].

Risaliti G., Harrison F.A., Madsen K.K., Walton D.J., Boggs S.E., Christensen F.E., Craig W.W., Grefenstette B.W., Hailey C.J., Nardini E., et al. (2013). "A rapidly spinning supermassive black hole at the centre of NGC1365". *Nature*, **494**:449–451. [ADS].

Robinson A., Young S., Axon D.J., Kharb P., Smith J.E. (2010). "Spectropolarimetric Evidence for a Kicked Supermassive Black Hole in the Quasar E1821+643". *Astrophysical Journal, Letters*, **717**:L122–L126. [ADS].

Rodriguez C., Taylor G.B., Zavala R.T., Pihlström Y.M., Peck A.B. (2009). "H I Observations of the Supermassive Binary Black Hole System in 0402+379". *Astrophysical Journal*, **697**:37–44. [ADS].

Roedig C., Dotti M., Sesana A., Cuadra J., Colpi M. (2011). "Limiting eccentricity of subparsec massive black hole binaries surrounded by self-gravitating gas discs". *Monthly Notices of the Royal Astronomical Society*, **415**:3033–3041. [ADS].

Roedig C., Sesana A., Dotti M., Cuadra J., Amaro-Seoane P., Haardt F. (2012). "Evolution of binary black holes in self gravitating discs. Dissecting the torques". *Astronomy and Astrophysics*, **545**:A127. [ADS].

Rosotti G.P., Lodato G., Price D.J. (2012). "Response of a circumbinary accretion disc to black hole mass loss". *Monthly Notices of the Royal Astronomical Society*, **425**:1958–1966. [ADS].

Rossi E.M., Lodato G., Armitage P.J., Pringle J.E., King A.R. (2010). "Black hole mergers: the first light". *Monthly Notices of the Royal Astronomical Society*, **401**:2021–2035. [ADS].

Ruiter A.J., Belczynski K., Fryer C. (2009). "Rates and Delay Times of Type Ia Supernovae". *Astrophysical Journal*, **699**:2026–2036. [ADS].

Ruiter A.J., Belczynski K., Sim S.A., Hillebrandt W., Fryer C.L., Fink M., Kromer M. (2011). "Delay times and rates for Type Ia supernovae and thermonuclear explosions from double-detonation sub-Chandrasekhar mass models". *Monthly Notices of the Royal Astronomical Society*, **417**:408–419. [ADS].

Ruiter A.J., Sim S.A., Pakmor R., Kromer M., Seitenzahl I.R., Belczynski K., Fink M., Herzog M., Hillebrandt W., Röpke F.K., et al. (2013). "On the brightness distribution of Type Ia supernovae from violent white dwarf mergers". *Monthly Notices of the Royal Astronomical Society*, **429**:1425–1436. [ADS].

Salpeter E.E. (1964). "Accretion of Interstellar Matter by Massive Objects." *Astrophysical Journal*, **140**:796–800. [ADS].

Santamaría L., Ohme F., Ajith P., Brügmann B., Dorband N., Hannam M., Husa S., Mösta P., Pollney D., Reisswig C., et al. (2010). "Matching post-Newtonian and numerical relativity waveforms: Systematic errors and a new phenomenological model for nonprecessing black hole binaries". *Physical Review D*, **82**(6):064016. [ADS].

Sathyaprakash B., Abernathy M., Acernese F., Ajith P., Allen B., Amaro-Seoane P., Andersson N., Aoudia S., Arun K., Astone P., et al. (2012). "Scientific objectives of Einstein Telescope". *Classical and Quantum Gravity*, **29**(12):124013. [ADS].

Sathyaprakash B.S., Schutz B.F. (2003). "Templates for stellar mass black holes falling into supermassive black holes". *Classical and Quantum Gravity*, **20**:209. [ADS].

Sathyaprakash B.S., Schutz B.F. (2009). "Physics, Astrophysics and Cosmology with Gravitational Waves". *Living Reviews in Relativity*, **12**:2. [ADS].

Saulson P.R. (1994). *Fundamentals of interferometric gravitational wave detectors*. Singapore: World Scientific Publishers, 1994, xvi, 299 p. ISBN 9810218206. [ADS].

Schäfer C., Speith R., Hipp M., Kley W. (2004). "Simulations of planet-disc interactions using Smoothed Particle Hydrodynamics". *Astronomy and Astrophysics*, **418**:325–335. [ADS].

Scheuer P.A.G., Feiler R. (1996). "The realignment of a black hole misaligned with its accretion disc". *Monthly Notices of the Royal Astronomical Society*, **282**:291. [ADS].

Schiff L.I. (1960). "Possible New Experimental Test of General Relativity Theory". *Physical Review Letters*, **4**:215–217. [ADS].

Schnittman J.D. (2004). "Spin-orbit resonance and the evolution of compact binary systems". *Physical Review D*, **70**(12):124020. [ADS].

Schnittman J.D. (2011). "Electromagnetic counterparts to black hole mergers". *Classical and Quantum Gravity*, **28**(9):094021. [ADS].

Schnittman J.D., Buonanno A. (2007). "The Distribution of Recoil Velocities from Merging Black Holes". *Astrophysical Journal, Letters*, **662**:L63–L66. [ADS].

Schnittman J.D., Krolik J.H. (2008). "The Infrared Afterglow of Supermassive Black Hole Mergers". *Astrophysical Journal*, **684**:835–844. [ADS].

Schödel R., Genzel R., Ott T., Eckart A. (2003). "The Galactic Center stellar cluster: The central arcsecond". *Astronomische Nachrichten Supplement*, **324**:535–541. [ADS].

Schödel R., Ott T., Genzel R., Hofmann R., Lehnert M., Eckart A., Mouawad N., Alexander T., Reid M.J., Lenzen R., et al. (2002). "A star in a 15.2-year orbit around the supermassive black hole at the centre of the Milky Way". *Nature*, **419**:694–696. [ADS].

Schutz B. (2009). *A First Course in General Relativity*. Cambridge University Press, 2009. ISBN: 9780521887052. [ADS].

Schwarzschild K. (1916). "On the Gravitational Field of a Mass Point According to Einstein's Theory". *Abh. Konigl. Preuss. Akad. Wissenschaften Jahre 1906,92, Berlin,1907*, pages 189–196. [ADS].

Semerák O. (1999). "Spinning test particles in a Kerr field - I". *Monthly Notices of the Royal Astronomical Society*, **308**:863–875. [ADS].

Sepinsky J., Kalogera V., Belczynski K. (2005). "Are Supernova Kicks Responsible for X-Ray Binary Ejection from Young Clusters?" *Astrophysical Journal, Letters*, **621**:L37–L40. [ADS].

Sepinsky J.F., Willems B., Kalogera V., Rasio F.A. (2009). "Interacting Binaries with Eccentric Orbits. II. Secular Orbital Evolution due to Non-conservative Mass Transfer". *Astrophysical Journal*, **702**:1387–1392. [ADS].

Sepinsky J.F., Willems B., Kalogera V., Rasio F.A. (2010). "Interacting Binaries with Eccentric Orbits. III. Orbital Evolution due to Direct Impact and Self-Accretion". *Astrophysical Journal*, **724**:546–558. [ADS].

Sesana A., Gair J., Berti E., Volonteri M. (2011). "Reconstructing the massive black hole cosmic history through gravitational waves". *Physical Review D*, **83**(4):044036. [ADS].

Shafee R., McClintock J.E., Narayan R., Davis S.W., Li L.X., Remillard R.A. (2006). "Estimating the Spin of Stellar-Mass Black Holes by Spectral Fitting of the X-Ray Continuum". *Astrophysical Journal, Letters*, **636**:L113–L116. [ADS].

Shakura N.I., Sunyaev R.A. (1973). "Black holes in binary systems. Observational appearance." *Astronomy and Astrophysics*, **24**:337–355. [ADS].

Shankar F., Salucci P., Granato G.L., De Zotti G., Danese L. (2004). "Supermassive black hole demography: the match between the local and accreted mass functions". *Monthly Notices of the Royal Astronomical Society*, **354**:1020–1030. [ADS].

Shankar F., Weinberg D.H., Miralda-Escudé J. (2013). "Accretion-driven evolution of black holes: Eddington ratios, duty cycles and active galaxy fractions". *Monthly Notices of the Royal Astronomical Society*, **428**:421–446. [ADS].

Shen Y. (2013). "The Mass of Quasars". *ArXiv*, (1302.2643). [ADS].

Shen Z.Q., Lo K.Y., Liang M.C., Ho P.T.P., Zhao J.H. (2005). "A size of ˜1AU for the radio source Sgr A* at the centre of the Milky Way". *Nature*, **438**:62–64. [ADS].

Shields G.A., Bonning E.W. (2008). "Powerful Flares from Recoiling Black Holes in Quasars". *Astrophysical Journal*, **682**:758–766. [ADS].

Shields G.A., Bonning E.W., Salviander S. (2009a). "Comment on the Black Hole Recoil Candidate Quasar SDSS J092712.65+294344.0". *Astrophysical Journal*, **696**:1367–1373. [ADS].

Shields G.A., Rosario D.J., Smith K.L., Bonning E.W., Salviander S., Kalirai J.S., Strickler R., Ramirez-Ruiz E., Dutton A.A., Treu T., et al. (2009b). "The Quasar SDSS J105041.35+345631.3: Black Hole Recoil or Extreme Double-Peaked Emitter?" *Astrophysical Journal*, **707**:936–941. [ADS].

Sijacki D., Springel V., Haehnelt M.G. (2011). "Gravitational recoils of supermassive black holes in hydrodynamical simulations of gas-rich galaxies". *Monthly Notices of the Royal Astronomical Society*, **414**:3656–3670. [ADS].

Simone L.E., Leonard S.W., Poisson E., Will C.M. (1997). "Gravitational waves from binary systems in circular orbits: does the post-Newtonian expansion converge?" *Classical and Quantum Gravity*, **14**:237–256. [ADS].

Skibo J.G. (1997). "Spallation of Iron in Black Hole Accretion Flows". *Astrophysical Journal*, **478**:522. [ADS].

Smith J.R. (2009). "The path to the enhanced and advanced LIGO gravitational-wave detectors". *Classical and Quantum Gravity*, **26**(11):114013. [ADS].

Soberman G.E., Phinney E.S., van den Heuvel E.P.J. (1997). "Stability criteria for mass transfer in binary stellar evolution." *Astronomy and Astrophysics*, **327**:620–635. [ADS].

Soltan A. (1982). "Masses of quasars". *Monthly Notices of the Royal Astronomical Society*, **200**:115–122. [ADS].

Somiya K. (2012). "Detector configuration of KAGRA-the Japanese cryogenic gravitational-wave detector". *Classical and Quantum Gravity*, **29**(12):124007. [ADS].

Spaans M., Silk J. (2000). "The Polytropic Equation of State of Interstellar Gas Clouds". *Astrophysical Journal*, **538**:115–120. [ADS].

Sperhake U., Berti E., Cardoso V. (2011a). "Numerical simulations of black-hole binaries and gravitational wave emission". *ArXiv*, (1107.2819). [ADS].

Sperhake U., Berti E., Cardoso V., González J.A., Brügmann B., Ansorg M. (2008a). "Eccentric binary black-hole mergers: The transition from inspiral to plunge in general relativity". *Physical Review D*, **78**(6):064069. [ADS].

Sperhake U., Berti E., Cardoso V., Pretorius F. (2012). "Universality, maximum radiation and absorption in high-energy collisions of black holes with spin". *ArXiv*, (1211.6114). [ADS].

Sperhake U., Berti E., Cardoso V., Pretorius F., Yunes N. (2011b). "Superkicks in ultrarelativistic encounters of spinning black holes". *Physical Review D*, **83**(2):024037. [ADS].

Sperhake U., Cardoso V., Pretorius F., Berti E., González J.A. (2008b). "High-Energy Collision of Two Black Holes". *Physical Review Letters*, **101**(16):161101. [ADS].

Spruit H., Phinney E.S. (1998). "Birth kicks as the origin of pulsar rotation". *Nature*, **393**:139–141. [ADS].

Srinivasan G. (2010). "Recycled pulsars". *New Astronomy Review*, **54**:93–100. [ADS].

Steiner J.F., McClintock J.E. (2012). "Modeling the Jet Kinematics of the Black Hole Microquasar XTE J1550-564: A Constraint on Spin-Orbit Alignment". *Astrophysical Journal*, **745**:136. [ADS].

Syer D., Clarke C.J. (1995). "Satellites in discs: regulating the accretion luminosity". *Monthly Notices of the Royal Astronomical Society*, **277**:758–766. [ADS].

Takahashi R. (2004a). "Shapes and Positions of Black Hole Shadows in Accretion Disks and Spin Parameters of Black Holes". *Astrophysical Journal*, **611**:996–1004. [ADS].

Takahashi R. (2004b). "Status of TAMA300". *Classical and Quantum Gravity*, **21**:403. [ADS].

Tan Y., Wang J.X., Shu X.W., Zhou Y. (2012). "A Possible Ultra Strong and Broad Fe Kα Emission Line in Seyfert 2 Galaxy IRAS 00521-7054". *Astrophysical Journal, Letters*, **747**:L11. [ADS].

Tanaka Y., Nandra K., Fabian A.C., Inoue H., Otani C., Dotani T., Hayashida K., Iwasawa K., Kii T., Kunieda H., et al. (1995). "Gravitationally redshifted emission implying an accretion disk and massive black hole in the active galaxy MCG-6-30-15". *Nature*, **375**:659–661. [ADS].

Taylor J.H., Weisberg J.M. (1982). "A new test of general relativity - Gravitational radiation and the binary pulsar PSR 1913+16". *Astrophysical Journal*, **253**:908–920. [ADS].

Taylor J.H., Weisberg J.M. (1989). "Further experimental tests of relativistic gravity using the binary pulsar PSR 1913 + 16". *Astrophysical Journal*, **345**:434–450. [ADS].

Tchekhovskoy A., Narayan R., McKinney J.C. (2011). "Efficient generation of jets from magnetically arrested accretion on a rapidly spinning black hole". *Monthly Notices of the Royal Astronomical Society*, **418**:L79–L83. [ADS].

Thirring H. (1918). "Über die Wirkung rotierender ferner Massen in der Einsteinschen Gravitationstheorie." *Physikalische Zeitschrift*, **19**:33. [ADS].

Thirring H. (1921). "Berichtigung zu meiner Arbeit: "Über die Wirkung rotierender Massen in der Einsteinschen Gravitationstheorie"". *Physikalische Zeitschrift*, **22**:29. [ADS].

Thorne K.S. (1974). "Disk-Accretion onto a Black Hole. II. Evolution of the Hole". *Astrophysical Journal*, **191**:507–520. [ADS].

Thorne K.S. (1980). "Multipole expansions of gravitational radiation". *Reviews of Modern Physics*, **52**:299–340. [ADS].

Thorne K.S. (1987). *Gravitational radiation.*, pages 330–458. Three Hundred Years of Gravitation. [ADS].

Thorne K.S. (1994). *Black holes and time warps: Einstein's outrageous legacy.* Commonwealth Fund Book Program, New York, NY: W.W. Norton and London: Picador, c1994. [ADS].

Thorne K.S., Hartle J.B. (1985). "Laws of motion and precession for black holes and other bodies". *Physical Review D*, **31**:1815–1837. [ADS].

Thorne K.S., Zytkow A.N. (1975). "Red giants and supergiants with degenerate neutron cores". *Astrophysical Journal, Letters*, **199**:L19–L24. [ADS].

Thorne K.S., Zytkow A.N. (1977). "Stars with degenerate neutron cores. I - Structure of equilibrium models". *Astrophysical Journal*, **212**:832–858. [ADS].

Timmes F.X., Woosley S.E., Weaver T.A. (1996). "The Neutron Star and Black Hole Initial Mass Function". *Astrophysical Journal*, **457**:834. [ADS].

Toonen S., Nelemans G., Portegies Zwart S. (2012). "Supernova Type Ia progenitors from merging double white dwarfs. Using a new population synthesis model". *Astronomy and Astrophysics*, **546**:A70. [ADS].

Török G., Abramowicz M.A., Kluźniak W., Stuchlík Z. (2005). "The orbital resonance model for twin peak kHz quasi periodic oscillations in microquasars". *Astronomy and Astrophysics*, **436**:1–8. [ADS].

Townsend P.K. (1997). "Black Holes". *ArXiv*, (9707012). [ADS].

Treister E., Urry C.M. (2006). "The Evolution of Obscuration in Active Galactic Nuclei". *Astrophysical Journal, Letters*, **652**:L79–L82. [ADS].

Tremaine S., Gebhardt K., Bender R., Bower G., Dressler A., Faber S.M., Filippenko A.V., Green R., Grillmair C., Ho L.C., et al. (2002). "The Slope of the Black Hole Mass versus Velocity Dispersion Correlation". *Astrophysical Journal*, **574**:740–753. [ADS].

Trilling D.E., Benz W., Guillot T., Lunine J.I., Hubbard W.B., Burrows A. (1998). "Orbital Evolution and Migration of Giant Planets: Modeling Extrasolar Planets". *Astrophysical Journal*, **500**:428. [ADS].

Tsoubelis D., Economou A., Stoghianidis E. (1986). "The geodetic effect along polar orbits in the Kerr spacetime". *Physics Letters A*, **118**:113–116. [ADS].

Tutukov A.V., Yungelson L.R. (1993a). "Formation of neutron stars in binary systems". *Astronomy Reports*, **37**:411–431. [ADS].

Tutukov A.V., Yungelson L.R. (1993b). "The merger rate of neutron star and black hole binaries". *Monthly Notices of the Royal Astronomical Society*, **260**:675–678. [ADS].

Ugliano M., Janka H.T., Marek A., Arcones A. (2012). "Progenitor-explosion Connection and Remnant Birth Masses for Neutrino-driven Supernovae of Iron-core Progenitors". *Astrophysical Journal*, **757**:69. [ADS].

van den Heuvel E.P.J., De Loore C. (1973). "The nature of X-ray binaries III. Evolution of massive close binaries with one collapsed component - with a possible application to Cygnus X-3." *Astronomy and Astrophysics*, **25**:387–395. [ADS].

van den Heuvel E.P.J., Habets G.M.H.J. (1984). "Observational lower mass limit for black hole formation derived from massive X-ray binaries". *Nature*, **309**:598–600. [ADS].

van Haasteren R., Levin Y., Janssen G.H., Lazaridis K., Kramer M., Stappers B.W., Desvignes G., Purver M.B., Lyne A.G., Ferdman R.D., et al. (2011). "Placing limits on the stochastic gravitational-wave background using European Pulsar Timing Array data". *Monthly Notices of the Royal Astronomical Society*, **414**:3117–3128. [ADS].

van Haasteren R., Levin Y., Janssen G.H., Lazaridis K., Kramer M., Stappers B.W., Desvignes G., Purver M.B., Lyne A.G., Ferdman R.D., et al. (2012). "Erratum: Placing limits on the stochastic gravitational-wave background using European Pulsar Timing Array data". *Monthly Notices of the Royal Astronomical Society*, **425**:1597–1597. [ADS].

van Meter J.R., Miller M.C., Baker J.G., Boggs W.D., Kelly B.J. (2010). "Test of a General Formula for Black Hole Gravitational Wave Kicks". *Astrophysical Journal*, **719**:1427–1432. [ADS].

Van Wassenhove S., Volonteri M., Mayer L., Dotti M., Bellovary J., Callegari S. (2012). "Observability of Dual Active Galactic Nuclei in Merging Galaxies". *Astrophysical Journal, Letters*, **748**:L7. [ADS].

Volonteri M. (2007). "Gravitational Recoil: Signatures on the Massive Black Hole Population". *Astrophysical Journal, Letters*, **663**:L5–L8. [ADS].

Volonteri M., Haardt F., Madau P. (2003). "The Assembly and Merging History of Supermassive Black Holes in Hierarchical Models of Galaxy Formation". *Astrophysical Journal*, **582**:559–573. [ADS].

Volonteri M., Lodato G., Natarajan P. (2008). "The evolution of massive black hole seeds". *Monthly Notices of the Royal Astronomical Society*, **383**:1079–1088. [ADS].

Volonteri M., Madau P., Quataert E., Rees M.J. (2005). "The Distribution and Cosmic Evolution of Massive Black Hole Spins". *Astrophysical Journal*, **620**:69–77. [ADS].

Volonteri M., Miller J.M., Dotti M. (2009). "Sub-Parsec Supermassive Binary Quasars: Expectations at z<1". *Astrophysical Journal, Letters*, **703**:L86–L89. [ADS].

Volonteri M., Rees M.J. (2005). "Rapid Growth of High-Redshift Black Holes". *Astrophysical Journal*, **633**:624–629. [ADS].

Volonteri M., Sikora M., Lasota J.P., Merloni A. (2012). "The evolution of active galactic nuclei and their spins". *ArXiv*, (1210.1025). [ADS].

Voss R., Tauris T.M. (2003). "Galactic distribution of merging neutron stars and black holes - prospects for short gamma-ray burst progenitors and LIGO/VIRGO". *Monthly Notices of the Royal Astronomical Society*, **342**:1169–1184. [ADS].

Wagh S.M., Dadhich N. (1989). "The energetics of black holes in electromagnetic fields by the penrose process". *Physics Reports*, **183**:137–192. [ADS].

Wald R.M. (1984). *General relativity.* Chicago, University of Chicago Press, 1984, 504 p. [ADS].

Walton D.J., Nardini E., Fabian A.C., Gallo L.C., Reis R.C. (2013). "Suzaku observations of 'bare' active galactic nuclei". *Monthly Notices of the Royal Astronomical Society*, **428**:2901–2920. [ADS].

Wang C., Lai D., Han J.L. (2006a). "Neutron Star Kicks in Isolated and Binary Pulsars: Observational Constraints and Implications for Kick Mechanisms". *Astrophysical Journal*, **639**:1007–1017. [ADS].

Wang J.M., Chen Y.M., Zhang F. (2006b). "Cosmological Evolution of the Duty Cycle of Quasars". *Astrophysical Journal, Letters*, **647**:L17–L20. [ADS].

Webbink R.F. (1984). "Double white dwarfs as progenitors of R Coronae Borealis stars and Type I supernovae". *Astrophysical Journal*, **277**:355–360. [ADS].

Webbink R.F. (1996). "Structure Parameters of Galactic Globular Clusters (Webbink 1985)". *VizieR Online Data Catalog*, **7151**:0. [ADS].

Webbink R.F. (2008). "Common Envelope Evolution Redux". In *Astrophysics and Space Science Library*, edited by E.F. Milone, D.A. Leahy, D.W. Hobill, volume 352 of *Astrophysics and Space Science Library*, page 233. [ADS].

Weber J. (1961). *General relativity and gravitational waves*. Interscience Tracts on Physics and Astronomy, New York: Interscience, 1961. [ADS].

Webster B.L., Murdin P. (1972). "Cygnus X-1-a Spectroscopic Binary with a Heavy Companion ?" *Nature*, **235**:37–38. [ADS].

Weinberg S. (1972). *Gravitation and Cosmology: Principles and Applications of the General Theory of Relativity*. pp. 688. ISBN 0-471-92567-5. Wiley-VCH , July 1972. [ADS].

Weisberg J.M., Nice D.J., Taylor J.H. (2010). "Timing Measurements of the Relativistic Binary Pulsar PSR B1913+16". *Astrophysical Journal*, **722**:1030–1034. [ADS].

Weisberg J.M., Romani R.W., Taylor J.H. (1989). "Evidence for geodetic spin precession in the binary pulsar 1913 + 16". *Astrophysical Journal*, **347**:1030–1033. [ADS].

Weisberg J.M., Taylor J.H. (2002). "General Relativistic Geodetic Spin Precession in Binary Pulsar B1913+16: Mapping the Emission Beam in Two Dimensions". *Astrophysical Journal*, **576**:942–949. [ADS].

Weisberg J.M., Taylor J.H. (2003). "The Relativistic Binary Pulsar B1913+16". In *Radio Pulsars*, edited by M. Bailes, D.J. Nice, S.E. Thorsett, volume 302 of *Astronomical Society of the Pacific Conference Series*, page 93. [ADS].

Weisberg J.M., Taylor J.H. (2005). "The Relativistic Binary Pulsar B1913+16: Thirty Years of Observations and Analysis". In *Binary Radio Pulsars*, edited by F.A. Rasio, I.H. Stairs, volume 328 of *Astronomical Society of the Pacific Conference Series*, page 25. [ADS].

Wettig T., Brown G.E. (1996). "The evolution of relativistic binary pulsars". *New Astronomy*, **1**:17–34. [ADS].

Wilkins D.C. (1972). "Bound Geodesics in the Kerr Metric". *Physical Review D*, **5**:814–822. [ADS].

Will C.M. (2011). "Finally, results from Gravity Probe B". *Physcs Online Journal*, **4**:43. [ADS].

Willems B., Kalogera V. (2004). "Constraints on the Formation of PSR J0737-3039: The Most Probable Isotropic Kick Magnitude". *Astrophysical Journal, Letters*, **603**:L101–L104. [ADS].

Willems B., Kalogera V., Vecchio A., Ivanova N., Rasio F.A., Fregeau J.M., Belczynski K. (2007). "Eccentric Double White Dwarfs as LISA Sources in Globular Clusters". *Astrophysical Journal, Letters*, **665**:L59–L62. [ADS].

Willems B., Kaplan J., Fragos T., Kalogera V., Belczynski K. (2006). "Formation and progenitor of PSR J0737-3039: New constraints on the supernova explosion forming pulsar B". *Physical Review D*, **74**(4):043003. [ADS].

Willke B., Aufmuth P., Aulbert C., Babak S., Balasubramanian R., Barr B.W., Berukoff S., Bose S., Cagnoli G., Casey M.M., et al. (2002). "The GEO 600 gravitational wave detector". *Classical and Quantum Gravity*, **19**:1377–1387. [ADS].

Wilms J., Reynolds C.S., Begelman M.C., Reeves J., Molendi S., Staubert R., Kendziorra E. (2001). "XMM-EPIC observation of MCG-6-30-15: direct evidence for the extraction of energy from a spinning black hole?" *Monthly Notices of the Royal Astronomical Society*, **328**:L27–L31. [ADS].

Winters W.F., Balbus S.A., Hawley J.F. (2003). "Gap Formation by Planets in Turbulent Protostellar Disks". *Astrophysical Journal*, **589**:543–555. [ADS].

Wise M.W., McNamara B.R., Nulsen P.E.J., Houck J.C., David L.P. (2007). "X-Ray Supercavities in the Hydra A Cluster and the Outburst History of the Central Galaxy's Active Nucleus". *Astrophysical Journal*, **659**:1153–1158. [ADS].

Wollman E.R., Geballe T.R., Lacy J.H., Townes C.H., Rank D.M. (1977). "NE II 12.8 micron emission from the galactic center. II". *Astrophysical Journal, Letters*, **218**:L103–L107. [ADS].

Wong T.W., Valsecchi F., Fragos T., Kalogera V. (2012). "Understanding Compact Object Formation and Natal Kicks. III. The Case of Cygnus X-1". *Astrophysical Journal*, **747**:111. [ADS].

Woosley S.E., Heger A., Weaver T.A. (2002). "The evolution and explosion of massive stars". *Reviews of Modern Physics*, **74**:1015–1071. [ADS].

Woosley S.E., Langer N., Weaver T.A. (1995). "The Presupernova Evolution and Explosion of Helium Stars That Experience Mass Loss". *Astrophysical Journal*, **448**:315. [ADS].

Wyithe J.S.B., Loeb A. (2005). "Constraints on the Process that Regulates the Growth of Supermassive Black Holes Based on the Intrinsic Scatter in the M_{bh}-σ_{sph} Relation". *Astrophysical Journal*, **634**:910–920. [ADS].

Xu X.J., Li X.D. (2010a). "ERRATUM: "On the Binding Energy Parameter λ of Common Envelope Evolution" (2010, ApJ, 716, 114)". *Astrophysical Journal*, **722**:1985–1988. [ADS].

Xu X.J., Li X.D. (2010b). "On the Binding Energy Parameter λ of Common Envelope Evolution". *Astrophysical Journal*, **716**:114–121. [ADS].

Yu Q. (2002). "Evolution of massive binary black holes". *Monthly Notices of the Royal Astronomical Society*, **331**:935–958. [ADS].

Yu Q., Tremaine S. (2002). "Observational constraints on growth of massive black holes". *Monthly Notices of the Royal Astronomical Society*, **335**:965–976. [ADS].

Yunes N. (2007). "Frankenstein's glue: transition functions for approximate solutions". *Classical and Quantum Gravity*, **24**:4313–4336. [ADS].

Yunes N., Berti E. (2008). "Accuracy of the post-Newtonian approximation: Optimal asymptotic expansion for quasicircular, extreme-mass ratio inspirals". *Physical Review D*, **77**(12):124006. [ADS].

Yunes N., Berti E. (2011). "Erratum: Accuracy of the post-Newtonian approximation: Optimal asymptotic expansion for quasicircular, extreme-mass ratio inspirals [Phys. Rev. D 77, 124006 (2008)]". *Physical Review D*, **83**(10):109901. [ADS].

Yunes N., Tichy W. (2006). "Improved initial data for black hole binaries by asymptotic matching of post-Newtonian and perturbed black hole solutions". *Physical Review D*, **74**(6):064013. [ADS].

Yunes N., Tichy W., Owen B.J., Brügmann B. (2006). "Binary black hole initial data from matched asymptotic expansions". *Physical Review D*, **74**(10):104011. [ADS].

Zahn J.P. (1975). "The dynamical tide in close binaries". *Astronomy and Astrophysics*, **41**:329–344. [ADS].

Zel'dovich Y.B., Ivanova L.N., Nadezhin D.K. (1972). "Nonstationary Hydrodynamical Accretion onto a Neutron Star." *Soviet Astronomy*, **16**:209. [ADS].

Zhang Z., Yunes N., Berti E. (2011). "Accuracy of the post-Newtonian approximation. II. Optimal asymptotic expansion of the energy flux for quasicircular, extreme mass-ratio inspirals into a Kerr black hole". *Physical Review D*, **84**(2):024029. [ADS].

Zhou X.L., Wang J.M. (2005). "Narrow Iron Kα Lines in Active Galactic Nuclei: Evolving Populations?" *Astrophysical Journal, Letters*, **618**:L83–L86. [ADS].

Zoghbi A., Fabian A.C., Uttley P., Miniutti G., Gallo L.C., Reynolds C.S., Miller J.M., Ponti G. (2010). "Broad iron L line and X-ray reverberation in 1H0707-495". *Monthly Notices of the Royal Astronomical Society*, **401**:2419–2432. [ADS].

Acknowledgments

The first part of this thesis has been mainly developed at the Physics Department of the University of Milan (Italy), while the second part has been developed at the California Institute of Technology (Pasadena CA, USA) and the University of Mississippi (Oxford MS, USA). This work was supported by Emanuele Berti's NSF CAREER Grant No. PHY-1055103 and the LIGO REU program at the California Institute of Technology. Computation has been performed using the LCM cluster in the Milan Physics Department, the TAPIR clusters in Caltech and a local machine owned by the Gravity Group of the University of Mississippi.

First, I would like to thank Emanuele Berti for all the help I received in developing the second part of this work. You taught me your passion for discoveries: it's a pleasure to be your student. Greetings to Michelle and Leonardo as well.

I thank Giuseppe Lodato, with whom I developed the first part of this thesis. I am especially grateful to your attention to every detail of the physical problem we addressed together.

I thank Michael Kesden, that carefully checked my results and realized the importance of mass-ratio reversal; Richard O'Shaughnessy, that stressed the role of tidal interactions and the implications of our work on previous population-synthesis results; and Ulrich Sperhake, that taught me how to run the PN code (thanks for your help with my Cambridge application as well).

I thank Tamara Bogdanovìc, Chris Reynolds, Cole Miller, Massimo Dotti, Monica Colpi for their constructive criticism on the timescale argument to predict spin-disc alignment in SMBH merger; Andrew King and Chris Nixon for that stimulating discussions we had in Como; Gordon Ogilvie for providing us the code to compute the effective viscosity coefficient in a warped disc; Marco Tazzari for insights on gap opening and planetary migration; Stefano Facchini for clarifications on the different warp-propagation regimes, and Giovanni Rosotti for discussions on electromagnetic signatures of recoiling BHs.

I thank Krzysztof Belczynski, Tomasz Bulik, Or Graur, Sterl Phinney for helpful discussions on the second part of this work; Marc Favata and Parameswaran Ajith for providing us higher-order PN terms to test our code. I thank all the people of the Gravity Group in Olemiss: Marco Cavaglià for his idea that later becomes Fig. 7.1; Michael Horbatsch for suggestions on how to address the pile-up effect; and all the students that listened to my presentations: Daniele Trifirò, Cody Arceneaux, Zhongyang Zhang, Caixia Sky Gao, Sagnik De, Hector Okada da Silva, Domizia Chericoni. I also would like to thank Lucien Cremaldi and the Phyiscs Department of the University of Mississippi for giving me the possibility to attend the 22^{nd} Midwest Relativity Meeting in Chicago, where I presented part of this work. I thank Yanbei Chen, Kennet Libbrecht and Alan Weinstein for the coordination of the SURF program in Caltech and the trip to LIGO Livingston; as well as my SURF fellows Derek Nelson, Maximiliano Isi, Irina Ene, Oleg Kiriukhin and Mikhail Korobko for early discussions on my simulations.

I thank all the friends from Pasadena: Filippo, Luca, Cristina, Paul, Nick, TJ, Ellynore and Angeline. A special thanks to Matt for the hospitality I received in New York and for his deep passion towards his work and his wishes. I thank also the friends I gained in Oxford: Cristina, Marco, Stacy, Elisa, Carla, Fabiana, Alessandra, Francesca; and particularly Santo and Luisa because they made me feel like home. I thank Mattia, Giuseppe and all the people

of the Physics CLU community in Milan: through you all I discovered that life is really a wonderful adventure. I thank my mum and my dad because anything of this would not have been possible without their support; my grandmas and my grandpa for all their prayers and thoughts; my brother Stefano and my sister Monica: good luck!; and my cousin Giacomino as well.

Finally, I thank most of all Sofia because she has always been there, despite the number of timezones between us and the difficulties of this year.